Effect of flexible supports on the frequencies of nanobeams with tip mass and axial load for applications in atomic force microscopy (AFM)

Malesela K. Moutlana

In fulfillment of a Doctor of Philosophy in Mechanical Engineering

College of Agriculture, Engineering and Science, University of KwaZulu-Natal

School of Engineering

September 2020

Supervisor:

Prof. Sarp Adali

Declaration I

Supervisor:

As the candidate's Supervisor I agree/do not agree to the submission of this dissertation.

Signed: ……..……..(Prof. Sarp Adali) Date: 13 September 2020

Candidate:

I, Malesela Kenneth Moutlana (207528577) declare that:

(i) The research reported in this dissertation, except where otherwise indicated, is my original work.

(ii) This dissertation has not been submitted for any degree or examination at any university.

(iii) This dissertation does not contain other person's data, pictures, graphs or other information, unless specifically acknowledged as being sourced from other persons.

(iv) This dissertation does not contain other person's writing, unless specifically acknowledged as being sourced from other researchers. Where written sources have been quoted, then:

   a) their words have been re-written but the general information attributed to them has been referenced;

   b) where their exact words have been used, their writing has been placed inside quotation marks, and referenced.

(v) Where I have reproduced a publication of which I am an author, co-author or editor, I have indicated in detail which part of the publication was actually written by myself alone and have fully referenced such publication.

(vi) This dissertation does not contain text, graphics or tables copied and pasted from the Internet, unless specifically acknowledged, and the source being detailed in the dissertation and in the References sections.

Signed:…… ……..….(MK Moutlana) Date:…14/09/2020……

Declaration II

Conferences.

1. Moutlana MK (2015) Analytical solution of a vibrating nano cantilevered beam used for atomic force microscopy (AFM) in tapping mode. *2nd International Conference on Composite and Biocomposites and Nanocomposites* (ICCBN-2), 28 – 30 October 2015, Durban.
2. Moutlana MK (2016) Fundamental frequencies of a cantilevered nano-beam used for atomic force microscopy (AFM) in tapping mode. *4th International Conference on Nanomechanics and Nanocomposites* (ICNN-4), 14 – 17 September 2016, Vicenza, Italy.
3. Moutlana MK (2017) Frequencies of a cantilevered nano-beam used for atomic force microscopy (AFM) in tapping mode. *9th International Conference of the African Materials Research Society* (AMRS2017) 11 – 14 December 2017, Gaborone, Botswana.
4. Moutlana MK (2018) Fundamental frequencies of a torsional cantilevered nano-beam used in atomic force microscopy (AFM) for pliable biological samples. *3rd International Conference on Composite and Biocomposites and Nanocomposites* (ICCBN-3), 7 – 9 November 2018, Port Elizabeth.
5. Moutlana MK (2019) Frequencies of a cantilevered nanobeam with arbitrary boundary conditions including surface effects. *26th International Congress on Sound and Vibration* (ICSV26), 7 – 11 July 2019, Montreal, Canada.

Journal publications.

1. Moutlana MK and Adali S (2014) *Vibration of a Cantilever Beam with extended tip mass subject to piezoelectric control*. *R&D Journal SAIMechE*, Stellenbosch.
2. Moutlana MK and Adali S (2018) *Effects of Elastic Restraints on the Fundamental Frequency of Nonlocal Nanobeams with Tip Mass*. The International Journal of Acoustics and Vibration (IJAV). , https://doi.org/10.20855/ijav.2019.24.31368.
3. Moutlana MK and Adali S (2018) *Fundamental frequencies of a nano beam used for atomic force microscopy (AFM) in tapping mode*. MRS Advances (doi.org/10.1557/adv.2018.321)
4. Moutlana MK and Adali S (2019) *Fundamental frequencies of a torsional cantilever nano-beam for dynamic Atomic Force Microscopy (dAFM) in tapping mode*. Microsystem Technologies Springer. (DOI: 10.1007/s00542-018-4166-x)

Signed:…… ……..….(MK Moutlana) Date: 28/07/2020

Acknowledgments

I would like to thank Prof. Sarp Adali for supervising my research in this project and for his support. His knowledge, guidance and experience has encouraged and motivated me throughout my research. I would like to thank my family: Zondi and Irene, the kids; Tswelopele, Keletso and Thato for their support and inspiration. I would also like thank my extended family who remain a shining beacon in my life. I love you very much.

Abstract

Summary: *This work provides a study of the natural frequencies of a nanobeam with tip mass, axial load and arbitrary boundary conditions.*

This aim of this investigation is to describe the mechanical performance of a beam (probe) used in dynamic atomic force microscopy (dAFM) which can be utilized in scanning the topographical features of biological samples or "pliable" samples in general. These nanobeams can also be used to modify samples by using high frequency oscillating contact forces to remove material or shape nano structures. A nanobeam with arbitrary boundary conditions is studied to investigate different configurations and the effects of the relevant parameters on the natural frequencies.

The nano structure is modelled using the Euler-Bernoulli theory and Eringen's theory of nonlocal continuum or first order stress-gradient theory is incorporated to simulate the dynamics of the system. This theory is effective at nanoscale because it considers the small-scale effects on the mechanical properties of the material. The theory of Nonlocal continuum is based on the assumption that the stress at a single point in the material is influenced by the strains at all the points in the material. This theory is widely applied to the vibration modelling of carbon nanotubes in several studies.

The system is modelled as a beam with a torsional spring boundary condition that is rigidly restrained in the transverse direction at one end. The torsional boundary condition can be tuned, by changing the torsional spring stiffness, such that the compliance of the system matches that of the sample to prevent mechanical damage of both the probe tip and the sample. When the torsional spring stiffness is zero, the beam is pinned and when the stiffness is infinite, the beam is a cantilever. In the first case, a mass is attached to the tip and a linear transverse spring is attached to the nanobeam. The mass and spring model the probe tip and contact force, respectively.

In the second case, at the free end is a transverse linear spring attached to the tip. The other end of the spring is attached to a mass, resulting in a single degree of freedom spring-mass system. When the linear spring constant is infinite, the free end behaves as a beam with a concentrated tip mass. When the mass is infinite, the boundary condition is that of a linear spring. When the tip mass is zero, the configuration is that of a torsionally restrained cantilever beam. When tip of the nanobeam vibrates, the system behaves like a hammer and chisel.

The motion of the tip of the beam and tip mass can be investigated to observe the tip frequency response, force, acceleration, velocity and displacement. The combined frequencies of the beam and spring-mass systems contain information about the maximum displacement amplitude and therefore the sample penetration depth.

Keywords: vibrations, nanobeam, stress-gradient theory, small-scale effects, surface effects, atomic force microscope (AFM), elastic restraints, tip mass.

Table of Contents

List of figures

List of figures in appendix

List of tables

Nomenclature

ε_{xx} or ε_x – Strain in the longitudinal direction.

σ_{xx} or σ_x – Stress in the longitudinal direction, (N/m^2).

σ_{zz} – Stress in the normal direction to σ_{xx}.

ρ – Density, (kg/m^3).

ρ_o – Density of surface layer, (kg/m^2).

ρ_c – Dimensionless density ratio of surface to beam.

ω_n – Natural frequency of the n^{th} mode, (1/s).

R_n – Dimensionless natural frequency of the n^{th} mode.

a_n – Frequency parameter for n^{th} mode, (1/m).

k_1 – Torsional spring constant, (N·m).

κ_1 – Dimensionless torsional spring constant.

k_2 – Linear spring constant, (N/m).

κ_2 – Dimensionless linear spring constant.

a_k – Spring mass frequency parameter, (1/m).

λ – Buckling frequency parameter, (1/m).

A – Cross-sectional area of beam, (m^2).

s^* – Cross-sectional area (perimeter) of surface, (m).

$b(x)$ – Width of beam, (m).

E_c – Young's Modulus for local beam, (N/m^2).

E^e – Young's Modulus for beam with surface effects, (N/m^2).

E – Young's Modulus for nonlocal beam, (N/m^2).

$\bar{\mu}$ – Nonlocal small-scale effects parameter, (m^2).

μ – Dimensionless nonlocal small-scale effects parameter, (m^2).

μ_o – Lamé's first parameter derived from Molecular Dynamics, (N/m).

λ_o – Lamé's second parameter derived from Molecular Dynamics, (N/m).

ν – Poisson's ratio.

τ_{xx} and τ_{zx} – In-plane components of the surface stress tensor, (N/m^2).

τ_o – Internal stress in the surface layer, (N/m).

τ_c – Dimensionless internal stress in the surface layer.

α – constant dependent on the cross-section of beam.

T_z – Normal contact traction, (N/m^2).

T_x – Tangential contact traction, (N/m^2).

$F_o(x,t)$ – Transverse external loading of beam, (N or N/m).

$F_L(x,t)$ – Transverse external loading due to spring-mass, (N).

H – Height of beam, (m).

H_0 – Intrinsic height of surface of beam, (m).

I_c – Moment of inertia for the local beam, (m^4).

I – Moment of inertia for the nonlocal beam, (m^4).

I^* – Moment of inertia for the surface layers of beam, (m^3).

L – Length of beam, (m).

$\bar{m}$ – Mass per unit length of composite, (kg/m).

M_T – Mass at tip of beam, (kg).

η – Dimension-less mass ratio = $M_T/(\bar{m}L)$.

$M_c(x,t)$ or M^s or M – Moment distribution along the composite, (Nm).

$Q_c(x,t)$ or Q^s or Q – Shear force distribution along the beam, (N).

$N(x)$ – Axial load, (N).

k – Dimensionless axial load ratio to critical buckling load.

N_{cr} – Euler's critical buckling load, (N).

β – Axial load parameter, ($1/m^2$).

p_1, p_2 – Characteristic values, (1/m).

p_{1n} , p_{2n} – Characteristic values for n^{th} mode, (1/m).

$w(x,t)$ – Transverse displacement of beam as a function of time.

t – Time, (s).

$T_n(t)$ – Time function

$X_n(x)$ – Transverse displacement along the length of beam

$\gamma(L,t)$ – Transverse displacement of tip mass due to beam

z_o – Initial transverse displacement of mass.

$z(t)$ – Transverse displacement of mass.

x– Lengthwise coordinate in the *x*-direction

y – Lengthwise coordinate in the *y*- direction.

Chapter 1 – Introduction

1.1 Background and motivation.

Carbon nanotubes and nanostructures have become prominent in a wide range of engineering applications and are starting to appear in commonplace devices like sensors and nano resonators. Nanotubes in vibration can be used as probes for scanning surface topology in Atomic Force Microscopy (AFM) at molecular and atomic level. Furthermore, advanced AFM devices can be used to manipulate the molecular and atomic composition of samples by using high frequency vibrations to dislodged molecules or atoms of interest [1-3]. The Atomic Force Microscope (AFM) follows the discovery of the Scanning Tunnel Microscope (STM) by Binnig *et al* [4]. The AFM produces 3D image whilst the STM produces 2D topological images at atomic level. The STM measures the current that passes between the probe and the surface of interest and therefore limited to conductive materials. The AFM measures the force between the probe and the surface and has enjoyed greater use because it can be used for all materials. The AFM has become the foremost scanning device with the discovery of carbon nanotubes which are used as sensor tips or chiselling tools in the form of a cantilever [5-8].

The scanning process for AFM involves taking the measurement of force as the tip of the vibrating cantilever beam interacts with the surface of interest. The measured value of the force at a distinct frequency contains information about the velocity and depth (topology) of the tip, see Figure 1-1. These contact forces represent the dominant component of the forces when the interaction takes place. In the process of fabrication of nano molecules and structures, high frequency oscillations of a tip mass are utilized with the purpose of deforming or shaping a material into a desired shape [9,10]. This process is popularly known as dynamic atomic force microscopy (dAFM)[7] or tapping mode atomic force microscopy (TM-AFM)[10]. For this reason, dynamic microscopy has become of great value in the field of biomolecular engineering, nanomedicine and nano-manufacturing.

Nanotubes are also used as biosensors by observing the vibration patterns when different foreign masses are attached. By analysing sensing data obtained, one can calculate the mass and several parameters of interest of the attached particle [12-16].

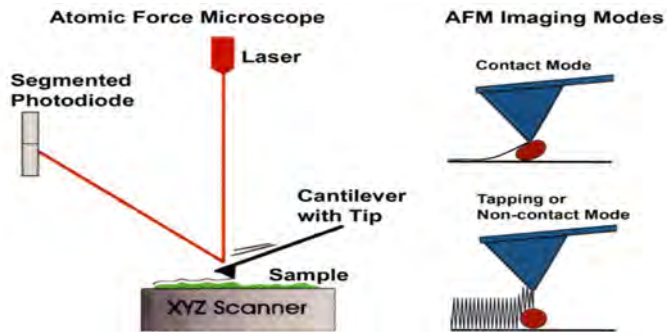

Figure 1-1: Atomic Force Microscope (AFM) configuration

The use of sensors is crucial in environmental monitoring, detecting minute particles in the air i.e. pollution, bioterrorism, etc.

These types of applications are generally referred to as nano-resonator sensors which are based on detecting shifts in resonant frequencies caused by a mass attached to the nanotube [17-24]. Carbon nanotubes are known to provide a high level of sensitivity and a significant improvement in the accuracy of measurement in comparison to conventional sensors.

The vibration characteristics of nanoscale beams are examined within the framework of nonlocal continuum theory and this basis has been applied to the vibration modelling of carbon nanotubes in several studies [25-34]. Vibrations of carbon nanotubes with a tip mass have been studied extensively due to their use in sensor applications [18,21-23,35-38] and a number of studies presented vibrations of nanotubes with elastically restrained boundaries [39-42]. In the current research, an elastically restrained nanobeam with a tip mass is modelled as an Euler-Bernoulli beam underpinned by Eringen's nonlocal or stress-gradient theory [25,26] to account for the small scale effects [43,44]. When the beams reach nanoscale length, non-local continuum (stress gradient) and strain gradient theories are incorporated in the modelling [45,46]. These stress gradient theories include Eringen's non-local theory (first order stress) and higher order theories like Reddy Beam Theory (RBT) and Levison Beam Theory (LBT). Eringen's theory provides a unified foundation for field equations of non-local continuum and provides a basis for several stress-gradient theories [44]. Higher order stress/strain gradient theories are constructed such that the transverse stress at the surface vanish as required. Ansari *et. al*. [45] and Lu *et. al*. [46] investigated strain gradient theories for beams at nanoscale by considering only the local higher order strains. All these theories above provide very accurate results compared to Molecular Dynamics (MD) simulations.

The boundary condition on one support ($x = 0$) is stipulated as a torsional spring and pin which replaces the clamped boundary condition reported in numerous studies. Two cases are reported in this investigation:

1) A tip mass is attached to the free end ($x = L$) of the beam and a transverse linear spring is attached to the tip of the beam. In this configuration [47,48], the tip mass serves as a probe tip and the linear transverse spring models the interaction force between the probe and surface of interest. The torsional spring is included to tune the system such that the compliance of the sample matches that of the vibrating beam [12,13]. These types of beams are generally referred to as torsional cantilevers and are much more versatile than conventional clamped cantilevers. These torsional nanobeams can therefore be

appropriate for cutting-edge atomic force microscopy in applications involving topological scanning.

2) A linear spring is attached to the free end ($x = L$) and a mass is attached to the other end of the spring, to form a spring-mass system. A torsional spring and pin are the boundary condition at the other end ($x = 0$) resulting in a torsional cantilever. In this configuration [48, 49], the tip of the beam behaves like a forcing function applied (hammer) to a spring-mass as it vibrates. In turn, the force is transmitted to the mass via the spring and the mass (chisel) is displaced in the lateral direction until it interacts with the sample. In this system, the frequencies of the beam can be manipulated by varying the torsional and linear stiffness. The frequencies of vibration are directly linked to the depth of penetration of the mass and the force induced. These two parameters are the most vital in transforming and reshaping materials at molecular level e.g. by knocking off atoms to alter the material's mechanical properties and nanofabrication in general.

The theories mentioned above on vibrations exhibit what is known softening or hardening of the nanobeam, were there is a slight underestimation or overestimation of the natural frequencies of vibration compared to results obtained using molecular dynamics according to Pishkenari *et. al* [50]. It is known and well documented that the lateral natural frequency of a string or thin rod increases if a tensile load is applied and decrease if a compressive load is applied. Moutlana and Adali [51] reported on the use of sandwiched piezoelectric actuators to alter the fundamental frequency of a cantilever by applying tensile and compressive loads. This is very important because it allows us to increase the frequency gap between: 1) buckling frequency and fundamental frequency or 2) fundamental frequency and second natural frequency, such that we can increase the frequency spectrum of the applied external load and prevent resonance failure. In the current investigation, an axial compressive/tensile load is applied at the free end ($x = L$) to simulate this softening/hardening effects exhibited by the piezo actuators.

The beams contemplated in this investigation are regarded as slender i.e. the thickness of the beam is small compared to the length ($h \ll L$) and at nanoscale, could be made up of several layers of atoms [52]. In view of this, we can design a composite beam with a flexoelectric layer at the top and bottom surface and implement active piezoelectric control at nanoscale. At these scales, the beams under investigation could be at minimum, three (3) atoms thick, and the bulk to surface volumes become comparable such that the surface energies have significant influence on the vibration of the system. This influence on the natural frequencies of vibration

is borne out of the fact that the different layers of the beam experience different environments. The bulk material is typically surrounded by other atoms, whilst the surface atoms are in contact with the bulk atoms on one side and a different "environment" on the other side (i.e. air or viscous fluid). In the present study Gurtin and Murdoch's Linear Surface Elasticity Theory (LSET) [53] is adopted to model the influence of surface effects on the system. The influence of the surface effects is studied in a system modelled as a nanobeam with a torsional boundary condition at one end and spring-mass at the free end and presented by Moutlana [54].

The lateral vibration of a beam is described using 4^{th} order homogenous equations of motion that satisfy four boundary conditions. The solution is determined by the method of separation of variables, made up of the modal and temporal domains. The general solution to the modal domain has four constants which are calculated simultaneously by ensuring that the general solution conforms to the equation of motion and the boundary condition.

1.2 Literature review.

In 1981, Binnig and Rohrer [55] received a Nobel Prize in Physics for the development of the Scanning Tunnelling Microscope (STM). The STM is the first instrument capable of directly obtaining images of solid surfaces. The STM is limited to the study of surfaces of electrically conductive materials because it relies on a voltage potential difference between the surface and the probe. One of the two electrodes is attached to a sharp metal tip at the end of the probe and the another is attached to the surface being scanned. The sharp metal tip is brought very close to the surface of interest until it is at approximately 0.3 to 1nm from the surface. After applying a voltage (10mV to 1V) a tunnelling current is observed between the probe and the surface, and this current can be measured to generate a topographic map of the surface [56, 57]. One of the greatest disadvantages is that if there are any different atomic species within the sample, the tunnelling current may not yield reliable results for the height of the specimen. Baratoff *et. al*. introduced new improvements on the types of surfaces that could be effectively scanned by studying the topology of semiconducting materials using STM [56]. The Atomic Force Microscope (AFM) represents an improvement on the Scanning Tunnelling Microscope (STM) and produces high resolution 3D images of surface topology.

Unlike the STM, the AFM probe comes into contact with the surface during scanning. This can be likened to using one's fingers to visualize a 3D object [58]. The AFM is presently the most powerful tool for determining surface topography of molecules at sub-nanometer resolution. The measuring probe for an AFM is made from a cantilevered carbon nano tube

(CNT) with a sharp tip that is used to probe the surface. The AFM measures the force induced at the tip of the cantilevered probe as it scans the surface and these forces are ultrasmall, on the order of 1nN (nano-Newton) [58]. The dynamic behaviour of the forces is extremely complicated and using precise analysis, the induced frequencies of vibration created by the interaction forces between the probe and surface can be detected and measured. The measured frequencies allow us to predict the displacement of the tip which can be in turn be used to map the topology of the surface. Furthermore, the information about the tip displacement can be used in nanofabrication and nanomanipulation of samples; because knowing the frequencies allows us to determine the penetration depth.

Nanotubes have found applications [59] in medical research to detect bacteria and viruses. These sensors are modelled as cantilevered beams with a tip mass [16, 60, 21]. The tip mass could be the bacteria or virus attached to the tip of the nanotube which behaves as a cantilever. AFM have been also used for mechanically unfolding proteins for mapping of DNA sequence [4] and these DNA sequences can be used to develop therapies for deadly pandemics. Cantilevered nanotubes can also be used for many other applications ranging from environmental monitoring to fighting bioterrorism [61, 24, 62].

Carbon nanotubes (CNT) were discovered in the early 1990's by Ijima [63]. These materials have received significant interest in the scientific community due to their exceptional properties. Carbon nanobeams cannot be modelled using classical beam theories such as Euler-Bernoulli and Timoshenko [64, 65]. These theories are accurate only up to micrometer scale and will breakdown at nanoscale level because engineering material properties are sensitive to size. The molecule size to bulk is small and therefore new theories were developed in order to take into account the small-scale effects.

The vibration characteristics of nano scale beams can be analysed within several frameworks depending on the size of the beam [25, 26]. At macro and micro level, the Euler-Bernoulli and Timoshenko bending theories are used with satisfactory results. When the beam dimensions reach nanoscale length, nonlocal continuum (stress gradient) and strain gradient theories are incorporated in the modelling [33 - 48]. These stress gradient theories include Eringen's non-local theory (first order stress) and higher order theories like Reddy Beam Theory (RBT) and Levison Beam Theory (LBT). Eringen's theory provides a unified foundation for field equations of nonlocal continuum and provides a basis for several stress-gradient theories [66]. Eringen proposed a theory based on nonlocal continuum mechanics were the strain on any point on a body is dependent on the strains in the entire body. This theory is suited to nanoscale modelling due to bulk to particle size ratio and the theory can

satisfactorily explain phenomenon at atomic and molecular scale such as vibrations and wave dispersion [25, 26]. Experimental findings and atomistic simulations have shown a significant size dependency in mechanical properties at nanoscale [67 - 70]. Higher order stress/strain gradient theories are constructed such that the transverse stress at the surface vanish as required. Ansari *et al.* [45] and Lu *et. al.* [46] investigated strain gradient theories for beams at nanoscale by taking into account only the local higher order strains. All these theories above provide very accurate results compared to Molecular Dynamics (MD) simulations and calibration of the small-scale parameters has been published by Pishkenari, H.N *et. al.* and Hossein, N.P., *et. al.* [50, 69].

Two different methods of modelling can be applied in simulating the dynamic behaviour: 1) atomistic modelling and 2) non-local continuum modelling. Atomistic models are significantly more accurate and reliable but have the following disadvantages: a) inapplicability of modelling for large number of atoms, b) requires very large amount of intensive computational analysis and c) model formulation is extremely complex and limited to small systems. In nonlocal continuum modelling the following advantages are realized: a) the influence of CNT chirality, intermolecular spacing and characteristic dimensions can be incorporated into the model, b) computational requirements are significantly lower and c) complex models can be constructed and evaluated within a shorter space of time. Early developments and applications of these theories were presented by Peddieson and Buchanan [68] and further developed by Reddy and others [67, 70 - 80].

The transverse motion of a bean in vibration can be determined using 4^{th} order differential equations of motion. Fourth order differential equations can be solved by separation of variables [40-45, 64, 65, 74], finite element method [16, 21 , 29, 37, 71] and Lagrange formulation [72, 73]. Various boundary conditions can be associated with the transverse vibration frequencies of systems. The majority of classic boundary conditions are studied extensively by Balachandran, Magrab and others [64, 65, 72, 73], and are used as the foundation to investigate nano electromechanical systems (NEMS) and micro electromechanical systems (MEMS). The analytical solution to solve for the frequencies of vibration is complex and used extensively in solving of buckling and vibration problems. Eigenfunctions can be used as the building blocks to construct a solution that satisfies the non-homogenous boundary condition. The eigenfunctions are associated with the distinct modes of vibration [72, 73] and related eigenfrequencies. The eigenfrequencies derived from the solution to the differential equations of motion are referred to as the natural frequencies of the system [64]. The natural frequencies of a structure are extremely important in engineering

design to prevent catastrophic failure due to resonance and to eliminate unwanted noises [72]. Resonance is a phenomenon whereby the frequency of a dynamic applied external load matches the natural frequency of the system. When that happens, the amplitude of vibration increases with every successive application of the external load until there is total collapse of the structure due to mechanical failure.

Beam elements are used in many prominent engineering structures in NEMS and MEMS. These beam structures can be distinguished by the boundary condition, typically two or four boundary conditions are applied, but in general, the number of boundary conditions are equal to the number of constants in the general solution for the differential equation of motion. Micro beams are modelled using classic continuum theory e.g. Euler-Bernoulli and Timoshenko beam theory. These theories have been adapted to give accurate predictions for beams at nano scale in what is referred to as stress (nonlocal) and strain gradient theories.

In Nonlocal theory, it is assumed that the stress at a single point in the material is influenced by the strains of all the points in the material. This theory is widely applied to the vibration modelling of carbon nanotubes in several studies [33, 34] and in particular, vibrations of carbon nanotubes with a tip mass have been studied extensively due to their use in sensor applications [19, 41, 42].

In many studies, the elasticity of the boundaries is not taken into account and the classical clamped or free boundary conditions are considered. In several studies, vibrations of nanotubes with elastically restrained boundaries have been conducted [43, 44], but only as a stand-alone system, that cannot be decomposed into sub-systems. The effects of the elastic restraints and tip mass on the frequencies have been investigated numerically and these problems have been solved in the case of beams based on the local (classical) theory of elasticity. Elastically supported beams with a tip mass have been studied in [43, 44] and the beam with torsional and translational springs with a tip mass has been studied in [45, 46, 47] based on the classic theory of Euler-Bernoulli beams.

The stiffness of a cantilever beam probe has been studied in the field of hydrodynamics and very important developments were reported by Basak *et. al*. [13] and Beyder *et. al*. [14]. According to Beyder and Basak, the boundary condition for a cantilever clamp end can be modified using a torsional spring to create what is called a torsional cantilever. This is very important when probing pliable or biological sample because the compliance of the probe can be matched to that of the sample. By doing so, damage to the tool and the sample can be prevented [13, 14]. This torsional cantilever also allows researchers to utilize short cantilevers, and at the same time, achieve large tip displacements. Natsuki *et. al*. [78] found that by

increasing the aspect ratio of a nanobeam, the sensitivity of measurement can be improved for nanomechanical mass sensors. While Natsuki *et. al*. [78] used high aspect ratio nanobeams to improve the sensitivity of measurement, the same can be achieved by using a torsional cantilever with a low aspect ratio nanobeams. Furthermore, torsional cantilevers can be utilized in applications requiring low force and high frequencies, such as topological mapping of biological samples embedded if a viscous medium [14].

Moutlana and Adali [51] published an article on the vibration of a beam with extended tip-mass subject to piezo control allowing one to alter the natural frequencies in order to actively prevent resonance. In their investigation [51], it was determined that an extended mass has an influence on the second mode (2^{nd}) of vibration and that the frequencies can give us information about the radius of the attached mass or radius of attached bacteria or virus. The frequency shift in the 2^{nd} mode allows us to determine the radius or diameter of the bacteria or virus, making it easier to identify. Seyed [83] investigated a tapered beam with spring-mass system using continuum theory like some of the above investigations, but small-scale effects were not taken into account.

Elastically restrained nanobeams with a tip mass are modelled as Euler-Bernoulli beams underpinned by Eringen's nonlocal theory [25, 26] to take into consideration the small-scale effects [44]. Some of the earlier work was performed by Esteshami and Hajabasi [84] for the most basic boundary condition: clamped, simply supported and free for both single and double walled nanotubes. In this work [84], the researchers recognised that, with the exception for a simply supported beam, the frequencies of vibration are influenced by the small-scale parameter. Li *et. al*. [85] studied nanobeams with the classic clamped-free, clamped-clamped and simply supported beams with a mass attached to region of maximum displacement. The modes shapes were also investigated by generating the shape functions from the natural frequencies and the initial conditions, which again showed that the small-scale parameter has an influence on the systems [86]. Ansari [45] has implemented strain gradient theory to solve similar problems with the results being in good agreement compared to Molecular Dynamics.

Nanobeams with non-classic boundary conditions (e.g. linear and torsional springs, masses, etc.) have received wide acceptance in NEMS. Nanobeams with tip mass can be used as accelerometers and nanobeams with piezo surface layers can readily be used as energy harvesters to create autonomous nanorobots according to an investigation by Managheb *et. al*. [86]. In their investigation, Managheb *et. al*. found that attaching a mass at the tip of a flexoelectric cantilever nanobeam improves the energy harvesting process. Bahrami *et. al*. [87, 88] studied a nanocantilever with tip mass and horizontal nonlinear spring that behaves like a

directed axial load on the beam and this research can be straightaway applied in NEMS. Some of the configurations of the boundary conditions were studied by Moutlana and Adali, Berretta *et. al.* and Mahmoudpour *et. al.* [49, 89, 90], where the clamped boundary condition is substituted by a torsional spring and the results were found to be consistent with Eringen's nonlocal stress theory. It was shown that the use of a torsional cantilever could benefit the process of scanning for AFM in viscous medium in studies conducted by Arda and Aydogdu [91], investigating biological nanomotors. Moutlana and Adali [54] investigated a torsional cantilever with tip-mass and linear spring boundary condition and showed that with elastic boundary conditions, the natural frequencies of vibration can be manipulated to the desired requirement. Most of the research above was conducted for a beam with discreet mechanical elements e.g. linear or torsional spring or concentrated mass attached to the boundaries.

NEMS are usually made up of several coupled discreet systems. These systems are expected to function simultaneously e.g. a cantilever coupled with a spring-mass system. Many such systems are well documented at micro and macro scale in dynamics textbooks [64, 65] and many researchers are investigating the mechanical behaviour of such system at nanoscale [92 - 100]. Earlier work on coupled systems was presented by Gheshlaghi and Mirzaei [99] were they investigated the sensitivity of lateral vibrations due to small scale effects. Gheshlaghi and Mirzaei studied a cantilever beam with spring-mass attached to the free end but the force due to the spring mass is not included in the shear boundary conditions. According to classic continuum theories, Magrab [65] maintains that the single degree system induces a force at the tip of the beam which manifests as a shear force.

Moutlana and Adali [49] presented new improvements by coupling a torsional cantilever with a single degree spring mass system. The model presented herein includes the induced force due to the spring-mass in the shear boundary condition, and therefore represents a more consistent treatment as opposed to Gheshlaghi and Mirzaei. In this research [49], the model shows that there is a strong link between the natural frequency of the beam and the natural frequency of the spring mass system; and this can be used to predict the beam tip deflection and the deflection of the tip-mass. This can be directly linked to the penetration depth of a tool like AFM for sample scanning or manipulation [49].

In most engineering applications the 1st natural frequency in the most important and dominant when the system undergoes vibrations and is typically referred to as the fundamental frequency of vibration [75, 76]. The frequencies of vibration for a beam under axial load are somewhat more complex in that the frequency parameter of the system are sensitive to compressive loads according to Pin *et. al.* [77]. This complication is brought about because if

the load becomes too big, the beam undergoes static buckling and thus fails. Further studies on a beam with axial load have been conducted by Natsuki *et. al*. [78] to determine the effects on the vibrations and they found that a tensile axial load increases the natural frequencies in concurrence with Moutlana and Adali [51]. Wang *et. al*. [101, 102] used an axially loaded nanobeam to determine or calibrate Eringen's small-scale coefficients by using discreet beam model (DBM) and Eringen's beam model (ENBM). This is achieved by solving the discrete beam formulation using the theory of linear central finite differences and compare the buckling loads and natural frequencies of the DBM with those of the ENBM, where local continualized discrete boundary conditions are applied to neighboring elements.

1.3 Research objectives.

The aim of this investigation is to develop a model to simulate the vibration characteristics of a nanobeam with flexible restraints, tip mass and axial load. The nanobeam is restrained by a torsional spring, carries a tip mass and linear spring . The torsional and linear stiffness and mass are utilized to modify the vibration characteristics of the system. To accomplish the aim of controlling and analyzing the vibration characteristics of the model, the following objectives must be met,

1. Development of the equations of motion governing the vibration of the nanobeam.
2. Development of the equations using the constitutive relations governing nonlocal continuum or stress-gradient theory.
3. Derive the characteristic equations to determine the natural frequencies.
4. Investigation of the effects of the critical parameters on the natural frequencies.
5. Investigate the effects of the spring-mass system on the motion of the system.
6. Investigate the vibration of the beam subject to axial loading.

Euler-Bernoulli theory is employed because we assume the beam is slender ($h/L<<1$) and therefore the shear deformations are not accounted for, without losing accuracy. To satisfy the stated objectives the research is divided into three major categories: (i) Problem formulation, (ii) Modelling and numerical solutions and (iii) Results and refinements.

(i) **Problem formulation**: This stage involves the assessment of the mechanical structure subjected to vibration. It also involves formulating the stress strain relationships which are used for developing the 4^{th} order differential equations of motion for the nanobeam and 2^{nd} order differential equations for the

spring-mass system. The differential equations of motion are coupled, and the total system dynamics can be determined.

(ii) **Modelling and numerical solutions:** At this stage, the analytical solution is developed using separation of variables and presented it in the form of an eigenfunction series expansion. The natural frequencies are generated numerically by plotting the characteristic equations for the vibrations of the system.

(iii) **Results and refinements**: The results for the analytical solutions are generated using Wolfram Mathematica[1] and *wx*Maxima[2]. The results will be plotted and tabulated to indicate the influence of the different parameters on the frequencies. The model is refined further to take into account surface effects because at nanoscale and pico-scale, "There is plenty of room at the bottom"-- Richard Feynman

1.4 References.

1. Li, C., Thostenson, E. T., and Chou, T. W. (2008) Sensors and actuators based on carbon nanotubes and their composites: a review. *Compos. Sci. Technol*. **68**: 1227-1249.
2. Bogue, R. (2009) Nanosensors: A review of recent progress. *Sens. Rev*. **29**(4): 310-315,
3. Feng, E. H. and Jones R. E. (2011) Carbon nanotube cantilevers for next-generation sensors. *Physical Review B* **83**: 195412.
4. Binnig, G., Quate, C. F., and Gerber, C. (1986) Atomic force microscope. *Phys. Rev. Lett*. **56**: 930–933.
5. Chang, W. J. (2002) Sensitivity of vibration modes of atomic force microscope cantilevers in continuous surface contact. *Nanotechnology* **13**: 510–514.
6. Hsu, J.C., Lee, H.L., and Chang, W.J. (2007) Flexural vibration frequency of atomic force microscope cantilevers using the Timoshenko beam model. *Nanotechnology* **18**: 285-503.
7. Raman, A., Melcher, J., and Tung, R. (2008) Cantilever dynamics in atomic force microscopy. *Nano Today*, **3**: 20-27.
8. Sadeghi, A. (2012) The flexural vibration of V shaped atomic force microscope cantilevers

[1] Mathematica is a computer algebra program used in symbolic mathematical computation for engineering, mathematics, physics, etc.

[2] Maxima computer algebra system (CAS) that is symbolic based. It is used for algebraic manipulation, calculus, matrix, linear algebra, etc.

by using the Timoshenko beam theory, *Zeitschriftfur Angewandte Mathematik und Mechanik* **92** 782–800.

9. Chang, W. J., Yang, Y. C., and Lee, H. L. (2013) Dynamic behaviour of atomic force microscope-based nanomachining based on a modified couple stress theory. *Micro Nano Lett*. **8**: 832–835.
10. Okamoto, R. and Naruo Sasaki, N. (2019) Effect of size and shape of graphene sheets on nanoscale peeling process by atomic force microscopy. *The Japan Society of Applied Physics: Japanese Journal of Applied Physics*, Volume **58**, Number 11.
11. Liu, W., Yan, Y., Hu, Z., Zhao, X., Yan, J., and Dong, S. (2012) Study on the nano machining process with vibrating AFM tip on the polymer surface. *Applied Surface Science* **258**: 2620-26261.
12. McCarthy, R., Carmichael, B., and Nima Mahmoodi, S. (2014) Dynamic analysis of tapping atomic force microscopy considering various boundary value problems. *Sensors and Actuators A*, **216**: 69-77.
13. Basak, S. Beyder, A, Spagnoli, C., Raman, A. and Sachs, F. (2007) Hydrodynamics of torsional probes for atomic force microscopy in liquids. *Jornal of Aplied Physics* **102**, 024914 .
14. Beyder, A., Frederick Sachs, F. (2006) Micro fabricated torsion levers optimized for low force and high-frequency operation in fluids. *Ultramicroscopy* **106**, 838–846.
15. Adhikari, S. and Chowdhury, R. (2010) The calibration of carbon nanotube based bionanosensors. *J. Appl. Phys.* **107**: 124322(1-8).
16. Murmu, T. and Adhikari, S. (2012) Nonlocal frequency analysis of nanoscale biosensors. *Sensors and Actuators A: Physical* **173**: 41-48.
17. Shen, Z. B., Sheng, L. P., Li, X. F., and Tang, G. J. (2012) Nonlocal Timoshenko beam theory for vibration of carbon nanotube-based biosensor. *Physica E* **44**: 1169-1175.
18. Joshi, A.Y., Harsha, S. P., and Sharma, S. C. (2010) Vibration signature analysis of single walled carbon nanotube based nanomechanical sensors. *Physica E* **42**: 2115-2123.
19. Chiu, H. Y., Hung, P., Postma, H. W. C., and Bockrath, M. (2008) Atomic-scale mass sensing using carbon nanotube resonators. *Nano Lett*. **8**: 4342–4346.
20. Liang, L.N., Ke, L.L., and Wang, Y.S. (2015) Flexural vibration of an atomic force microscope cantilever based on modified couple stress theory. *Int. J. Struct. Stability Dyn.* **15**: 1540025.
21. Mehdipour, I., Barari, A., and Domairy, G. (2011) Application of a cantilevered SWCNT with mass at the tip as a nanomechanical sensor. *Comput. Mater. Sci*. **50**: 1830-1833.

22. Lee, H.-L., Hsu, J.-C., and Chang, W.-J. (2010) Frequency shift of carbon nanotube-based mass sensor using nonlocal elasticity theory. *Nanoscale Research Letters* **5**: 1774-1778.
23. Shen, Z. B., Li, X. F., Sheng, L. P., and Tang, G. J. (2012) Transverse vibration of nanotube-based micro-mass sensor via nonlocal Timoshenko beam theory. *Comput. Mater. Sci*. **53**: 340-346.
24. Wang, Q., and Arash, B. (2014) A review on applications of carbon nanotubes and graphenes as nano-resonator sensors. *Computational Materials Science* **82**: 350–360.
25. Eringen, A. C., and Edelen, D. (1972) On nonlocal elasticity. *Int. J. Eng. Sci*. **10** (3): 233–248.
26. Eringen, A. C. (2002) Nonlocal Continuum Field Theories, Springer-Verlag, New York.
27. Sakhaee-Pour, A., Ahmadian, M., and Vafai, A. (2009) Vibrational analysis of single-walled carbon nanotubes using beam element. *Thin Walled Struct.* **47** (6-7): 646–652.
28. Artan, R., and Lehmann, L. (2009) The vibrations of carbon nanotubes in nonlocal elasticity. *J. Comp. Theoretical Nanosci*. **6**: 653–661.
29. Eltaher, M. A., Alshorbagy, A. E., and Mahmoud, F. F. (2013) Vibration analysis of Euler–Bernoulli nanobeams by using finite element method. *Appl. Math. Modelling* **37**: 4787–4797.
30. Behera, L., and Chakraverty, S. (2014) Free vibration of Euler and Timoshenko nanobeams using boundary characteristic orthogonal polynomials. *Appl. Nanosci*. **4**:347–358.
31. Li, X.F., Tang, G.J., Shen, Z.B., and Lee, K. Y. (2015) Resonance frequency and mass identification of zeptogram-scale nanosensor based on nonlocal theory beam theory. *Ultrasonics* **55**: 75-84.
32. Arefi, A., and Salimi, M. (2015) Investigations on vibration and buckling of carbon nanotubes with small initial curvature by nonlocal elasticity theory. *Fullerenes, Nanotubes and Carbon Nanostructures* **23**(2): pg. 105-112.
33. Rahmanian, M., Torkaman-Asadi, M. A., Firouz-Abadi, R. D., and Kouchakzadeh, M. A. (2016) Free vibrations analysis of carbon nanotubes resting on Winkler foundations based on nonlocal models. *Physica B* **484**: pg. 83–94.
34. Rosa, M. A. D., and Lippiello, M. (2016) Nonlocal frequency analysis of embedded single-walled carbon nanotube using the Differential Quadrature Method. *Compos. Part B: Eng*. **84**: 41–51.
35. Murmu, T., and Adhikari, S. (2011) Nonlocal vibration of carbon nanotubes with attached bucky-balls at tip. *Mech. Res. Commun*. **38**: 62-67.

36. Elishakoff, I., Versaci, C., and Muscolino, G. (2011) Clamped-free double-walled carbon nanotube-based mass sensor. *Acta Mech*. **219**: 29–43.
37. Mehdipour, I., Barari, A., and Domairy, G. (2011) Application of a cantilevered SWCNT with mass at the tip as a nanomechanical sensor. *Comput. Mater. Sci*. **50**: 1830-1833.
38. Horng, T.-L. (2012) Analytical solution of vibration analysis on fixed-free single-walled carbon nanotube-based mass sensor. *J. Surface Engineered Materials Adv. Technology* **2**: 47-52.
39. Kiani, K. (2010) A meshless approach for free transverse vibration of embedded single-walled nanotubes with arbitrary boundary conditions accounting for nonlocal effect. *Int. J. Mech. Sci.* **52**: 1343-1356.
40. Kiani, K. (2013) Vibration analysis of elastically restrained double-walled carbon nanotubes on elastic foundation subjected to axial load using nonlocal shear deformable beam theories. *Int. J. Mech. Sci*. **68**: 16–34.
41. Kiani, K. (2015) Nanomechanical sensors based on elastically supported double-walled carbon nanotubes. *Appl. Math. Comput*. **270**: 216–241.
42. Kiani, K., Ghaffari, H., and Mehri, B. (2013) Application of elastically supported single-walled carbon nanotubes for sensing arbitrarily attached nano-objects. *Curr. Appl. Phys.* **13**: 107–120.
43. Reddy, J. N. (2006) Nonlocal theories for bending, buckling and vibration of beams. *Int. J. Eng. Sci*. **45**: 288-307.
44. Reddy, J. N., and Pang, S. N. (2008) Nonlocal continuum theories of beams for the analysis of carbon nanotubes. *J. App. Phys.* **103**: 023511.
45. Ansari, R., Gholami, R. and Rouhi, H. (2012) Vibration analysis of single-walled carbon nanotubes using different gradient elasticity theories. *Composites: Part B*: **43**: 2985-2989.
46. Lu, L., Gou, X and Zhao, J. (2017) Size-dependent vibration analysis of nanobeams based on the nonlocal strain gradient. *International Journal of Engineering Science*. 116: 12-24.
47. Moutlana, M.K. and Adali, S. (2019) Effects of Elastic Restraints on the Fundamental Frequency of Nonlocal Nanobeams with Tip Mass. *International Journal of Acoustics and Vibration*. Vol. **24**, No. 3, pg. 520-53. https://doi.org/10.20855/ijav.2019.24.31368.
48. Moutlana, M.K. and Adali, S. (2018). Fundamental frequencies of a nano beam used for atomic force microscopy (AFM) in tapping mode. *MRS Advances*, **3** (42-43), 2617-2626. doi:10.1557/adv.2018.321.

49. Moutlana, M.K., Adali, S. (2019) Fundamental frequencies of a torsional cantilever nano beam for dynamic atomic force microscopy (dAFM) in tapping mode. *Microsystems Technologies.* **25**, 1087–1098. https://doi.org/10.1007/s00542-018-4166-x
50. Pishkenari, H.N., Afsharmanesh, B. and Tajaddodianfar, F. (2016) Continuum models calibrated with atomistic simulations for the transverse vibrations of silicon nanowires. *International Journal of Engineering Science*. Volume **100**. Pages 8-24. ISSN 0020-7225. https://doi.org/10.1016/j.ijengsci.2015.11.005.
51. Moutlana, M. K., and Adali, S. (2015) Vibration of a cantilever beam with extended tip mass and axial load subject to piezoelectric control. *R & D J. South African Institution of Mech. Eng.* **31**: 60-65.
52. Moutlana, M. K., and Adali, S. (2020) Fundamental frequencies of a nanobeam with arbitrary boundary conditions including axial load. [**in preparation**]
53. Gurtin, M.E. and Murdoch, A. (1975) A continuum theory of elastic material surfaces. *Archive for Rational Mechanics and Analysis* (**57**) pg. 291-323.
54. Moutlana, M. K., and Adali, S. (2019) Fundamental frequencies of a nanobeam with arbitrary boundary conditions including surface affects. *Proceedings: The 26th International Congress on Sound and Vibration* (ICSV26) | 2019-07-07 - 2019-07-11, Montreal, Canada.
55. Binnig, G. and Rohrer H. (1983) Scanning tunneling microscopy. *Surface Science* Volume **126**, Issues 1–3, Pages 236-244.
56. Baratoff, A., Binnig, G., Fuchs, H., Salvan, F. and Stoll, E. (1986). Tunneling microscopy and spectroscopy of semiconductor surfaces and interfaces *Surface Science* Volume **168**, Issues 1–3, Pages 734-743.
57. Sutter P. (2019) Scanning Tunneling Microscopy in Surface Science. In: Hawkes P.W., Spence J.C.H. (eds) Springer Handbook of Microscopy. Springer Handbooks. Springer, Cham.
58. Rief, M., Gautel, M., Oesterhelt, F., Fernandez, J M and Gaub, H E (1997). "Reversible Unfolding of Individual Titin Immunoglobulin Domains by AFM". *Science*. **276** (5315): 1109–1112. doi:10.1126/science.276.5315.1109.
59. Rafiee, R. and Moghadam, R. M. (2014) On the modelling of carbon nanotubes: A critical review. *Composites Part B: Engineering,* **56,** 435-449.
60. Mehdipour, I., Erfani-Moghadam, A. and Mehdipour, C. (2013) Application of an electrostatically actuated cantilevered carbon nanotube with an attached mass as a bio-mass sensor. *Current Applied Physics,* **13,** 1463-1469.

61. Mittala, M. and Kumara, A. (2014) Carbon nanotube (CNT) gas sensors for emissions from fossil fuel burning. *Sensors and Actuators B: Chemical,* **203,** 349–362.
62. Gohardani, O., Elola, M.C. and Elizetxea, C. (2014) Potential and prospective implementation of carbon nanotubes on next generation aircraft and space vehicles: A review of current and expected applications in aerospace sciences. *Progress in Aerospace Sciences,* **70,** 42–68.
63. Iijima, S. (1991) Helical microtubules of graphitic carbon. *Nature* **354**, 56–58 https://doi.org/10.1038/354056a0.
64. Balachandran, B. and Magrab, B. E. (2009) *Magrab_Vibrations,* Toronto, Cengage Learning.
65. Magrab, B. E. 2012. *Magrab_Vibrations of Elastic Systems: With Applications to MEMS and NEMS,* New York, Springer.
66. Eltaher, M.A., Khater, M.E. and Emam, S.A (2016) A review on nonlocal elastic models for bending, buckling, vibrations and wave propagation of nanoscale beams. *Applied Mathematical Modelling* **40** 4109-4128.
67. Reddy, J. N., and Pang, S. N. (2008) Nonlocal continuum theories of beams for the analysis of carbon nanotubes. *J. App. Phys.* **103**: 023511.
68. Peddieson, J, Buchanan, G.R. and McNitt, R.P. (2003) Application of nonlocal continuum models to nanotechnology. *International Journal of Engineering Science,* **41,** 305-312.
69. Hossein, N.P., Bahram, A. and Farid, T (2016) Continuum models calibrated with atomistic simulations for the transverse vibrations of silicon nanowires. *International Journal of Engineering Science*, Volume **100**, Pages 8-24, ISSN 0020-7225, https://doi.org/10.1016/.
70. Bar On, B., Altus, E. and Tadmor, E. B. (2010). Surface effects in non-uniform nanobeams: Continuum vs atomistic modelling. *International Journal of Solids and Structures*, Volume **47**, Issue 9, Pages 1243-1252, ISSN 0020-7683, https://doi.org/10.1016/j.ijsolstr.2010.01.010.
71. Norouzzadeh A. and Ansari, R (2017) Finite element analysis of nano-scale Timoshenko beams using the integral model of nonlocal elasticity. *Physica E: Low-dimensional Systems and Nanostructures*. Volume **88**, Pages 194-200, ISSN 1386-9477, https://doi.org/10.1016/j.physe.2017.01.006.
72. Dowell, E. H. (1978) On some general properties of combined dynamical systems. *American Society of Mechanical Engineers,* Vol. **46**, Pages 206-209, Winter Annual Meeting, San Francisco, Calif., Dec. 10-15.

73. Gürgöze, M. (1996) On the eigenfrequencies of a cantilever beam with attached tip mass and spring-mass system. Journal of Sound and Vibration. **190**(2): 149-162.
74. Azrar, A., Azrar, L. and Aljinaidi, A.A. (2011). Length scale effect analysis on vibration behavior of single walled Carbon NanoTubes with arbitrary boundary conditions. *Revue de Mécanique Appliquée et Théorique,* **2,** 475-485.
75. Wu, Der & Chien, Wen & Chen, Cheng & Chen, Hsin. (2006). Resonant frequency analysis of fixed-free single-walled carbon nanotube-based mass sensor. *Sensors and Actuators A: Physical*. **126**. 117-121. 10.1016/j.sna.2005.10.005.
76. Gibson, R.F., Ayorinde, E.O. and Wen, Y.F. (2007) Vibrations of carbon nanotubes and their composites: A review. *Composites Science and Technology,* **67,** 1-28.
77. Pin Lu, H., Lee, P. and Lu, C (2006) Dynamic properties of flexural beams using a nonlocal elasticity model. *Journal of Applied Physics* **99**, 073510; https://doi.org/10.1063/1.2189213.
78. Natsuki, T., Matsuyama, N., Jin-Xing, S. and Qing-Qing, N. (2014) Vibration analysis of nanomechanical mass sensor using carbon nanotubes under axial tensile loads. *Appl. Phys. A* **116**, 1001–1007. https://doi.org/10.1007/s00339-014-8289-3.
79. Maurizi, M. J., Rossi, R. E., and Reyes, J. A. (1976) Vibration frequencies for a uniform beam with one end spring hinged and subjected to a translational restraint at the other end. *J. Sound Vib*. **48**(4): 565-568.
80. Laura, P. A. A., Grossi, R. O., and Alvarez, S. (1982) Transverse vibrations of a beam elastically restrained at one end and with a mass and spring at the other subjected to an axial force. *Nuclear Eng. Design* **74**: 299-302.
81. Zhou, D. (1997) The vibrations of a cantilever beam carrying a heavy tip mass with elastic supports. *J. Sound Vib*. **206**: 275-279.
82. Gürgöze, M. (1996) On the eigenfrequencies of a cantilever beam with attached tip mass and spring-mass system. *J. Sound Vib*. **190**(2): 149-162.
83. Seyed Mojtaba Hozhabrossadati (2015) Exact solution for free vibration of elastically restrained cantilever non-uniform beams joined by a mass-spring system at the free end, *The IES Journal Part A: Civil & Structural Engineering*, **8**:4, 232-239, DOI: 10.1080/19373260.2015.1054957.
84. Ehteshami, H and Mohammad A. Hajabasi, M.A. (2011) Analytical approaches for vibration analysis of multi-walled carbon nanotubes modeled as multiple nonlocal Euler beams. *Physica E: Low-dimensional Systems and Nanostructures*. Volume **44**, Issue 1. Pages 270-285, ISSN 1386-9477, https://doi.org/10.1016/j.physe.2011.08.023.

85. Li, X.F., Tang, G.J., Shen, Z.B. and Lee, K.Y. (2015) Resonance frequency and mass identification of zeptogram-scale nanosensor based on the nonlocal beam theory. *Ultrasonics*, **55**, 75-84.
86. Managheb, S.A.M., Ziaei-Rad, S. and Tikani, R (2018) Energy harvesting from vibration of Timoshenko nanobeam under base excitation considering flexoelectric and elastic strain gradient effects. *Journal of Sound and Vibration*. Volume **421**, Pages 166-189. ISSN 0022-460X. https://doi.org/10.1016/j.jsv.2018.01.059.
87. Bahrami, A., Zargaripoor, A., Shiri, H. and Khosravi, N. (2019). Size-dependent free vibration of axially functionally graded tapered nanorods having non-linear spring constraint with a tip nanoparticle. *Journal of Vibration and Control*. **25**. 10.1177/1077546319870921.
88. Maenaka, K., Ioku, S., Sawai, N., Fujita, T. and Takayama, Y. (2005) Design,fabrication and operation of MEMS gimbal gyroscope. *Sensors and Actuators A: Physical*. Vol.**121**, No.1, pp.6-15.
89. Barretta, R., Feo, L., Luciano, R., Marotti de Sciarra, F. and Penna, R. (2017), Nano-beams under torsion: a stress-driven nonlocal approach. *PSU Research Review*. Vol. **1** No. 2, pp. 164-169. https://doi.org/10.1108/PRR-05-2017-0030.
90. Mahmoudpour, E., Hosseini-Hashemi, S.H., Faghidian, S.A. (2018) Nonlinear vibration analysis of FG nano-beams resting on elastic foundation in thermal environment using stress-driven nonlocal integral model. *Applied Mathematical Modelling*. Volume **57**, p. 302-315. ISSN 0307-904X. https://doi.org/10.1016/j.apm.2018.01.021.
91. Arda, M. and Aydogdu, M. (2019). Torsional dynamics of coaxial nanotubes with different lengths in viscoelastic medium. *Microsystem Technologies*. **25,** 3943–3957. 10.1007/s00542-019-04446-8.
92. Yayli, Mustafa. (2016). An efficient solution method for the longitudinal vibration of nanorods with arbitrary boundary conditions via a hardening nonlocal approach. *Journal of Vibration and Control*. **24**. 10.1177/1077546316684042.
93. Bahrami, Arian & Teimourian, Amir. (2015). Nonlocal scale effects on buckling, vibration and wave reflection in nanobeams via wave propagation approach. *Composite Structures.* **134**. 1061–1075. 10.1016/j.compstruct.2015.09.007.
94. Bedroud, M. and Kamali, K. (2018). An analytical study on the size dependent longitudinal vibration analysis of thick nanorods. *Materials Research Express*. **5**. 075016. 10.1088/2053-1591/aacf6e.

95. Numanoğlu, H., Akgöz, B. and Civalek, Ö. (2018). On dynamic analysis of nanorods. *International Journal of Engineering Science*. **130**. pg. 33-50.
96. Barretta, R., Faghidian, S., Marotti de Sciarra, F. and Vaccaro, M. (2019). Nonlocal strain gradient torsion of elastic beams: variational formulation and constitutive boundary conditions. *Archive of Applied Mechanics*. **90**. 10.1007/s00419-019-01634-w.
97. Sneha Rupa, N., Ray, M.C. (2017) Analysis of flexoelectric response in nanobeams using nonlocal theory of elasticity. *Int J Mech Mater Des* **13**, 453–467. https://doi.org/10.1007/s10999-016-9347-0.
98. Xiao-Jian, X., Xuan-Cang, W., Mu-Lian, Z and Zheng, M. (2017) Bending and buckling of nonlocal strain gradient elastic beams. *Composite Structures*. Volume **160**. pg. 366-377. ISSN 0263-8223. https://doi.org/10.1016/j.compstruct.2016.10.038.
99. Gheshlaghi, B. and Mirzaei, Y. (2012) Flexural sensitivity and resonance of cantilever micro-sensors based on nonlocal elasticity theory. *Optics Communications*. Vol **285**. (12), Pages 2798-2801. ISSN 0030-4018. https://doi.org/10.1016/j.optcom.2012.01.050.
100. Ryoji Okamoto and Naruo Sasaki (2019) Effect of size and shape of graphene sheets on nanoscale peeling process by atomic force microscopy. *The Japan Society of Applied Physics: Japanese Journal of Applied Physics*. Volume **58**, Number 11.
101. Wang, C., Zhang, H., Challamel, N. and Duan, W. (2017). Eringen's small length scale coefficient for vibration of axially loaded nonlocal Euler beams with elastic end restraints. *Journal of Modeling in Mechanics and Materials*. 10.1515/jmmm-2016-0158.
102. Challamel, N., Zhang, Z., Wang, C.M. Reddy, J. N. and Michelitsch, T. (2014) On nonconservativeness of Eringen's nonlocal elasticity in beam mechanics: correction from a discrete-based approach. *Arch Appl Mech* **84,** 1275–1292 (2014). https://doi.org/10.1007/s00419-014-0862-x.

Chapter 2 – Governing equations for a vibrating nanobeam

2.1 Derivation of the governing equations for the nanobeam.

2.1.1 Moment-curvature relation for beam.

In Fig. 2.1, a uniform beam is vibrating freely under constant axial load $N(x,t)$. The left-end of the beam is mechanically constrained by use of an elastic support i.e. torsional spring, while the right-hand side has mechanical elements i.e. a tip mass and elastic supports arranged in a desired configuration. There are moments $M(x,t)$ and shear forces $Q(x,t)$ along the beam and the mechanical elements contribute moments, $M(0,t)$ and $M(L,t)$ and shear forces, $Q(0,t)$ and $Q(L,t)$ at the boundaries as indicated in the diagram [1, 2]. Let $w(x,t)$ be the transverse displacement of the beam anywhere along the *x-dir*. at any time (*t*). The Euler-Bernoulli theory can be applied to the deformation of the beam, where the fiber along the neutral axis of the beam experiences zero strain. The fibers above the neutral axis experience a contraction, whilst the fibers at the bottom of the neutral axis experience an extension.

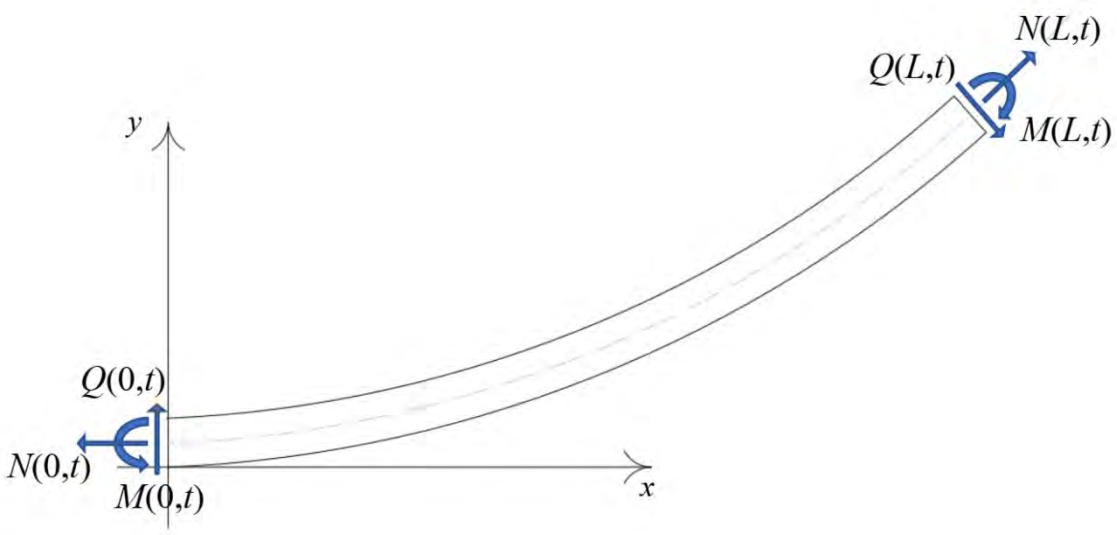

According to Euler-Bernoulli theory, when a slender beam experience's bending:

i. The neutral axis remains undeformed,
ii. Plane sections normal to the neutral axis remain normal before and after bending,
iii. The transverse normals experience zero strain along the normal direction.
iv. The material obeys Hooke's law.

A single fiber undergoing deflection can be isolated to form a basis for the discussion as shown in the Fig. (2.2),

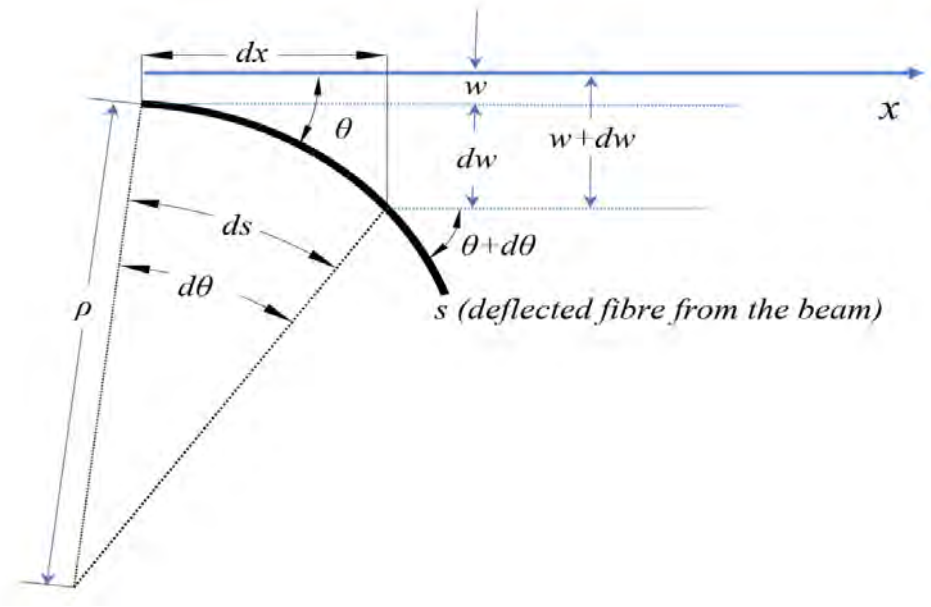

For small deflection ($d\theta$) the fibers along the thickness of the beam create concentric arches and the fiber length (s) is extended by a small length (ds) as shown above. The relation between the deflection, the arc-length and radius of curvature (ρ) can be deduced from Fig. (2.2) and presented as follows,

$$\frac{d\theta}{ds} = \frac{1}{\rho} \quad \text{..... (2.1)}$$

and the strain relation is,

$$\varepsilon_x(y) = -y \cdot \frac{d\theta}{ds} = -(y/\rho) \quad \text{..... (2.2)}$$

and therefore, the stress-strain relation can be expressed as,

$$\sigma_x(y) = E_c \cdot \varepsilon_x = -y \cdot (E_c/\rho) \quad \text{..... (2.3)}$$

The resultant bending moment of curvature[3] (M_c) due to σ_x must equal the integral of the bending moment across the cross-sectional area and thus,

$$M_c = -\int_A y \cdot [\sigma_x dA] \quad \text{(2.4a)}$$

and, after combining Eqs. (2.3) and (2.4a),

$$M_c = -(E_c/\rho) \cdot \int_A y^2 dA \quad \text{(2.4b)}$$

also,

$$I_c = \int_A y^2 dA \quad \text{(2.4c)}$$

therefore,

$$M_c = -E_c I_c \cdot \frac{1}{\rho} \qquad \text{and} \qquad \frac{1}{\rho} = \frac{d\theta}{ds} \quad \text{(2.4d)}$$

It can be shown that the relation below holds for beam deflection,

[3] The subscript "c" denotes local or classic parameters e.g. moment, shear force and material constants

$$\frac{d\theta}{ds} = \frac{\frac{d^2w}{dx^2}}{\left[1+\left(\frac{dw}{dx}\right)^2\right]^{\frac{3}{2}}} \tag{2.5}$$

when $\left(\frac{dw}{dx}\right)^2 << 1$ the slope and the deflection are small it leads to the following moment curvature relation,

$$\frac{d^2w}{dx^2} = -\frac{M_c(x)}{E_c I_c} \text{ ……..……..…… (2.6)}$$

When the beam moves from its natural position; internal forces, shear forces and moments acting on each infinitesimal element of the beam are induced, as shown in Fig. (2.3). The element has a length dx along the beam in the x-direction.

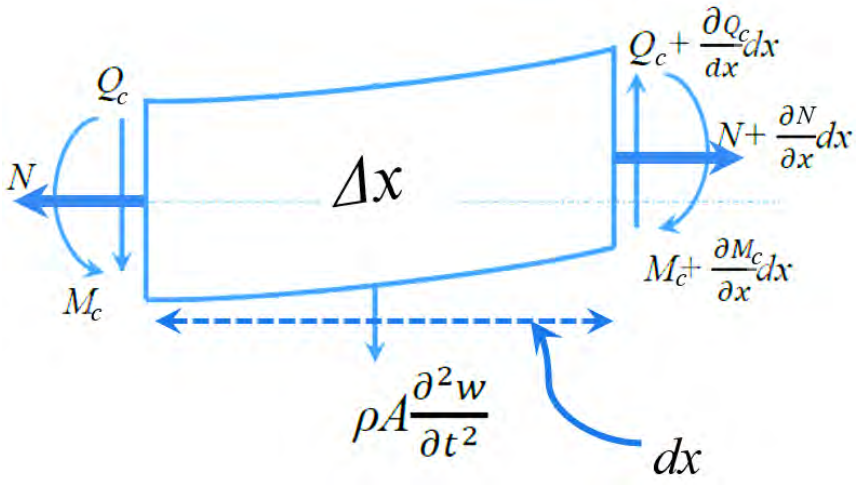

Taking the sum of the forces and moments in both co-ordinates (x and y) we derive the equilibrium conditions for the element in a form of these equations:

$$\frac{\partial Q_c(x,t)}{\partial x} - \rho A \frac{\partial^2 w(x,t)}{\partial t^2} = 0 \tag{2.7}$$

$$\frac{\partial M_c(x,t)}{\partial x} + N(x)\frac{\partial w(x,t)}{\partial x} - Q_c(x,t) = 0 \tag{2.8}$$

The local or classic moment and shear force are shown in Eqs. (2.9a) and (2.9b).

$$M_c = -E_c I_c \frac{\partial^2 w(x,t)}{\partial x^2} \tag{2.9a}$$

$$Q_c = E_c I_c \frac{\partial^3 w(x,t)}{\partial x^3} + N\frac{\partial^2 w(x,t)}{\partial x^2} \tag{2.9b}$$

After combining Eqs. (2.7) and (2.8) we can determine the local or classic differential equation of motion for the beam.

$$E_c I_c \frac{\partial^4 w(x,t)}{\partial x^4} - N\frac{\partial^2 w(x,t)}{\partial x^2} - \rho A \frac{\partial^2 w(x,t)}{\partial t^2} = F_0(x) \tag{2.10}$$

where E_c is the modulus of elasticity, I_c is the moment of inertia, ρ is the density, A is the cross-sectional area and $F_0(x)$ is the forcing function which is taken as $F_0(x) = 0$ for a free vibration of the beam.

2.1.2. Eringen's nonlocal stress gradient theory for small-scale effects.

The moment curvature relation derived for Euler-Bernoulli theory is valid for micro and macro scale beams but needs to be modified in order to be valid for nanoscale beams. The Euler-Bernoulli beam theory [1, 2] can be applied to the transverse vibrations of nanobeams by applying the Eringen's theory on nonlocal continuum [3], with consistent results. Eringen's nonlocal stress tensor σ at a point **x** is stated as,

$$\sigma = \int_V K(|\mathbf{x}' - \mathbf{x}|, \tau)\mathbf{t}(\mathbf{x}')dx' \tag{2.11}$$

The integral above represents the weighted average of the influence of the strain field of all the points in the bulk to the stress field at a point. The first term in the integral $K(|\mathbf{x}' - \mathbf{x}|, \tau)$ is the kernel function and denotes the nonlocal modulus with $|\mathbf{x}' - \mathbf{x}|$ being the distance. The second term $\mathbf{t}(\mathbf{x}')$ is the local or classic stress tensor at a point **x**, such that **x** is the reference point in a body in which the stress tensor is calculated at any other point $\mathbf{x}'$. The material constant (τ), depends on the internal and external characteristic lengths. The 4th order local or bulk stress tensor obeys Hookean Laws and is described as,

$$\mathbf{t}(\mathbf{x}) = \mathbf{C}_{ijkl}(\mathbf{x})\varepsilon_{kl}(\mathbf{x}) \tag{2.12}$$

The integral in Eq. (2.11) makes the linear elasticity problem challenging to resolve. The integral equivalent can be expressed in differential form by,

$$\mathbf{t}(\mathbf{x}) = \left(1 - \tau^2 l_e^2 \frac{\partial^2}{\partial x^2}\right)\sigma \quad \text{and} \quad \bar{\mu}, \tau = \frac{e_o l_i}{l_e} \tag{2.13a}$$

or,

$$\left(1 - \tau^2 l_e^2 \frac{\partial^2}{\partial x^2}\right) M^{nl} = EI \frac{\partial^2 w(x,t)}{\partial x^2} \tag{2.13b}$$

when written in terms of moments, where M^{nl} is the nonlocal (nl) moments, e_o is a material constant that can be accurately estimated using molecular dynamics, l_i and l_e are the internal and external characteristic length which depend on lattice spacing and wavelength [4]. Applying Eq. (2.13b) the nonlocal moment and shear force are,

$$M^{nl} = EI \frac{\partial^2 w(x,t)}{\partial x^2} + \bar{\mu}\left[N \frac{\partial^2 w(x,t)}{\partial x^2} - \rho A \frac{\partial^2 w(x,t)}{\partial t^2}\right] \tag{2.14a}$$

$$Q^{nl} = EI \frac{\partial^3 w(x,t)}{\partial x^3} + N \frac{\partial w(x,t)}{\partial x} - \bar{\mu}\left[N \frac{\partial^3 w(x,t)}{\partial x^3} - \rho A \frac{\partial^3 w(x,t)}{\partial x \partial t^2}\right] \tag{2.14b}$$

Using Eqs. (2.7), (2.8) and (2.13b) to incorporate the nonlocal effects, the equation of motion for a nonlocal nanobeam in transverse vibration is,

$$EI \frac{\partial^4 w(x,t)}{\partial x^4} + N \frac{\partial^2 w(x,t)}{\partial x^2} - \bar{\mu} N \frac{\partial^4 w(x,t)}{\partial x^4} + \bar{\mu}\rho A \frac{\partial^4 w(x,t)}{\partial x^2 \partial t^2} - \rho A \frac{\partial^2 w(x,t)}{\partial t^2} = F_o(x,t) \tag{2.15}$$

2.1.3 Surface energies consideration for nano and sub-nano beams.

Scientists and engineers studying nano mechanical structures are now venturing into much smaller structures in the picometer(pm) or atomic range. At this miniscule size, the beams under consideration could be composed of a minimum of three or four atomic layers as show in the Fig. (2.4) below.

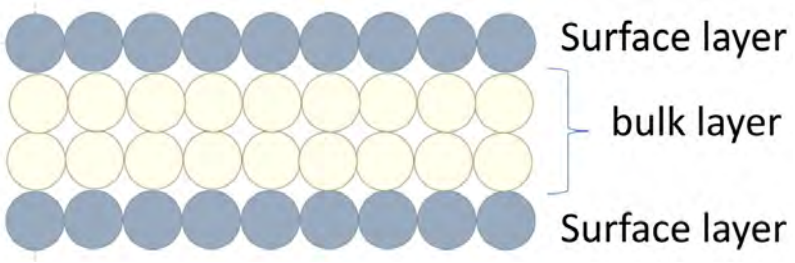

Figure 2-4: Beam composed of four layers of atoms, two bulk layers and top and bottom surface layers.

From the diagram it is noted that the bulk to surface volume are comparable and therefore the energies in the atoms at the surface will be comparable to the energies in the bulk. In this case, the surface layers will have an influence on the natural frequencies of the beam. The influence is bourne out the fact that the different atoms experience a different environment i.e. the surface is in contact with air and an atom on the other side, whereas the bulk material is surrounded by atoms. This leads to contact tractions in Eq. (2.16), at the interface between bulk and the surface layer.

T_z – Normal Contact Traction
T_x – Tangential Contact Traction

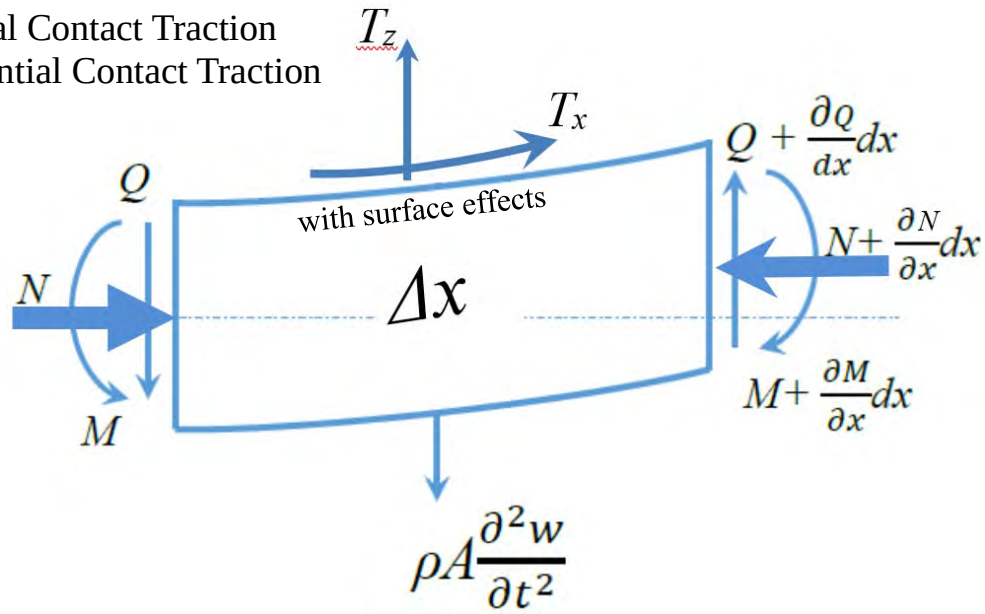

Figure 2-5: Internal shear forces, moments and external forces on the beam with traction forces at the surface.

A section of the beam (dx) including the moments (M^s), shear forces (Q^s), axial load(N), and the contact tractions (T_x and T_z), which are integrated over the surface, is shown in Fig. (2.5). The sum of the forces and bending moments[4] are,

$$\frac{\partial M^s}{\partial x} = Q^s + \oiint T_x z ds + \left(N \frac{\partial w}{\partial x}\right) \tag{2.17}$$

$$\frac{\partial Q^s}{\partial x} = -\oiint T_z ds + \rho A \frac{\partial^2 w}{\partial t^2} \tag{2.18}$$

In order to capture more complex material behaviour, the Gurtin and Murdoch surface layer equilibrium equations [5] are introduced, Eqs. (2.19) and (2.20). When the surface tractions are considered, a second-order tensor characterizing the surface stress is introduced [5,6]. The surface stress tensor is associated with the bulk stress tensor and the external loads by means of a force equilibrium equation created at the solid surface [5,6].

$$\frac{\partial \tau_{xx}}{\partial x} - T_x = \rho_0 \frac{\partial^2 u}{\partial t^2} \tag{2.19}$$

$$\frac{\partial \tau_{zx}}{\partial x} - T_z = \rho_0 \frac{\partial^2 w}{\partial t^2} \tag{2.20}$$

were the first terms in Eqs. (2.19) and (2.20) contain the derivative of the in-plane components of the surface stress tensor, τ_{xx} and τ_{zx}.

$$\tau_{xx} = \tau_o + (2\mu_o + \lambda_o) \frac{\partial u_x}{\partial x} \tag{2.21a}$$

$$u_x = -z \frac{\partial w(x)}{\partial x} \tag{2.21b}$$

$$\tau_{zx} = \tau_o \frac{\partial u_z}{\partial x} \tag{2.21c}$$

$$u_z = w(x) \tag{2.21d}$$

The mechanical properties of the surface are contained in the constants μ_o and λ_o, which are the Lamé's constants that arise in strain-stress relationships and can be determined using molecular dynamics (MD), τ_o is the residual surface stress and ρ_0 is the surface density. The constitutive equation for stress-strain can be written as,

$$\sigma_{xx} = E\varepsilon_{xx} + \nu\sigma_{zz} \tag{2.22}$$

where ν is the Poisson's ratio and σ_{zz} is the stress in the normal direction to σ_{xx}. The strain is expressed as,

$$\varepsilon_{xx} = \frac{\partial u_x}{\partial x} \tag{2.23}$$

and the normal stress,

$$\sigma_{zz} = \frac{2z}{h}\left[\tau_o \frac{\partial^2 w}{\partial x^2} - \rho_o \frac{\partial^2 w}{\partial t^2}\right] \tag{2.24}$$

[4] The bending moments and shear forces due to surface effects are denoted by "s"

Solving for T_x and T_z in Eqs. (2.19) and (2.20) and solving the moment equation in Eq. (2.25) below, the results can be substituted into Eqs. (2.17) and (2.18).

$$M = -\int_A \sigma_{xx} dA \tag{2.25}$$

This results in the moment and shear force equation for a nanobeam with axial load, small-scale and surface effects are conveyed in Eqs. (2.26a) and (2.26b) which are comparable to the equations developed by Juntarasaid *et. al.* [7].

$$M^s = E^e I^e \frac{\partial^2 w(x,t)}{\partial x^2} + \frac{2\nu I \rho_o}{H} \frac{\partial^2 w(x,t)}{\partial t^2} - \bar{\mu}\left[N \frac{\partial^2 w(x,t)}{\partial x^2} - (\rho A + \rho_o s^*) \frac{\partial^2 w(x,t)}{\partial t^2} - \tau_o s^* \frac{\partial^2 w(x,t)}{\partial x^2}\right] \tag{2.26a}$$

$$Q^s = E^e I^e \frac{\partial^3 w(x,t)}{\partial x^3} + \frac{2\nu I \rho_o}{H} \frac{\partial^3 w(x,t)}{\partial x \partial t^2} - \tau_o s^* \frac{\partial w(x,t)}{\partial x} - N \frac{\partial w(x,t)}{\partial \mathrm{x}} + \bar{\mu}\left[N \frac{\partial^3 w(x,t)}{\partial x^3} - (\rho A + \rho_o s^*) \frac{\partial^3 w(x,t)+}{\partial x \partial t^2}\right] \tag{2.26b}$$

where,

$$E^e I^e = EI + (2\mu_o + \lambda_o) I^* - \frac{2\nu I \tau_o}{H}$$

After solving for Q^sin Eq. (2.17), differentiate Q^s with respect to *x* and substitute into Eq. (2.18) to derive the equation of motion for a nanobeam with , small-scale and surface effects.

$$E^e I^e \frac{\partial^4 w(x,t)}{\partial x^4} - \tau_o s^* \frac{\partial^2 w(x,t)}{\partial x^2} + \bar{\mu} \tau_o s^* \frac{\partial^4 w(x,t)}{\partial x^4} (\rho A + \rho_o s^*) \frac{\partial^2 w(x,t)}{\partial t^2} + \frac{2\nu I \rho_o}{H} \frac{\partial^4 w(x,t)}{\partial x^2 \partial t^2} + N \frac{\partial^2 w(x,t)}{\partial x^2} - \bar{\mu} N \frac{\partial^4 w(x,t)}{\partial x^4} + (\bar{\mu} \rho A + \bar{\mu} \rho_o s^*) \frac{\partial^4 w(x,t)}{\partial x^2 \partial t^2} = F_o(x,t) \tag{2.27}$$

The Young's modulus of the bulk is E, I is the moment of inertia of the bulk and I^* is the perimeter moment of inertia of the surface. The density of the bulk is ρ, ρ_o is the surface density, A is the cross-sectional area, H is the height of the beam and $s^* = \oint n_z^2 ds$ is the cross-sectional area/perimeter of the surface layer. $F_o(x,t)$ is the forcing function which is taken as $F_o(x,t) = 0$ for a nanobeam under free vibration.

Case 1: Topological scanning tool model.

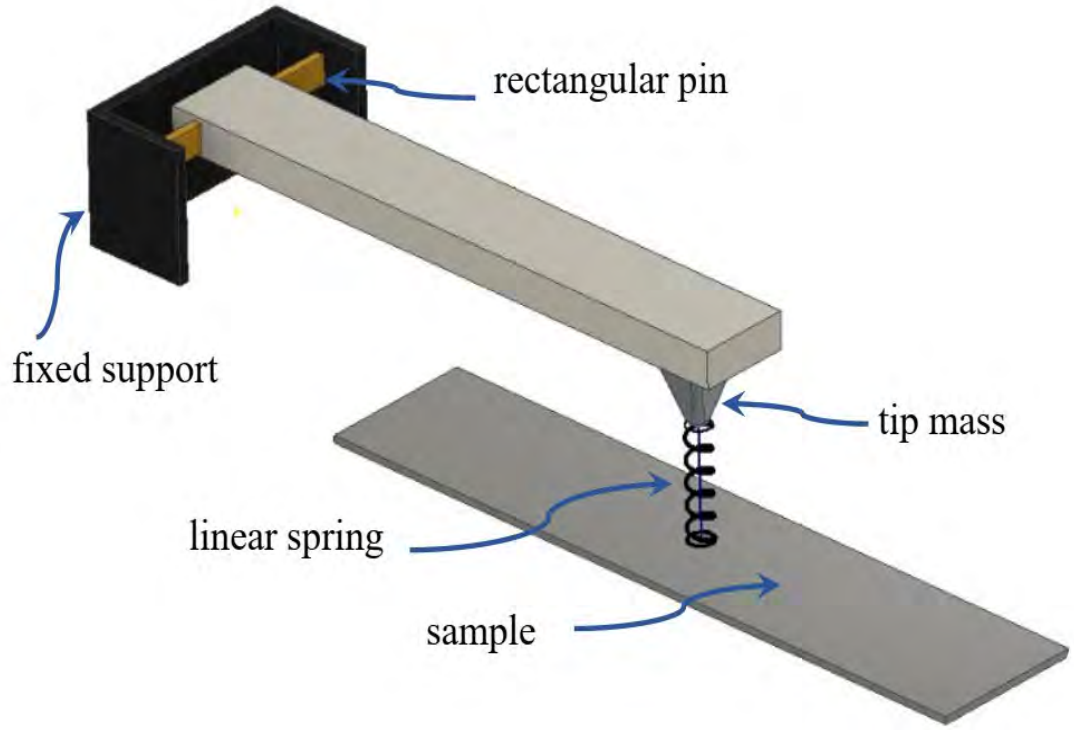

Figure 2-6: Nanobeam with tip-mass and lateral linear spring.

In bending and vibration, the nanobeam experiences displacements, velocity and acceleration which lead to forces and moments for every infinitesimal cross-section. Eqs. (2.26a), (2.26b) and (2.27) account for intermediate motion of the nanobeam for $0 < x < L$. Different mechanical elements can be added to model actual applications. In Fig. (2.6), a rectangular cross-section pin is included and acts as a torsional spring (k_1) at $x = 0$. The boundary conditions *without surface effects* are the following,

$$w(0,t) = 0 \tag{2.28a}$$

$$EI\frac{d^2w(0,t)}{dx^2} - \bar{\mu}^2\rho A\frac{\partial^2 w(0,t)}{\partial t^2} - k_1\frac{dw(0,t)}{dx} = 0 \tag{2.28b}$$

$x = L$), taking into account the small-scale effects, the tip mass and the linear spring, the moment and shear boundary conditions can be expressed as,

$$EI\frac{d^2w(L,t)}{dx^2} + \bar{\mu}^2\rho A\frac{\partial^2 w(L,t)}{\partial t^2} = 0 \tag{2.29a}$$

$$EI\frac{d^3w(L,t)}{dx^3} - \bar{\mu}^2\rho A\frac{\partial^3 w(x,t)}{\partial x\partial t^2} - M_T w(L) + k_2 w(L) = 0 \tag{2.29b}$$

where M_T is the tip mass, k_1 and k_2 are the torsional and linear spring constants, respectively.

Case 2: Sculpting and removal tool model.

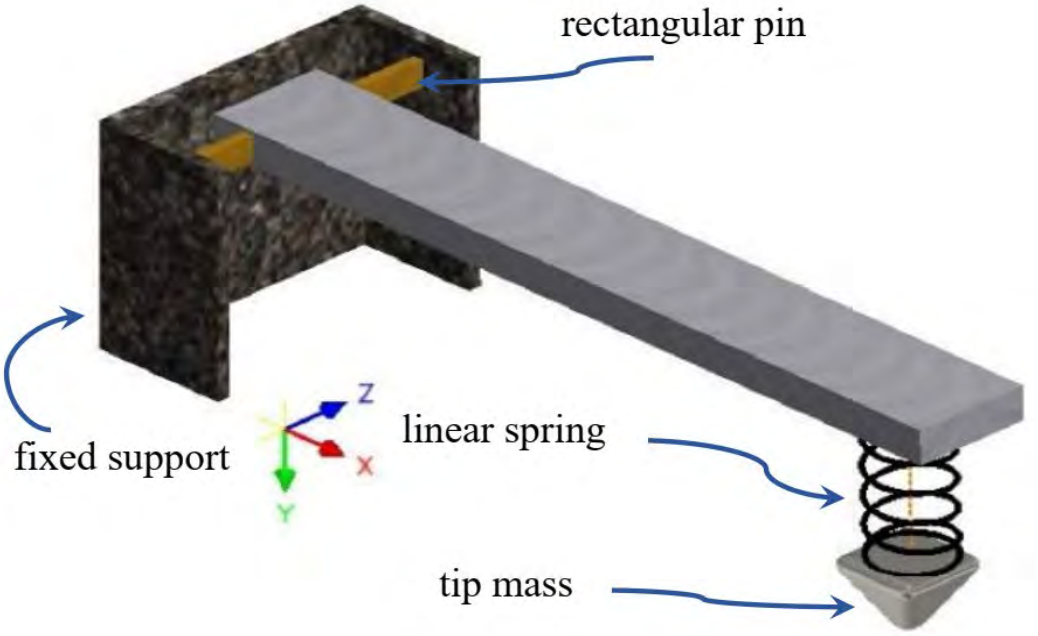

Figure 2-7: Nanobeam with single degree spring-mass system.

In this configuration the nanobeam has a linear spring attached to the tip and a mass attached to other end of the spring. Once more, Eqs. (2.26a), (2.26b) and (2.27) are employed to derive the moment and shear boundary condition at $x = 0$ and $x = L$. The boundary conditions *with surface effects* are,

$$w(0) = 0 \tag{2.30a}$$

$$E^e I^e \frac{\partial^2 w(x,t)}{\partial x^2} + \frac{2\nu I \rho_o}{H} \frac{\partial^2 w(x,t)}{\partial t^2} - \bar{\mu}\left[N \frac{\partial^2 w(x,t)}{\partial x^2} - (\rho A + \rho_o s^*) \frac{\partial^2 w(x,t)}{\partial t^2} - \tau_o s^* \frac{\partial^2 w(x,t)}{\partial x^2}\right] - k_1 \frac{\partial w(x,t)}{\partial x} = 0 \tag{2.30b}$$

At the free end ($x = L$), taking into account the small-scale effects, surface effects and the single degree of freedom spring-mass system, the moment and shear boundary conditions can be expressed as,

$$E^e I^e \frac{\partial^3 w(x,t)}{\partial x^3} + \frac{2\nu I \rho_o}{H} \frac{\partial^3 w(x,t)}{\partial x \partial t^2} - \tau_o s^* \frac{\partial w(x,t)}{\partial x} - N \frac{\partial w(x,t)}{\partial x} + \bar{\mu}\left[N \frac{\partial^3 w(x,t)}{\partial x^3} - \tau_o s^* \frac{\partial^3 w(x,t)}{\partial x^3} - (\rho A + \rho_o s^*) \frac{\partial^3 w(x,t)+}{\partial x \partial t^2}\right] = F_L(x,t) \tag{2.31b}$$

In the system depicted in Fig. (2.7), $F_L(x,t)$ in the shear boundary condition of Eq. (2.31b) is the force due to the compression or extension of the spring. The linear spring force has the form of a spring constant times a displacement , $F_L(x,t) = k_2 * \gamma(L,t)$, where $\gamma(L,t)$ is the displacement calculated from solving a 2nd order differential equation of motion in Section 2.2.2 below.

2.1.4 Critical buckling load for nanobeams under axial load.

The axial load is applied in both compression and tension and therefore we need to consider the magnitude of the force in order prevent failure. The choice of axial load is made by referencing the applied load (N) to the critical buckling load (N_{cr}) of the beam.

$$N = k \cdot N_{cr} \tag{2.32}$$

where k is the axial load fraction and allows the for the axial load to be selected in an acceptable range, k = -0.8, -0.4, 0, +0.4, +0.8. To determine the critical buckling load of the system, the equation of motion Eq. (2.15) is written below with the terms involving time or derivative with respect to time set to zero.

$$EI\frac{\partial^4 w(x)}{\partial x^4} + N\frac{\partial^2 w(x)}{\partial x^2} - \bar{\mu}N\frac{\partial^4 w(x)}{\partial x^4} = 0 \tag{2.33}$$

The 4th order differential equation of motion can be reduced to a 2nd order differential equation by integrating twice with respect to x, and after integration twice we derive an equation with two integration constants, E and F.

$$(EI - \bar{\mu}N)\frac{\partial^2 w(x)}{\partial x^2} + Nw(x) = Ex + F \tag{2.34}$$

The LHS side of Eq. (2.34) has a homogeneous solution of the form,

$$\frac{\partial^2 w(x)}{\partial x^2} + \lambda^2 w(x) = 0 \tag{2.35a}$$

Let, $$\lambda^2 = \frac{N}{(EI - \bar{\mu}N)} \quad \text{or} \quad N = \frac{\lambda^2}{(1+\bar{\mu}\lambda^2)}EI \tag{2.35b}$$

The solution for this second order differential equation of motion Eq. (2.34) has two solutions: 1) a homogenous solution and 2) a particular solution which is derived from the boundary conditions. The total solution is a sum of the homogenous and particular solution and can be expressed as,

$$w(x) = Asin(\lambda x) + Bcos(\lambda x) + \frac{1}{\lambda^2}(Ex + F) \tag{2.36}$$

The constants can be determined to satisfy the displacement and moment boundary conditions.

Displacement at $x = 0$:

$$w(0) = 0 \tag{2.37}$$

$$Asin(0) + Bcos(0) + \frac{1}{\lambda^2}(0 + F) = 0$$

$$F = -\lambda^2 B$$

$$w(x) = Asin(\lambda x) - Bcos(\lambda x) + \frac{1}{\lambda^2}(Ex - \lambda^2 B) \tag{2.38}$$

Moment at $x = 0$:

$$EI\frac{\partial^2 w(0)}{\partial x^2} - \bar{\mu}N\frac{\partial^2 w(0)}{\partial x^2} - k_1\frac{\partial w(0)}{\partial x} = 0 \tag{2.39}$$

$$\frac{(EI-\bar{\mu}N)}{k_1}\frac{\partial^2 w(0)}{\partial x^2}-\frac{\partial w(0)}{\partial x}=0$$

$$\frac{\left(-A\lambda^2\sin(x\lambda)-B\lambda^2\cos(x\lambda)\right)\left(1-\beta^2\mu\right)}{k_1}+B\lambda=0$$

$$A=\frac{B\lambda^4\left(\beta^2\mu-B\right)-k_1E}{k_1\lambda^3}$$

$$X(x)=\frac{B\beta^2\lambda^4\,sin(x\lambda)\mu+\left(-B\lambda^4-k_1E\right)sin(x\lambda)+k_1B\lambda^3\,cos(x\lambda)-k_1B\lambda^3+k_1Ex\lambda}{k_1\lambda^3} \tag{2.40}$$

The general solution Eq. (2.40) is in terms of B and E alone. This can then be inserted into the two boundary conditions for the moment and shear forces at $x=L$. There after the two equations Eqs. (2.42) and (2.44) can be solved for E. The E derived from the moment boundary condition can be equated to the E derived from the shear boundary condition which leads to the characteristic equation for buckling of the system.

Moment at $x=L$:

$$EI\frac{\partial^2 w(L)}{\partial x^2}-\bar{\mu}N\frac{\partial^2 w(L)}{\partial x^2}=0 \tag{2.41}$$

$$(EI-\bar{\mu}N)\frac{\partial^2 w(L)}{\partial x^2}=0$$

Then,
$$-\frac{-B\beta^2\lambda^6\sin(x\lambda)\mu-\lambda^2\left(-B\lambda^4-k_1E\right)\sin(x\lambda)-k_1B\lambda^5\cos(x\lambda)}{k_1\lambda^3}=0$$

$$E=\frac{B\beta^2\lambda^4\sin(L\lambda)\mu-B\lambda^4\sin(L\lambda)+k_1B\lambda^3\cos(L\lambda)}{k_1\sin(L\lambda)} \tag{2.42}$$

Shear at $x=L$:

$$EI\frac{\partial^3 w(L)}{\partial x^3}-\bar{\mu}N\frac{\partial^3 w(L)}{\partial x^3}-N\frac{\partial w(L)}{\partial \mathrm{x}}=0 \tag{2.43}$$

$$\frac{\partial^3 w(L)}{\partial x^3}-\frac{N}{(EI-\bar{\mu}N)}\frac{\partial w(L)}{\partial \mathrm{x}}=0$$

$$\frac{\partial^3 w(L)}{\partial x^3}-\lambda^2\frac{\partial w(L)}{\partial \mathrm{x}}=0$$

then,
$$-\frac{\beta^2\left(\frac{B\beta^2\lambda^2\cos(x\lambda)\mu}{k_1}-B\lambda\sin(x\lambda)-\frac{B\lambda^2\cos(x\lambda)}{k_1}-\frac{E\cos(x\lambda)}{\lambda^2}+\frac{E}{\lambda^2}\right)}{1-\mu\beta^2}+\frac{B\beta^2\lambda^4\cos(x\lambda)\mu}{k_1}-$$
$$B\lambda^3\sin(x\lambda)-\frac{B\lambda^4\cos(x\lambda)}{k_1}-E\cos(x\lambda)=0$$

$$E=\frac{((B\mu\beta^4-B\beta^2)\lambda^6+B\beta^4\lambda^4)\cos(x\lambda)\mu+((k_1B-k_1B\mu\beta^2)\lambda^5}{\left((k_1\mu\beta^2-k_1)\lambda^2+k_1\beta^2\right)\cos(x\lambda)-k_1\beta^2}+$$
$$\frac{-k_1B\beta^2\lambda^3)\sin(x\lambda)+((B-B\mu\beta^2)\lambda^6-B\beta^2\lambda^4)\cos(x\lambda)}{\left((k_1\mu\beta^2-k_1)\lambda^2+k_1\beta^2\right)\cos(x\lambda)-k_1\beta^2} \tag{2.44}$$

After inserting the general solution into the boundary conditions, only three constants can be determined, and we therefore set $B=1$, and this results in a transcendental equation with roots corresponding to the various buckling modes. The lowest root of Eq. (2.45) corresponds to the critical buckling load and the transcendental equation is,

$$-\frac{\sin(\lambda L)}{k_1} + \lambda\cos(\lambda L) = 0 \tag{2.45}$$

The lowest buckling load, $\lambda = 0$ is a trivial solution and therefore the transcendental equation is solved numerically for the non-trivial solutions. When $\lambda \to 0$ the transcendental equation is that of a simply supported beam, $\sin(\lambda L) = 0$ and when $\lambda \to \infty$ the equation is that of a cantilever beam, $\lambda\cos(\lambda L) = 0$. The 1st root of the equation is substituted into Eq. (2.35b) to obtain the critical buckling load of the system (N_{cr}).

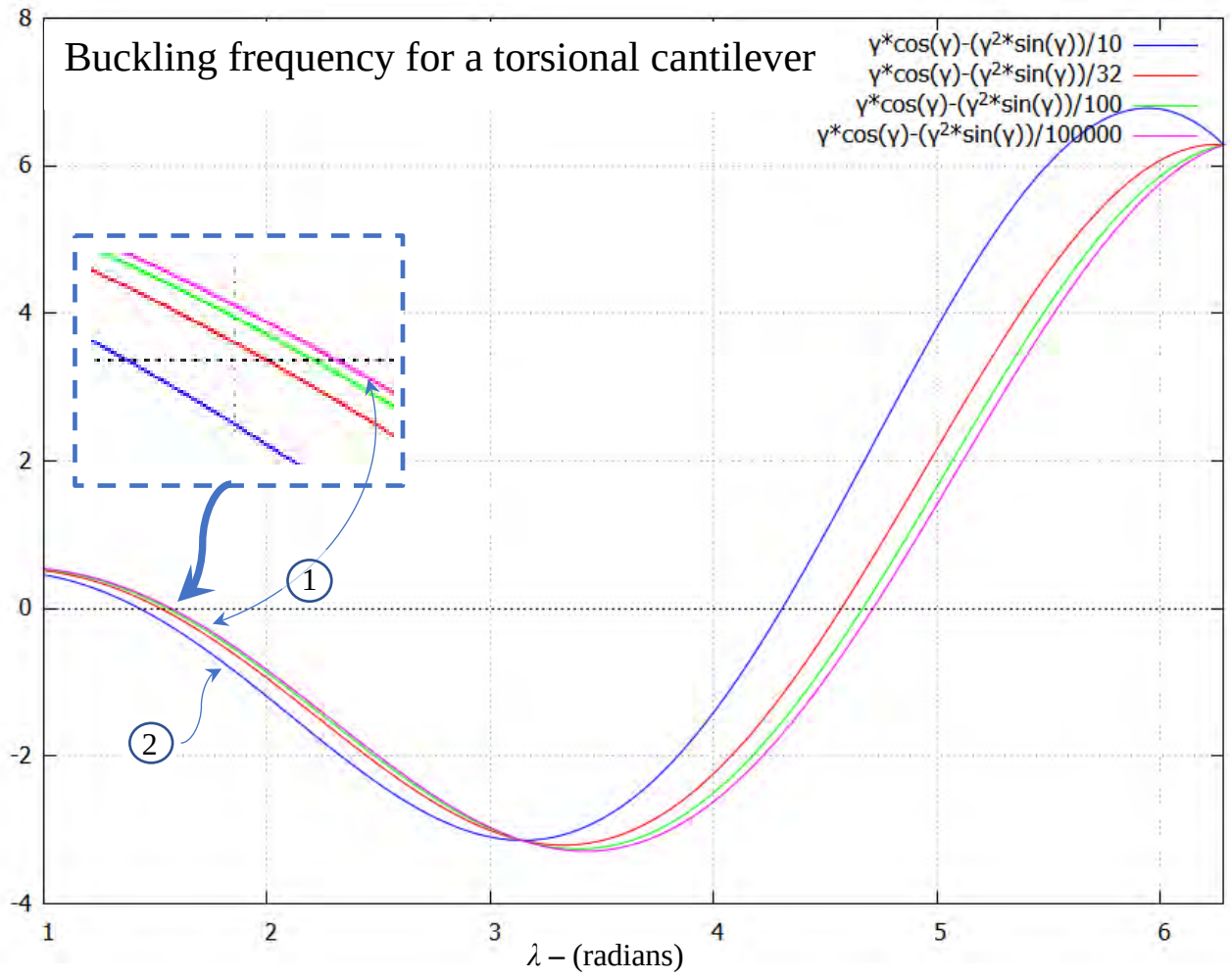

Figure 2-8: Transcendental equation for buckling of a single degree spring mass system.

Figure (2.8) shows the plots of the transcendental equations in buckling for varying torsional stiffness (k_1). The blue graph ② is for the lowest torsional spring ratio ($k_1 = 10$) and pink graph ① highest spring ratio ($k_1 = 10^6$), i.e. a cantilever nanobeam. The highest buckling load is associated with the pink graph, and this is the critical buckling load used in this investigation.

2.2 Solution of the governing equations of motion by separation of variables.

2.2.1 Solution of the governing equations for nanobeam.

In free vibration the external transverse load is set to zero, $F_o(x,t) = 0$, in Eq. (2.27) and the axial force $N(x,t)$, is kept the constant along the length of the beam. This problem can be solved by obtaining the eigenvalues and taking the sum of the eigenfunctions. The solution of the governing Eq. (2.27) is obtained by eigenfunction expansion of the displacement function using separation of variables. The displacement functions $w(x,t)$ and $\gamma(L,t)$ for the nanobeam and the tip-mass are dynamic and can be split into modal and temporal components.

$$w(x,t) = \sum_{n=1}^{\infty} X_n(x)T_n(t) \tag{2.46a}$$

$$\gamma(L,t) = \sum_{n=1}^{\infty} z_o T_n(t) \tag{2.46b}$$

$$\ddot{T}_n(t) + \omega_n^2 T_n(t) = 0 \tag{2.46c}$$

Inserting Eq. (2.46a) into Eq. (2.27) and using Eq. (2.46c), we obtain the differential equation of motion for the beam in the modal domain[5].

$$E^e I^e \frac{\partial^4 X_n(x)T_n(t)}{\partial x^4} - \bar{\mu} N \frac{\partial^4 X_n(x)T_n(t)}{\partial x^4} + N \frac{\partial^2 X_n(x)T_n(t)}{\partial x^2} - \tau_o s^* \frac{\partial^2 X_n(x)T_n(t)}{\partial x^2} + \bar{\mu}\tau_o s^* \frac{\partial^4 X_n(x)T_n(t)}{\partial x^4} (\rho A + \rho_o s^*) \frac{\partial^2 X_n(x)T_n(t)}{\partial t^2} + \frac{2\nu I \rho_o}{H} \frac{\partial^4 X_n(x)T_n(t)}{\partial x^2 \partial t^2} + (\bar{\mu}\rho A + \bar{\mu}\rho_o s^*) \frac{\partial^4 X_n(x)T_n(t)}{\partial x^2 \partial t^2} = 0 \tag{2.47a}$$

$$E^e I^e X'''' T - \bar{\mu} N X'''' T + \bar{\mu}\tau_o s^* X'''' T + N X'' T - \tau_o s^* X'' T + (\rho A + \rho_o s^*) X \ddot{T} + \frac{2\nu I \rho_o}{H} X'' \ddot{T} + (\bar{\mu}\rho A + \bar{\mu}\rho_o s^*) X'' \ddot{T} = 0 \tag{2.47b}$$

divide Eq. (2.47b) by T.

$$E^e I^e \frac{X''''T}{T} - \bar{\mu} N \frac{X''''T}{T} + N \frac{X''T}{T} + \bar{\mu}\tau_o s^* \frac{X''''T}{T} - \tau_o s^* \frac{X''T}{T} + (\rho A + \rho_o s^*) \frac{X\ddot{T}}{T} + \frac{2\nu I \rho_o}{H} \frac{X''\ddot{T}}{T} + (\bar{\mu}\rho A + \bar{\mu}\rho_o s^*) \frac{X''\ddot{T}}{T} = 0 \tag{2.47c}$$

$$E^e I^e X'''' - \bar{\mu} N X'''' + N X'' + \bar{\mu}\tau_o s^* X'''' - \tau_o s^* X'' + (\rho A + \rho_o s^*) X \frac{\ddot{T}}{T} + \frac{2\nu I \rho_o}{H} X'' \frac{\ddot{T}}{T} + (\bar{\mu}\rho A + \bar{\mu}\rho_o s^*) X'' \frac{\ddot{T}}{T} = 0 \tag{2.47d}$$

solving Eq. (2.46c) for the angular velocity ($\omega_n^2 = -\ddot{T}/T$) and substituting into Eq. (2.47d).

$$E^e I^e X'''' - \bar{\mu} N X'''' + N X'' + \bar{\mu}\tau_o s^* X'''' - \tau_o s^* X'' + (\rho A + \rho_o s^*)(-\omega_n^2) X + \frac{2\nu I \rho_o}{H} (-\omega_n^2) X'' + (\bar{\mu}\rho A + \bar{\mu}\rho_o s^*)(-\omega_n^2) X'' = 0 \tag{2.47e}$$

The natural frequency ω_n is the frequency of the n^{th} mode of vibration. The differential equation in the modal mode then becomes

$$P \cdot X'''' + \mathrm{Q} \cdot X'' - R \cdot X = 0 \tag{2.48}$$

[5] The subscript "*n*" and input variables (*x*,*t*) are dropped for clarity of presentation.

where,

$$P = 1 + \left[\frac{(2\mu_o+\lambda_o)}{E} - \frac{2\nu\tau_c}{\alpha}\right]\frac{\alpha}{H} - \mu\beta^2 + \bar{\mu}\tau_o s^*$$
$$Q = \frac{2\nu}{A}\frac{I^*}{\alpha}\rho_c a_n^4 + \mu\left(1 + \rho_c\frac{s^*}{A}\right)a_n^4 + \beta^2 - \tau_c\frac{s^*}{I}$$
$$R = \left(1 + \rho_c\frac{s^*}{A}\right)a_n^4$$

and,

$$\alpha = \frac{I^*}{I}H \quad , \quad \tau_c = \frac{\tau_0}{EL} \quad , \quad \mu = \left(\frac{\bar{\mu}}{l_i}\right)^2 L^2 \quad , \quad \rho_c = \frac{\rho_o}{\rho L}$$
$$N_{cr} = \frac{EI}{L^2}\left(\frac{\pi^2}{4+\mu\pi^2}\right) \quad , \quad N = k \cdot N_{cr} \quad , \quad \beta^2 = \frac{N}{EI}L^2 \quad \text{and} \quad a_n^4 = \frac{\rho A\omega^2}{EI}$$

The ratio alpha (α) that depends on the cross-sectional geometry [9, 10] is introduced to determine change of bending stiffness due to surface effects on the local or classic bending stiffness.

$$E^e I^e = EI + (2\mu_o + \lambda_o)I^* - \frac{2\nu I\tau_o}{H}$$

therefore,

$$\frac{E^e I^e - EI}{EI} = \frac{\left[(2\mu_o+\lambda_o) - \frac{2\nu I\tau_o}{\alpha}\right]}{E}\cdot\frac{\alpha}{H} = \alpha\frac{H_0}{H}$$
$$\frac{E^e I^e - EI}{EI} = \alpha\frac{E^s}{E}\frac{1}{H} = \alpha\frac{H_0}{H}$$

where α is a non-dimensional constant that is dependents on the structural geometry of the element, H is a height of the size of the structure. The parameter, $H_0 = E^s/E$ is a dimension at which the effect of the free surfaces become significant and for a square or circular cross-section, $\alpha = 8$. The quantity E^s is the elastic constant of the surface of the nanobeam and E is the corresponding elastic modulus of the bulk material. For $H >> H_0$, the bulk properties dominate, but as H, approaches H_0, the effect of the surface cannot be ignored and $H_0 = [(2\mu_o + \lambda_o) - 2\nu I\tau_o/\alpha]/E$ is referred to as the intrinsic length for bending [9, 10]. The ratio above shows that if $\alpha H_0 \cong H$ the surface effects need to be considered for improved model accuracy.

The frequency parameter a_n is associated with the natural frequency ω_n of vibration, α is a constant ratio that depends on the moment of inertia of the cross-section geometry of the bulk and surface, τ_c, μ , β^2, and ρ_c are the dimensionless constants corresponding to the residual stress, small-scale parameter, axial load and bulk to surface density ratio, respectively. The maximum axial load is taken to be 80% of the critical buckling load (N_{cr}) and therefore k = -0.8, -0.4, 0, +0.4, +0.8, with (-*ve*) being the tensile load and (+*ve*) compressive load. The general solutions of the differential equation Eq. (2.48) is given by,

$$X_n(x) = A_n\cos p_{2n} + B_n\sin p_{2n} + C_n\cosh p_{1n} + D_n\sinh p_{1n} \qquad (2.49)$$

and,

$$T_n(t) = E_n \sin\omega_n t + F_n \cos\omega_n t \qquad (2.50)$$

p_{1n} and p_{2n} are the roots of the 4th order differential equation or the wave numbers,

$$p_{1n} = \sqrt{\frac{Q+\sqrt{Q^2+4PR}}{2P}} \quad \text{and} \quad p_{2n} = \sqrt{\frac{Q-\sqrt{Q^2+4PR}}{2P}} \tag{2.51}$$

where A_n, B_n, C_n, and D_n, are constants to be determined from the boundary conditions; and E_n and F_n from the initial conditions. The characteristic equation can be used to determine the natural frequencies from the stipulated boundary conditions.

2.2.2 Governing equations for spring-mass system.

The spring mass system is a discreet system that is coupled to the tip of the nanobeam as indicated in Fig. (2.7). This system is governed by 2nd order differential equation of motion Eq. (2.52a),

$$M_T \frac{\partial^2 z(t)}{\partial t^2} + k_2 z(t) = k_2 w(L,t) \tag{2.52a}$$

$$M_T \frac{\partial^2 z(t)}{\partial t^2} = k_2\big(w(L,t) - z(t)\big)$$

let,

$$\gamma(L,t) = w(L,t) - z(t)$$

$$z(t) = w(L,t) - \gamma(L,t)$$

$$M_T \frac{\partial^2 \big(w(L,t) - \gamma(L,t)\big)}{\partial t^2} = k_2 \gamma(L,t)$$

$$M_T \frac{\partial^2 w(L,t)}{\partial t^2} = k_2 \gamma(L,t) + M_T \frac{\partial^2 \gamma(L,t)}{\partial t^2}$$

substitute Eqs. (2.46b) and (2.46c) dropping the subscript "*n*" and input variables (*x*,*t*) for clarity of presentation. Divide by M_T and then by T.

$$M_T \frac{\partial^2 (XT)}{\partial t^2} = k_2 z_o T + M_T \frac{\partial^2 (z_o T)}{\partial t^2}$$

$$\frac{M_T}{M_T} X \frac{\ddot{T}}{T} = \frac{k_2}{M_T} z_o \frac{T}{T} + \frac{M_T}{M_T} z_o \frac{\ddot{T}}{T}$$

$$X(-\omega_n^2) = \frac{k_2}{M_T} z_o + z_o(-\omega_n^2)$$

$$X(-\omega_n^2) = z_o\left(\frac{k_2}{M_T} - \omega_n^2\right)$$

$$z_o = \frac{X(-\omega_n^2)}{\left(\frac{k_2}{M_T} - \omega_n^2\right)} \tag{2.52b}$$

Let $\overline{m} = \rho A$ and multiply Eq. (2.52b) numerator and denominator by $\overline{m}/EI$

$$\frac{z_o}{X} = \frac{(-\omega_n^2)}{\left(\frac{k_2}{M_T} - \omega_n^2\right)} \frac{\overline{m}/_{EI}}{\overline{m}/_{EI}} \tag{2.52c}$$

$$\frac{z_o}{X} = -\frac{\left(\frac{\overline{m}\omega_n^2}{EI}\right)}{\left(\frac{\overline{m}}{M_T}\frac{k_2}{EI} - \frac{\overline{m}\omega_n^2}{EI}\right)}$$

$$\frac{z_o}{X} = -\frac{a_n^4}{(a_k^4 - a_n^4)} \tag{2.52d}$$

were the nondimensional parameters are: $\kappa_2 = \frac{k_2}{EI}$, $\eta = \frac{M_T}{\bar{m}L}$ and $a_k^4 = \frac{\kappa_2}{\eta}$. We obtain the equation of motion of the tip mass in the modal domain and time domain:

$$\gamma(L,t) = \frac{a_n^4 X(L)}{a_k^4\left(1 - \frac{a_n^4}{a_k^4}\right)} T_n(t) \tag{2.53}$$

where $a_k^4 = \kappa_2/\eta$ is frequency parameter for the spring-mass system; κ_2 and η represent the linear spring constant ratio and the tip-mass ratio, respectively.

2.3 References

1. Balachandran, B. and Magrab, B. E. (2009) Vibrations, Toronto, Cengage Learning.
2. Magrab, B. E. 2012. Magrab_Vibrations of Elastic Systems: With Applications to MEMS and NEMS, New York, Springer. Eringen, A. C., and Edelen, D. (1972) On nonlocal elasticity. *Int. J. Eng. Sci*. **10** (3): 233–248.
3. Eringen, A. C., (2002) Nonlocal Continuum Field Theories, Springer-Verlag, New York.
4. Reddy, J. N., and Pang, S. N. (2008) Nonlocal continuum theories of beams for the analysis of carbon nanotubes. *J. App. Phys*. **103**: 023511.
5. Gurtin, M.E. and Murdoch, A. (1975) A continuum theory of elastic material surfaces. *Archive for Rational Mechanics and Analysis* (**57**) 291-323.
6. Yichao Zhu, Yihai Wei, Xu Guo,(2017) Gurtin-Murdoch surface elasticity theory revisit: An orbital-free density functional theory perspective. *Journal of the Mechanics and Physics of Solids*. Volume **109**, Pages 178-197. ISSN 0022-5096. https://doi.org/10.1016/j.jmps.2017.08.009.
7. Juntarasaid, C., Pulngern, T. and Chucheepsakul, S. (2012) Bending and buckling of nanowires including the effects of surface stress and nonlocal elasticity. *Physica E*: *Low-dimensional Systems and Nanostructures*. Volume **46**. Pages 68-76. ISSN 1386-9477. https://doi.org/10.1016/j.physe.2012.08.005.
8. Ansari, R., Gholami, R. and Rouhi, H. (2012) Vibration analysis of single-walled carbon nanotubes using different gradient elasticity theories. Composites: Part B: **43**: 2985-2989.
9. Liu, C. and Rajapakse, N. (2010). Continuum Models Incorporating Surface Energy for Static and Dynamic Response of Nanoscale Beams. *Nanotechnology, IEEE Transactions* on. **9**. 422 - 431. 10.1109/TNANO.2009.2034142.

10. Miller, R.E. and Shenoy, V.B. (2000) Size-dependent elastic properties of nanosized structural elements. *Nanotechnology*, Volume **11**, Number 3. pages 139-147}, https://doi.org/10.1088/0957-4484/11/3/301
11. Soleimany, M.R., Jamal-Omidi, M., Nabavi, S.M. and Tavakolian, M (2021). Molecular dynamics predictions of thermo-mechanical properties of carbon nanotube/polymeric composites. *International Nano Leterst* **11,** 179–194. https://doi.org/10.1007/s40089-021-00329-x

Chapter 3 - Computation of the characteristic equation for the fundamental frequencies of the system

3.1 Natural frequencies for a torsional cantilever beam (without surface effects).

Discreet elements can be attached to the ends of the beam to influence the vibration profile of the beam. For one end of the beam, $x = 0$, a rectangular cross-section pin is used to keep the beam in a fixed position as indicated in Fig. (2.6). The pin prevents lateral motion and allows angular motion depending on the material's Hookean strength of the pin, resulting in a torsional spring (k_1) effect, see Fig. (3.1). On the other end of the beam, $x = L$, a tip mass is attached such that the centre of gravity of the mass coincides with the tip of the beam (rotary effects of the mass are neglected). A linear spring (k_2) is attached to the mass to simulate the contact force.

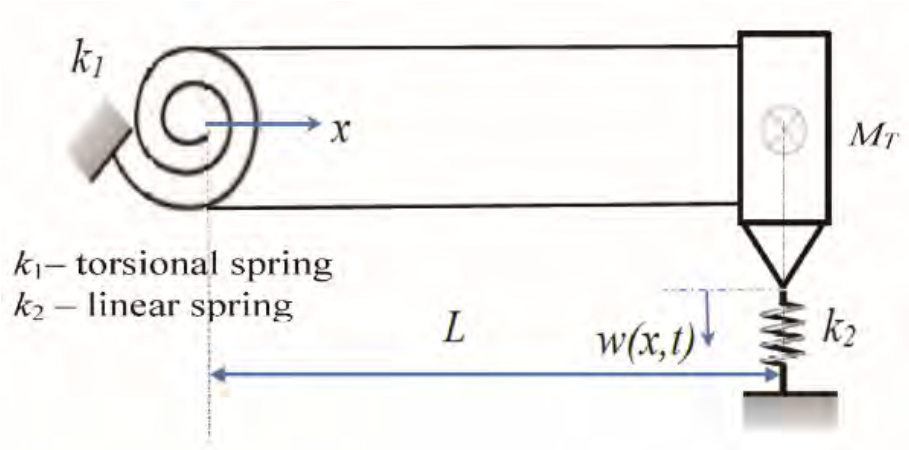

Figure 3-1: Geometry of the nano beam with concentrated mass and linear spring at free end.

Therefore, the boundary condition at $x = 0$ are zero lateral displacement in Eq. (3.1) and a state of equilibrium for the sum of moments in Eq. (3.2).

$$w(0) = 0 \tag{3.1}$$

$$EI\frac{d^2w(0)}{dx^2} - \bar{\mu}^2\rho A\frac{\partial^2 w(0,t)}{\partial t^2} - k_1\frac{dw(0)}{dx} = 0 \tag{3.2}$$

and at $x = L$, the moment and shear boundary conditions can be expressed as,

$$EI\frac{d^2w(L,t)}{dx^2} + \bar{\mu}^2\rho A\frac{\partial^2 w(L,t)}{\partial t^2} = 0 \tag{3.3}$$

$$EI\frac{d^3w(L,t)}{dx^3} - \bar{\mu}^2\rho A\frac{\partial^3 w(L,t)}{\partial x\partial t^2} - M_T\frac{\partial^3 w(L,t)}{\partial x\partial t^2} + k_2 w(L,t) = 0 \tag{3.4}$$

The above boundary conditions are 2nd and 3rd order differential equations which are decomposed into the modal and temporal domains by separation of variables using the displacement function, $w(x,t) = \sum_{n=1}^{\infty} X_n(x)T_n(t)$.

Displacement at $x = 0$:

$$w(0) = 0$$

$$X_n(0)T_n(t) = 0$$

divide by $T_n(t)$ and therefore in the modal domain,

$$X_n(0) = 0 \tag{3.5}$$

Moment at $x = 0$:

$$EI\frac{\partial^2 w(x,t)}{\partial x^2} - \bar{\mu}^2\rho A\frac{\partial^2 w(x,t)}{\partial t^2} - k_1\frac{\partial w(x,t)}{\partial x} = 0$$

$$EI\frac{\partial^2 X_n(x)T_n(t)}{\partial x^2} - \bar{\mu}^2\rho A\frac{\partial^2 X_n(x)T_n(t)}{\partial t^2} - k_1\frac{\partial X_n(x)T_n(t)}{\partial x} = 0$$

$$EI\frac{\partial^2 X_n(x)}{\partial x^2}T_n(t) - \bar{\mu}^2\rho AX_n(x)\frac{\partial^2 T_n(t)}{\partial t^2} - k_1\frac{\partial X_n(x)}{\partial x}T_n(t) = 0$$

$$EIX_n''(x)T_n(t) - \bar{\mu}^2\rho AX_n(x)\ddot{T}_n(t) - k_1X_n'(x)T_n(t) = 0$$

$$EIX_n''(x)T_n(t) - \bar{\mu}^2\rho AX_n(x)\ddot{T}_n(t) - k_1X_n'(x)T_n(t) = 0$$

Insert $\ddot{T}_n(t) = -\omega_n^2 T(t)$,

$$EIX_n''(x)T_n(t) - \bar{\mu}^2\rho AX_n(x)\left(-\omega_n^2 T(t)\right) - k_1X_n'(x)T_n(t) = 0$$

divide by $T_n(t)$ and reduce the equation to the modal domain,

$$EIX_n''(x) + \bar{\mu}^2\rho A\omega_n^2 X_n(x) - k_1X_n'(x) = 0$$

divide by EI and simplify to non-dimensional constants.

$$X_n''(x) + \bar{\mu}^2\frac{\rho A\omega_n^2}{EI}X_n(x) - \frac{k_1}{EI}X_n' = 0$$

$$X_n''(x) + \mu a_n^4 X_n(x) - \kappa_1 X_n' = 0 \tag{3.6}$$

Where a_n^4 , μ , and κ_1 are the dimensionless constant for the frequency parameter, the small-scale parameter and torsional spring ratio.

$$a_n^4 = \frac{\rho A\omega_n^2}{EI} \quad , \quad \mu = \left(\frac{\bar{\mu}}{l_i}\right)^2 L^2 \quad , \quad \kappa_1 = \frac{k_1 L}{EI} \qquad \text{(dimensionless constants)}$$

In a similar manner, the boundary conditions at $x = L$ can be reduced to the modal domain with dimensionless constants.[6]

Moment at $x = L$:

$$EI\frac{d^2 w(x,t)}{dx^2} - \bar{\mu}^2\rho A\frac{\partial^2 w(x,t)}{\partial t^2} = 0$$

$$EI\frac{d^2 XT}{dx^2} - \bar{\mu}^2\rho A\frac{\partial^2 XT}{\partial t^2} = 0$$

[6] The subscript "*n*" and input variables (*x*,*t*) are dropped for clarity of presentation.

$$EIX^{''}T - \bar{\mu}^2 \rho A X \ddot{T} = 0$$
$$EIX^{''}T - \bar{\mu}^2 \rho A X(-\omega_n^2 T) = 0$$
$$X^{''}T + \bar{\mu}^2 \frac{\rho A \omega_n^2}{EI} XT = 0$$
$$X^{''} + \mu a_n^4 X = 0 \tag{3.7}$$

Shear at $x = L$:

$$EI\frac{d^3 w(L,t)}{dx^3} - \bar{\mu}^2 \rho A \frac{\partial^3 w(L,t)}{\partial x \partial t^2} - M_T \frac{\partial^3 w(L,t)}{\partial x \partial t^2} + k_2 w(L) = 0$$
$$EI\frac{d^3 XT}{dx^3} - \bar{\mu}^2 \rho A \frac{\partial^3 XT}{\partial x \partial t^2} - M_T \frac{\partial^3 XT}{\partial x \partial t^2} + k_2 XT = 0$$
$$EIX^{'''}T - \bar{\mu}^2 \rho A X' \ddot{T} - M_T X' \ddot{T} + k_2 XT = 0$$
$$EIX^{'''}T - \bar{\mu}^2 \rho A X'(-\omega_n^2 T) - M_T X'(-\omega_n^2 T) + k_2 XT = 0$$
$$EIX^{'''}T + \bar{\mu}^2 \rho A \omega_n^2 X' T + M_T \omega_n^2 XT + k_2 XT = 0$$

divide by T and EI,

$$X^{'''} + \bar{\mu}^2 \frac{\rho A \omega_n^2}{EI} X' + \frac{M_T}{\rho A}\frac{\rho A \omega_n^2}{EI} X + \frac{k_2}{EI} X = 0$$
$$X^{'''} + \mu a_n^4 X' - \eta a_n^4 X + \kappa_2 X = 0 \tag{3.8}$$

where,

$$\eta = \frac{M_T L}{\rho A} \quad \text{and} \quad \kappa_2 = \frac{k_2 L^3}{EI} \qquad \text{(dimensionless constants)}$$

where η is the tip mas ratio and κ_2 is the linear spring ratio.

The general solution to the modal domain of the 4th order differential equation of motion Eq. (2.15) is expressed as,

$$X_n(x) = A_n \cos p_{2n} x + B_n sin p_{2n} x + C_n cosh p_{1n} x + D_n sinh p_{1n} x \tag{3.9}$$

This order of equation requires four constants A_n , B_n , C_n and D_n which are determined from the boundary conditions were, the boundary conditions.

Displacement at $x = 0$:

$$X_n(0) = 0 \tag{3.10a}$$
$$A_n \cos(0) + B_n \sin(0) + C_n \cosh(0) + D_n \sinh(0) = 0$$
$$A_n(1) + C_n(1) = 0$$
$$A_n = -C_n$$

therefore,

$$\begin{aligned} X_n(x) &= B\sin(p_2 x) + C(\cosh(p_1 x) - \cos(p_2 x)) + D\sinh(p_1 x) \\ X_n'(x) &= +p_2 B\cos(p_2 x) + C(p_2 \sin(p_2 x) + p_1 \sinh(p_1 x)) + p_1 D\cosh(p_1 x) \\ X_n''(x) &= -p_2^2 B\sin(p_2 x) + C(p_2^2 \cos(p_2 x) + p_1^2 \cosh(p_1 x)) + p_1^2 D\sinh(p_1 x) \\ X_n'''(x) &= -p_2^3 B\cos(p_2 x) + C(p_1^3 \sinh(p_1 x) - p_2^3 \sin(p_2 x)) + p_1^3 D\cosh(p_1 x) \\ X_n''''(x) &= p_2^4 B\sin(p_2 x) + C(p_1^4 \cosh(p_1 x) - p_2^4 \cos(p_2 x)) + p_1^4 D\sinh(p_1 x) \end{aligned} \tag{3.10b}$$

Moment at $x = 0$:

$$X_n''(0) + \mu a_n^4 X_n(0) - \kappa_1 X_n'(0) = 0 \tag{3.11a}$$

$$-p_2^2 B\sin(p_2x) + C(p_2^2\cos(p_2x) + p_1^2\cosh(p_1x)) + p_1^2 D\sinh(p_1x) + \mu a_n^4 [B\sin(p_2x) + C(\cosh(p_1x) - \cos(p_2x)) + D\sinh(p_1x)] - \kappa_1[p_2 B\cos(p_2x) + C(p_2\sin(p_2x) + p_1\sinh(p_1x)) + p_1 D\cosh(p_1x)] = 0$$

$$-p_2^2 B\sin(0) + C(p_2^2\cos(0) + p_1^2\cosh(0)) + p_1^2 D\sinh(0) + \mu a_n^4 [B\sin(0) + C(\cosh(0) - \cos(0)) + D\sinh(0)] - \kappa_1[p_2 B\cos(0) + C(p_2\sin(0) + p_1\sinh(0)) + p_1 D\cosh(0)] = 0$$

$$-0 + C\big(p_2^2(1) + p_1^2(1)\big) + 0 + \mu a_n^4\big[0 + C\big((1) - (1)\big) + 0\big] - \kappa_1[p_2 B(1) + \mathrm{C}(0+0) + p_1 D(1)] = 0$$

$$C\big(p_2^2(1) + p_1^2(1)\big) - \kappa_1[p_2 B(1) + p_1 D(1)] = 0$$

therefore,

$$B = \frac{(p_2^2 + p_1^2)C - \kappa_1 p_1 D}{\kappa_1 p_2} \tag{3.11b}$$

and B is substituted into Eq. (3.10b) and the general solution can be stated in terms of C and D in Eq. (3.12), and procced to solve the boundary conditions at $x = L$.

$$X_n(x) = C\left[(\cosh(p_1x) - \cos(p_2x)) + \frac{(p_2^2+p_1^2)}{\kappa_1 p_2}\sin(p_2x)\right] + D\left[\sinh(p_1x) - \frac{p_1}{p_2}\sin(p_2x)\right] \tag{3.12}$$

<u>Moment at</u> $x = L$:

$$X_n''(L) + \mu a_n^4 X_n(L) = 0 \tag{3.13a}$$

$$-\left(\frac{\left((p_2^2+p_1^2)C - \kappa_1 p_1 D\right)\sin(p_2L)}{\kappa_1 p_2} - C\cos(p_2L) + D\sinh(p_1L) + C\cosh(p_1L)\right)a_n^4\mu - \frac{p_2\left((p_2^2+p_1^2)C - k_1 p_1 D\right)\sin(p_2L)}{\kappa_1} + p_2^2 C\cos(p_2L) + p_1^2 D\sinh(p_1L) + p_1^2 C\cosh(p_1L) = 0$$

After substituting the general solution and it is derivatives from Eq. (3.12) into Eq. (3.13a), the above equation is solved for C which we rename C_moment,

$$C\_moment = C = \frac{C11}{C12} \tag{3.13b}$$

$$C11 = (\kappa_1 p_1 D\sin(p_2L) - \kappa_1 p_2 D\sinh(p_1L))a_n^4\mu + \kappa_1 p_1 p_2^2 D\sin(p_2L) + \kappa_1 p_1^2 p_2 D\sinh(p_1L)$$

$$C12 = \big((p_2^2 + p_1^2)\sin(p_2L) - \kappa_1 p_2\cos(p_2L) + \kappa_1 p_2\cosh(p_1L)\big)a_n^4\mu + (p_2^4 + p_1^2 p_2^2)\sin(p_2L) - \kappa_1 p_2^3\cos(p_2L) - \kappa_1 p_1^2 p_2\cosh(p_1L)$$

For the shear moment at $x = L$ the same operations are applied as above to solve for $C = C\_shear$.

<u>Shear at</u> $x = L$:

$$X_n'''(L) + \mu a_n^4 X_n'(L) - \eta a_n^4 X_n(L) + \kappa_2 X_n(L) = 0 \tag{3.14a}$$

$$-\left(p_2 C\sin(p_2L)+\frac{\left((p_2^2+p_1^2)C-k_1p_1D\right)\cos(p_2L)}{\kappa_1}+p_1C\sinh(p_1L)+\right.$$
$$\left.p_1D\cosh(p_1L)\right)a_n^4\mu-\left(\frac{\left((p_2^2+p_1^2)C-\kappa_1p_1D\right)sin(p_2L)}{\kappa_1p_2}-C\,cos(p_2L)+D\,sinh(p_1L)+\right.$$
$$\left.C\,cosh(p_1L)\right)\eta a_n^4+\kappa_2\left(\frac{\left((p_2^2+p_1^2)C-\kappa_1p_1D\right)\sin(p_2L)}{\kappa_1p_2}-C\cos(p_2L)+D\sinh(p_1L)+\right.$$
$$\left.C\cosh(p_1L)\right)-p_2^3C\sin(p_2L)-\frac{p_2^2\left((p_2^2+p_1^2)C-k_1p_1D\right)\cos(p_2L)}{\kappa_1}+p_1^3C\sinh(p_1L)+$$
$$p_1^3D\cosh(p_1L)=0$$

$$C\_shear=C=\frac{C21}{C22} \tag{3.14b}$$

$$\begin{aligned}C21=&(\kappa_1p_1p_2D\cos(p_2L)-\kappa_1p_1p_2D\cosh(p_1L))a_n^4\mu+(\kappa_1p_1D\sin(p_2L)-\\&\kappa_1p_2D\sinh(p_1L))\eta a_n^4-\kappa_1p_1\kappa_2D\sin(p_2L)+\kappa_1p_1p_2^3D\cos(p_2L)+\\&\kappa_1\kappa_2p_2D\sinh(p_1L)+\kappa_1p_1^3p_2D\cosh(p_1L)\end{aligned}$$

$$\begin{aligned}C22=&(\kappa_1p_2^2\sin(p_2L)+(p_2^3+p_1^2p_2)\cos(p_2L)+\kappa_1p_1p_2\sinh(p_1L))a_n^4\mu+\\&\left((p_2^2+p_1^2)\sin(p_2L)-\kappa_1p_2\cos(p_2L)+\kappa_1p_2\cosh(p_1L)\right)\eta a_n^4+\\&(\kappa_1p_2^4-\kappa_2p_2^2-p_1^2\kappa_2)\sin(p_2L)+(p_2^5+p_1^2p_2^3+\kappa_1\kappa_2p_2)\cos(p_2L)-\\&\kappa_1p_1^3p_2\sinh(p_1L)-\kappa_1\kappa_2p_2\cosh(p_1L)\end{aligned}$$

The dummy constants C_moment and C_shear are in terms of D alone, which can be set to unity. The new constants are equated ($C\_moment=C\_shear$) to generate the characteristics equation for the natural frequency of the system. Therefore, the characteristic equation is,

$$C\_moment-C\_shear=0$$
$$\frac{C11\cdot C22-C21\cdot C12}{C12\cdot C22}=0$$
$$C11\cdot C22-C21\cdot C12=0 \tag{3.15}$$

To find the roots of the characteristic equation Eq. (3.15), let $R_n^4=a_n^4L^4$, such that R_n becomes a non-dimensional constant, then $a_n=R_n/L$. Therefore,

$$\left(\frac{R_n}{L}\right)^4=\frac{\rho A{\omega_n}^2}{EI} \tag{3.16}$$

therefore,

$$\omega_n=\left(\frac{R_n}{L}\right)^2\sqrt{\frac{EI}{\rho A}} \tag{3.17}$$

using the relationship in Eq. (3.17) R_n can be determined numerically and thus the characteristic value for the nanobeam (a_n^4).

3.2 Natural frequencies for a cantilevered beam (with surface effects).

Complex mechanical systems are usually made of several assemblies that are coupled together to function in unison. These coupled systems will have their own unique natural frequencies and when acting together, they produce another set of universal natural frequencies. When the systems interact, the dynamics of each system behavior produces an external force that is experienced by the other systems. In the previous section we added mechanical elements (e.g. tip mass and linear spring) and in this instance, we add a mechanical system in the form of a spring-mass as indicated in Fig. (3.2).

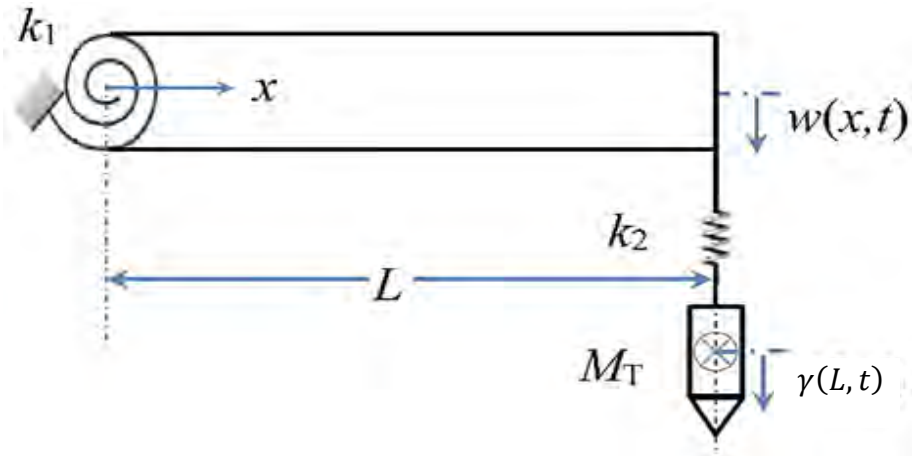

Figure 3-2: Geometry of the elastically restrained nanobeam with spring-mass at the free end.

Therefore, the boundary condition at $x = 0$ are zero lateral displacement and a state of equilibrium for the moments,

$$w(x) = 0 \tag{3.18}$$

$$E^e I^e \frac{\partial^2 w(x,t)}{\partial x^2} + \frac{2\nu I \rho_o}{H}\frac{\partial^2 w(x,t)}{\partial t^2} - \bar{\mu}\left[N\frac{\partial^2 w(x,t)}{\partial x^2} - (\rho A + \rho_o s^*)\frac{\partial^2 w(x,t)}{\partial t^2} - \tau_o s^* \frac{\partial^2 w(x,t)}{\partial x^2}\right] - k_1 \frac{\partial w(x,t)}{\partial x} = 0 \tag{3.19}$$

and at $x = L$, the moment and shear boundary conditions can be expressed as,

$$E^e I^e \frac{\partial^2 w(x,t)}{\partial x^2} + \frac{2\nu I \rho_o}{H}\frac{\partial^2 w(x,t)}{\partial t^2} - \bar{\mu}\left[N\frac{\partial^2 w(x,t)}{\partial x^2} - (\rho A + \rho_o s^*)\frac{\partial^2 w(x,t)}{\partial t^2} - \tau_o s^* \frac{\partial^2 w(x,t)}{\partial x^2}\right] = 0 \tag{3.20}$$

$$E^e I^e \frac{\partial^3 w(x,t)}{\partial x^3} + \frac{2\nu I \rho_o}{H}\frac{\partial^3 w(x,t)}{\partial x \partial t^2} - \tau_o s^* \frac{\partial w(x,t)}{\partial x} - N\frac{\partial w(x,t)}{\partial x} + \bar{\mu}\left[N\frac{\partial^3 w(x,t)}{\partial x^3} + \tau_o s^* \frac{\partial^3 w(x,t)}{\partial x^3} - (\rho A + \rho_o s^*)\frac{\partial^3 w(x,t)}{\partial x \partial t^2}\right] = F_L(x,t) \tag{3.21}$$

$$E^e I^e = EI + (2\mu_o + \lambda_o)I^* - \frac{2\nu I \tau_o}{H}$$

The shear boundary condition contains a term $F_L(x,t)$ that is the force due to the spring effect,

$$F_L(x,t) = k_2 \cdot \gamma(L,t) \tag{3.22}$$

and the displacement function $\gamma(L,t)$ is derived in detail in Section (2.2.2) and is express as,

$$\gamma(L,t) = \frac{a_n^4 X(L)}{a_k^4\left(1-\frac{a_n^4}{a_k^4}\right)} T_n(t) \tag{3.23}$$

Displacement at $x = 0$:

The general solution for the 4th order differential equations (Eq. (2.10), (2.33) and (2.47a)) is,

$$X_n(x) = A_n \cos p_{2n}x + B_n sinp_{2n}x + C_n coshp_{1n}x + D_n sinhp_{1n}x \tag{3.24a}$$

After inserting the value of $x = 0$ into Eq. (3.24a),

$$X_n(0) = A_n \cos p_{2n}(0) + B_n sinp_{2n}(0) + C_n coshp_{1n}(0) + D_n sinhp_{1n}(0) \tag{3.24b}$$

Substitute Eq. (3.24a) into the boundary condition Eq. (3.18),

$$X_n(0) = 0 \tag{3.25a}$$

$$A_n = -C_n \tag{3.25b}$$

substituting Eq. (3.25b) into Eq. (3.24a) the displacement function gives,

$$X_n(x) = B_n \sin p_{2n}(x) + D_n \sinh p_{1n}(x) + (\cos p_{2n}(x) - \cosh p_{1n}(x))C_n \tag{3.25c}$$

Moment at $x = 0$:

$$E^e I^e \frac{\partial^2 w(0,t)}{\partial x^2} + \frac{2\nu I \rho_o}{H}\frac{\partial^2 w(0,t)}{\partial t^2} - \bar{\mu}\left[N\frac{\partial^2 w(0,t)}{\partial x^2} - (\rho A + \rho_o s^*)\frac{\partial^2 w(0,t)}{\partial t^2} - \tau_o s^* \frac{\partial^2 w(0,t)}{\partial x^2}\right] - k_1 \frac{\partial w(0,t)}{\partial x} = 0 \tag{3.26a}$$

$$E^e I^e X''T + \frac{2\nu I \rho_o}{H} X\ddot{T} - \bar{\mu}\left[NX''T - (\rho A + \rho_o s^*)X\ddot{T} - \tau_o s^* X''T\right] - k_1 X'T = 0$$

$$E^e I^e X''T + \frac{2\nu I \rho_o}{H} X(-\omega_n^2 T) - \bar{\mu}[NX''T - (\rho A + \rho_o s^*)X(-\omega_n^2 T) - \tau_o s^* X''T] - k_1 X'T = 0$$

divide by T,

$$\left(EI + (2\mu_o + \lambda_o)I^* - \frac{2\nu I \tau_o}{H}\right)X'' - \frac{2\nu I \rho_o}{H}\omega_n^2 X - \bar{\mu}[NX'' + (\rho A + \rho_o s^*)\omega_n^2 X - \tau_o s^* X''] - k_1 X' = 0$$

divide by EI and non-dimensionalize the material constants,

$$\left(1 + \frac{(2\mu_o+\lambda_o)}{E}\frac{I^*}{I} - \frac{2\nu I}{HI}\frac{\tau_o}{E}\right)X'' - \frac{2\nu I \rho_o}{H}\frac{\omega_n^2}{EI}X - \bar{\mu}\left[\frac{N}{EI}X'' + \left(\frac{\rho A}{EI} + \frac{\rho_o s^*}{EI}\right)\omega_n^2 X - \frac{\tau_o}{E}\frac{s^*}{I}X''\right] - \frac{k_1}{EI}X' = 0$$

$$\left[1 + \left(\frac{(2\mu_o+\lambda_o)}{E} - \frac{2\nu}{\alpha}\frac{\tau_o}{E}\right)\frac{\alpha}{H}\right]X'' - \bar{\mu}\frac{N}{EI}X'' + \bar{\mu}\frac{\tau_o}{E}\frac{s^*}{I}X'' - \frac{2\nu}{A}\frac{I^*}{\alpha}\frac{\rho_o}{\rho}\frac{\rho A\omega_n^2}{EI}X - \bar{\mu}\frac{\rho A\omega_n^2}{EI}X - \bar{\mu}\frac{\rho_o}{\rho}\frac{s^*}{A}\frac{\rho A\omega_n^2}{EI}X - \frac{k_1}{EI}X' = 0$$

$$\left[1+\left(\frac{(2\mu_o+\lambda_o)}{E}-\frac{2\nu}{\alpha}\frac{\tau_o}{E}\right)\frac{\alpha}{H}-\bar{\mu}\frac{N}{EI}+\bar{\mu}\frac{\tau_o}{E}\frac{s^*}{I}\right]X''-\left[\frac{2\nu}{A}\frac{I^*}{\alpha}\frac{\rho_o}{\rho}\frac{\rho A\omega_n^2}{EI}-\bar{\mu}\frac{\rho A\omega_n^2}{EI}-\bar{\mu}\frac{\rho_o}{\rho}\frac{s^*}{A}\frac{\rho A\omega_n^2}{EI}\right]X-\frac{k_1}{EI}X'=0$$

$$\left[1+\left(\frac{(2\mu_o+\lambda_o)}{E}-\frac{2\nu}{\alpha}\tau_c\right)\frac{\alpha}{H}-\bar{\mu}\beta^2+\bar{\mu}\tau_c\frac{s^*}{I}\right]X''-\left[\frac{2\nu}{A}\frac{I^*}{\alpha}\rho_c a_n^4-\bar{\mu}\left(1+\rho_c\frac{s^*}{A}\right)a_n^4\right]X-\kappa_1 X'=0 \quad (3.26b)$$

$$\alpha=\frac{I^*}{I}H \quad , \quad \tau_c=\frac{\tau_0}{EL} \quad , \quad \mu=\left(\frac{\bar{\mu}}{l_i}\right)^2L^2 \quad , \quad \rho_c=\frac{\rho_o}{\rho L}$$

$$N_{cr}=\frac{EI}{L^2}\left(\frac{\pi^2}{4+\mu\pi^2}\right) \quad , \quad N=k\cdot N_{cr} \quad , \quad \beta^2=\frac{N}{EI}L^2 \quad \text{and} \quad a_n^4=\frac{\rho A\omega^2}{EI}$$

Let, $$\Gamma_1=1+\left(\frac{(2\mu_o+\lambda_o)}{E}-\frac{2\nu}{\alpha}\tau_c\right)\frac{\alpha}{H}-\bar{\mu}\beta^2+\bar{\mu}\tau_c\frac{s^*}{I}$$

and, $$\Gamma_2=\left[\frac{2\nu}{A}\frac{I^*}{\alpha}\rho_c-\bar{\mu}\left(1+\rho_c\frac{s^*}{A}\right)\right]a_n^4$$

therefore, $$\Gamma_1 X''-\Gamma_2 X-\kappa_1 X'=0 \quad (3.26c)$$

and, after using the general solution Eq. (3.25b) the constant B is determined in terms of C and D,

$$B=-\frac{p_1\kappa_1 D+\left(-\Gamma_1 p_2^2-p_1^2\Gamma_1\right)C}{\kappa_1 p_2} \quad (3.26d)$$

and the general equation is,

$$X_n(x)=\frac{C\left(\Gamma_1 p_2\sin(p_2x)+\frac{p_1^2\Gamma_1\sin(p_2x)}{p_2}\right)}{\kappa_1}+D\left(\sinh(p_1x)-\frac{p_1\sin(p_2x)}{p_2}\right)+C(\cosh(p_1x)-\cos(p_2x)) \quad (3.26e)$$

Moment at $x=L$:

$$E^eI^e\frac{\partial^2w(L,t)}{\partial x^2}+\frac{2\nu I\rho_o}{H}\frac{\partial^2w(L,t)}{\partial t^2}-\bar{\mu}\left[N\frac{\partial^2w(L,t)}{\partial x^2}-(\rho A+\rho_o s^*)\frac{\partial^2w(L,t)}{\partial t^2}-\tau_o s^*\frac{\partial^2w(L,t)}{\partial x^2}\right]=0 \quad (3.27a)$$

The same procedures used above to calculate the modal domain function for the moment at $x=L$ and leads to the following,

$$\left[1+\left(\frac{(2\mu_o+\lambda_o)}{E}-\frac{2\nu}{\alpha}\tau_c\right)\frac{\alpha}{H}-\mu\beta^2+\bar{\mu}\tau_c\frac{s^*}{I}\right]X''-\left[\frac{2\nu}{A}\frac{I^*}{\alpha}\rho_c a_n^4-\bar{\mu}\left(1+\bar{\mu}\rho_c\frac{s^*}{A}\right)a_n^4\right]X=0$$

therefore, $$\Gamma_1 X''-\Gamma_2 X=0 \quad (3.27b)$$

From Eq. (3.28b) we determine the constant C in terms of D for the moment boundary condition at $x=L$,

$$C\_moment=C=\frac{C_{11}}{C_{12}} \quad (3.27c)$$

$$C_{11}=(p_1\kappa_1\Gamma_2+p_1\Gamma_1\kappa_1p_2^2)D\sin(p_2L)+(p_1^2\Gamma_1\kappa_1p_2-\kappa_1p_2\Gamma_2)D\sinh(p_1L)$$

$$C_{12}=\left((\Gamma_1p_2^2+p_1^2\Gamma_1)\Gamma_2+\Gamma_1^2p_2^4+p_1^2\Gamma_1^2p_2^2\right)sin(p_2L)+(-\kappa_1p_2\Gamma_2-\Gamma_1\kappa_1p_2^3)cos(p_2L)+(\kappa_1p_2\Gamma_2-p_1^2\Gamma_1\kappa_1p_2)\cosh(p_1L)$$

Shear at $x=L$:

The shear boundary condition is reduced to the modal domain in Eq. (3.28) and Eq. (3.26e), with the constants C and D, is used to solve for the constant C.

$$E^e I^e \frac{\partial^3 w(L,t)}{\partial x^3} + \frac{2\nu I \rho_o}{H} \frac{\partial^3 w(L,t)}{\partial x \partial t^2} - \tau_o s^* \frac{\partial w(L,t)}{\partial x} - N \frac{\partial w(L,t)}{\partial x} + \bar{\mu}\left[N \frac{\partial^3 w(L,t)}{\partial x^3} + \tau_o s^* \frac{\partial^3 w(x,t)}{\partial x^3} - (\rho A + \rho_o s^*) \frac{\partial^3 w(L,t)}{\partial x \partial t^2}\right] = k_2 \cdot \gamma(L,t) \quad (3.28a)$$

$$E^e I^e X''' T + \frac{2\nu I \rho_o}{H} X' \ddot{T} - \tau_o s^* X' T - N X' T + \bar{\mu}\left[N X''' T + \tau_o s^* X''' T - (\rho A + \rho_o s^*) X' \ddot{T}\right] = k_2 \cdot \frac{a_n^4 X T}{a_k^4\left(1 - \frac{a_n^4}{a_k^4}\right)}$$

$$E^e I^e X''' T + \frac{2\nu I \rho_o}{H} X'(-\omega_n^2 T) - \tau_o s^* X' T - N X' T + \bar{\mu}[N X''' T + \tau_o s^* X''' T - (\rho A + \rho_o s^*) X'(-\omega_n^2 T)] = k_2 \cdot \frac{a_n^4 X T}{a_k^4\left(1 - \frac{a_n^4}{a_k^4}\right)}$$

$$\left(EI + (2\mu_o + \lambda_o) I^* - \frac{2\nu I \tau_o}{H}\right) X''' T + \frac{2\nu I \rho_o}{H} X'(-\omega_n^2 T) - \tau_o s^* X' T - N X' T + \bar{\mu}[N X''' T + \tau_o s^* X''' T - (\rho A + \rho_o s^*) X'(-\omega_n^2 T)] - k_2 \frac{a_n^4 X T}{a_k^4\left(1 - \frac{a_n^4}{a_k^4}\right)} = 0$$

divide by T and EI then non-dimensionalize parameters,

$$\left(EI + (2\mu_o + \lambda_o) I^* - \frac{2\nu I \tau_o}{H}\right) X''' - \frac{2\nu I \rho_o}{H} \omega_n^2 X' - \tau_o s^* X' - N X' + \bar{\mu}[N X''' + + \tau_o s^* X''' + (\rho A \omega_n^2 + \rho_o s^* \omega_n^2) X'] - k_2 \frac{a_n^4 X}{a_k^4\left(1 - \frac{a_n^4}{a_k^4}\right)} = 0$$

$$\left[1 + \left(\frac{(2\mu_o + \lambda_o)}{E} - \frac{2\nu}{\alpha}\tau_c\right)\frac{\alpha}{H}\right] X''' - \frac{2\nu}{A}\frac{I^*}{\alpha}\rho_c a_n^4 X' - \tau_c \frac{s^*}{I} X' - \beta^2 X' + \bar{\mu}\left[\beta^2 X''' + \tau_c \frac{s^*}{I} X''' + \left(1 + \rho_c \frac{s^*}{A}\right) a_n^4 X'\right] - \frac{\kappa_2 a_n^4 X}{\frac{\kappa_2}{\eta}\left(1 - \frac{a_n^4}{a_k^4}\right)} = 0$$

$$\left[1 + \left(\frac{(2\mu_o + \lambda_o)}{E} - \frac{2\nu}{\alpha}\tau_c\right)\frac{\alpha}{H}\right] X''' - \frac{2\nu}{A}\frac{I^*}{\alpha}\rho_c a_n^4 X' - \tau_c \frac{s^*}{I} X' - \beta^2 X' + \bar{\mu}\left[\beta^2 X''' + \tau_c \frac{s^*}{I} X''' + \left(1 + \rho_c \frac{s^*}{A}\right) a_n^4 X'\right] - \frac{\eta a_n^4 X}{\left(1 - \frac{a_n^4}{a_k^4}\right)} = 0$$

$$\left[1 + \left(\frac{(2\mu_o + \lambda_o)}{E} - \frac{2\nu}{\alpha}\tau_c\right)\frac{\alpha}{H}\right] X''' - \frac{2\nu}{A}\frac{I^*}{\alpha}\rho_c a_n^4 X' - \tau_c \frac{s^*}{I} X' - \beta^2 X' + \bar{\mu}\left[\beta^2 X''' + \tau_c \frac{s^*}{I} X''' - \left(1 + \rho_c \frac{s^*}{A}\right) a_n^4 X'\right] - \frac{\eta a_n^4 X}{\frac{1}{a_k^4}(a_k^4 - a_n^4)} = 0 \quad (3.28b)$$

The form of the last term in the equation above i.e. $1/(a_k^4 - a_n^4)$, indicates that $a_k^4 \neq a_n^4$ because that will lead to a divide by zero $(1/0)$ or infinity which is notoriously referred to as resonance. This phenomenon arises when the nanobeam system frequency approaches the spring-mass system frequency, or vice-versa. This knowledge is essential for NEMS and MEMS electro-mechanical system performance improvement.

$$\left[1+\left(\frac{(2\mu_o+\lambda_o)}{E}-\frac{2\nu}{\alpha}\tau_c\right)\frac{\alpha}{H}\right]X'''-\bar{\mu}\beta^2X'''+\bar{\mu}\tau_c\frac{s^*}{I}X'''\pm\frac{2\nu}{A}\frac{I^*}{\alpha}\rho_c a_n^4X'-\tau_c\frac{s^*}{I}X'-\beta^2X'+\bar{\mu}\left(1+\rho_c\frac{s^*}{A}\right)a_n^4X'-\frac{\eta a_k^4a_n^4X}{(a_k^4-a_n^4)}=0$$

$$\left[1+\left(\frac{(2\mu_o+\lambda_o)}{E}-\frac{2\nu}{\alpha}\tau_c\right)\frac{\alpha}{H}-\bar{\mu}\beta^2+\bar{\mu}\tau_c\frac{s^*}{I}\right]X'''-\left[\frac{2\nu}{A}\frac{I^*}{\alpha}\rho_c a_n^4-\bar{\mu}\left(1+\rho_c\frac{s^*}{A}\right)a_n^4\right]X'-\left(\tau_c\frac{s^*}{I}+\beta^2\right)X'-\frac{\eta a_k^4a_n^4X}{(a_k^4-a_n^4)}=0 \quad (3.28c)$$

Let,

$$\Gamma_1=1+\left(\frac{(2\mu_o+\lambda_o)}{E}-\frac{2\nu}{\alpha}\tau_c\right)\frac{\alpha}{H}-\bar{\mu}\beta^2+\bar{\mu}\tau_c\frac{s^*}{I}$$

$$\Gamma_2=\left[\frac{2\nu}{A}\frac{I^*}{\alpha}\rho_c-\bar{\mu}\left(1+\rho_c\frac{s^*}{A}\right)\right]a_n^4$$

and,

$$\Gamma_3=\tau_c\frac{s^*}{I}+\beta^2$$

therefore,

$$\Gamma_1X'''-\Gamma_2X'-\Gamma_3X'-\frac{\eta a_k^4a_n^4X}{(a_k^4-a_n^4)}=0 \quad (3.28d)$$

$$C\_shear=C=\frac{C_{21}}{C_{22}}$$

$$\begin{aligned}C_{21}=&\big((p_1\kappa_1D\sin(p_2L)-\kappa_1p_2D\sinh(p_1L))\eta a_k^4+(p_1\kappa_1p_2\Gamma_3-p_1\kappa_1p_2\Gamma_2-\\&p_1\Gamma_1\kappa_1p_2^3)D\cos(p_2L)+(-p_1\kappa_1p_2\Gamma_3+p_1\kappa_1p_2\Gamma_2-\\&p_1^3\Gamma_1\kappa_1p_2)D\cosh(p_1L)\big)a_n^4+\big((-p_1\kappa_1p_2\Gamma_3+p_1\kappa_1p_2\Gamma_2+\\&p_1\Gamma_1\kappa_1p_2^3)D\cos(p_2L)+(p_1\kappa_1p_2\Gamma_3-p_1\kappa_1p_2\Gamma_2+\\&p_1^3\Gamma_1\kappa_1p_2)D\cosh(p_1L)\big)a_k^4\end{aligned}$$

$$\begin{aligned}C_{22}=&a_k^4(\Gamma_1p_2^2\sin(p_2L)\,\eta a_n^4+p_1^2\Gamma_1\sin(p_2L)\,\eta a_n^4-\kappa_1p_2\cos(p_2L)\,\eta a_n^4+\\&\kappa_1p_2\cosh(p_1L)\,\eta a_n^4-\kappa_1p_2^2\Gamma_3\sin(p_2L)+\kappa_1p_2^2\Gamma_2\sin(p_2L)+\\&\Gamma_1\kappa_1p_2^4\sin(p_2L)-\Gamma_1p_2^3\Gamma_3\cos(p_2L)-p_1^2\Gamma_1p_2\Gamma_3\cos(p_2L)+\\&\Gamma_1p_2^3\Gamma_2\cos(p_2L)+p_1^2\Gamma_1p_2\Gamma_2\cos(p_2L)+\Gamma_1^2p_2^5\cos(p_2L)+\\&p_1^2\Gamma_1^2p_2^3\cos(p_2L)-p_1\kappa_1p_2\Gamma_3\sinh(p_1L)+p_1\kappa_1p_2\Gamma_2\sinh(p_1L)-\\&p_1^3\Gamma_1\kappa_1p_2\sinh(p_1L))+\kappa_1p_2^2\Gamma_3\sin(p_2L)\,a_n^4-\kappa_1p_2^2\Gamma_2\sin(p_2L)\,a_n^4-\\&\Gamma_1\kappa_1p_2^4\sin(p_2L)\,a_n^4+\Gamma_1p_2^3\Gamma_3\cos(p_2L)\,a_n^4+p_1^2\Gamma_1p_2\Gamma_3\cos(p_2L)\,a_n^4-\\&\Gamma_1p_2^3\Gamma_2\cos(p_2L)\,a_n^4-p_1^2\Gamma_1p_2\Gamma_2\cos(p_2L)\,a_n^4-\Gamma_1^2p_2^5\cos(p_2L)\,a_n^4-\\&p_1^2\Gamma_1^2p_2^3\cos(p_2L)\,a_n^4+p_1\kappa_1p_2\Gamma_3\sinh(p_1L)\,a_n^4-\\&p_1\kappa_1p_2\Gamma_2\sinh(p_1L)\,a_n^4+p_1^3\Gamma_1\kappa_1p_2\sinh(p_1L)\,a_n^4\end{aligned}$$

$$C\_moment-C\_shear=0$$

$$\frac{C_{11}}{C_{12}}-\frac{C_{21}}{C_{22}}=0$$

$$\frac{C_{11}C_{22}-C_{12}C_{21}}{C_{12}C_{22}}=0$$

$$C_{11}C_{22}-C_{12}C_{21}=0 \quad (3.28e)$$

The constants, C_moment and C_shear are equated and Eq. (3.28e) provides the eigenfrequencies of the system. These eigenfrequencies are used to construct eigenfunctions for the different modes of vibration of the system. The calculation for the frequencies of vibration is detailed in subsequent Chapters.

Chapter 4 – Paper 1: *International Journal of Acoustics and Vibration*

4.1 Effects of Elastic Restraints on the Fundamental Frequency of Nonlocal Nanobeams with Tip Mass.

In this Section, Case 1 is studied in more detail and the findings are published in the *International Journal of Acoustics and Vibration*, Vol. 24, No. 3, 2019.

Effects of Elastic Restraints on the Fundamental Frequency of Nonlocal Nanobeams with Tip Mass

Malesela K. Moutlana

Department of Mechanical Engineering, Durban University of Technology, Durban 4001, South Africa.

Sarp Adali

Discipline of Mechanical Engineering, University of KwaZulu-Natal, Durban 4041, South Africa.

(Received 4 April 2017; accepted 2 February 2018)

The fundamental frequencies of an elastically restrained nanobeam with a tip mass are studied based on the nonlocal Euler-Bernoulli beam theory. The nanobeam has a torsional spring at one end and a translational spring at the other end where a tip mass is attached. The aim is to model a tapping mode atomic force microscope (TM-AFM), which can be utilized in imaging and the manufacture of Nano-scale structures. A TM-AFM uses high frequency oscillations to remove material, shape structures or scan the topology of a Nano-scale structure. The nonlocal theory is effective at modelling Nano-scale structures, as it takes small scale effects into account. Torsional elastic restraints can model clamped and pinned boundary conditions, as their stiffness values change between zero and infinity. The effects of the stiffness of the elastic restraints, tip mass and the small-scale parameter on the fundamental frequency are investigated numerically.

1. INTRODUCTION

The vibrations of carbon nanotubes have been studied extensively due to their use as sensors in a number of applications such as an atomic force microscope (AFM), biosensors and Nano-resonators.[1–3] The atomic force microscope, discovered in the late eighties by Binnig et al,[4] has become more accurate with the discovery of carbon nanotubes which are used as sensor tips in the form of a cantilever.[5–8] An AFM cantilever provides dynamic interaction with the surface leading to transverse vibrations. Contact forces represent the dominant component of the forces when the interaction takes place. In the fabrication of nano-scale structures, the high frequency oscillations of a tip mass attached to a beam are employed with the purpose of deforming or shaping a material into a desired shape.[9,10] This process is widely known as either dynamic atomic force microscopy (DAFM)[7] or TM-AFM.[11] Cantilever nanotubes are also used as biosensors as their vibration patterns are analysed to obtain sensing data.[12–16] Nanotubes are also used as Nano-resonator sensors that are based on detecting shifts in resonant frequencies caused by a mass attached to the nanotube tip.[17–23] Nano-resonators improve the accuracy of the measurements by providing a high level of sensitivity as compared to conventional sensors. A review of the applications of carbon nanotubes as nano-resonator sensors is given in Wang and Arash.[24]

The vibration characteristics of Nano-scale beams can be analysed by modelling them within the framework of nonlocal continuum theory.[25,26] Nonlocal theory has been applied to the vibration modelling of carbon nanotubes in several studies[27–34] and, in particular, vibrations of carbon nanotubes with a tip mass have been studied extensively due to their use in sensor applications.[18,21–23,35–37] In these studies the flexibility of the boundaries were not taken into account and the classical boundary conditions were considered. The vibrations of nanotubes with elastically restrained boundaries have been analysed in a number of studies.[38–41]

In the present study, an elastically restrained nanobeam with a tip mass was modelled as a Euler-Bernoulli beam based on the nonlocal theory[25,26] to take into account the small scale effects.[42,43] The restraint at one support was specified as a torsional spring which replaced the clamped end boundary condition used in a number of studies. A translational spring was attached to the other end where a tip mass was attached. The governing differential equation of motion was solved analytically to determine the fundamental vibration frequency. The effects of the elastic restraints, tip mass and the small-scale parameter on the fundamental frequency were investigated numerically. Similar problems have been solved in the case of beams based on the local (classical) theory of elasticity. Elastically supported beams with a tip mass had been studied in literature[44–48] and a beam with torsional and translational springs with a tip mass had been studied in Zhou[49] based on the local theory of Euler-Bernoulli beams.

Most researchers model TM-AFM as a clamped-free beam in which case the clamped end can be considered 'ideal'.[6–8,50,51] A model replacing the clamped end with a torsional spring represents a more 'realistic' boundary condition, allowing for the flexibility of the attachment. This class of AFM is commonly referred to as torsion cantilevers and has been proven to exhibit some advantageous properties in subjects of research involving hydrated or soft biological samples and improved resolution and sensitivity of force in AFM probes subject to liquid environments.[52,53] Torsional cantilevers are important in the field of Nano-manufacturing because they allow for compliance matching or mismatching between the machining tool and the sample to be shaped. Matching the compliance of the machining tool and the sample prevents the destruction of the sample during manufacturing. Probing and compliance matching allows for the 'effortless' shaping of a sample. In TM-AFM, the free end carries a fabrication/cutting tool which is modelled as concentrated mass

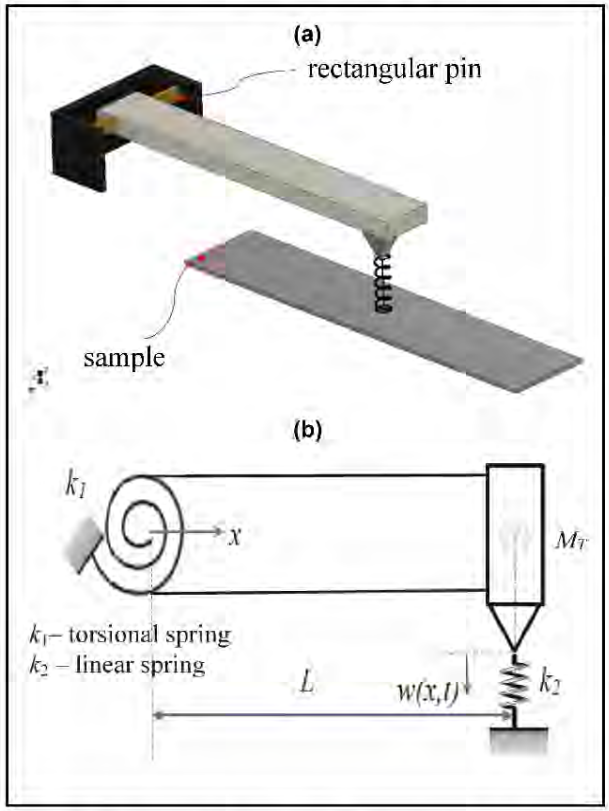

Figure 1. Geometry of the nanobeam with torsional restraint, concentrated mass and linear spring at free end. (a) 3D isometric model. (b) Engineering model showing the different system parameters under investigation.

such that the centre of the mass of the tool coincides with the sharp end of the cutting tool and the tip of the beam. A translational linear spring was attached to the tip of the mass and modelled the contact force with the sample of interest.

2. ELASTICALLY RESTRAINED NANOBEAM WITH TIP MASS

The beam under consideration was a Nano cantilever with the attachment at $x = 0$ modelling an elastic restraint due to a torsional spring of constant k_1 as shown in Fig. 1. A machining tool that modelled a concentrated mass with a sharp tip was attached to the free end of the beam at $x = L$. Figure 1 shows that the tip mass's centre of gravity coincided with the end of the beam. During the machining process, a contact force was generated between the tip mass and the object to be shaped. This contact force was modelled as a linear spring with a spring constant k_2. Figure 1 shows the configuration of the system where the beam was mounted by using a rectangular pin. The rectangular pin in Fig. 1(a) restricted vertical motion in the y-direction while restraining the lateral motion of the beam as it rotated about the rectangular pin. Therefore, the boundary conditions were that of a pinned and torsionally restrained end.

The constitutive relation of stress-strain, which was based on the nonlocal theory of elasticity, was expressed as

$$\sigma_{xx} - \overline{\mu}\frac{d^2\sigma_{xx}}{dx^2} = E\varepsilon_{xx}; \tag{1}$$

where E was the Young's modulus, $\overline{\mu} = e_0 l_i$ was the small scale parameter with e_0 denoting a material constant and l_i was the characteristic length. The expression for moment $M(x)$ was given by

$$M(x) - \overline{\mu}\frac{d^2M_z(x)}{dx^2} = -EI\frac{d^2w}{dx^2}; \tag{2}$$

where I was the moment of inertia. The equation of motion for a nonlocal nanobeam undergoing bending vibrations was given in Reddy[42,43] and was expressed as

$$EI\frac{d^4w}{dx^4} - \overline{\mu}^2\rho A\frac{d^2w}{dx^2} + \rho Aw = F_0(x); \tag{3}$$

where I was the moment of inertia, ρ was the density, A was the cross-sectional area and $F_0(x)$ was the forcing function which was taken as $F_0(x) = 0$ for a freely vibrating beam.

3. METHOD OF SOLUTION

The solution for the governing Eq. (3) was obtained by the eigenfunction expansion of the displacement function as

$$w(x) = \sum_{n=1}^{\infty} X_n(x). \tag{4}$$

Inserting Eq. (4) into Eq. (3) and after rearrangement, we obtained the equation in the modal domain given by

$$X_n''''(x) + \overline{\mu}^2 a_n^4 X_n''(x) - a_n^4 X_n(x) = 0. \tag{5}$$

The frequency parameter a_n was defined as

$$a_n^4 = \frac{\rho A\omega_n^2}{EI}; \tag{6}$$

where ω_n was the natural frequency for the n^{th} mode of vibration. The general solutions of Eq. (5) were given by

$$X_n(x) = A_n\cos p_{2n}x + B_n\sin p_{2n}x + C_n\cosh p_{1n}x + D_n\sinh p_{1n}x; \tag{7}$$

where p_{1n} and p_{2n} were

$$p_{1n,2n} = \sqrt{\frac{a_n^8\overline{\mu}^2 \pm \sqrt{a_n^8\overline{\mu}^2 + 4a_n^4}}{2}} = a_n\sqrt{\frac{a_n^6\overline{\mu}^2 \pm \sqrt{a_n^4\overline{\mu}^2 + 4}}{2}}. \tag{8}$$

The constants A_n, B_n, C_n and D_n were determined from the boundary conditions. The boundary conditions at $x = 0$ were zero displacement and the moment induced by the torsional spring and was expressed as

$$w(0) = 0; \tag{9a}$$

$$EI\frac{d^2w(0)}{dx^2} - \overline{\mu}^2\rho Aw - k_1\frac{dw(0)}{dx} = 0. \tag{9b}$$

From Eq. (9b), it followed that, if the torsional spring constant is infinite, only the third term became nonzero. This corresponded with the clamped boundary condition. For a beam with a tip mass M_T, the mass's centre of gravity was located at $x = L$. At the free end, taking into account the small scale

effect, the tip mass and the linear spring, the moment and shear boundary conditions were expressed as

$$EI\frac{d^2w(L)}{dx^2} + \overline{\mu}^2\rho A w(L) = 0; \tag{10a}$$

$$EI\frac{d^3w(L)}{dx^3} - \overline{\mu}^2\rho A w(L) - M_T w(L) + k_2 w(L) = 0. \tag{10b}$$

Eigenfunction expansions at $x = 0$ and $x = L$ were given by

$$w(0) = \sum_{n=1}^{\infty} X_n(0); \qquad w(L) = \sum_{n=1}^{\infty} X_n(L). \tag{11}$$

By substituting $w(0)$ in Eq. (11) into the boundary conditions at $x = 0$, we obtained

$$X_n(0) = 0; \tag{12a}$$

$$X_n''(0) + \mu^2 a_n^4 X_n(0) - \kappa_1 X_n'(0) = 0; \tag{12b}$$

where $\kappa_1 = \frac{k_1 L}{EI}$ was the dimensionless torsional spring constant. By substituting $w(L)$ in Eq. (11) into Eqs. (10a) and (10b), moment and shear force expressions at the boundary $x = L$ were obtained as

$$X_n''(L) + \mu^2 a_n^4 X_n(L) = 0; \tag{13a}$$

$$X_n'''(L) + \mu^2 a_n^4 X_n'(L) + \eta a_n^4 X_n(L) + \kappa_2 X_n(L) = 0; \tag{13b}$$

where

$$\eta = \frac{M_T L}{\rho A}; \quad \text{(dimensionless mass ratio);}$$

$$\kappa_2 = \frac{k_2 L^3}{EI}; \quad \text{(dimensionless linear spring constant);}$$

$$\mu = \left(\frac{\overline{\mu}}{l_i}\right)^2 L^2; \quad \text{(dimensionless small scale parameter).}$$

With the substitution of Eq. (7) into the boundary condition for Eq. (12a), we obtained

$$A_n - C_n = 0. \tag{14}$$

The general solution for Eq. (7) was be expressed as

$$X_n(x) = D_n \sinh p_{1n}x - B_n \sin p_{2n}x + C_n\left(\cos p_{2n}x - \cosh p_{1n}x\right). \tag{15}$$

Substituting Eq. (15) into Eq. (12b) gave

$$\kappa_1 p_1 D_n - \left(p_{2n}^2 + p_{1n}^2\right) C_n + \kappa_1 p_2 B_n = 0. \tag{16}$$

Solving for B_n and substituting into Eq. (15) allowed for the general solution to be expressed in terms of constants C_n and D_n alone. This result was substituted into the moment boundary conditions Eq. (10a) at $x = L$ to obtain

$$C_n \cdot \Gamma_{1n} + D_n \cdot \Gamma_{2n} = 0; \tag{17}$$

where

$$\begin{aligned}\Gamma_{1n} = &\Big[\left(p_{2n}^2 + p_{1n}^2\right)\sin p_{2n}L - \\ &\kappa_1 p_{2n}\left(\cos p_{2n}L - \cosh p_{1n}L\right)\Big]\mu a_n^4 + \\ &\left(p_{2n}^4 + p_{1n}^2 p_{2n}^2\right)\sin p_{2n}L - \\ &\kappa_1 p_{2n}\left(p_{2n}^2\cos p_{2n}L + p_{1n}^2\cosh p_{1n}L\right); \\ \Gamma_{2n} = &\frac{1}{p_{2n}}\Big[a_n^4\left(p_{2n}\sinh p_{1n}L - p_{1n}\sin p_{2n}L\right)\mu - \\ &p_{1n}p_{2n}\left(p_{2n}\sin p_{2n}L - p_{1n}\sinh p_{1n}L\right)\Big].\end{aligned}$$

Shear boundary condition Eq. (10b) at was expressed as

$$C_n \cdot \Gamma_{3n} + D_n \cdot \Gamma_{4n} = 0; \tag{18}$$

where

$$\begin{aligned}\Gamma_{3n} = &\Big[\kappa_1 a_n^4\left(p_{1n}p_{2n}\sinh p_{1n}L + p_{2n}^2\sin p_{2n}L\right) + \\ &\left(p_{2n}^3 + p_{1n}^2 p_{2n}\right)a_n^4\cos p_{2n}L\Big]\mu + \\ &\Big[\left(p_{2n}^2 + p_{1n}^2\right)a_n^4\eta + \kappa_1 p_{2n}^4 - \\ &\kappa_2\left(p_{2n}^2 + p_{1n}^2\right)\Big]\sin p_{2n}L + \\ &p_{2n}\left(\kappa_1 a_n^4\eta + p_{2n}^4 + p_{1n}^2 p_{2n}^2 + \kappa_1\kappa_2\right)\cos p_{2n}L - \\ &\kappa_1 p_{1n}^3 p_{2n}\sinh p_{1n}L + \\ &\left(\kappa_1 p_{2n}a_n^4\eta - \kappa_1\kappa_2 p_{2n}\right)\cosh p_{1n}L;\end{aligned}$$

and

$$\begin{aligned}\Gamma_{4n} = &\kappa_1\Big[p_{1n}p_{2n}\left(a_n^4\cosh p_{1n}L - a_n^4\cos p_{2n}L\right)\mu + \\ &p_{1n}\left(\kappa_2 - a_n^4\eta\right)\sin p_{2n}L\Big] + \\ &\kappa_1\Big[p_{2n}\left(a_n^4\eta - \kappa_2\right)\sinh p_{1n}L - \\ &p_{1n}p_{2n}\left(p_{2n}^2\cos p_{2n}L - p_{1n}^2\cosh p_{1n}L\right)\Big].\end{aligned}$$

The results from the moment and shear boundary conditions were given in Eqs. (17) and (18) was expressed in matrix form as

$$\begin{bmatrix}\Gamma_{1n} & \Gamma_{2n}\\ \Gamma_{3n} & \Gamma_{4n}\end{bmatrix}\begin{bmatrix}C_n\\ D_n\end{bmatrix} = \begin{bmatrix}0\\ 0\end{bmatrix}; \tag{19}$$

and the characteristic equation was obtained from the determinant of Eq. (19) as:

$$\Gamma_{1n}\Gamma_{4n} - \Gamma_{2n}\Gamma_{3n} = 0. \tag{20}$$

The characteristic Eq. (20) was solved numerically to compute the roots. For the cases of infinite torsional spring constant at $x = 0$, ($\kappa_1 \to \infty$), zero tip mass, ($\eta = 0$), zero linear spring constant at $x = L$, ($\kappa_2 = 0$), and zero small scale parameter ($\mu = 0$), Eq. (20) was reduced to the frequency equation of a cantilever given in Magrab and Bokaian.[54,55]

4. NUMERICAL RESULTS

Using the characteristic Eq. (20) and substituting $a_n = R_n/L$ allow for the dimensionless roots R_n of the characteristic equation to be computed. Equation (6) shows that

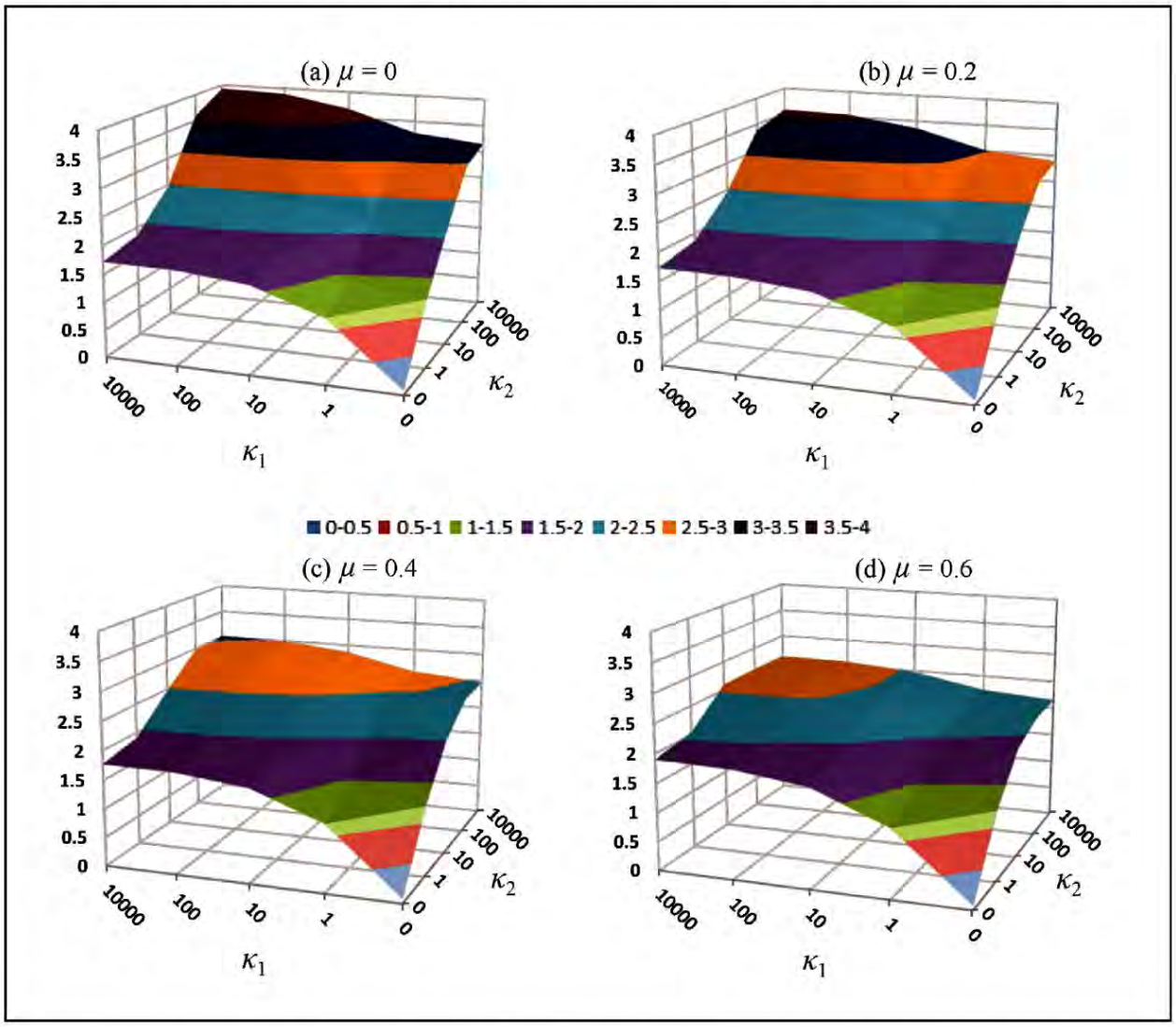

Figure 2. Fundamental frequency plotted against spring constants κ_1 and κ_2 with tip mass ratio $\eta = 0.1$, a) $\mu = 0.0$, b) $\mu = 0.2$, c) $\mu = 0.4$, d) $\mu = 0.6$.

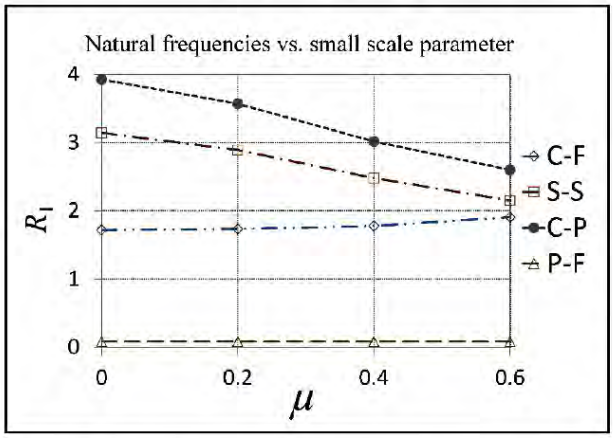

Figure 3. The natural frequencies of a nanobeam with classical boundary conditions.

these roots are directly associated with the natural frequencies ω_n by the relation $R_n = L\omega^{1/2}(\rho A/EI)^{1/4}$. Numerical results are given using dimensionless R_n values. Figure 2 shows the fundamental frequencies of the system with respect to the torsional spring constant κ_1 and the linear spring constant κ_2 for different values of the small scale parameter $\mu = 0, 0.2, 0.4, 0.6$. Figure 2(a) corresponds to a local beam with $\mu = 0$, which is based on the classical continuum model. The results in Figs. 2(b) to 2(d) take nonlocal effects into account and clearly demonstrate that these effects are important in the analysis of the nanobeams.

The results of Fig. 2(a) are in accordance with the results obtained by Magrab[54] for different boundary conditions. The boundary conditions include clamped-pinned, simply supported, clamp free, pinned-free beams. When the spring constants for the torsional spring at $x = 0$ and the linear spring at $x = L$ are infinite, i.e., $\kappa_1, \kappa_2 \to \infty$, the nanobeam behaves like a clamped-pinned beam. The frequency for this case is $R_1 = 3.9266$ and the corresponding result in Magrab is 1.25π. For the case when $\kappa_1 = 0$ and $\kappa_2 \to \infty$, the nanobeam becomes simply-supported with the frequency given by $R_1 = \pi$. For a clamped-free beam, $\kappa_1 \to \infty$ and $\kappa_2 \to 0$. For this case and with a tip mass of $\eta = 0.1$, the frequency is $R_1 = 1.7227$ which is the same result (0.5484π) as the one given in Ma-

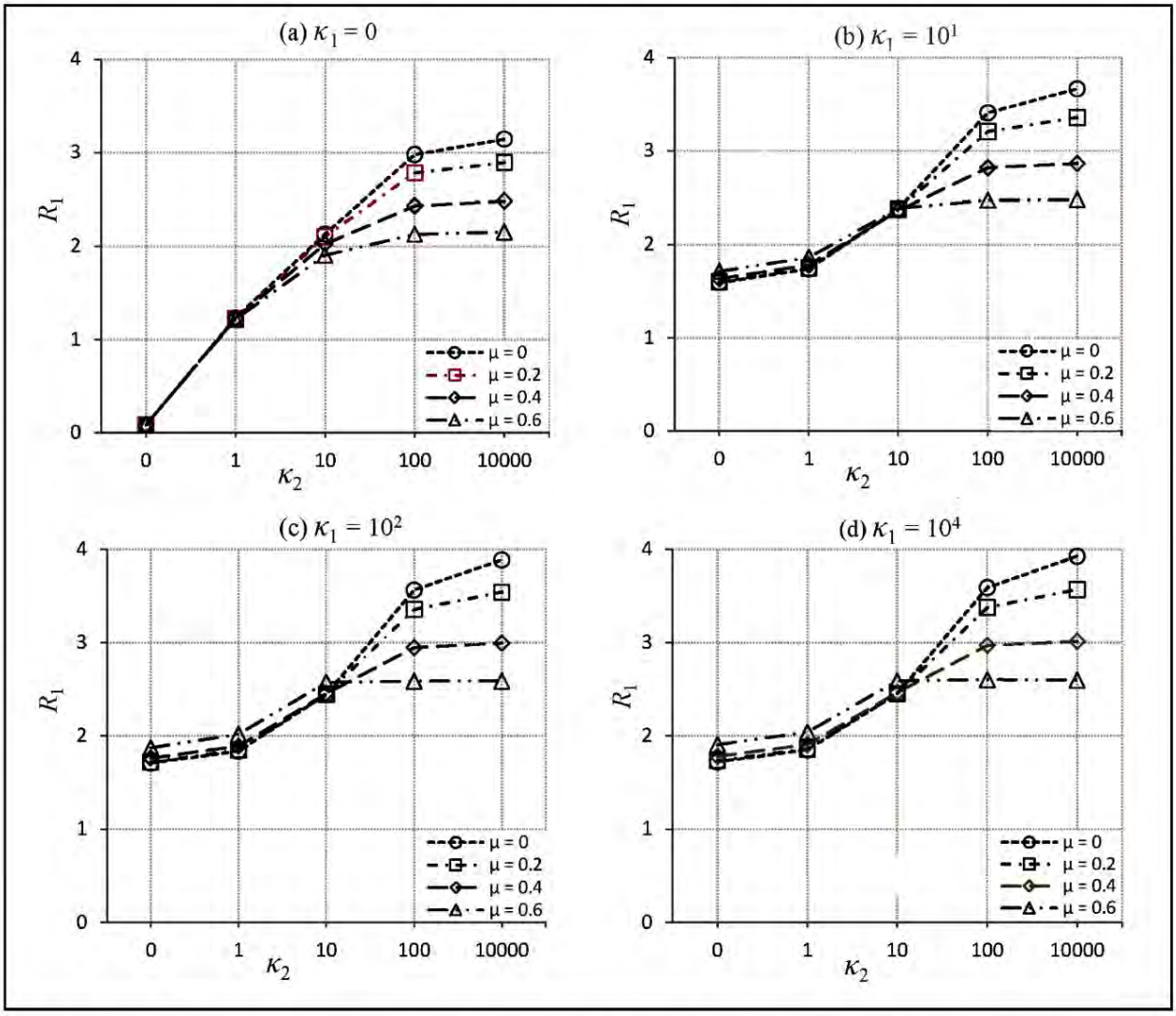

Figure 4. Fundamental frequency plotted against κ_2 for various values of κ_1 and μ with tip mass ratio $\eta = 0.1$, a) $\kappa_1 = 0$, b) $\kappa_1 = 10$, c) $\kappa_1 = 10^2$, d) $\kappa_1 = 10^4$.

grab.[54] For zero torsional and linear spring constants, i.e., $\kappa_1, \kappa_2 \to 0$, the frequencies approach zero ($R_1 \to 0$) for all values of the small scale parameter μ. A similar observation was made by Behera and Chakraverty.[30]

Frequencies of a cantilever nanobeam given by Ehteshami and Hajabasi,[56] Murmu and Adhikari[15] indicate that, as the small-scale parameter increases, the fundamental frequency of the cantilever nanobeam also increases. When the boundaries have a finite stiffness, the frequencies may increase or decrease depending on the problem parameters as the small-scale parameter increases. The graphs of the natural frequencies shown in Figs. 2(a) to 2(d) indicate this phenomenon.

For a simply supported nanobeam, the torsional spring constant at $x = 0$ is zero ($\kappa_1 = 0$) and the linear constant at $x = L$ is infinity ($\kappa_2 \to \infty$). For this case, Figs. 2(a) to 2(d) indicate that the frequencies decrease as the small scale parameter increases. Figures 2(a) to 2(d) indicate that, for a clamped-pinned case ($\kappa_1, \kappa_2 \to \infty$), the frequencies decrease as the small scale parameter increases. The effect of the small scale parameter on frequency is investigated in Fig. 3, which shows the trend in the frequencies as the small scale parameter increases for classical boundary conditions. It is observed that frequencies decrease for clamped-free (C-F) and simply-supported-simply-supported (S-S) boundary conditions, but increase for the clamped-pinned (C-P) case. These results are supported by the results obtained by Behera and Chakraverty.[30] For a pinned-free (P-F) nanobeam, i.e., $\kappa_1, \kappa_2 \to 0$, the frequencies are extremely small and approach zero in the limit.

The effect of the linear spring constant κ_2 at $x = L$ is investigated in Fig. 4, which shows the curves of frequency plotted against κ_2 for $\kappa_1 = 0, 10, 100, 10000$ and for different values of the small scale parameter. The curves represent the frequency profile for a particular torsional spring constant at $x = 0$ and small scale parameter. In Fig. 4, the frequency increases steadily as the stiffness κ_2 increases while κ_1 at $x = 0$ is kept constant. It is noted that the boundary condition at $x = L$ becomes a simple support when $\kappa_2 \to \infty$.

Figure 5 shows the curves of frequency plotted against the small scale parameter for $\kappa_1 = 0, 10, 100, 10000$ and for different values of κ_2 It is observed that the frequency increases as the small scale parameter increases at low values of κ_2, but decreases at high values of κ_2 indicating the effect of the spring

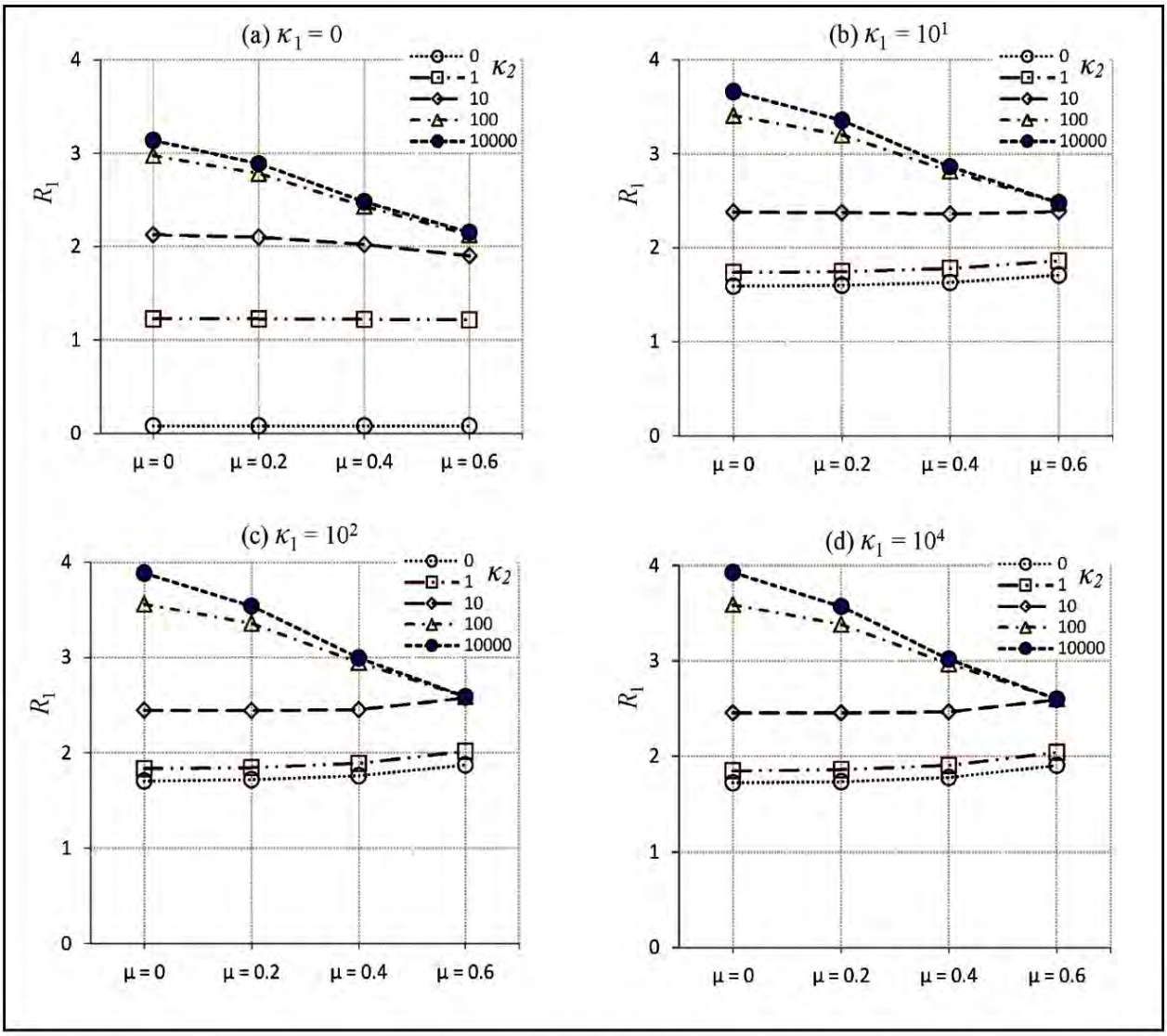

Figure 5. Fundamental frequency plotted against μ for various values of κ_1 and κ_2 and with tip mass ratio $\eta = 0.1$, a) $\kappa_1 = 0$, b) $\kappa_1 = 10$, c) $\kappa_1 = 10^2$, d) $\kappa_1 = 10^4$.

at $x = L$. Figure 5 shows that, for $\kappa_1 = 0$ and $\kappa_2 = 0$, the frequency is very small and its value is independent of the small scale parameter. As κ_1 increases from $\kappa_1 = 10$ to $\kappa_1 = 10^4$ (Figs. 5(b) to 5(d)) for $\kappa_2 = 0$, frequency increases from $R_1 = 1.5912$ to $R_1 = 1.7070$ to $R_1 = 1.7227$. The frequency $R_1 = 1.7227$ is widely published as the natural frequency of a local cantilever beam ($\mu = 0$) with tip mass ratio of $\eta = 0.1$.[54] From Figs. 5(b), 5(c) and 5(d), we note that frequencies increase as μ increases for $\kappa_2 = 0, 1, 10$ and they decrease for $\kappa_2 = 10^2, 10^4$. For cantilever nanobeam ($\kappa_1 = 10000$) in Fig. 5(d), the results in Li et al.[57] show similar trends for the frequencies.

In Fig. 6, the frequency is plotted against the linear spring constant κ_2 for different values of κ_1 and μ. Figure 6(a) shows that, when the end of the beam is free ($\kappa_2 = 0$), the small scale parameter has minimal effect on the frequency. However, Fig. 6(d) shows that its effect increases as the end $x = L$ becomes simply supported when $\kappa_2 = 10^4$. The frequency increases as the boundaries at $x = 0$ and $x = L$ become stiffer, i.e., as $\kappa_1, \kappa_2 \to 10^4$ with the amount of increase depending on the small scale parameter.

Next, the effect of the rigidity of the end $x = L$ is investigated by plotting the frequency against μ in Fig. 7. It is observed that the frequency may increase or decrease as μ increases depending on κ_1 and the rigidity of the end point as measured by κ_2. As κ_2 increases, decrease in the frequency with increasing μ becomes more pronounced.

Next, the effect of the tip mass on frequency is studied in Fig. 8 for the following boundary conditions: 1) $\kappa_1 = 10$ and $\kappa_2 = 0$, restrained-free (R-F), 2) $\kappa_1 = 10$ and $\kappa_2 = 10$, restrained-restrained (R-R), 3) $\kappa_1 \to \infty$ and $\kappa_2 = 0$, clamped-free (C-F) and 4) $\kappa_1 \to \infty$ and $\kappa_2 = 10$, clamped-restrained (C-R). It is observed that as the tip mass ratio increases, frequency decreases as observed in Moutlana and Adali.[58] It is observed that, for a C-F local cantilever ($\mu = 0$), the fundamental frequencies are $R_1 = 1.875$, $R_1 = 1.723$, $R_1 = 1.420$ and $R_1 = 1.248$ corresponding to the tip mass ratios $\eta = 0$, $\eta = 0.1$, $\eta = 0.5$ and $\eta = 1.0$, respectively, which are the same as the results obtained by Balachandran and Magrab,[59] which were based on classical continuum theory. It is also noted that

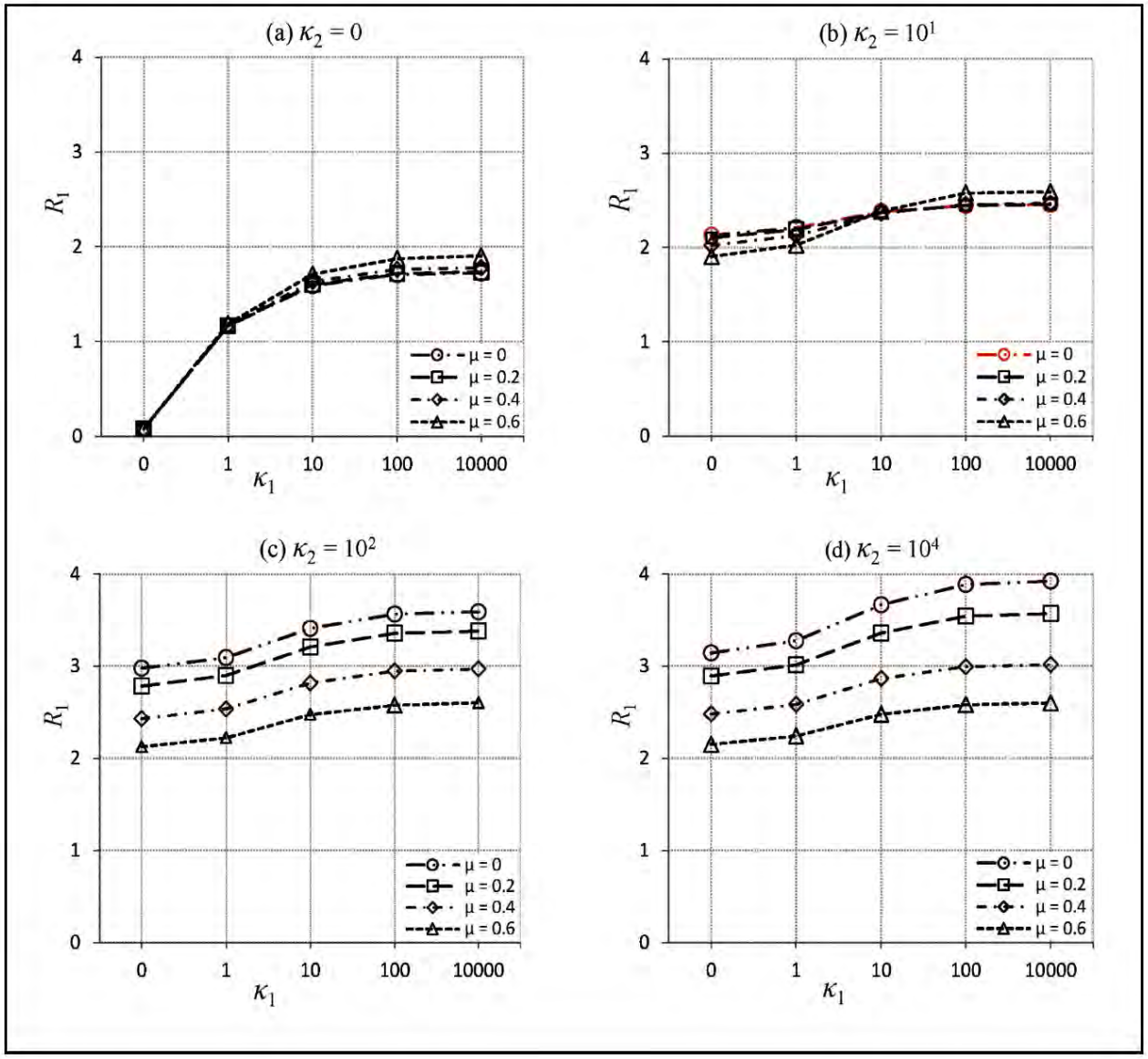

Figure 6. Fundamental frequency plotted against κ_1 for various values of κ_2 and μ with tip mass ratio $\eta = 0.1$, a) $\kappa_2 = 0$, b) $\kappa_2 = 10$, c) $\kappa_2 = 10^2$, d) $\kappa_2 = 10^4$.

frequencies for $\mu = 0.0, 0.2, 0.4, 0.6$ in Fig. 8(a) for zero tip mass ($\eta = 0$), are verified by Lu et al.[60]

It is observed from Fig. 8 that when the support at $x = 0$ is clamped, the frequency increases with increasing μ. However, when the support at $x = 0$ is restrained with $\kappa_1 = 10$, the frequency decreases with increasing μ when $\eta \leq 0.1$. Similar observations were made in Azrar et al.[61] for the case $\eta = 0$. When $\eta \geq 0.5$, frequency increases with increasing μ for all boundary conditions. As expected frequencies are reduced when the tip mass ratio increases. It is noted that for $\eta = 0$ with $\kappa_1 \to \infty$ and $\kappa_2 = 10$ (clamped-restrained case), $R_a = 2.5954$ for $\mu = 0.565$, and for $\mu > 0.565$ a non-trivial real eigenvalue (R_1) does not exist as also observed in Lu.[62] A similar situation is encountered for the same boundary conditions when the tip mass ratio is $\eta = 0.1$ where $R_1 = 2.4627$ for $\mu = 0.58$ and there are no real non-trivial eigenvalues beyond this point. It is noted that for a clamped-free beam, there are no real non-trivial eigenvalues beyond $\mu = 0.62$.[60]

5. CONCLUSIONS

In the present paper, small scale effects on the fundamental frequency are investigated for a nanobeam with elastically restrained end conditions and carrying a tip mass. The solution for the beam is obtained analytically by expanding the deflection in terms of its eigenfunctions and solving the resulting characteristic equation numerically. The results are given in the form of three-dimensional plots in terms of the fundamental frequencies, small scale parameter, torsional and linear spring constants. Further numerical results are presented for parametric studies of the effect of support elasticity and tip mass on the fundamental frequencies of the nanobeam.

It is observed that the effect of the small-scale parameter depends on several problem parameters and may lead to an increase or decrease of the fundamental frequency depending on the support flexibility. Boundary conditions are expressed in terms of a torsional spring at $x = 0$ and a linear spring at

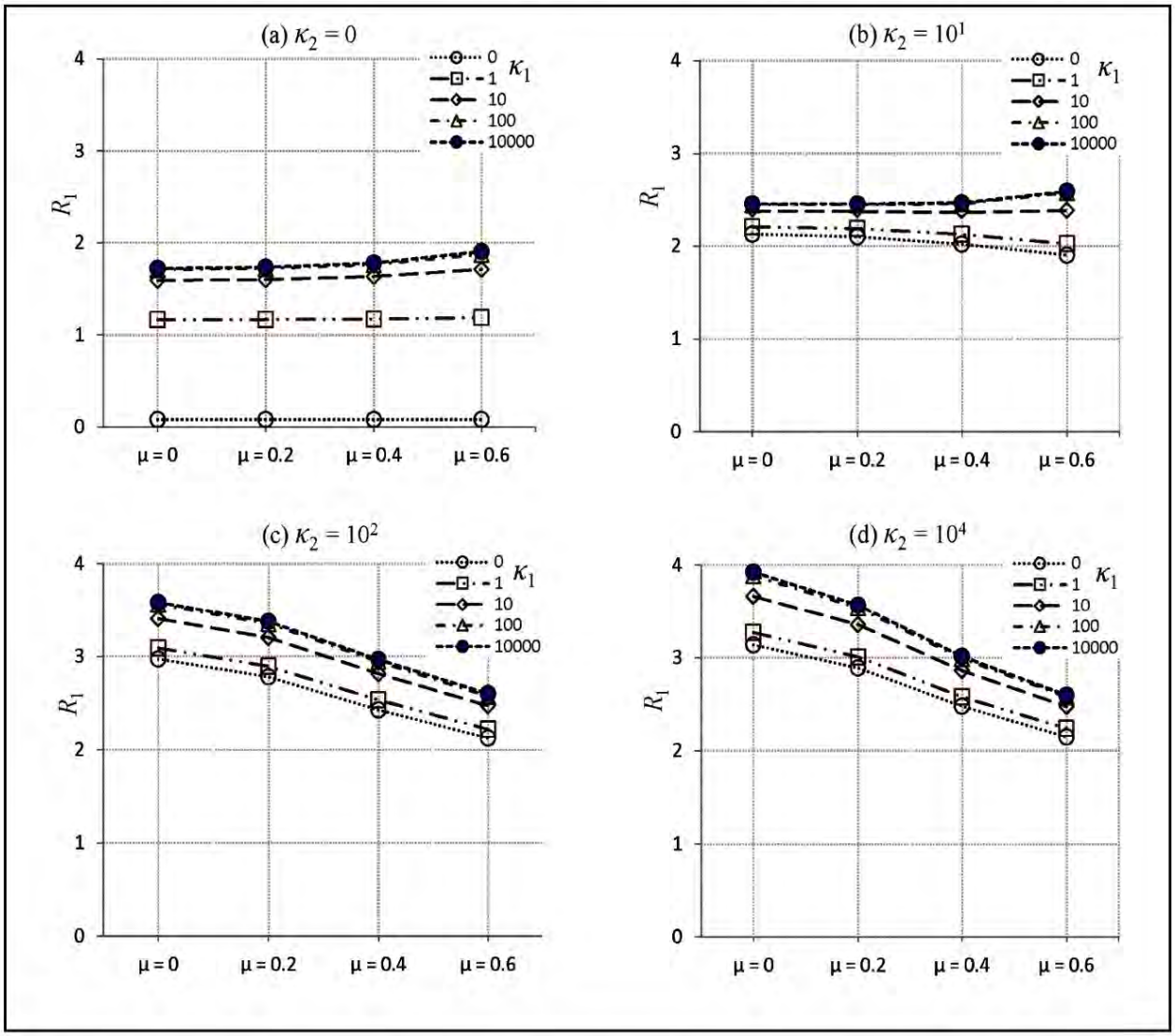

Figure 7. Fundamental frequency plotted against μ for various values of κ_1 and κ_2 and with tip mass ratio $\eta = 0.1$, a) $\kappa_2 = 0$, b) $\kappa_2 = 10$, c) $\kappa_2 = 10^2$, d) $\kappa_2 = 10^4$.

$x = L$ and the classical boundary conditions correspond to setting the torsional and linear spring constants to zero ($\kappa_{1,2} \to 0$) or infinity ($\kappa_{1,2} \to \infty$). It was observed that low torsional spring stiffness and high linear spring stiffness leads to a decrease in the fundamental frequency and high torsional spring stiffness and low linear spring stiffness to an increase in the fundamental frequency as the small-scale parameter increases (Figs. 5 and 7). The rates of decrease and increase depend on the relative values of the spring constants. The effect of the tip mass on the frequencies are studied in Fig. 8 and it is observed that in some cases a real eigenvalue cannot be obtained as also observed in Lu et al. and Lu.[60,62]

ACKNOWLEDGEMENT

The research of the second author was supported by research grants from the University of KwaZulu-Natal (UKZN) and from National Research Foundation (NRF) of South Africa. The author gratefully acknowledges the support provided by UKZN and NRF.

REFERENCES

[1] Li, C., Thostenson, E. T., and Chou, T. W. Sensors and actuators based on carbon nanotubes and their composites: a review, *Composites Science and Technology*, **68**, 1227–1249, (2008). https://dx.doi.org/10.1016/j.compscitech.2008.01.006

[2] Bogue, R. Nanosensors: A review of recent progress, *Sensor Review*, **29** (4), 310–315, (2009). https://dx.doi.org/10.1108/02602280810849965

[3] Feng, E. H. and Jones R. E. Carbon nanotube cantilevers for next-generation sensors, *Physical Review B*, **83**, 195412, (2011). https://dx.doi.org/10.1103/PhysRevB.83.195412

[4] Binnig, G., Quate, C. F., and Gerber, C. Atomic force microscope, *Physical Review Letters*, **56**, 930–933, (1986). https://dx.doi.org/10.1103/PhysRevLett.56.930

[5] Chang, W. J. Sensitivity of vibration modes of atomic force

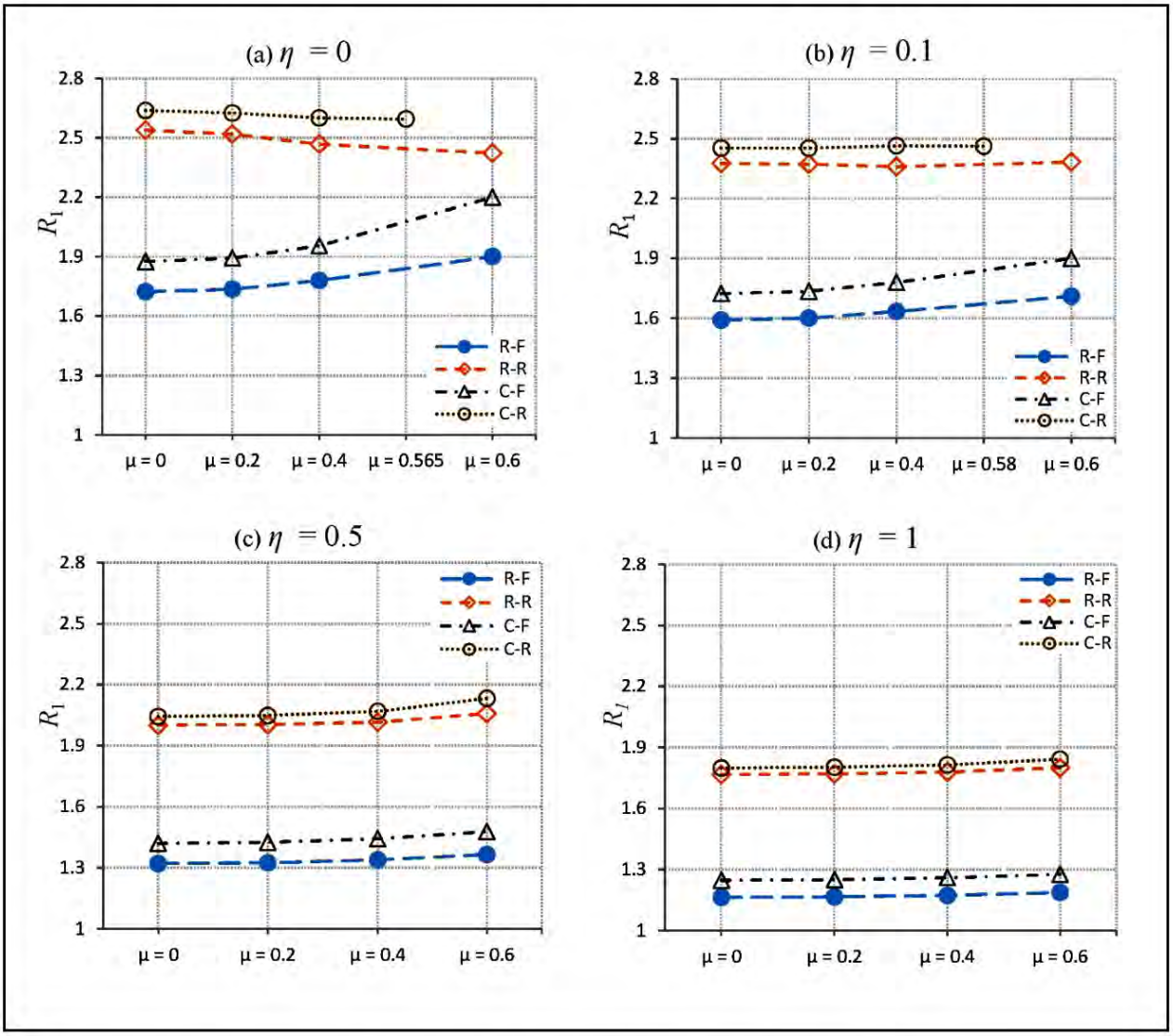

Figure 8. Fundamental frequency plotted against μ for various boundary conditions, a) $\eta = 0$, b) $\eta = 0.1$, c) $\eta = 0.5$, d) $\eta = 1.0$.

microscope cantilevers in continuous surface contact, *Nanotechnology*, **13**, 510–514, (2002).

[6] Hsu, J.-C., Lee, H.-L., and Chang, W.-J. Flexural vibration frequency of atomic force microscope cantilevers using the Timoshenko beam model, *Nanotechnology*, **18**, 285–503, (2007).

[7] Raman, A., Melcher, J., and Tung, R. Cantilever dynamics in atomic force microscopy, *Nano Today*, **3**, 20–27, (2008). https://dx.doi.org/10.1016/S1748-0132(08)70012-4

[8] Sadeghi, A. The flexural vibration of V shaped atomic force microscope cantilevers by using the Timoshenko beam theory, *Zeitschriftfur Angewandte Mathematik und Mechanik*, **92**, 782–800, (2012). https://dx.doi.org/10.1002/zamm.201100100

[9] Chang, W. J., Yang, Y. C., and Lee, H. L. Dynamic behaviour of atomic force microscope based nano-machining based on a modified couple stress theory, *Micro & Nano Letters*, **8**, 832–835, (2013). https://dx.doi.org/10.1049/mnl.2013.0493

[10] Liu, W., Yan, Y., Hu, Z., Zhao, X., Yan, J., and Dong, S. Study on the nano machining process with vibrating AFM tip on the polymer surface, *Applied Surface Science*, **258**, 2620–2626, (2012). https://dx.doi.org/10.1016/j.apsusc.2011.10.107

[11] McCarthy, R., Carmichael, B., and Nima Mahmoodi, S. Dynamic analysis of tapping atomic force microscopy considering various boundary value problems, *Sensors and Actuators A: Physical*, **216**, 69–77, (2014). https://dx.doi.org/10.1016/j.sna.2014.04.036

[12] Balasubramanian, K., Burghard, M. Biosensors based on carbon nanotubes, *Analytical and Bioanalytical Chemistry*, **385** (3), 452–468, (2006). https://dx.doi.org/10.1007/s00216-006-0314-8

[13] Chowdhury, R., Adhikari, S., and Mitchell, J. Vibrating car-

bon nanotube based biosensors, *Physica E*, **42**, 104–109, (2009). https://dx.doi.org/10.1016/j.physe.2009.09.007

[14] Adhikari, S. and Chowdhury, R. The calibration of carbon nanotube based bionanosensors, *Journal of Applied Physics*, **107**, 124322, (2010). https://dx.doi.org/10.1063/1.3435316

[15] Murmu, T. and Adhikari, S. Nonlocal frequency analysis of nanoscale biosensors, *Sensors and Actuators A: Physical*, **173**, 41–48, (2012). https://dx.doi.org/10.1016/j.sna.2011.10.012

[16] Shen, Z. B., Sheng, L. P., Li, X. F., and Tang, G. J. Nonlocal Timoshenko beam theory for vibration of carbon nanotube-based biosensor, *Physica E*, **44**, 1169–1175, (2012). https://dx.doi.org/10.1016/j.physe.2012.01.005

[17] Joshi, A. Y., Harsha, S. P., and Sharma, S. C. Vibration signature analysis of single walled carbon nanotube based nanomechanical sensors, *Physica E*, **42**, 2115–2123, (2010). https://dx.doi.org/10.1016/j.physe.2012.01.005

[18] Wu, D. H., Chien, W. T., Chen, C. S., and Chen, H. H. Resonant frequency analysis of fixed-free single-walled carbon nanotube-based mass sensor, *Sensors and Actuators A: Physical*, **126**, 117–121, (2006). https://dx.doi.org/10.1016/j.sna.2005.10.005

[19] Chiu, H. Y., Hung, P., Postma, H. W. C., and Bockrath, M. Atomic-scale mass sensing using carbon nanotube resonators, *Nano Letters*, **8**, 4342–4346, (2008). https://dx.doi.org/10.1021/nl802181c

[20] Bichoutskaia, E., Popov, A. M., Lozovik, Y. E., Ershova, O. V., Lebedeva, I. V., and Knizhnik, A. A. Nanoresonator based on relative vibrations of the walls of carbon nanotubes, *Fullerenes, Nanotubes and Carbon Nanostructures*, **18** (4–6), 523–530, (2010). https://dx.doi.org/10.1080/1536383X.2010.488524

[21] Mehdipour, I., Barari, A., and Domairy, G. Application of a cantilevered SWCNT with mass at the tip as a nanomechanical sensor, *Computational Materials Science*, **50**, 1830–1833, (2011). https://dx.doi.org/10.1016/j.commatsci.2011.01.025

[22] Lee, H.-L., Hsu, J.-C., and Chang, W.-J. Frequency shift of carbon nanotube-based mass sensor using nonlocal elasticity theory, *Nanoscale Research Letters*, **5**, 1774–1778, (2010). https://dx.doi.org/10.1007/s11671-010-9709-8

[23] Shen, Z. B., Li, X. F., Sheng, L. P., and Tang, G. J. Transverse vibration of nanotube-based micromass sensor via nonlocal Timoshenko beam theory, *Computational Materials Science*, **53**, 340–346, (2012). https://dx.doi.org/10.1016/j.commatsci.2011.09.023

[24] Wang, Q. and Arash, B. A review on applications of carbon nanotubes and graphenes as nano-resonator sensors, *Computational Materials Science*, **82**, 350–360, (2014). https://dx.doi.org/10.1016/j.commatsci.2013.10.010

[25] Eringen, A. C. and Edelen, D. On nonlocal elasticity, *International Journal of Engineering Science*, **10** (3), 233–248, (1972). https://dx.doi.org/10.1016/0020-7225(72)90039-0

[26] Eringen, A. C. *Nonlocal Continuum Field Theories*, Springer-Verlag, New York, (2002).

[27] Sakhaee-Pour, A., Ahmadian, M., and Vafai, A. Vibrational analysis of single-walled carbon nanotubes using beam element, *Thin-Walled Structures*, **47** (6–7), 646–652, (2009). https://dx.doi.org/10.1016/j.tws.2008.11.002

[28] Artan, R. and Lehmann, L. The vibrations of carbon nanotubes in nonlocal elasticity, *Journal of Computational and Theoretical Nanoscience*, **6**, 653–661, (2009). https://dx.doi.org/10.1166/jctn.2009.1088

[29] Eltaher, M. A., Alshorbagy, A. E., and Mahmoud, F. F. Vibration analysis of Euler–Bernoulli nanobeams by using finite element method, *Applied Mathematical Modelling*, **37**, 4787–4797, (2013). https://dx.doi.org/10.1016/j.apm.2012.10.016

[30] Behera, L. and Chakraverty, S. Free vibration of Euler and Timoshenko nanobeams using boundary characteristic orthogonal polynomials, *Applied Nanoscience*, **4**, 347–358, (2014). https://dx.doi.org/10.1007/s13204-013-0202-4

[31] Baghdadi, H., Tounsi, A., Zidour, M., and Benzair, A. Thermal effect on vibration characteristics of armchair and zigzag single-walled carbon nanotubes using nonlocal parabolic beam theory, *Fullerenes, Nanotubes and Carbon Nanostructures*, **23** (3), 266–272, (2015). https://dx.doi.org/10.1080/1536383X.2013.787605

[32] Arefi, A. and Salimi, M. Investigations on vibration and buckling of carbon nanotubes with small initial curvature by nonlocal elasticity theory, *Fullerenes, Nanotubes and Carbon Nanostructures*, **23** (2), 105–112, (2015). https://dx.doi.org/10.1080/1536383X.2013.771171

[33] Rahmanian, M., Torkaman-Asadi, M. A., Firouz-Abadi, R. D., and Kouchakzadeh, M. A. Free vibrations analysis of carbon nanotubes resting on Winkler foundations based on nonlocal models, *Physica B*, **484**, 83–94, (2016). https://dx.doi.org/10.1016/j.physb.2015.12.041

[34] Rosa, M. A. D. and Lippiello, M. Nonlocal frequency analysis of embedded single-walled carbon nanotube using the Differential Quadrature Method, *Composites Part B: Engineering*, **84**, 41–51, (2016). https://dx.doi.org/10.1016/j.compositesb.2015.08.065

[35] Murmu, T. and Adhikari, S. Nonlocal vibration of carbon nanotubes with attached buckyballs at tip, *Mechanics Research Communications*, **38**, 62–67, (2011). https://dx.doi.org/10.1016/j.mechrescom.2010.11.004

[36] Elishakoff, I., Versaci, C., and Muscolino, G. Clamped-free double-walled carbon nanotube-based mass sensor, *Acta Mechanica*, **219**, 29–43, (2011). https://dx.doi.org/10.1007/s00707-010-0435-1

[37] Horng, T.-L. Analytical solution of vibration analysis on fixed-free single-walled carbon nanotube-based mass sensor, *Journal of Surface Engineered Materials and Advanced Technology*, **2**, 47–52, (2012). https://dx.doi.org/10.4236/jsemat.2012.21009

[38] Kiani, K. A meshless approach for free transverse vibration of embedded single-walled nanotubes with arbitrary boundary conditions accounting for nonlocal effect, *International Journal of Mechanical Sciences*, **52**, 1343–1356, (2010). https://dx.doi.org/10.1016/j.ijmecsci.2010.06.010

[39] Kiani, K. Vibration analysis of elastically restrained double-walled carbon nanotubes on elastic foundation subjected to axial load using nonlocal shear deformable beam theories, *International Journal of Mechanical Sciences*, **68**, 16–34, (2013). https://dx.doi.org/10.1016/j.ijmecsci.2012.11.011

[40] Kiani, K. Nanomechanical sensors based on elastically supported double-walled carbon nanotubes, *Applied Mathematics and Computation*, **270**, 216–241, (2015). https://dx.doi.org/10.1016/j.amc.2015.07.114

[41] Kiani, K., Ghaffari, H., and Mehri, B. Application of elastically supported single-walled carbon nanotubes for sensing arbitrarily attached nano-objects, *Current Applied Physics*, **13**, 107–120, (2013). https://dx.doi.org/10.1016/j.cap.2012.06.023

[42] Reddy, J. N. Nonlocal theories for bending, buckling and vibration of beams, *International Journal of Engineering Science*, **45**, 288–307, (2006). https://dx.doi.org/10.1016/j.ijengsci.2007.04.004

[43] Reddy, J. N. and Pang, S. N. Nonlocal continuum theories of beams for the analysis of carbon nanotubes, *Journal of Applied Physics*, **103**, 023511, (2008). https://dx.doi.org/10.1063/1.2833431

[44] Lee, T. W. Vibration frequencies for a uniform beam with one end spring-hinged and carrying a mass at the other free end, *ASME Journal of Applied Mechanics*, **40**, 813–815, (1973). https://dx.doi.org/10.1115/1.3423097

[45] Grant, D. A. Vibration frequencies for a uniform beam with one end elastically supported and carrying a mass at the other end, *ASME Journal of Applied Mechanics*, **42**, 878–880, (1975). https://dx.doi.org/10.1115/1.3423723

[46] Laura, P. A. A., Maurizi, M. J., and Pombo, J. L. A note on the dynamic analysis of an elastically restrained-free beam with a mass at the free end, *Journal of Sound and Vibration*, **41**, 397–405, (1975). https://dx.doi.org/10.1016/S0022-460X(75)80104-0

[47] Maurizi, M. J., Rossi, R. E., and Reyes, J. A. Vibration frequencies for a uniform beam with one end spring hinged and subjected to a translational restraint at the other end, *Journal of Sound and Vibration*, **48** (4), 565–568, (1976). https://dx.doi.org/10.1016/0022-460X(76)90559-9

[48] Laura, P. A. A., Grossi, R. O., and Alvarez, S. Transverse vibrations of a beam elastically restrained at one end and with a mass and spring at the other subjected to an axial force, *Nuclear Engineering and Design*, **74**, 299–302, (1982). https://dx.doi.org/10.1016/0029-5493(83)90068-7

[49] Zhou, D. The vibrations of a cantilever beam carrying a heavy tip mass with elastic supports, *Journal of Sound and Vibration*, **206**, 275–279, (1997). https://dx.doi.org/10.1006/jsvi.1997.1087

[50] Kahrobaiyan, M. H., Asghari, M., Rahaeifard, M., and Ahmadian, M. T. Investigation of the size-dependent dynamic characteristics of atomic force microscope microcantilevers based on the modified couple stress theory, *International Journal of Engineering Science*, **48**, 1985–1994, (2010). https://dx.doi.org/10.1016/j.ijengsci.2010.06.003

[51] Liang, L.-N., Ke, L.-L., and Wang, Y.-S. Flexural vibration of an atomic force microscope cantilever based on modified couple stress theory, *International Journal of Structural Stability and Dynamics*, **15**, 1540025, (2015). https://dx.doi.org/10.1142/S0219455415400258

[52] Basak, S., Beyder, A., Spagnoli, C., Raman, A., and Sachs, F. Hydrodynamics of torsional probes for atomic force microscopy in liquids, *Journal of Aplied Physics*, **102**, 024914, (2007). https://dx.doi.org/10.1063/1.2759197

[53] Beyder, A., Sachs, F. Micro fabricated torsion levers optimized for low force and high-frequency operation in fluids, *Ultramicroscopy*, **106**, 838–846 (2006). https://dx.doi.org/0.1016/j.ultramic.2005.11.014

[54] Magrab, B. E. *Vibrations of Elastic Systems: With Applications to MEMS and NEMS*, New York, Springer, (2012).

[55] Bokaian, A. Natural frequencies of beams under tensile axial loads, *Journal of Sound and Vibration*, **142**, 481–498, (1990). https://dx.doi.org/10.1016/0022-460X(90)90663-K

[56] Ehteshami, H. and Hajabasi, M. A. Analytical approaches for vibration analysis of multi-walled carbon nanotubes modelled as multiple nonlocal Euler beams, *Physica E*, **44**, 270–285, (2011). https://dx.doi.org/10.1016/j.physe.2011.08.023

[57] Li, X. F., Tang, G. J., Shen, Z.-B., and Lee, K. Y. Resonance frequency and mass identification of zeptogram-scale nanosensor based on nonlocal theory beam theory, *Ultrasonics*, **55**, 75–84, (2015). https://dx.doi.org/10.1016/j.ultras.2014.08.002

[58] Moutlana, M. K. and Adali, S. Vibration of a cantilever beam with extended tip mass and axial load subject to piezoelectric control, *R & D Journal of the South African Institution of Mechanical Engineering*, **31**, 60–65, (2015).

[59] Balachandran, B. and Magrab, E. B. *Vibrations*, CENGAGE Learning, Toronto, Canada, (2009).

[60] Lu, P., LEE, H. P., Lu, C., and Zhang, P. Q. Dynamic properties of flexural beams using a nonlocal elasticity model, *Journal of Applied Physics*, **99**, 073510, (2006). https://dx.doi.org/10.1063/1.2189213

[61] Azrar, A., Azrar, L., and Aljinaidi, A. A. Length scale effect analysis on vibration behaviour of single walled carbon nano tubes with arbitrary boundary conditions, *Revue de Mecanique Appliquee et Theorique*, **25**, 475–485, (2011).

[62] Lu, P. Dynamic analysis of axially pre-stressed micro/nano beam structures based on nonlocal beam theory, *Journal of Applied Physics*, **101**, 073504, (2007). https://dx.doi.org/10.1063/1.2717140

Chapter 5 – Paper 2: *Microsystem Technologies*

5.1 Fundamental frequencies of a torsional cantilever nano beam for dynamic atomic force microscopy (dAFM) in tapping mode.

In this Section, Case 2 is studied in more detail and the findings are published in *Microsystem Technologies*, Received: 15 May 2018 / Accepted: 1 October 2018.

Fundamental frequencies of a torsional cantilever nano beam for dynamic atomic force microscopy (dAFM) in tapping mode

Malesela K. Moutlana & Sarp Adali

Microsystem Technologies
Micro- and Nanosystems Information Storage and Processing Systems

ISSN 0946-7076
Volume 25
Number 3

Microsyst Technol (2019) 25:1087-1098
DOI 10.1007/s00542-018-4166-x

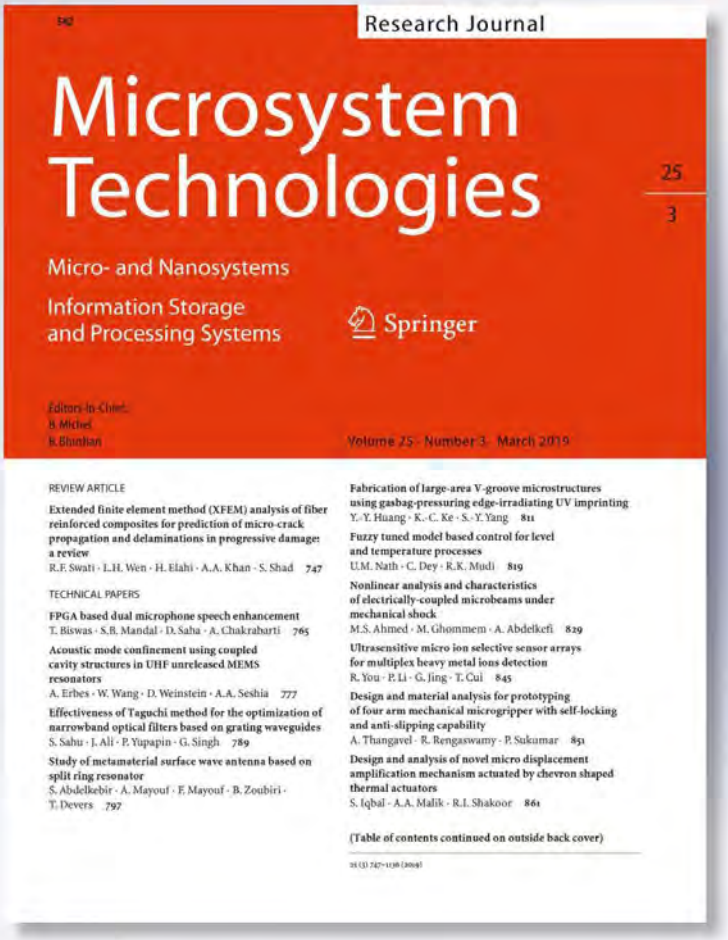

Springer

Microsystem Technologies (2019) 25:1087–1098
https://doi.org/10.1007/s00542-018-4166-x

TECHNICAL PAPER

Fundamental frequencies of a torsional cantilever nano beam for dynamic atomic force microscopy (dAFM) in tapping mode

Malesela K. Moutlana[1] · Sarp Adali[2]

Received: 15 May 2018 / Accepted: 1 October 2018 / Published online: 22 October 2018

Abstract
The aim of this investigation is to study the motion of an elastically restrained beam used in tapping mode atomic force microscopy (TM-AFM), which is to be utilized in manufacturing at nano-scale. TM-AFM uses high frequency oscillations to remove material or shape nano structures. Euler–Bernoulli theory and Eringen's theory of non-local continuum are used to model the nano machining structure composed of a nanobeam and a single degree of freedom, spring-mass system. The system is modelled as a beam with a torsional spring boundary condition that is rigidly restrained in the transverse direction at one end; and at the free end is a transverse linear spring attached to the tip. The other end of the spring is attached to a mass, resulting in a single degree of freedom spring-mass system. When the linear spring constant is infinite, the free end behaves as a beam with a concentrated tip mass. When the mass is infinite, the boundary condition is that of a linear spring. When the tip mass is zero, the configuration is that of a torsionally restrained-free beam. The motion of the tip of the beam and tip mass can be investigated to observe the tip frequency response, displacement and force. The tip displacement frequency contains information about the maximum displacement amplitude and therefore the sample penetration depth.

1 Introduction

Since the discovery of the atomic force microscope (AFM), in the late eighties by Binnig et al. (1986), its accuracy has improved with the discovery of carbon nanotubes which are used as sensor tips or fabrication tools in the form of a cantilever (Feng and Jones 2011; Sadeghi 2012). Vibrations of carbon nanotubes have been studied extensively in the last decade due to their use as sensors in a number of applications such as in atomic force microscopes (AFM), nano-resonators and biosensors (Murmu and Adhikari 2012; Shen et al. 2012; Joshi et al. 2010). AFM cantilever in transverse vibrations provides dynamic interactions with the surface of interest. In the fabrication of nano structures, high frequency oscillations of a tip mass attached to a beam is employed with the purpose of deforming or shaping a material into a desired shape (Chang et al. 2013; Liu et al. 2012; McCarthy et al. 2014). Contact forces represent the dominant component of the forces when the interaction takes place. This process is widely known as dynamic atomic force microscopy (dAFM) or tapping mode atomic force microscopy (TM-AFM) (McCarthy et al. 2014). Cantilever nanotubes are also used as biosensors and their vibration patterns are analyzed to obtain sensing data (Mehdipour et al. 2011; Shen et al. 2012). Another area where nanotubes are used is nano-resonator sensors which are based on detecting resonant frequency shifts caused by a mass attached to the nanotube tip (Wang and Arash 2014; Bichoutskaia et al. 2010). Nano-resonators improve the accuracy of the measurements by providing a high level of sensitivity as compared to conventional sensors. A review on the applications of carbon nanotubes as nano-resonator sensors is given in Wang and Arash (2014).

Vibration characteristics of nano scale beams can be analyzed by modelling them within the framework of nonlocal continuum theory (Eringen and Edelen 1972; Eringen 2002). Nonlocal theory is based on the assumption that the stress at a single point in the material is influenced by the strains of all the points in the material. This theory is widely applied to the vibration modelling of carbon nanotubes in several studies (Eltaher et al. 2013; Behera and

✉ Malesela K. Moutlana
moutlanam@dut.ac.za

Sarp Adali
ADALI@ukzn.ac.za

[1] Department of Mechanical Engineering, Durban University of Technology, Durban, South Africa

[2] Discipline of Mechanical Engineering, University of KwaZulu-Natal, Durban 4041, South Africa

Chakraverty 2014; Eltaher et al. 2016; Ansari et al. 2012; Rahmanian et al. 2016; Rosa and Lippiello 2016), and in particular, vibrations of carbon nanotubes with a tip mass have been studied extensively due to their use in sensor applications (Mehdipour et al. 2011; Shen et al. 2012; Wang and Arash 2014; Bichoutskaia et al. 2010; Lu et al. 2017; Elishakoff et al. 2011; Horng 2012). In these studies the flexibility of the boundaries are not taken into account and the classical boundary conditions are considered. A number of studies relating to the vibrations of nanotubes with elastically restrained boundaries have been conducted in literature (Kiani 2013, 2015; Kiani et al. 2013). Most of these studies are based on single degree freedom systems in transverse vibration at micro or macro scale. In the present study, the work of the above mentioned researchers is extended by adding a single degree of freedom (SDOF) spring-mass system to the tip of an infinite degree of freedom nanobeam.

The present study extends the results of previous research to the case of a nanobeam with a spring-mass system attached to the free end. In the current investigation, an elastically restrained nanobeam with a tip mass is modelled using Euler–Bernoulli beam theory (EBT) based on the nonlocal theory (Eringen and Edelen 1972; Eringen 2002) and Eringen's theory of non-local continuum is used to take into account the small scale effects (Reddy 2006; Reddy and Pang 2008). Several beam theories have been proposed to solve problems dealing with non-local continuum which are underpinned by Eringen's theory which provides a unified foundation for field equations of non-local continuum (Eltaher et al. 2016). Timeshenko beam theory (TBT), Reddy beam theory (RBT) and Levinson beam theory (LBT) have been applied in deriving the equations of motion from the principle of virtual displacements. EBT presents the simplest forms of the equations of motion. TBT requires that one chooses the shear correction factor to correct an error in the assumption that the shear stresses are constant in the transverse direction. In higher order theories (i.e., RBT and LBT) the transverse strains vanish at the bottom and top surfaces as required. All these theories above will produce similar results for the natural frequencies of beams with high aspect ratio (L/h) and when the aspect ratio (L/h) is small, TBT, RBT and LBT produce similar results, while EBT tends to underestimate the natural frequencies of vibration. Gradient theories tend to predict a stiffer response compared to classic theories (Reddy 2006).

Ansari et al. (2012) presented an investigation of stress gradient elasticity theory (i.e. nonlocal elasticity theory), strain gradient elasticity theory and combined strain-inertia gradient elasticity theory, in which they compared the results of the above mentioned theories to molecular dynamics (MD) simulations. Stress gradient elasticity theory includes nonlocal first order stresses but does not account for non-locality of higher-order stresses and strain gradient elasticity theory accounts only for local higher order strain gradients and no non-local effects are considered (Lu et al. 2017). Strain-inertia elasticity theory takes strain gradients and inertia gradients into account and therefore utilizes two length scale parameters for material strain and inertia. In the above investigations (Ansari et al. 2012; Lu et al. 2017; Reddy 2006) it was concluded that Euler–Bernoulli beam theory (EBT) produces similar results to all the theories mentioned above for slender beams or beams with high aspect ratio ($L/h > 15$).

The restraint at one support is specified as a torsional spring which replaces the 'ideal' clamped end boundary condition used in a number of studies. A translational spring is attached to the other end where a tip mass is attached to form a spring-mass system. The governing differential equations of motion are solved analytically using separation of variables to compute the vibration frequencies. The effects of the elastic restraints, tip mass and the small-scale parameter on the frequencies are investigated numerically. Similar problems have been solved in the case of beams based on the local (classical) theory of elasticity where size effects are not taken into account. Elastically supported beams with a tip mass have been studied in Lee (1973), Grant (1975), Laura et al. (1975), and Gürgöze (1996) and the beam with torsional and translational springs with a tip mass has been studied in Balachandran and Magrab (2009), Azrar et al. (2011), and Yayli (2016, 2018a, b, c) based on the classic theory of Euler–Bernoulli beams. Gürgöze (1996) has investigated the frequencies of vibration for such a system using the Dunkerley-based approximations for the fundamental frequencies and the results are in agreement with the results obtained in this study. The present model makes a huge improvement on the model proposed by Gürgöze (1996) by having a torsional elastic support and incorporating non-local continuum theories to determine the natural frequencies at nano scale.

Many research papers have been published on the modelling of TM-AFM as a clamped-free beam in which case the clamped end can be considered 'ideal' (Liu et al. 2012; Yayli 2018c; Laura et al. 1982; Magrab 2012; Hozhabrossadati 2015; Liang et al. 2015). In the present study the clamped end contains a torsional spring and this type of boundary condition is commonly referred to as a torsional cantilever (Basak et al. 2007; Beyder and Frederick Sachs 2006). This represents a more 'realistic' boundary condition allowing for flexibility at the built-in boundary. In TM-AFM, the free end carries a fabrication/cutting tool which is modelled as concentrated mass such that the centre of the mass of the tool coincides with the sharp end of the cutting tool and the tip of the beam. In

the current model a translational linear spring is attached to the tip of the beam with the spring a mass is attached. The spring-mass system behaves like a forcing function at the tip of the beam as the nanobeam and the spring mass system are coupled and vice verse.

2 Elastically restrained nanobeam with a single degree of freedom system at $x = L$

The beam under consideration is restrained by a torsional spring with a spring constant k_1 at $x = 0$ which provides a flexible restraint as shown in Fig. 1 instead of a clamped boundary. Attached to the free end of the beam at $x = L$ is a machining tool which can be modelled as a concentrated mass with a sharp tip. It is attached to the beam by means of a linear spring having a spring constant k_2 and the centre of gravity of the tip mass coincides with the end of the beam (Fig. 1). This constitutes a single degree of freedom spring-mass system at the tip of the beam, at $x = L$. The spring-mass system is excited by the motion of the tip of the nanobeam. During the machining process, a contact force is generated between the tip mass and the object to be shaped.

The constitutive equation relating the stress (σ_{xx}) to strain (ε_{xx}) based on the nonlocal theory of elasticity can be expressed as

$$\sigma_{xx} - \bar{\mu}\frac{\partial^2 \sigma_{xx}}{\partial x^2} = E\varepsilon_{xx} \tag{1}$$

where E is the Young's modulus, $\bar{\mu} = e_0 l_i$ is the small scale parameter with e_0 denoting a material constant and l_i the characteristic length. The expression for moment $M(x)$ is given by

$$M(x) - \bar{\mu}\frac{\partial^2 M(x)}{\partial x^2} = -EI\frac{\partial^2 w(x,t)}{\partial x^2} \tag{2}$$

where I is the moment of inertia. The equation of motion for a nonlocal nanobeam undergoing transverse bending vibrations is given in Reddy (2006), and Magrab (2012) and can be expressed as

$$EI\frac{\partial^4 w(x,t)}{\partial x^4} - \bar{\mu}^2\rho A\frac{\partial^2 w(x,t)}{\partial x^2} + \rho A\frac{\partial^2 w(x,t)}{\partial t^2} - \frac{k_2}{L}[w(L,t) - z(L,t)]\delta(x-L) = F_0(x) \tag{3a}$$

where $w(x,t)$ represents the transverse motion of the beam and $z(L,t)$ the motion of the tip mass at $x = L$ along the length of the beam. The boundary conditions at the free end are expressed as

$$EI\frac{\partial^2 w(L,t)}{\partial x^2} + \bar{\mu}^2\rho A w(L,t) = 0 \text{ and } EI\frac{\partial^3 w(L,t)}{\partial x^3} - \bar{\mu}^2\rho A\frac{\partial w^3(L,t)}{\partial x \partial t^2} = 0. \tag{3b}$$

The last two terms of the left-hand-side (LHS) of Eq. (3a) represent an impulse response which can be include in the equation of motion using a step function or a Dirac delta function, in which case the boundary conditions at the free end are simplified to that of an ordinary cantilever nanobeam (McCarthy et al. 2014; Magrab 2012) i.e. moment and shear are zero, see Eq. (3b). Equation (3a) allows us to include the spring-mass system at any position along the beam by choosing the displacement terms $w(x,t)$ and the spring compression/extension parameter between $x = 0$ and $x = L$. When the effect of the spring mass system is considered in the free end boundary, the last two terms on the LHS of Eq. (3a) are not included and the equation of motion can be represented in Eq. (4a) and the spring mass system is considered in the boundary conditions (Hozhabrossadati 2015).

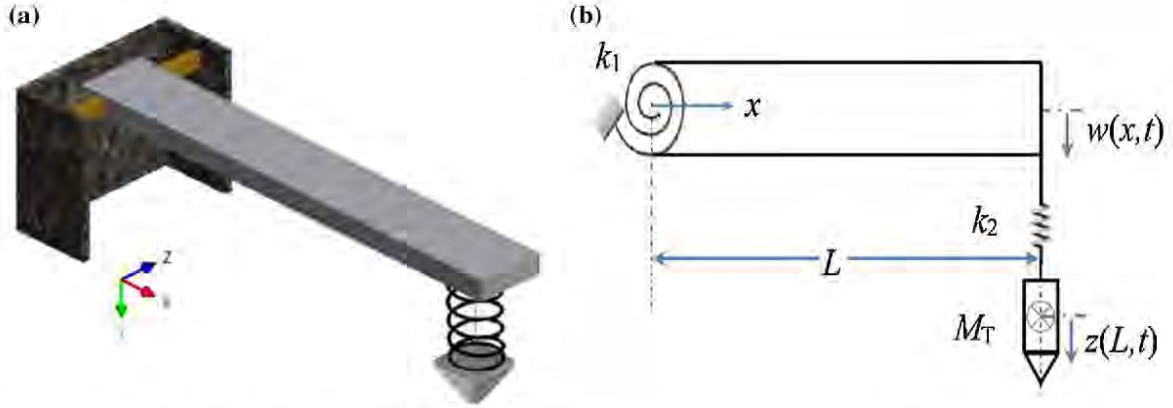

Fig. 1 Geometry of the elastically restrained nanobeam with concentrated mass and linear spring at the free end

$$EI\frac{\partial^4 w(x,t)}{\partial x^4} - \bar{\mu}^2\rho A\frac{\partial^2 w(x,t)}{\partial x^2} + \rho A\frac{\partial^2 w(x,t)}{\partial t^2} = F_0(x) \tag{4a}$$

$$M_T\frac{d^2 z(L,t)}{dt^2} + k_2 z(L,t) = k_2 w(L,t) \tag{4b}$$

where ρ is the density, A is the cross-sectional area and $F_0(x)$ is the forcing function which is taken as $F_0(x) = 0$ for a freely vibrating beam. The transverse motion of the tip mass is described by $z(L,t)$ where $x = L$ is the coordinate along the length of the beam. The dynamic motion of the tip mass denoted by M_T is expressed in Eq. (4b) and the two Eqs. (4a) and (4b) are coupled through the motion of the tip $w(L,t)$. In the present study the vibration problem is solved by using the formulation given in Eqs. (4a) and (4b).

3 Method of solution

Solution of the governing Eqs. (3a) and (4a) is obtained by eigenfunction expansion of the displacement function as shown in Eqs. (5a)–(5c) where $X_n(L)$ represents the modal domain on the beam and $Z_n(L)$ the transverse compression/extension of the spring associated with the mode of vibration of the beam. $T_n(t)$ represents the temporal domain of the eigen expansion series.

$$w(x,t) = \sum_{n-1}^{\infty} X_n(x)\,T_n(t) \tag{5a}$$

$$z(L,t) = \sum_{n-1}^{\infty} Z_n(L)T_n(t) \tag{5b}$$

$$T_n(t) + \omega_n^2 T_n(t) = 0. \tag{5c}$$

Inserting Eqs. (5a) into (3a) and after rearrangement, we obtain the differential equation of motion for the beam in the modal domain given by Eqs. (6a) and (6b) when the spring-mass system is not included in the equation of motion, but included in the boundary conditions. After inserting Eqs. (5b) into (4b) and rearrangement, we obtain the equation of motion of the tip mass in the modal domain given in Eq. (7), viz.

$$X_n^{iv}(x) + \mu^2 a_n^4 X_n''(x) + \frac{\kappa_2}{L}[Z_n(L) - a_n^4 X_n(x)]\delta(x-L) = 0 \tag{6a}$$

$$X_n^{iv}(x) + \mu^2 a_n^4 X_n''(x) = 0 \tag{6b}$$

$$Z_n(L) = X_n(L)\left(\frac{a_k^4}{a_k^4 - a_n^4}\right) \tag{7}$$

where $\mu = \left(\frac{\mu}{l_i}\right)^2 L^2$ and ω_n is the natural frequency for the nth mode of vibration. The non-dimensional frequency parameter a_n for the beam and the non-dimensional frequency parameter a_k for the single degree freedom spring mass system are defined as

$$a_n^4 = \frac{\rho A\omega_n^2}{EI} \tag{8a}$$

$$a_k^4 = \frac{\kappa_2}{\eta} \tag{8b}$$

where $\kappa_2 = \frac{k_2}{EI}$, $\eta = \frac{M_T L}{\rho A}$. The general solutions of Eqs. (6a, 6b) is given by

$$X_n(x) = A_n\cos p_{2n}x + B_n\sin p_{2n}x + C_n\cosh p_{1n}x + D_n\sinh p_{1n}x \tag{9}$$

where p_{1n} and p_{2n} are defined as

$$p_{1n,2n} = a_n\sqrt{\frac{a_n^6\bar{\mu}^2 \pm \sqrt{a_n^4\bar{\mu}^2 + 4}}{2}}. \tag{10}$$

The constants A_n, B_n, C_n and D_n in Eq. (9) are determined from the boundary conditions. The boundary conditions at $x = 0$ are zero displacement and zero moment, and can be expressed as

$$w(0,t) = 0 \tag{11a}$$

$$EI\frac{\partial^2 w(0,t)}{\partial x^2} - \bar{\mu}^2\rho A\frac{\partial^2 w(0,t)}{\partial t^2} - k_1\frac{\partial w(0,t)}{\partial x} = 0. \tag{11b}$$

For a beam with a tip mass M_T, the centre of gravity of the mass is located at $x = L$. At the free end $x = L$, taking into account the small scale effect, the tip mass and the linear spring, the moment and shear boundary conditions at can be expressed as

$$EI\frac{\partial^2 w(L,t)}{\partial x^2} + \bar{\mu}^2\rho A w(L,t) = 0 \tag{12a}$$

$$EI\frac{\partial^3 w(L,t)}{\partial x^3} - \bar{\mu}^2\rho A\frac{\partial w^3(L,t)}{\partial x\partial t^2} = F_L(L,t) \tag{12b}$$

where $F_L(L,t)$ is the transverse force due to the linear spring at $x = L$,

$$F_L(L,t) = k_2 z(L,t)$$

and $z(L,t)$ is expressed in Eq. (5b). The eigenfunction expansions at $x = 0$ and $x = L$ are given by

$$w(0,t) = \sum_{n=1}^{\infty} X_n(0)\,T_n(t) \quad w(L,t) = \sum_{n=1}^{\infty} X_n(L)\,T_n(t). \tag{13}$$

By substituting $w(0,t)$ given by Eq. (13) into the boundary conditions (11a) and (11b) at $x = 0$, we obtain

$$X_n(0) = 0 \tag{14a}$$

$$X_n''(0) + \mu^2 a_n^4 X_n(0) - \kappa_1 X_n'(0) = 0 \tag{14b}$$

where $\kappa_1 = \frac{k_1 L}{EI}$. Substituting $w(L,t)$ in Eqs. (13) into (12a)

and (12b), moment and shear force expressions at the boundary $x = L$ are obtained as

$$X_n''(L) + \mu^2 a_n^4 X_n(L) = 0 \tag{15a}$$

$$X_n'''(L) + \mu^2 a_n^4 X_n'(L) + \eta a_n^4 Z_n(L) = 0. \tag{15b}$$

Substitution of Eq. (9) into the boundary condition (14a) gives

$$A_n + C_n = 0. \tag{16}$$

The general solution (9) can now be expressed as

$$X_n(x) = D_n \sinh p_{1n}x - B_n \sin p_{2n}x + (\cos p_{2n}x - \cosh p_{1n}x)C_n. \tag{17}$$

Substituting Eqs. (17) into (14b) gives

$$\kappa_1 p_1 D_n - (p_{2n}^2 + p_{1n}^2) C_n + \kappa_1 p_{2n} B_n = 0. \tag{18}$$

Solving for B_n in Eq. (18) and substituting into (17) gives, the general solution can be obtained in terms of constants C_n and D_n as

$$X_n(x) = -\left(\sinh p_{1n}x + \frac{p_{1n}}{p_{2n}} \sin p_{2n}x\right) D_n + \left(\frac{p_{2n} \sin p_{2n}x}{\kappa_1} + \frac{p_{1n}^2 \sin p_{2n}x}{\kappa_1 p_{2n}}\right) C_n - (\cos p_{2n}x - \cosh p_{1n}x)C_n. \tag{19}$$

This result can be substituted into the moment boundary condition (15a) at $x = L$ to obtain

$$C_n \cdot \Gamma_{1n} + D_n \cdot \Gamma_{2n} = 0 \tag{20}$$

where

$$\Gamma_{1n} = \left(\left(p_{2n}^2 + p_{1n}^2\right) a_n^4 \sin p_{2n}L - \kappa_1 p_{2n} a_n^4 \cos p_{2n}L + \kappa_1 p_{2n} a_n^4 \cosh p_{1n}L\right)\mu + \left(p_{2n}^4 + p_{1n}^2 p_{2n}^2\right) \sin p_{2n}L - \kappa_1 p_{2n}^3 \cos p_{2n}L - \kappa_1 p_{1n}^2 p_{2n} \cosh p_{1n}L$$

$$\Gamma_{2n} = \kappa_1 \left(p_{1n} a_n^4 \sin p_{2n}L - p_{2n} a_n^4 \sinh p_{1n}L\right)\mu + \kappa_1 p_{1n} p_{2n}^2 \sin p_{2n}L + \kappa_1 p_{1n}^2 p_{2n} \sinh p_{1n}L.$$

After substituting Eqs. (7) and (19) into the shear boundary condition (15b) at $x = L$, the result can be expressed as

$$C_n \cdot \Gamma_{3n} + D_n \cdot \Gamma_{4n} = 0 \tag{21}$$

where

$$\Gamma_{3n} = \left[\left(\kappa_1 p_{2n}^2 a_n^8 - \kappa_1 p_{2n}^2 a_k^4 a_n^4\right) \sin p_{2n}L + \left(\kappa_1 p_{1n} p_{2n} a_n^8 - \kappa_1 p_{1n} p_{2n} a_k^4 a_n^4\right) \sinh p_{1n}L\right]\mu + \left[\left(\left(p_{2n}^3 + p_{1n}^2 p_{2n}\right) a_n^8 + \left(-p_{2n}^3 - p_{1n}^2 p_{2n}\right) a_k^4 a_n^4\right) \cos p_{2n}L\right]\mu + \left[\left(\left(-p_{2n}^2 - p_{1n}^2\right)\eta a_k^4 - \kappa_1 p_{2n}^4\right) a_n^4 + \kappa_1 p_{2n}^4 a_k^4\right] \sin p_{2n}L + \left[\left(\kappa_1 p_{2n} \eta a_k^4 - p_{2n}^5 - p_{1n}^2 p_{2n}^3\right) a_n^4 + \left(p_{2n}^5 + p_{1n}^2 p_{2n}^3\right) a_k^4\right] \cos p_{2n}L + \left(\kappa_1 p_{1n}^3 p_{2n} a_n^8 - \kappa_1 p_{1n}^3 p_{2n} a_k^4\right) \sinh p_{1n}L - \kappa_1 p_{2n} \eta a_k^4 a_n^4 \cosh p_{1n}L$$

and

$$\Gamma_{4n} = \left[\left(\kappa_1 p_{1n} p_{2n} a_n^8 - \kappa_1 p_{1n} p_{2n} a_k^4 a_n^4\right) \cos p_{2n}L + \left(\kappa_1 p_{1n} p_{2n} a_k^4 a_n^4 - \kappa_1 p_{1n} p_{2n} a_n^8\right) \cosh p_{1n}L\right]\mu - \kappa_1 p_{1n} \eta a_k^4 a_n^4 \sin p_{2n}L + \kappa_1 p_{2n} \eta a_k^4 a_n^4 \sinh p_{1n}L + \left(\kappa_1 p_{1n} p_{2n}^3 a_k^4 - \kappa_1 p_{1n} p_{2n}^3 a_n^4\right) \cos p_{2n}L + \left(\kappa_1 p_{1n}^3 p_{2n} a_k^4 - \kappa_1 p_{1n}^3 p_{2n} a_n^4\right) \cosh p_{1n}L.$$

The results from the moment and shear boundary conditions given in Eqs. (20) and (21) can be expressed in matrix form as

$$\begin{bmatrix} \Gamma_{1n} & \Gamma_{2n} \\ \Gamma_{3n} & \Gamma_{4n} \end{bmatrix} \begin{bmatrix} C_n \\ D_n \end{bmatrix} = \begin{bmatrix} 0 \\ 0 \end{bmatrix} \tag{22}$$

and the characteristic equation can be obtained from the determinant of Eq. (22) as

$$\Gamma_{1n}\Gamma_{4n} - \Gamma_{2n}\Gamma_{3n} = 0. \tag{23}$$

The characteristic Eq. (23) can be solved numerically to compute the roots to determine the eigenfrequencies. For the cases of infinite torsional spring constant at $x = 0$, zero tip mass ($\eta = 0$), zero linear spring constant ($\kappa_2 = 0$) at $x = L$, and zero small scale parameter ($\mu = 0$), Eq. (23) reduces to the frequency equation of a classical cantilever given in Balachandran and Magrab (2009) and Magrab (2012), i.e.,

$$1 + \cos a_n L \cosh a_n L = 0. \tag{24}$$

4 Numerical results

The numerical solution for the roots of Eq. (23) yields the eigenvalues which are associated with the natural frequencies of the system shown in Fig. 2. The natural frequencies of the system R_n are obtained by making a substitution, $a_n = R_n/L$, into the into Eq. (23). The values of R_n are dimensionless natural frequencies used below to analyze the numerical results. The system under consideration shown in Fig. 1 shows that the tip mass M_T is attached to the tip of the beam through a linear spring. The deformation of the spring depends on the presence of a tip mass and its magnitude. If the tip mass is removed and the tip mass ratio is zero, the spring will not deform and therefore the spring will not have an effect on the natural frequencies of the system. If the tip mass ratio is zero, we note that in Eq. (15b) the third term in the shear boundary condition disappears and by extension, the frequency parameter (a_k), contained in $Z_n(L)$vanishes and therefore the single degree of freedom systems has no effect on the vibrations of the beam. The first two terms of the Eq. (15b) represent the shear boundary condition of a nano cantilever beam. From these observations, we can conclude that the beam behaves in a similar manner to a torsionally clamped

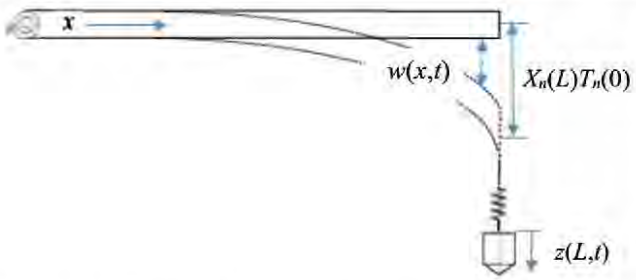

Fig. 2 Deflection of a nanobeam with linear spring and mass at the free end

beam or a cantilever beam when the torsional spring constant approaches infinity ($\kappa_1 \to \infty$).

From Eq. (8b) it is noted that if the mass approaches zero in the limit ($\eta \to 0$) the frequency parameter for the spring-mass system approaches infinity ($a_k^4 \to \infty$) and furthermore, in Eq. (7), the ratio of the frequency parameter of the beam and the spring-mass system approaches zero($a_n^4/a_k^4 \to 0$). Therefore the ratio of the displacement of the point of attachment of the mass (z_0) and the displacement of the tip of the beam $X_n(L)$ approaches unity ($Z_n(L)/X_n(L) \to 1$) when the tip mass approaches zero($\eta \to 0$) in the limit. This means that the tip of the beam moves in-sync with the spring displacement. The literature on the behaviour of these types of beams is published in Gürgöze (1996), Yayli (2016, 2018a, b, c), and Laura et al. (1982). For meaningful results in the context of this investigation, the tip mass will be taken to be non-zero (η = 0.1, 0.5 and 1), representing 10, 50 and 100% the mass of the nano beam, respectively.

When $\kappa_1 \to \infty$ the torsional spring becomes rigid and the boundary condition behaves like that of a cantilevered beam. The classic cantilever configuration can be obtained by setting the mass to zero ($\eta = 0$) and the fundamental natural frequency of the system is $R_1 = 1.8750$ which corresponds to the results obtained by Magrab (2012) $R_1 = 0.5969\pi$.

Furthermore, when $k_2 \to \infty$ the linear spring is rigid and the system behaves like a cantilever beam with a concentrated tip mass because the centre of gravity of the attached mass coincides with the tip of the beam.

For a tip mass ratio $\eta = 0.1$ and $\eta = 1$ the fundamental natural frequencies are $R_1 = 1.7227$ and $R_1 = 1.2479$ which are the same result obtained by Gürgöze ($R_1 = 1.2479$) and Magrab ($R_1 = 0.5484\pi$), respectively (Gürgöze 1996; Magrab 2012). The boundary conditions for upper and lower limits of the system parameters are shown in Table 1. In practical applications, the values for the parameters of interest will vary between zero and infinity($0 < \kappa_1, \kappa_2, \eta < \infty$).

Table 1 Classical boundary condition derived from the system

Boundary conditions	κ_1	κ_2	η
Clamped-free	∞	0 or ∞	0
Simply supported-free	0	0 or ∞	0
Simply supported-simply supported	0	∞	∞
Clamped-simply supported	∞	∞	∞

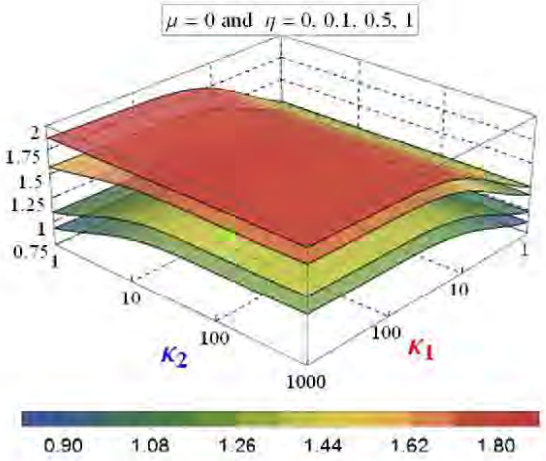

Fig. 3 Fundamental frequency plotted against spring constants κ_1 and κ_2 with small scale parameter $\mu = 0$ and varying tip mass ratio η

Figure 3 shows the natural frequencies for varying torsional and linear spring whilst the tip mass fluctuates between zero and unity. The contour plots are plotted for differing tip mass ratio, where the top 1st (Fig. 4a) contour represents zero tip mass ratio ($\eta = 0$) and the 2nd (Fig. 4b), 3rd (Fig. 4c) and 4th (Fig. 4d) contour from the top represents $\eta = 0.1$, 0.5 and 1, respectively. As expected, the frequencies of vibration will decrease as the tip mass ratio increases if all the other parameters are kept constant (Li et al. 2015; Dowell 1979). The boundary conditions discussed above relate to extreme rigidity of the torsional and linear spring. The results show that the when the torsional spring is completely elastic ($k_1 \to 0$) the fundamental natural frequencies approach zero in the limit ($R_1 \to 0$) and the other variables have minimal effect on the frequencies. Therefore the fundamental frequencies for completely elastics torsional spring ($k_1 \to 0$) and linear spring ($\kappa_2 \to 0$) will be observed only, but additional attention will be given to spring constant ratios between zero and infinity($0 < \kappa_1, \kappa_2 < \infty$).

For intermediate values of the spring constants (κ_1, κ_2 = 1, 10, 100) the solution generated in this investigation can be readily verified for $\kappa_1 \to \infty$, $\kappa_2 \to 10$ and $\eta \to 1$. The fundamental frequency for this set of parameters is $R_1 = 1.1914$ which is reported by Hozhabrossadati (2015).

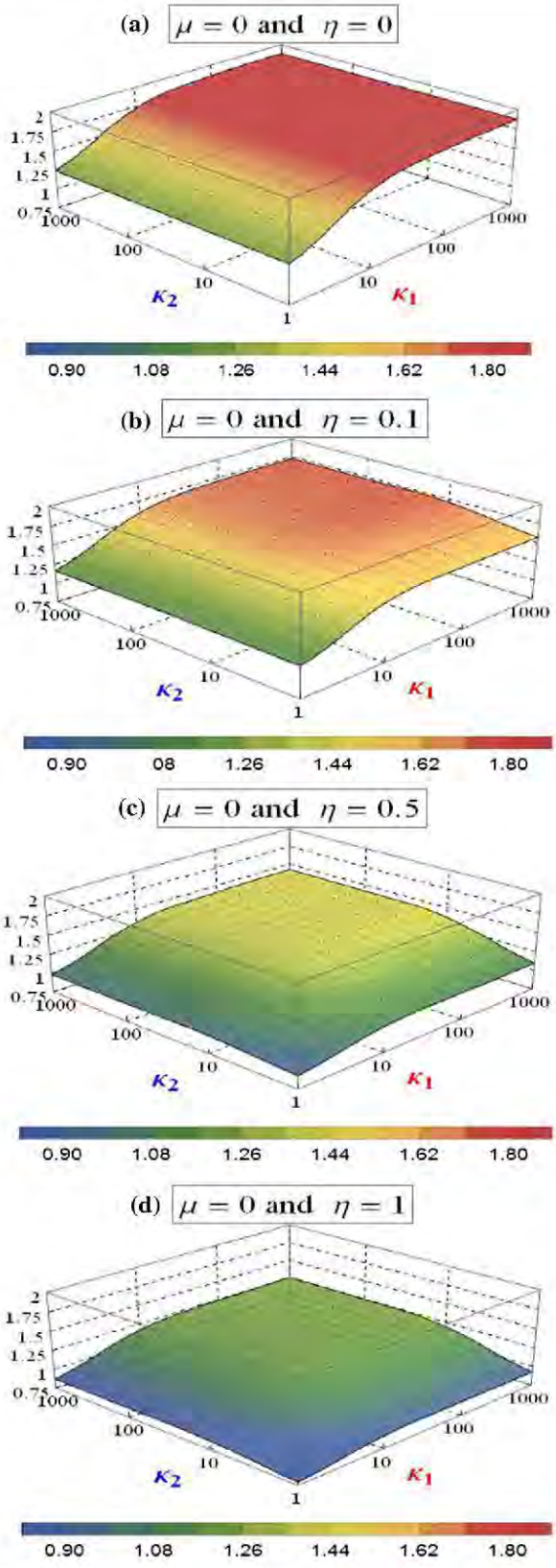

Fig. 4 Frequency for spring constants κ_1 and κ_2 with small scale parameter $\mu = 0$: **a** $\eta = 0$, **b** $\eta = 0.1$, **c** $\eta = 0.5$ and **d** $\eta = 1$

When the system is elastically restrained at $x = 0$ with $\kappa_1 = 10$, $\kappa_2 = 10$ and $\eta = 1$the fundamental natural frequency is $R_1 = 1.1240$ which can be verified by Hozhabrossadati (2015). By and large, the solution generated in this investigation will accurately yield the fundamental frequencies of the system in Fig. 1, using classic continuum theory, when small scale parameter is set to zero ($\mu = 0$) in the present solution.

If $\kappa_1 \to \infty$ and tip mass ratio $\eta \to 0$ the beam behaves like a cantilevered beam and the results for the natural frequencies have been published by Lu et al. (2006), Lu (2007), Azrar et al. (2011) and Li et al. (2015); for the values for small scale parameter, μ = 0, 0.2, 0.4 and 0.6 and these are R_1 = 1.875, 1.8919, 1.9543 and 2.1989, respectively. This model makes an improvement to the models presented by the above researchers by allowing the torsional rigidity at $x = 0$ to vary between spring ratios of zero$\kappa_1 = 0$ and infinity $\kappa_1 = \infty$. Similar results are obtained using the present solution. Furthermore, Li et al. (2015) studied a cantilever beam with concentrated tip mass of $\eta = 0.5$ and obtained a fundamental frequency of R_1 = 1.4200, 1.4253, 1.4427 and 1.4778 for small scale parameter μ = 0, 0.2, 0.4 and 0.6, respectively.

Figure 5 shows the fundamental frequencies for tip mass ratio $\eta = 0.1$ and varying small scale parameter. The contour plots are plotted for differing torsional and linear spring ratio in Fig. 6a–d for varying small scale parameter.

The bottom 1st (Fig. 6a) contour represents zero small scale parameter ($\mu = 0$); and the 2nd (Fig. 6b), 3rd (Fig. 6c) and 4th (Fig. 6d) contour from the bottom represents $\mu = 0.2$, 0.4 and 0.6, respectively. When we consider that the parameters are selected such that the system behaves like a cantilevered beam the percentage difference in the fundamental frequency for $\mu = 0$ and $\mu = 0.2$ is minimal at approximately 0.9%.

This difference increases dramatically between small scale parameter of $\mu = 0.4$ and $\mu = 0.6$ to approximately 12%. Form the data above, a similar trend is observed when mass ($\eta = 0.5$) is rigidly attached ($\kappa_2 \to \infty$) to the tip of the beam and the percentage difference is approximately 0.4% for $\mu = 0$ and $\mu = 0.2$; and 2.5% for $\mu = 0.4$ and $\mu = 0.6$. In Fig. 5 we observed that the 1st and 2nd contour almost overlap and a small change in the fundamental frequencies is noted due to the above mentioned consideration. Figure 6a, b show the separated contour plots. It is again noted in Fig. 6d that the highest fundamental frequencies occurs for maximum small scale parameter $\mu = 0.6$ and at maximum spring ratio constant ($\kappa_1 \to \infty, \kappa_2 \to \infty$).

The noteworthy difference between the model in the present investigation and the model by Li et al. (2015) is that in the present model, the tip mass is elastically supported by a linear spring and therefore allowed to move

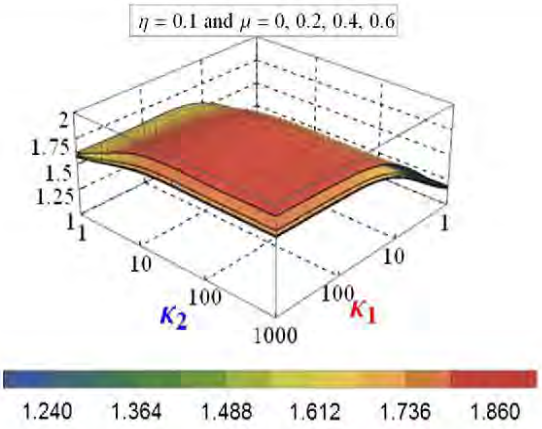

Fig. 5 Fundamental frequency plotted against spring constants κ_1 and κ_2 with tip mass ratio $\eta = 0.1$ for varying small scale parameter (μ)

relative to the tip of the beam. The present model allows us to compare the present results with that of Li et al. (2015) by setting the linear spring constant to infinity ($\kappa_2 \to \infty$). Yayli (2016, 2018a) investigated a nano beam with concentrated mass ($\eta = 1$) using Stoke's transformations and attained the fundamental frequencies: R_1 = 1.2530 and 1.2630 for small scale parameter, μ = 0.2 and 0.4. In the present study, the values for fundamental frequency obtained are R_1 = 1.2508 and 1.2600 using non-local Euler–Bernoulli theory. The results from the two models mentioned above are similar to within 0.5%.

The intermediate values for torsional and linear spring constant are plotted in Figs. 3 and 5 and when the spring constants are kept constant in order to determine the effects of the small scale parameter in combination with the tip mass, the results are shown in Fig. 7 below.

In his investigation, Gürgöze (1996) determined the natural frequencies for a cantilevered beam with $\eta = 1$ and $\kappa_2 = 1$, with small scale parameters neglected, to be $R_1^2 = 0.8409$ and in the present study, the results show that the fundamental natural frequency is $R_1 = 0.9270$ which represent a percentage difference of $\approx$ 1%. In the context of the present model, the torsional spring constant ratio at $x = 0$ is considered extremely large ($\kappa_1 = 1000$); and at $x = L$ the linear spring constant is unity ($\kappa_2 = 1$) and this is demonstrated in Fig. 7 element (2,3) and Table 2. In Fig. 7, the first row of plots represent a lightly restrained beam ($\kappa_1 = 1$) and a cantilevered beam ($\kappa_1 = 1000$) for linear spring constant of $\kappa_2 = 1$ and 1000, element (1,2) and (1,3), respectively. The first column of plots represent a lightly restrained tip mass ($\kappa_2 = 1$) and a ridigly restrained tip mass ($\kappa_2 = 1000$) for torsional spring constants of $\kappa_1 = 1$ and 1000, element (2,1) and (3,1), respectively. Element (2,2) and (3, 2) are combined in element (1,2) and element (2,3) and (3,3) are a combination of element (1,3), and that represents the columns. The rows are arranged such that,

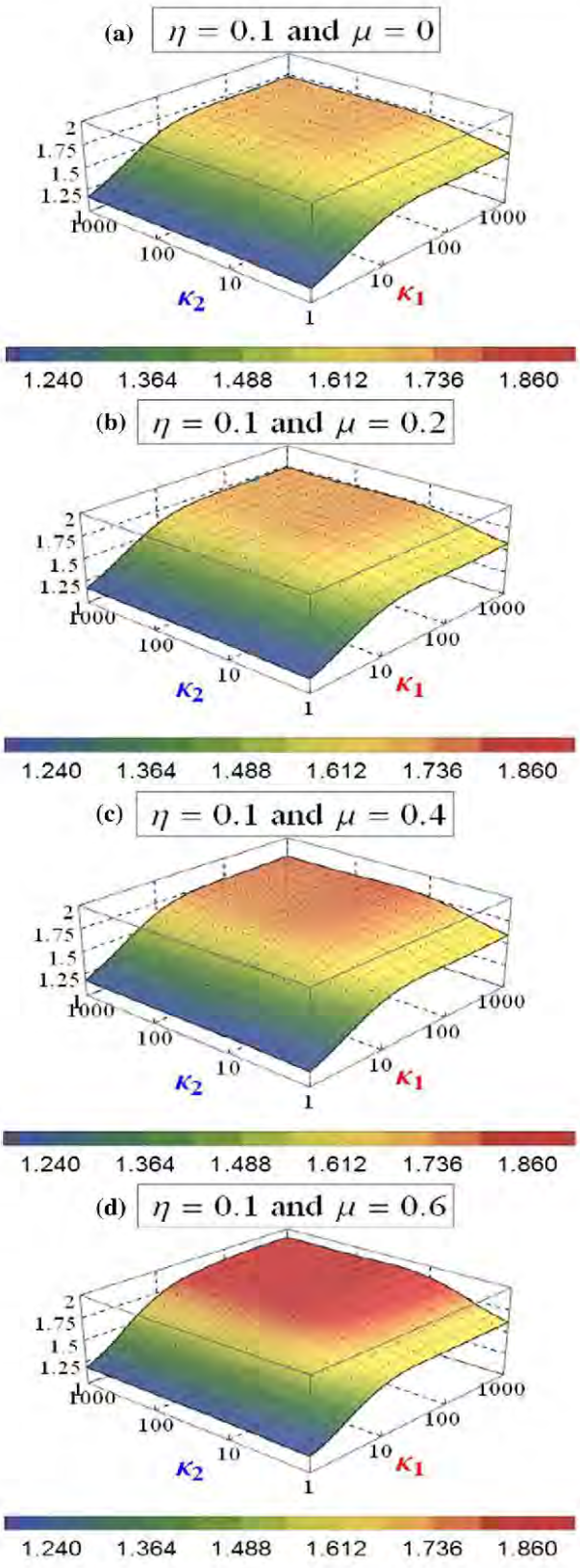

Fig. 6 Frequency for spring constants κ_1 and κ_2 with tip mass ratio $\eta = 0.1$: **a** $\mu = 0$, **b** $\mu = 0.2$, **c** $\mu = 0.4$ and **d** $\mu = 0.6$.

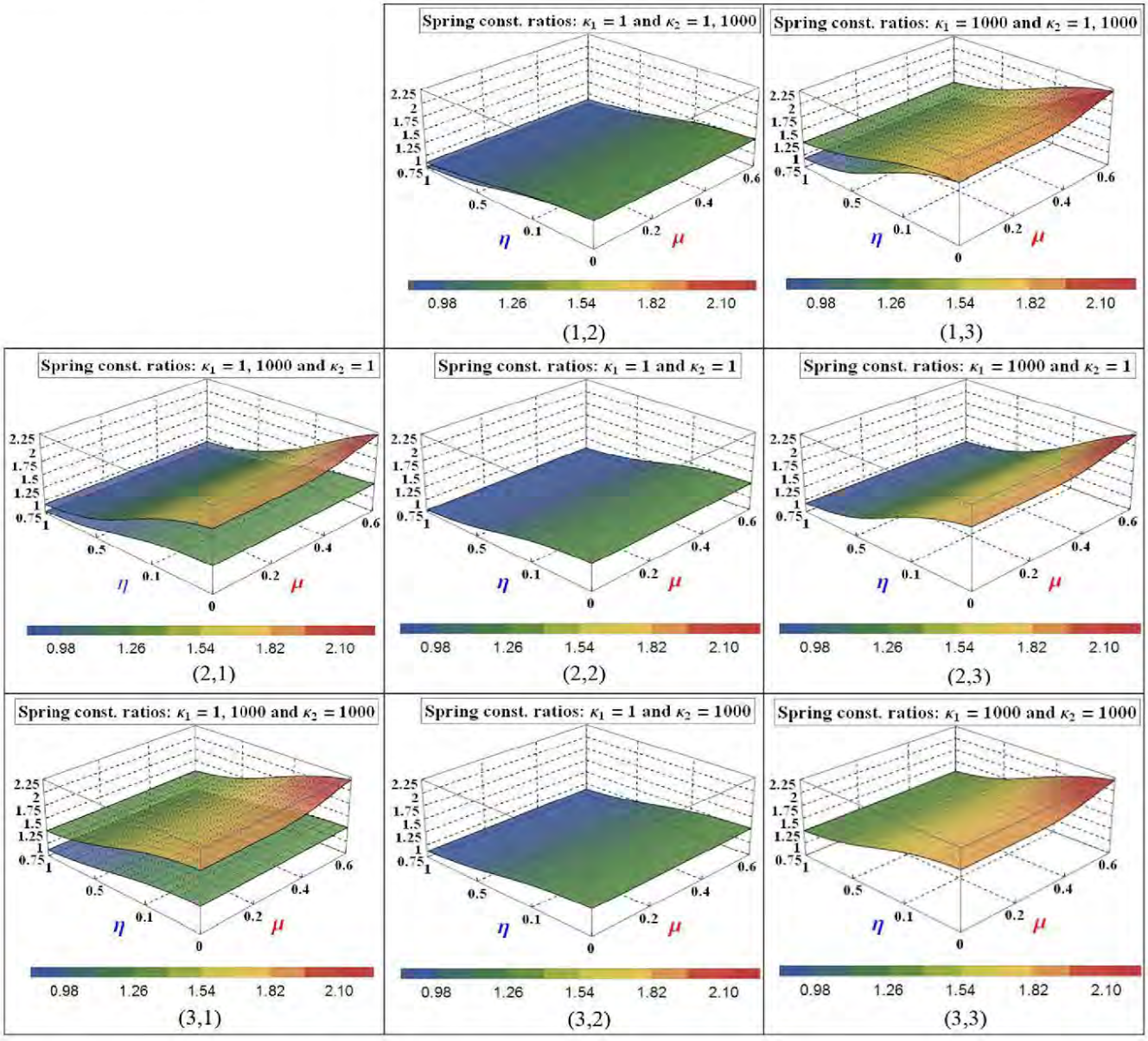

Fig. 7 Fundamental frequency plotted for varying tip mass ratio (η) and small scale parameter(μ)for spring constants $\kappa_1 = 1$, 1000 and $\kappa_2 = 1$, 1000

Table 2 Fundamental frequencies for elastic boundary conditions, varying tip mass (η) and small scale (μ) parameter for the system

		$\mu = 0$		$\mu = 0.6$	
κ_1	κ_2	$\eta = 0$	$\eta = 1$	$\eta = 0$	$\eta = 1$
1	1	1.2479	0.7890	1.2769	0.7910
1	10^3	1.2479	1.2769	0.8705	0.8770
10^3	1	1.8750	0.9270	2.1989	0.9290
10^3	10^3	1.8750	1.2479	2.1989	1.2769

element (2,1) is a combination of elements (2,2) and (2,3) and element (3,1) is a combination of elements (3,2) and (3,3). From this arrangement with can clearly see the changes in the natural frequencies for varying combinations of small scale parameter and tip mass ratios.

The spring-mass system can be isolated as shown in Fig. 8. This represents a single degree of freedom system and the frequency value for different combinations of linear spring constant and tip mass ratio is tabulated in Table 3. The frequencies of the beam are directly coupled to the frequencies of the spring-mass system and the information in Table 3 can reveal pertinent details about the vibration characteristics of the entire system.

Equation (7) can be rearranged and written in the form below, where the left hand side represents the ratio of the displacement of the mass from its equilibrium position to the displacement of the tip of the beam,

$$\frac{Z_n(L)}{X_n(L)} = \left(\frac{a_k^4}{a_k^4 - a_n^4}\right).$$

It is clear from the relationship above that this ratio depends entirely on the frequency parameters of the beam

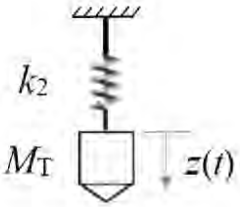

Fig. 8 Spring-mass system at $x = L$

Table 3 Frequency parameter (a_k) of spring-mass system

	$a_k^4 = \kappa_2/\eta$			
κ_2	$\eta = 0$	$\eta = 0.1$	$\eta = 0.5$	$\eta = 1$
0	∞	0	0	0
1	∞	1.7783	1.1892	1
10	∞	3.1623	2.1147	1.7783
100	∞	5.6234	3.7606	3.1623
1000	∞	10	6.6874	5.6234

(a_n) and the frequency parameters of the single degree of freedom system (a_k) and therefore we can obtain information about sample penetration depth. Using the frequencies in Figs. 3, 4, 5, 6, 7 and Table 3 we can calculate the displacement ratio and these results are shown in Table 4. When the linear spring constant is zero ($\kappa_2 = 0$) the ratio is zero indication that the mass does not move from the equilibrium position irrespective of the values of the other variables. It is noted that when the rigidity of the linear spring increases ($\kappa_2 \to \infty$) the ratio is non-zero meaning that the tip mass moves relative to the beam tip displacement. In the context of this investigation, it is observed in Table 4 that the biggest ratio occurs when the linear spring is at its least rigid value ($\kappa_2 = 1$) and tends to unity ($Z_n(L)/X_n(L) \to 1$) as the linear spring becomes extremely rigid ($\kappa_2 \to \infty$). When the linear spring constant is infinite, the mass is rigidly attached to the beam and therefore the tip moves in synch with the mass. These trends are confirmed in Magrab (2012), Dowell (1979) and Moutlana and Adali (2015).

Table 4 Ratio of mass displacement position from equilibrium to beam displacement for $\eta = 0.1$

		$Z_n(L)/X_n(L)$			
κ_1	κ_2	$\mu = 0$	$\mu = 0.2$	$\mu = 0.4$	$\mu = 0.6$
10^0	0	0	0	0	0
10^0	10^0	1.212	1.214	1.220	1.231
10^0	10^1	1.019	1.019	1.019	1.020
10^0	10^2	1.002	1.002	1.002	1.002
10^0	10^3	1.000	1.000	1.000	1.000
		$Z_n(L)/X_n(L)$			
κ_1	κ_2	$\mu = 0$	$\mu = 0.2$	$\mu = 0.4$	$\mu = 0.6$
10^1	0	0	0	0	0
10^1	10^0	2.008	2.036	2.133	2.353
10^1	10^1	1.067	1.069	1.075	1.090
10^1	10^2	1.006	1.007	1.007	1.009
10^1	10^3	1.000	1.000	1.000	1.000
		$Z_n(L)/X_n(L)$			
κ_1	κ_2	$\mu = 0$	$\mu = 0.2$	$\mu = 0.4$	$\mu = 0.6$
10^2	0	0	0	0	0
10^2	10^0	2.474	2.520	2.674	3.020
10^2	10^1	1.090	1.093	1.103	1.133
10^2	10^2	1.009	1.009	1.010	1.012
10^2	10^3	1.000	1.000	1.000	1.000
		$Z_n(L)/X_n(L)$			
κ_1	κ_2	$\mu = 0$	$\mu = 0.2$	$\mu = 0.4$	$\mu = 0.6$
10^3	0	0	0	0	0
10^3	10^0	2.548	2.596	2.758	3.120
10^3	10^1	1.094	1.097	1.107	1.140
10^3	10^2	1.009	1.009	1.010	1.013
10^3	10^3	1.000	1.000	1.000	1.000

As discussed earlier, the results for zero torsional spring ratio are worth noting, but will not serve any practical purpose in the present model and thus $\kappa_1 = 0$ is omitted from Table 4. When the torsional spring constant is at its lowest value ($\kappa_1 = 1$) the displacement ratio is the lowest and gradually increases as the torsional spring constant increases to a value almost double the initial value from a ratio of 1.2–2.6. Also, the fact that the values of the ratios are positive numbers tells us that the motion of the tip of the beam is in phase with that of the mass. A negative sign indicates that the respective motions are out of phase and therefore the phase is particularly important in controlling the motion of the machining tool in the context of nano manufacturing. These results give us essential understanding of sample penetration depth in the field of nano

manufacturing using dynamic atomic force microscopy (dAFM).

Equation (7) articulates the relation between the frequency parameter (a_n) of the beam and the frequency parameter (a_k) of single degree of freedom system. The form of the equation shows that if the denominator on the right-hand side is equal to zero ($a_n = a_k$), this term tends to infinity; i.e. $a_k^4/(a_k^4 - a_n^4) \to \infty$. When this occurs, the term on the left-hand side must be infinite by necessity. Either the numerator tends to infinity or the denominator tends to zero in the limit. When displacement of the mass from the equilibrium $Z_n(L)$ is infinite, the system undergoes the phenomenon of resonance which should be avoided in manufacturing tools. Furthermore, the displacement of the mass from the equilibrium $Z_n(L)$ also appears in the shear boundary condition [Eqs. (15b), (21)] and ultimately in the characteristic equation expressed in Eq. (23). When plotting the characteristic equation, the resonance frequencies of the whole system can be identified and the information is key to the design of mechanical systems.

This investigation is concerned with beams at nano scale and therefore the non-local effects have to be taken into account. When the small scale parameter is varied μ = 0, 0.2, 0.4 and 0.6 the ratio of the displacements increases by a maximum value of 2, 14, 18.1 and 18.3%, respectively. Table 3 shows that ratio of the displacements increase as the small scale parameter varies from μ = 0 to 0.6; and also, that the increase occurs due to the increase in the torsional spring constant where the maximum increase is observed at maximum rigidity ($\kappa_1 \to \infty$). Therefore but altering the rigidity of the torsional spring, we can influence the penetration depth; and in addition, if the small scale parameter is adjusted, the penetration depth can be predicted.

5 Conclusions

In the present paper, small scale effects on the fundamental frequency are investigated for a nanobeam with elastically restrained end conditions and carrying a tip mass attached via a linear spring to the end of the beam. The solution for the beam is obtained analytically by expanding the deflection in terms of its eigenfunctions and solving the resulting characteristic equation numerically. The results are given in the form of contour plots in terms of the fundamental natural frequencies, small scale parameter, tip mass, torsional and linear springs. Further numerical results are presented for parametric studies of the effect of support elasticity and tip mass on the fundamental frequencies of the nanobeam.

It is observed that the effect of the small scale parameter depends on varying problem parameters and boundary condition which may lead to an increase or decrease of the fundamental frequency depending on the support flexibility. Boundary conditions can be expressed in terms of a torsional spring at $x = 0$, linear spring and tip mass at $x = L$. The classical boundary conditions correspond to setting the small scale parameter to zero ($\mu = 0$) the torsional and linear spring constants to zero ($\kappa_{1,2} \to 0$) or infinity ($\kappa_{1,2} \to \infty$). It was observed that low torsional spring stiffness leads to a decrease in the fundamental frequency and high torsional spring stiffness to an increase in the fundamental frequency as the small scale parameter increases. The rates of decrease and increase depend on the relative values of the spring constants. The effect of the tip mass on the frequencies is to lower the natural frequencies (Moutlana and Adali 2017, 2018).

Acknowledgements The research of the second author was supported by research grants from the University of KwaZulu-Natal (UKZN) and from National Research Foundation (NRF) of South Africa. The author gratefully acknowledges the support provided by UKZN and NRF.

References

Ansari R, Gholami R, Rouhi H (2012) Vibration analysis of single-walled carbon nanotubes using different gradient elasticity theories. Compos Part B 43:2985–2989

Azrar A, Azrar L, Aljinaidi AA (2011) Length scale effect analysis on vibration behaviour of single walled carbon nano tubes with arbitrary boundary conditions. Revue de Mecanique Appliquee et Theorique 2(5):475–485

Balachandran B, Magrab EB (2009) Vibrations. CENGAGE Learning, Toronto

Basak S, Beyder A, Spagnoli C, Raman A, Sachs F (2007) Hydrodynamics of torsional probes for atomic force microscopy in liquids. J Appl Phys 102:024914

Behera L, Chakraverty S (2014) Free vibration of Euler and Timoshenko nanobeams using boundary characteristic orthogonal polynomials. Appl Nanosci 4:347–358

Beyder A, Frederick Sachs F (2006) Micro fabricated torsion levers optimized for low force and high-frequency operation in fluids. Ultramicroscopy 106:838–846

Bichoutskaia E, Popov AM, Lozovik YE, Ershova OV, Lebedeva IV, Knizhnik AA (2010) Nanoresonator based on relative vibrations of the walls of carbon nanotubes. Fuller Nanotubes Carbon Nanostruct 18(4–6):523–530

Binnig G, Quate CF, Gerber C (1986) Atomic force microscope. Phys Rev Lett 56:930–933

Chang WJ, Yang YC, Lee HL (2013) Dynamic behaviour of atomic force microscope based nano-machining based on a modified couple stress theory. Micro Nano Lett 8:832–835

Dowell EH (1979) On some properties of combined dynamical systems. J Appl Mech 46:206–209

Elishakoff I, Versaci C, Muscolino G (2011) Clamped-free double-walled carbon nanotube-based mass sensor. Acta Mech 219:29–43

Eltaher MA, Alshorbagy AE, Mahmoud FF (2013) Vibration analysis of Euler-Bernoulli nanobeams by using finite element method. Appl Math Model 37:4787–4797

Eltaher MA, Khater ME, Emam SA (2016) A review on nonlocal elastic models for bending, buckling, vibrations and wave propagation of nanoscale beams. Appl Math Model 40:4109–4128

Eringen AC (2002) Nonlocal continuum field theories. Springer, New York

Eringen AC, Edelen D (1972) On nonlocal elasticity. Int J Eng Sci 10(3):233–248

Feng EH, Jones RE (2011) Carbon nanotube cantilevers for next-generation sensors. Phys Rev B 83:195412

Grant DA (1975) Vibration frequencies for a uniform beam with one end elastically supported and carrying a mass at the other end. ASME J Appl Mech 42:878–880

Gürgöze M (1996) On the eigenfrequencies of a cantilever beam with attached tip mass and spring-mass system. J Sound Vib 190(2):149–162

Horng T-L (2012) Analytical solution of vibration analysis on fixed-free single-walled carbon nanotube-based mass sensor. J Surf Eng Mater Adv Technol 2:47–52

Hozhabrossadati SM (2015) Exact solution for free vibration of elastically restrained cantilever non-uniform beams joined by a spring-mass system at the free end. Civ Struct Eng IES J Part A. https://doi.org/10.1080/19373260.2015.1054957

Joshi AY, Harsha SP, Sharma SC (2010) Vibration signature analysis of single walled carbon nanotube based nanomechanical sensors. Phys E 42:2115–2123

Kiani K (2013) Vibration analysis of elastically restrained double-walled carbon nanotubes on elastic foundation subjected to axial load using nonlocal shear deformable beam theories. Int J Mech Sci 68:16–34

Kiani K (2015) Nanomechanical sensors based on elastically supported double-walled carbon nanotubes. Appl Math Comput 270:216–241

Kiani K, Ghaffari H, Mehri B (2013) Application of elastically supported single-walled carbon nanotubes for sensing arbitrarily attached nano-objects. Curr Appl Phys 13:107–120

Laura PAA, Maurizi MJ, Pombo JL (1975) A note on the dynamic analysis of an elastically restrained-free beam with a mass at the free end. J Sound Vib 41:397–405

Laura PAA, Grossi RO, Alvarez S (1982) Transverse vibrations of a beam elastically restrained at one end and with a mass and spring at the other subjected to an axial force. Nucl Eng Des 74:299–302

Lee TW (1973) Vibration frequencies for a uniform beam with one end spring-hinged and carrying a mass at the other free end. ASME J Appl Mech 40:813–815

Li X-F, Tang G-J, Shen Z-B, Lee KY (2015) Resonance frequency and mass identification of zeptogram-scale nanosensor based on nonlocal theory beam theory. Ultrasonics 55:75–84

Liang L-N, Ke L-L, Wang Y-S (2015) Flexural vibration of an atomic force microscope cantilever based on modified couple stress theory. Int J Struct Stab Dyn 15:1540025

Liu W, Yan Y, Hu Z, Zhao X, Yan J, Dong S (2012) Study on the nano machining process with vibrating AFM tip on the polymer surface. Appl Surf Sci 258:2620–26261

Lu P (2007) Dynamic analysis of axially pre-stressed micro/nano-beam structures based on nonlocal beam theory. J Appl Phys 101:073504

Lu P, Lee HP, Lu C, Zhang PQ (2006) Dynamic properties of flexural beams using a nonlocal elasticity model. J Appl Phys 99:073510

Lu L, Gou X, Zhao J (2017) Size-dependent vibration analysis of nanobeams based on the nonlocal strain gradient. Int J Eng Sci 116:12–24

Magrab BE (2012) Magrab vibrations of elastic systems: with applications to MEMS and NEMS. Springer, New York

McCarthy R, Carmichael B, Nima Mahmoodi S (2014) Dynamic analysis of tapping atomic force microscopy considering various boundary value problems. Sens Actuators A 216:69–77

Mehdipour I, Barari A, Domairy G (2011) Application of a cantilevered SWCNT with mass at the tip as a nanomechanical sensor. Comput Mater Sci 50:1830–1833

Moutlana MK, Adali S (2015) Vibration of a cantilever beam with extended tip mass and axial load subject to piezoelectric control. R & D J S Afr Inst Mech Eng 31:60–65

Moutlana MK, Adali S (2017) Fundamental frequencies of a nano beam used for atomic force microscopy (AFM) in tapping mode. In: The 9th international conference of the African materials research society (AMRS2017) Gaborone, 11–14 Dec 2017. MRS advances, Warrendale. https://doi.org/10.1557/adv.2018.321

Moutlana MK, Adali S (2018) Effects of elastic restraints on the fundamental frequency of nonlocal nanobeams with tip mass. Int J Acoust Vib (IJAV) **(accepted for publication)**

Murmu T, Adhikari S (2012) Nonlocal frequency analysis of nanoscale biosensors. Sens Actuators A 173:41–48

Rahmanian M, Torkaman-Asadi MA, Firouz-Abadi RD, Kouchakzadeh MA (2016) Free vibrations analysis of carbon nanotubes resting on Winkler foundations based on nonlocal models. Phys B 484:83–94

Reddy JN (2006) Nonlocal theories for bending, buckling and vibration of beams. Int J Eng Sci 45:288–307

Reddy JN, Pang SN (2008) Nonlocal continuum theories of beams for the analysis of carbon nanotubes. J Appl Phys 103:023511

Rosa MAD, Lippiello M (2016) Nonlocal frequency analysis of embedded single-walled carbon nanotube using the differential quadrature method. Compos Part B Eng 84:41–51

Sadeghi A (2012) The flexural vibration of V shaped atomic force microscope cantilevers by using the Timoshenko beam theory. Zeitschriftfur Angewandte Mathematik und Mechanik 92(2012):782–800

Shen ZB, Sheng LP, Li XF, Tang GJ (2012a) Nonlocal Timoshenko beam theory for vibration of carbon nanotube-based biosensor. Phys E 44:1169–1175

Shen ZB, Li XF, Sheng LP, Tang GJ (2012b) Transverse vibration of nanotube-based micro-mass sensor via nonlocal Timoshenko beam theory. Comput Mater Sci 53:340–346

Wang Q, Arash B (2014) A review on applications of carbon nanotubes and graphenes as nano-resonator sensors. Comput Mater Sci 82:350–360

Yayli MÖ (2016) A compact analytical method for vibration analysis of single-walled carbon nanotubes with restrained boundary conditions. J Vib Control 22(10):2542–2555

Yayli MÖ (2018a) Torsional vibrations of restrained nanotubes using modified couple stress theory. Microsyst Technol 24(8):3425–3435

Yayli MÖ (2018b) Free longitudinal vibration of a nanorod with elastic spring boundary conditions made of functionally graded material. Micro Nano Lett 13(7):1031–1035. https://doi.org/10.1049/mnl.2018.0181

Yayli MÖ (2018c) Free vibration analysis of a single-walled carbon nanotube embedded in an elastic matrix under rotational restraints. Micro Nano Lett 13(2):202–206. https://doi.org/10.1049/mnl.2017.0463

Chapter 6 – Paper 3: *MRS Advances*

6.1 Fundamental frequencies of a nano beam for atomic force microscopy (AFM) in tapping mode.

In this Section, Case 2 is studied, and the findings are published in *MRS Advances* © 2018 Materials Research Society, 11 Apr 2018.

MRS Advances © 2018 Materials Research Society
DOI: 10.1557/adv.2018.321

Fundamental frequencies of a nano beam used for atomic force microscopy (AFM) in tapping mode

MALESELA K. MOUTLANA[1] and SARP ADALI[2]

[1]*Department of Mechanical Engineering, Durban University of Technology, Durban, South Africa*

[2]*Discipline of Mechanical Engineering, University of KwaZulu-Natal, Durban, South Africa*

Corresponding author: moutlanam@dut.ac.za

ABSTRACT

In this study we investigate the motion of a torsionally restrained beam used in tapping mode atomic force microscopy (TM-AFM), with the aim of manufacturing at nano-scale. TM-AFM oscillates at high frequency in order to remove material or shape nano structures. Euler-Bernoulli theory and Eringen's theory of non-local continuum are used to model the nano machining structure composed of two single degree of freedom systems. Eringen's theory is effective at nano-scale and takes into account small-scale effects. This theory has been shown to yield reliable results when compared to modelling using molecular dynamics.

The system is modelled as a beam with a torsional boundary condition at one end; and at the free end is a transverse linear spring attached to the tip. The other end of the spring is attached to a mass, resulting in a single degree of freedom spring-mass system. The motion of the tip of the beam and tip mass can be investigated to observe the tip frequency response, displacement and contact force. The beam and spring–mass frequencies contain information about the maximum displacement amplitude and therefore the sample penetration depth and this allows

INTRODUCTION

Vibration characteristics of nano scale beams can be analysed by modelling them within the framework of nonlocal continuum theory (1, 2). Nonlocal theory is based on the assumption that the stress at a single point in the material is influenced by the strains of all the points in the material. This theory is widely applied to the vibration modelling of carbon nanotubes in several studies (3, 4), and in particular, vibrations of carbon nanotubes with a tip mass have been studied extensively due to their use in sensor applications (5, 6). In these studies the flexibility of the boundaries are not taken into account and the classical boundary conditions are considered. In a number of studies vibrations of nanotubes with elastically restrained boundaries have been studied (7, 8) but only as single degree freedom systems.

In the current investigation, an elastically restrained nanobeam with a tip mass is modelled as an Euler-Bernoulli beam based on the nonlocal theory (1, 2) to take into account the small scale effects (9). The restraint at one support is specified as a torsional spring which replaces the 'ideal' clamped end boundary condition used in a number of studies. A translational spring is attached to the other end where a tip mass is attached to form a spring-mass system. The governing differential equation of motion is solved analytically using separation of variables to determine the vibration frequencies. The effects of the elastic restraints, tip mass and the small-scale parameter on the frequencies are investigated numerically. Similar problems have been solved in the case of beams based on the local (classical) theory of elasticity. Elastically supported beams with a tip mass have been studied (10, 11) and the beam with torsional and translational springs with a tip mass has been studied in (12) based on the classic theory of Euler-Bernoulli beams.

A model swapping the clamped end for a torsional spring represents a more 'realistic' boundary condition allowing for the flexibility at the boundary. In TM-AFM, the free end carries a fabrication/cutting tool which is modelled as concentrated mass such that the centre of the mass of the tool coincides with the sharp end of the cutting tool and the tip of the beam. In the current model a translational linear spring attached to the tip of the beam and on the other end spring a mass is attached.

NANOBEAM ELASTICALLY RESTRAINED WITH A SPRING –MASS SYSTEM AT $x = L$.

The beam under consideration is restrained by a torsional spring at $x = 0$ modelled as a flexible restraint shown in Figure 1. During the machining process, a contact force is generated between the tip mass and the object to be shaped. Attached to the free end of the beam at $x = L$ is a machining tool which can be modelled as a mass with a sharp tip, attached to the beam by means of a linear spring (k_2) and the centre of gravity of the tip mass coincides with the tip of the beam and this constitutes the spring-mass system.

The spring-mass system is excited by the motion of the tip of the nanobeam and the constitutive relation of stress-strain for the based on nonlocal theory of elasticity can be expressed as

$$\sigma_{xx} - \bar{\mu}\frac{d^2\sigma_{xx}}{dx^2} = E\varepsilon_{xx} \tag{1}$$

where E is the Young's modulus, $\bar{\mu} = e_0 l_i$ is the small scale parameter with e_0 denoting a material constant and l_i the characteristic length.

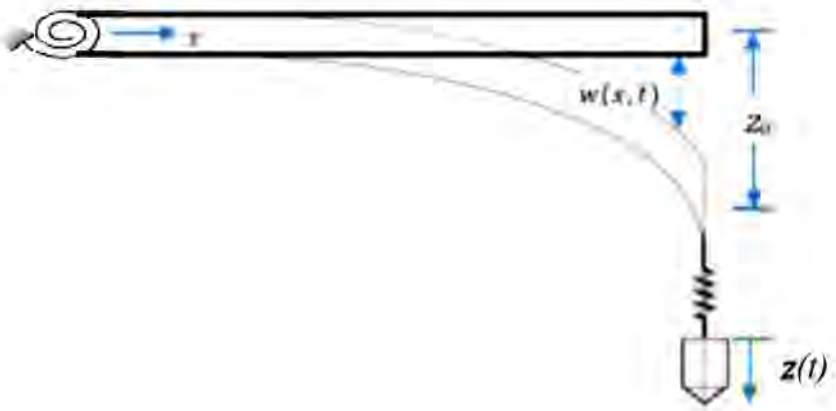

Fig. 1. Deflection of the beam with spring-mass attached at free end.

The expression for moment $M(x)$ is given by

$$M(x) - \bar{\mu}\frac{d^2 M_z(x)}{dx^2} = -EI\frac{d^2 w}{dx^2} \tag{2}$$

where I is the moment of inertia. The equation of motion for a nonlocal nanobeam undergoing transverse motion is given in (9) and can be expressed as

$$EI\frac{d^4 w(x,t)}{dx^4} - \bar{\mu}^2 \rho A\frac{d^2 w(x,t)}{dx^2} + \rho A\frac{d^2 w(x,t)}{dt^2} - \frac{k_2}{L}[w(L,t) - z(t)] = F_0(x) \tag{3}$$

$$M_T\frac{d^2 z(t)}{dt^2} + k_2 z(t) = k_2 w(L,t) \tag{4}$$

where ρ is the density, A is the cross-sectional area and $F_o(x)$ is the forcing function which is taken as $F_o(x) = 0$ for a beam under free vibration. The dynamic motion of the tip mass is expressed in equation (4) and the two equations (3) and (4) are coupled through the motion of the tip $w(L,t)$.

METHOD OF SOLUTION

The solution of the governing equation (3) is obtained by eigenfunction expansion of the displacement function as

$$w(x) = \sum_{n=1}^{\infty} X_n(x)\, T_n(t) \tag{5a}$$

$$z(t) = \sum_{n=1}^{\infty} z_0 T_n(t) \tag{5b}$$

$$\ddot{T}_n(t) + \omega_n^2 T_n(t) = 0 \tag{5c}$$

Inserting equation (5a) into equation (3) and using equation (5c), we obtain the differential equation of motion for the beam in the modal domain. For the spring-mass, after inserting equation (5b) into equation (4) and using equation (5c), we obtain the equation of motion of the tip mass in the modal domain. The natural frequency ω_n is the frequency of the n^{th} mode of vibration and the general solutions of equation (3) is given by

$$X_n(x) = A_n \cos p_{2n}x + B_n \sin p_{2n}x + C_n \cosh p_{1n}x + D_n \sinh p_{1n}x \tag{6}$$

where p_{1n} and p_{2n} are

$$p_{1n,2n} = \sqrt{\frac{a_n^8 \bar{\mu}^2 \pm \sqrt{a_n^8 \bar{\mu}^2 + 4a_n^4}}{2}} \tag{7}$$

The constants A_n, B_n ,C_n and D_n are determined from the boundary conditions where, the boundary conditions at $x = 0$ are zero displacement and moment; and can be expressed as

$$w(0) = 0 \tag{8a}$$

$$EI\frac{d^2w(0)}{dx^2} - \bar{\mu}^2 \rho A \frac{d^2w(0)}{dt^2} - k_1 \frac{dw(0)}{dx} = 0 \tag{8b}$$

At the free end, taking into account the small scale effect, the tip mass and the linear spring, the moment and shear boundary conditions at $x = L$ can be expressed as

$$EI\frac{d^2w(L)}{dx^2} + \bar{\mu}^2 \rho A w(L) = 0 \tag{9a}$$

$$EI\frac{d^3w(L)}{dx^3} - \bar{\mu}^2 \rho A w(L) = F_L \tag{9b}$$

where F_L is the transverse force due to the motion of the linear spring,

$$F_L = k_2 z_0$$

and z_0 can be determined from equation (4). Substitution of equation (6) into the boundary condition (8a), we obtain

$$A_n + C_n = 0 \tag{10}$$

The general solution (6) can now be expressed as

$$X_n(x) = D_n \sinh p_{1n}x - B_n \sin p_{2n}x + \left(\cos p_{2n}x - \cosh p_{1n}x\right)C_n \tag{11}$$

substituting equation (11) into equation (8b) gives

$$\kappa_1 p_1 D_n - \left(p_{2n}^2 + p_{1n}^2\right)C_n + \kappa_1 p_{2n} B_n = 0 \tag{12}$$

and substituting B_n in equation (12) into equation (11) gives the general solution expressed in terms of constants $C_n$and D_n alone.

$$\begin{aligned} X_n(x) = &-\left(\sinh p_{1n}x + \frac{p_{1n}}{p_{2n}} \sin p_{2n}x\right)D_n \\ &+ \left(\frac{p_{2n} \sin p_{2n}x}{\kappa_1} + \frac{p_{1n}^2 \sin p_{2n}x}{\kappa_1 p_{2n}}\right)C_n \\ &- \left(\cos p_{2n}x - \cosh p_{1n}x\right)C_n \end{aligned} \tag{13}$$

This result can be substituted into the moment boundary conditions (9a) at $x = L$ to obtain

$$C_n \cdot \Gamma_{1n} + D_n \cdot \Gamma_{2n} = 0 \tag{14}$$

where,

$$\begin{aligned} \Gamma_{1n} = &\left(\left(p_{2n}^2 + p_{1n}^2\right)a_n^4 \sin p_{2n}L - \kappa_1 p_{2n} a_n^4 \cos p_{2n}L + \kappa_1 p_{2n} a_n^4 \cosh p_{1n}L\right)\mu \\ &+ \left(p_{2n}^4 + p_{1n}^2 p_{2n}^2\right)\sin p_{2n}L - \kappa_1 p_{2n}^3 \cos p_{2n}L - \kappa_1 p_{1n}^2 p_{2n} \cosh p_{1n}L \end{aligned}$$

and,

$$\begin{aligned} \Gamma_{2n} = &\kappa_1\left(p_{1n} a_n^4 \sin p_{2n}L - p_{2n} a_n^4 \sinh p_{1n}L\right)\mu \\ &+ \kappa_1 p_{1n} p_{2n}^2 \sin p_{2n}L + \kappa_1 p_{1n}^2 p_{2n} \sinh p_{1n}L \end{aligned}$$

After substituting the results of equation (4) and (13) the shear boundary condition (9b) at $x = L$ can be expressed as

$$C_n \cdot \Gamma_{3n} + D_n \cdot \Gamma_{4n} = 0 \tag{15}$$

where,

$$\Gamma_{3n} = \mu\left(\kappa_1 p_{2n}^2 a_n^8 - \kappa_1 p_{2n}^2 a_k^4 a_n^4\right)\sin p_{2n}L + \mu\left(\kappa_1 p_{1n} p_{2n} a_n^8 - \kappa_1 p_{1n} p_{2n} a_k^4 a_n^4\right)\sinh p_{1n}L + \left(\left(\left(p_{2n}^3 + p_{1n}^2 p_{2n}\right)a_n^8 + \left(-p_{2n}^3 - p_{1n}^2 p_{2n}\right)a_k^4 a_n^4\right)\cos p_{2n}L\right)\mu + \left(\left(\left(-p_{2n}^2 - p_{1n}^2\right)\eta a_k^4 - \kappa_1 p_{2n}^2\right)a_n^4 + \kappa_1 p_{2n}^2 a_k^4\right)\sin p_{2n}L + \left(\left(\kappa_1 p_{2n}\eta a_k^4 - p_{2n}^5 - p_{1n}^2 p_{2n}^3\right)a_n^4 + \left(p_{2n}^5 + p_{1n}^2 p_{2n}^3\right)a_k^4\right)\cos p_{2n}L + \left(\kappa_1 p_{1n}^3 p_{2n} a_n^8 - \kappa_1 p_{1n}^3 p_{2n} a_k^4\right)\sinh p_{1n}L - \kappa_1 p_{2n}\eta a_k^4 a_n^4 \cosh_{1n} L$$

and,

$$\Gamma_{4n} = \mu\left(\kappa_1 p_{1n} p_{2n} a_n^8 - \kappa_1 p_{1n} p_{2n} a_k^4 a_n^4\right)\cos p_{2n}L + \mu\left(\kappa_1 p_{1n} p_{2n} a_k^4 a_n^4 - \kappa_1 p_{1n} p_{2n} a_n^8\right)\cosh p_{1n}L - \kappa_1 p_{1n}\eta a_k^4 a_n^4 \sin p_{2n}L + \kappa_1 p_{2n}\eta a_k^4 a_n^4 \sinh p_{1n}L + \left(\kappa_1 p_{1n} p_{2n}^3 a_k^4 - \kappa_1 p_{1n} p_{2n}^3 a_n^4\right)\cos p_{2n}L + \left(\kappa_1 p_{1n}^3 p_{2n} a_k^4 - \kappa_1 p_{1n}^3 p_{2n} a_n^4\right)\cosh p_{1n}L$$

The results from the moment and shear boundary conditions given in equations (14) and (15) can be expressed in matrix form as

$$\begin{bmatrix} \Gamma_{1n} & \Gamma_{2n} \\ \Gamma_{3n} & \Gamma_{4n} \end{bmatrix}\begin{bmatrix} C_n \\ D_n \end{bmatrix} = \begin{bmatrix} 0 \\ 0 \end{bmatrix} \tag{16}$$

and the characteristic equation can be obtained from the determinant of equation (16) as

$$\Gamma_{1n}\Gamma_{4n} - \Gamma_{2n}\Gamma_{3n} = 0 \tag{17}$$

The characteristic equation (17) can be solved numerically to compute the roots where κ_1, κ_2, η, a_n^4 and a_k^4 are the dimensionless constants for the beam and the spring-mass system.

RESULTS

The natural frequencies of the system R_n are obtained by making a substitution, $a_n = R_n/L$, into equation (17). The values of R_n are dimensionless natural frequencies used below to analyse the numerical results. When $\kappa_1 \to \infty$ the torsional spring becomes rigid and the boundary condition behaves like that of a cantilevered beam. The classic cantilever configure can be obtained by setting the mass to zero $\eta = 0$ and the fundamental natural frequency of the system is $R_1 = 1.875$ which corresponds to the results obtained by Magrab(13) $R_1 = 0.5969\pi$. Furthermore, when $\kappa_2 \to \infty$ the linear spring is rigid and the system behaves like a cantilevered beam with concentrated tip mass because the centre of gravity of the attached mass coincides with the tip of the beam (see Figure 2).

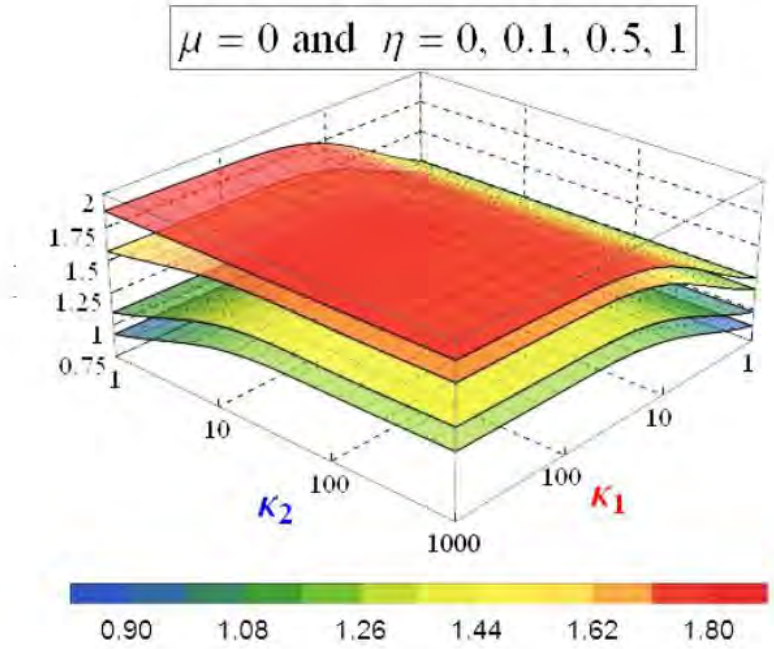

Fig. 2. Fundamental frequency plotted against spring constants κ_1 and κ_2 with tip mass ratio $\mu = 0$: a) $\eta = 0$, b) $\eta = 0.1$, c) $\eta = 0.5$ and d) $\eta = 1$.

For a tip mass ratio $\eta = 0.1$ and $\eta = 1$ the fundamental natural frequency is $R_1 = 1.7227$ and $R_1 = 1.2479$ which are the same result obtained by Magrab ($R_1 = 0.5484\pi$) and Gürgöze ($R_1 = 1.2479$), respectively (13, 14). In practical applications, the values for the parameters of interest will vary between zero and infinity ($0 < \kappa_1, \kappa_2 < \infty$). The boundary conditions discussed above relate to extreme rigidity of the torsional and linear spring. It is also noted that when the torsional spring is completely elastic $\kappa_1 \to 0$ the fundamental natural frequencies approach zero in the limit ($R_1 \to 0$) and the other variables have minimal effect on the frequencies as seen in Figure 2 above.

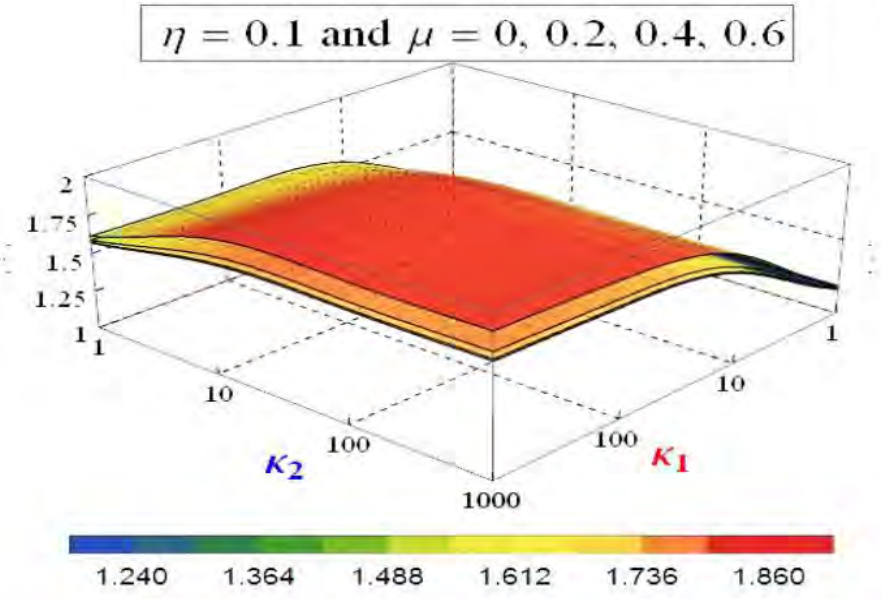

Fig. 3. Fundamental frequency plotted against spring constants κ_1 and κ_2 with tip mass ratio $\eta = 0.1$: a) $\mu = 0$, b) $\mu = 0.2$, c) $\mu = 0.4$ and d) $\mu = 0.6$.

The results for the natural frequencies have been published by Azrar(15) and Xiang-Fang Li(16); for the values for small scale parameter, $\mu = 0, 0.2, 0.4$ and 0.6; and these are $R_1 = 1.875, 1.8919, 1.9543$ and 2.1989, respectively. Similar results are obtained using the present solution. Furthermore, Xiang-Fang Li(31) studied a cantilever beam with concentrated tip mass of $\mu = 0.5$ and obtained a fundamental frequency of $R_1 = 1.4200, 1.4253, 1.4427$ and 1.4778 for small scale parameter $\mu = 0, 0.2, 0.4$ and 0.6, respectively. The intermediate values for torsional and linear spring constant are plotted in Figure (3). The spring constants are kept constant – Table 2 – in order to determine the effects of the small scale parameter in combination with the tip mass.

Table 1: Fundamental frequencies for elastic boundary conditions, varying tip mass (η) and small scale, (μ) parameter for the system.

		$\mu = 0$		$\mu = 0.6$	
κ_1	κ_2	$\eta = 0$	$\eta = 1$	$\eta = 0$	$\eta = 1$
1	1	1.2479	0.7890	1.2769	0.7910
1	1000	1.2479	1.2769	0.8705	0.8770
1000	1	1.8750	0.9270	2.1989	0.9290
1000	1000	1.8750	1.2479	2.1989	1.2769

In his investigation, Gürgöze determined the natural frequencies for $\eta = 1$ and $\kappa_2 = 1$ to be $R_1^2 = 0.8409$ and in the present study, the results show that the fundamental natural frequency is $R_1 = 0.9270$ which represent a percentage difference of 1%.

The frequencies of the beam are directly coupled to the frequencies of the spring-mass system and the information in Table 2 can reveal pertinent details about the vibration characteristics of the entire system. Equation (4) can be rearranged and written in the form below, where the left hand side represents the ratio of the displacement of the mass from its equilibrium position to the displacement of the tip of the beam.

$$\frac{z_0}{X_n(L)} = \left(\frac{a_k^4}{a_k^4 - a_n^4} \right) \tag{18}$$

It is clear from the relationship above that this ratio depends entirely on the frequency parameters of the beam (a_n) and the single degree of freedom system (a_k). Using the frequencies in Figure (2) and (3); and Table 1 and 2; we can calculate the displacement ratios. These results give us essential understanding of sample penetration depth in the field of nano manufacturing using dynamic atomic force microscopy (dAFM).

Equation (18) articulates the relation between the frequency parameter (a_n) of the beam and the frequency parameter (a_k) of single degree of freedom system. Therefore by altering the rigidity of the torsional spring, we can influence the penetration depth and in addition, if the small scale parameter is adjusted, the penetration depth can be predicted.

Table 2: Frequency parameter (a_k) of spring-mass system.

	$a_k^4 = \kappa_2 / \eta$			
$\kappa_2 \setminus \eta$	0	0.1	0.5	1
0	∞	0	0	0
1	∞	1.7783	1.1892	1
10	∞	3.1623	2.1147	1.7783
100	∞	5.6234	3.7606	3.1623
1000	∞	10	6.6874	5.6234

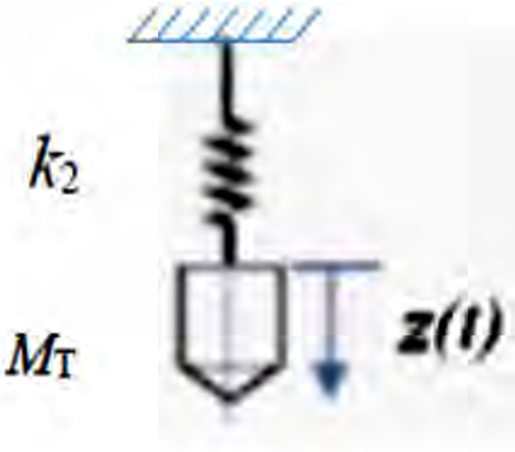

Fig. 4. Spring-mass system at $x = L$.

CONCLUSIONS

In the present paper, small scale effects on the fundamental frequency are investigated for a nanobeam with elastically restrained end conditions and carrying a tip mass attached via a linear spring to the end of the beam. The solution for the beam is obtained analytically by expanding the deflection in terms of its eigenfunctions and solving the resulting characteristic equation numerically. Further numerical results are presented for parametric studies of the effect of support elasticity and tip mass on the fundamental frequencies of the nanobeam.

It is observed that the effect of the small scale parameter depends on varying problem parameters and boundary condition which may lead to an increase or decrease of the fundamental frequency depending on the support flexibility. Boundary conditions can be expressed in terms of a torsional spring at $x = 0$, linear spring and tip mass at $x = L$. The classical boundary conditions correspond to setting the small scale parameter to zero ($\mu = 0$) the torsional and linear spring constants to zero ($\kappa_{1,2} \to 0$) or infinity($\kappa_{1,2} \to \infty$). It was also observed that low torsional spring stiffness leads to a decrease in the fundamental frequency and high torsional spring stiffness to an increase in the fundamental frequency as the small scale parameter increases. The rates of decrease and increase depend on the relative values of the spring constants. The effect of the tip mass on the frequencies is to lower the natural frequencies as observed in (17).

ACKNOWLEDGMENT

The research of the second author was supported by research grants from the University of KwaZulu-Natal (UKZN) and from National Research Foundation (NRF) of South Africa. The author gratefully acknowledges the support provided by UKZN and NRF.

REFERENCES

1. Eringen, A. C., and Edelen, D. (1972) On nonlocal elasticity. *Int. J. Eng. Sci.* 10 (3): 233–248.
2. Eringen, A. C., (2002) Nonlocal Continuum Field Theories, Springer-Verlag, New York.
3. Rahmanian, M., Torkaman-Asadi, M. A., Firouz-Abadi, R. D., and Kouchakzadeh, M. A. (2016) Free vibrations analysis of carbon nanotubes resting on Winkler foundations based on nonlocal models. *Physica B* 484: 83–94.
4. Rosa, M. A. D., and Lippiello, M. (2016) Nonlocal frequency analysis of embedded single-walled carbon nanotube using the Differential Quadrature Method. *Compos. Part B: Eng.* 84: 41–51.
5. Wu, D. H. Chien, W. T., Chen, C. S., and Chen, H. H. (2006) Resonant frequency analysis of fixed-free single-walled carbon nanotube-based mass sensor. *Sens. Actuators A* 126: 117-121.
6. Chiu, H. Y., Hung, P., Postma, H. W. C., and Bockrath, M. (2008) Atomic-scale mass sensing using carbon nanotube resonators. *Nano Lett.* 8: 4342–4346.
7. Kiani, K. (2015) Nanomechanical sensors based on elastically supported double-walled carbon nanotubes. *Appl. Math. Comput.* 270: 216–241.
8. Kiani, K., Ghaffari, H., and Mehri, B. (2013) Application of elastically supported single-walled carbon nanotubes for sensing arbitrarily attached nano-objects. *Curr. Appl. Phys.* 13: 107–120.
9. Reddy, J. N., and Pang, S. N. (2008) Nonlocal continuum theories of beams for the analysis of carbon nanotubes. *J. App. Phys.* 103: 023511.
10. Maurizi, M. J., Rossi, R. E., and Reyes, J. A. (1976) Vibration frequencies for a uniform beam with one end spring hinged and subjected to a translational restraint at the other end. *J. Sound Vib.* 48(4): 565-568.
11. Laura, P. A. A., Grossi, R. O., and Alvarez, S. (1982) Transverse vibrations of a beam elastically restrained at one end and with a mass and spring at the other subjected to an axial force. *Nuclear Eng. Design* 74: 299-302.
12. Zhou, D. (1997) The vibrations of a cantilever beam carrying a heavy tip mass with elastic supports. *J. Sound Vib.* 206: 275-279.
13. Magrab, B. E. (2012) Magrab Vibrations of Elastic Systems: With Applications to MEMS and NEMS, New York, Springer.
14. Gürgöze M. (1996) On the eigenfrequencies of a cantilever beam with attached tip mass and spring-mass system. *J. Sound Vib.* 190(2): 149-162.
15. Azrar, A., Azrar, L., and Aljinaidi, A. A. (2011) Length scale effect analysis on vibration behaviour of single walled carbon nano tubes with arbitrary boundary conditions. *Revue de Mecanique Appliquee et Theorique* 2.5: 475-485.
16. Li, X.-F., Tang, G.-J., Shen, Z.-B., and Lee, K. Y. (2015) Resonance frequency and mass identification of zeptogram-scale nanosensor based on nonlocal theory beam theory. *Ultrasonics* 55: 75-84.
17. Moutlana, M. K., and Adali, S. (2015) Vibration of a cantilever beam with extended tip mass and axial load subject to piezoelectric control. *R & D J. South African Institution of Mech. Eng.* 31: 60-65

Chapter 7 – Paper 4: *Proceedings 26th International Congress on Sound and Vibration* (ICSV26)

7.1 Fundamental frequencies of a cantilevered nanobeam with arbitrary boundary conditions including surface effects.

In this Section, Case 2 is studied in more detail with surface effects and the findings are published in the Proceedings *26th International Congress on Sound and Vibration* (ICSV26), 7 – 11 July 2019, Montreal, Canada.

26th International Conference on Sound and Vibration
7-11 July 2019, Montréal

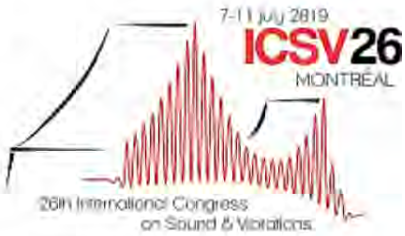

FUNDAMENTAL FREQUENCIES OF A CANTILEVERED NANOBEAM WITH ARBITRARY BOUNDARY CONDITIONS INCLUDING SURFACE EFFECTS.

Malesela K. Moutlana
Department of Mechanical Engineering, Durban University of Technology, Durban, 4001, RSA
email: moutlanam@dut.ac.za

Abstract

This investigation is about the motion of a cantilevered beam used in dynamic atomic force microscopy (dAFM) which can be utilized in scanning the topographical features of biological samples or "pliable" samples in general. These cantilevered beams can be used to modify samples by using high frequency oscillations to remove material or shape nano structures. A cantilever nanobeam with arbitrary boundary conditions is studied to investigate different configurations and the effects on the relevant parameters.

The nano structure is modelled using the Euler-Bernoulli theory. Eringen's theory of non-local continuum is incorporated to simulate the dynamics of the system. This theory is effective at nano-scale because it takes into account the small-scale effects of the structure. The scanning process is achieved by tapping/contact with the sample surface to determine the topographical profile of the sample. The tapping contact force can also be used to deform the sample surface or remove material using high frequency oscillations.

The fixed end is modelled as a torsional spring with zero transverse displacement instead of the "ideal" or clamped boundary condition. The torsional boundary condition can be tuned, by changing the torsional spring stiffness, such that the compliance of the system matches that of the sample to prevent mechanical damage of both the cantilever tip and the sample. The boundary condition at the free end is a tip-mass attached to a transverse linear spring which models a contact force.

At nano scale, the surface area to bulk ratio increases and surface effects becomes a significant factor when determining the natural frequencies of the system. The motions of the tip of the beam and the tip-mass is investigated to frequency response and force. The tip response frequency includes information about the maximum displacement amplitude and therefore the sample penetration depth.

Keywords: atomic force microscope, tip mass, elastic restraints, vibrations, nanobeam, small scale effects.

1. Introduction.

The vibration characteristics of nano scale beams can be analysed within the several frameworks depending on the size of the beam [1,2]. At macro and micro level, the Euler-Bernoulli and Timoshenko bending theories are used with a satisfactory results. When the beams reach nanoscale length, non-local continuum (stress gradient) and strain gradient theories are incorporated in the modelling [3-8]. These stress gradient theories include Eringen's non-local theory (first order stress) and higher order theories like Reddy Beam Theory (RBT) and Levison Beam Theory (LBT). Eringen's theory provides a unified foundation for field equations of non-local continuum and provides a basis for several stress-gradient theories [9]. Higher order stress/strain gradient theories are constructed such that the transverse stress at the surface vanish as required. Ansari et al. [10] and Lu et. al. [11] investigated strain gradient theories for beams at nanoscale by taking into account only the local higher order strains. All these theories above provide very accurate results compared to Molecular Dynamics (MD) simulations.

According to literature, scientist and engineers are presently extending their investigations to probe the behaviour of beam at pico-meter (pm) scale [12,13]. At these scales, the beams under investigation could be at minimum, three (3) atoms thick , and the bulk to surface volumes become comparable such the surface energies have significant influence on the vibration of the system. This influence on the natural frequencies of vibration is borne out of the fact that the different layers of the beam experience different environments.

The bulk material is typically surrounded by other atoms, whilst the surface atoms are in contact with the bulk atoms on one side and a different "environment" on the other side (i.e. air or viscous fluid). In the present study Gurtin and Murdoch's Linear Surface Elasticity Theory (LSET) is adopted to model the influence of surface effects on the system [14]. The system is modelled as a nanobeam with a torsional boundary condition at one end and spring-mass at the free end.

2. Elastically restrained nanobeam with spring–mass system at $x = L$.

The nanobeam under investigation is restrained by a torsional spring to at $x = 0$ and is modelled as a flexible restraint, and with a single degree of freedom spring-mass system attached at the other end $x = L$. Fig. (1a) shows the dAFM tip and Fig. (1b) shows the dAFM interacting with the sample.

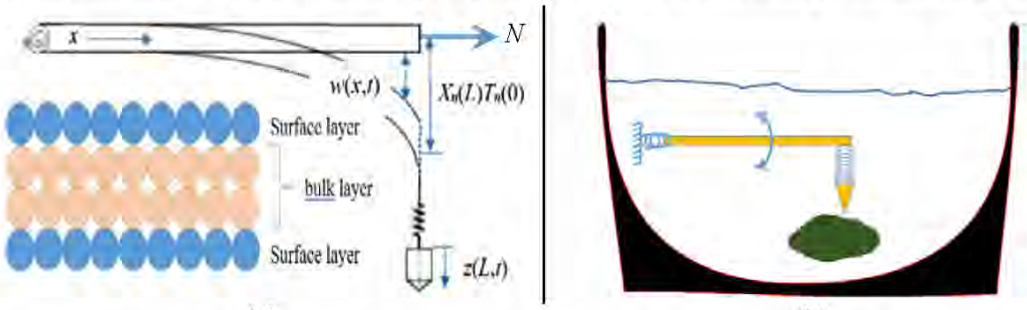

(a) (b)

Fig. 1. (a) Deflection of the beam with spring-mass attached at free end (b) sample in viscous fluid medium.

Attached to the free end of the beam at $x = L$ is a scanning tool which can be modelled as a mass with a sharp tip, attached to the beam by means of a linear spring (k_2) and the centre of gravity of the tip mass coincides with the tip of the beam and this constitutes the spring-mass system. During the scanning process, a contact force is generated between the tip mass and the object to be profiled. The spring-mass system is excited by the motion of the tip of the nanobeam as it vibrates and the constitutive relation of stress-strain for the beam based on nonlocal theory of elasticity can be expressed as

$$\sigma_{xx} - \bar{\mu}\frac{\partial^2 \sigma_{xx}}{\partial x^2} = E^e \varepsilon_{xx} \tag{1}$$

where E^e is the effective Young's modulus including surface effects, $\bar{\mu} = e_o l_i$ is the small scale parameter with e_o denoting a material constant and l_i the characteristic length. The expression for moment $M(x)$ is given by

$$M(x) - \bar{\mu}\frac{\partial^2 M(x)}{\partial x^2} = E^e I^e \frac{\partial^2 w}{\partial x^2} \tag{2}$$

where I^e is the effective moment of inertia. The equation of motion for a nonlocal nano beam undergoing transverse motion is given in (9) and can be expressed as

$$E^e I^e \frac{\partial^4 w(x,t)}{\partial x^4} - \tau_o s^* \frac{\partial^2 w(x,t)}{\partial x^2} + (\rho A + \rho_o s^*)\frac{\partial^2 w(x,t)}{\partial t^2} + \frac{2\nu l \rho_o}{H}\frac{\partial^4 w(x,t)}{\partial x^2 \partial t^2} + N\frac{\partial^2 w(x,t)}{\partial x^2} - \bar{\mu}N\frac{\partial^2 w(x,t)}{\partial x^2} + (\bar{\mu}\rho A + \bar{\mu}\rho_o s^*)\frac{\partial^4 w(x,t)}{\partial x^2 \partial t^2} = F_o(x,t) \tag{3}$$

where,

$$E^e I^e = EI + (2\mu_o + \lambda_o)I^* - \frac{2\nu l \tau_o}{H}$$

$$M_T \frac{\partial^2 z(t)}{\partial x^2} k_2 z(t) = k_2 w(L,t) \tag{4}$$

The Young's modulus of the bulk is E, μ_o and λ_o are the Lamme's constant that can be determined using molecular dynamics MD. I is the moment of inertia of the bulk and and I^* is the perimeter moment of inertia of the surface layer and ν is the Poisson's ratio whilst τ_o is the residual surface stress under unconstrained conditions. The density of the bulk is ρ and ρ_o that of the surface, A is the cross-sectional area and $s^* = \oint n_z^2 ds$ is the cross-sectional area of the surface layer. $F_o(x,t)$ is the forcing function which is taken as $F_o(x,t) = 0$ for a beam under free vibration. The dynamic motion of the tip mass is expressed in Eq. (4) and the two Eqs. (3) and (4) are coupled through the motion of the tip $w(L,t)$.

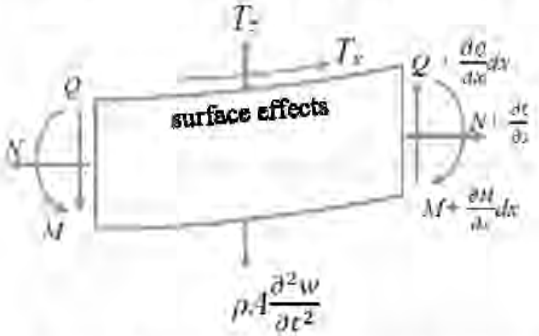

T_z – Normal Contact Traction
T_x – Tangential Contact Traction

Contact Tractions at the interface between bulk and the surface layer.

$$T_i = \sigma_{ij} n_i$$

Fig. 2. Section of beam showing forces and moments when beam is displaced from equilibrium position.

3. Method of solution.

Solution of the governing Eq. (3) is obtained by eigenfunction expansion of the displacement function as

$$w(x,t) = \sum_{n=1}^{\infty} X_n(x) T_n(t) \tag{5a}$$

$$z(L,t) = \sum_{n=1}^{\infty} z_o T_n(t) \tag{5b}$$

$$\ddot{T}_n(t) + \omega_n^2 T_n(t) = 0 \tag{5c}$$

Inserting Eq. (5a) into Eq. (3) and using Eq. (5c), we obtain the differential equation of motion for the beam in the modal domain. For the spring-mass, after inserting Eq. (5b) into Eq. (4) and using Eq. (5c), we obtain the equation of motion of the tip mass in the modal domain. The natural frequency ω_n is the frequency of the n^{th} mode of vibration. The differential equation in the modal mode then becomes

$$P \cdot X'''' + Q \cdot X'' - R \cdot X = 0 \tag{6a}$$

where,

$$P = 1 + \left[\frac{(2\mu_o + \lambda_o)}{E} - \frac{2\nu\tau_o}{\alpha}\right]\frac{\alpha}{H} - \mu\beta^2,$$

$$Q = \frac{2\nu}{A}\frac{I^*}{\alpha}\rho_c a_n^4 + \mu\left(1+\rho_c\frac{s^*}{A}\right)a_n^4 + \beta^2 - \tau_c\frac{s^*}{I},$$

$$R = \left(1+\rho_c\frac{s^*}{A}\right)a_n^4$$

and, $$\alpha = \frac{I^*}{I}H \quad , \quad \tau_c = \frac{\tau_0}{EL} \quad , \quad \mu = \frac{\bar{\mu}}{EI}L \quad , \quad \beta^2 = \frac{N}{EI}L^2 \quad , \quad \rho_c = \frac{\rho_o}{\rho L}$$

The motion of the tip-mass can also be written in the modal domain and the modal displacement of the system is

$$z(L,t) = \frac{\mathrm{X}(L)}{\left(1-\frac{a_n^4}{a_k^4}\right)} \tag{6b}$$

where $a_k^4 = \kappa_2/\eta$ is frequency parameter for the spring-mass system; κ_2 and η represent the linear spring constant ratio and the tip-mass ratio, respectively.

The frequency parameter a_n is associated with the natural frequency ω_n of vibration, α is a constant ratio that depends on the moment of inertia of the cross-section geometry of the bulk and surface, τ_c, μ, β^2, and ρ_c are the dimensionless constants corresponding to the residual stress, small-scale parameter, axial load and bulk to surface density ratio, respectively. The general solutions of Eq. (3) is given by

$$X_n(x) = A_n\cos p_{2n} + B_n\sin p_{2n} + C_n\cosh p_{1n} + D_n\sinh p_{1n} \tag{7a}$$

where p_{1n} and p_{2n} are

$$p_{1n} = \sqrt{\frac{Q+\sqrt{Q^2+4PR}}{2P}} \quad \text{and} \quad p_{2n} = \sqrt{\frac{Q-\sqrt{Q^2+4PR}}{2P}} \tag{7b}$$

The constants A_n, B_n, C_n and D_n are determined from the boundary conditions where, the boundary conditions at $x = 0$ are zero displacement and moment and can be expressed as

$$w(0) = 0 \tag{8a}$$

$$E^e I^e\frac{\partial^2 w(x,t)}{\partial x^2} + \frac{2\nu I\rho_o}{H}\frac{\partial^2 w(x,t)}{\partial t^2} + \bar{\mu}\left[N\frac{\partial^2 w(x,t)}{\partial x^2} - (\rho A + \rho_o s^*)\frac{\partial^2 w(x,t)}{\partial t^2} - (2\mu_o + \lambda_o)I^*\frac{\partial^4 w(x,t)}{\partial x^4} + \frac{2\nu I\rho_o}{H}\frac{\partial^4 w(x,t)}{\partial x^2\partial t^2}\right] - k_1\frac{\partial w(x,t)}{\partial \mathrm{x}} = 0 \tag{8b}$$

where k_1 is the torsional spring constant. Using Eqs. (5a) and (5b) the moment boundary condition can the transformed and written in the modal mode in Eqs. (9a) and (9b), where κ_1 the torsional is spring constant ratio.

$$X(0) = 0 \tag{9a}$$

$$\mu\frac{(2\mu_o+\lambda_o)}{E}\frac{I^*}{I}X'''' - \left\{1 + \left[\frac{(2\mu_o+\lambda_o)}{E} - \frac{2\nu\tau_c}{\alpha}\right]\frac{\alpha}{H} - \mu\beta^2 + \frac{2\nu}{A}\frac{I^*}{\alpha}\rho_c a_n^4 + \tau_c\frac{s^*}{I}\right\}X'' + a_n^4\left[\mu\left(1+\rho_c\frac{s^*}{A}\right) - \frac{2\nu}{A}\frac{I^*}{\alpha}\rho_c\right]X - \kappa_1 X' = 0 \tag{9b}$$

At the free end, taking into account the small scale effect, tip mass and the linear spring, the shear boundary condition at $x = L$ can be expressed as

$$E^e I^e\frac{\partial^3 w(x,t)}{\partial x^3} + \tau_o s^*\frac{\partial w(x,t)}{\partial x} + \frac{2\nu I\rho_o}{H}\frac{\partial^4 w(x,t)}{\partial x^2\partial t^2} - N\frac{\partial w(x,t)}{\partial \mathrm{x}} + \bar{\mu}\left[N\frac{\partial^3 w(x,t)}{\partial x^3} - (\rho A + \rho_o s^*)\frac{\partial^3 w(x,t)}{\partial x\partial t^2} + \frac{2\nu I\rho_o}{H}\frac{\partial^5 w(x,t)}{\partial x^3\partial t^2}\right] = F_L(x,t) \tag{10a}$$

where $F_L(x,t) = k_2 \cdot z(x,t)$ is force due to the spring-mass system and k_2 is the linear spring constant. Equation (6b) is the solution to Eq. (4) is used to represent $z(L,t)$ in the shear boundary. Using Eqs. (5a) and (5b) the shear boundary condition Eq. (10a) can the transformed and written in the modal mode in Eq. (10b),

$$\mu\frac{(2\mu_o+\lambda_o)}{E}\frac{I^*}{I}X''''' + \left\{1+\left[\frac{(2\mu_o+\lambda_o)}{E}-\frac{2\nu\tau_c}{\alpha}\right]\frac{\alpha}{H}+\mu\left(\beta^2+\tau_c\frac{s^*}{I}-\frac{2\nu}{A}\frac{I^*}{\alpha}\rho_c a_n^4\right)\right\}X''' + a_n^4\left[\mu\left(1+\rho_c\frac{s^*}{A}\right)-\frac{2\nu}{A}\frac{I^*}{\alpha}\rho_c\right]X' - \left(\tau_c\frac{s^*}{I}+\beta^2\right)X' - \frac{a_n^4\eta}{\left(1-\frac{a_n^4}{a_k^4}\right)}X = 0 \quad (10b)$$

Substitution of Eq. (7a) into the boundary condition Eq. (9a), we obtain

$$A_n + C_n = 0 \quad (11)$$

The general solution Eq. (7a) can now be expressed as

$$X_n(x) = B_n\sin p_{2n} + D_n\sinh p_{1n} + (\cos p_{2n} - \cosh p_{1n})C_n \quad (12)$$

substituting Eq. (12) into Eq. (8b) gives

$$B_n = \frac{C_n}{\kappa_1}\left(-\frac{p_{1n}^4(2\mu_o+\lambda_o)}{p_2E}\frac{I^*}{I}+\frac{p_{2n}^3(2\mu_o+\lambda_o)}{p_2E}\frac{I^*}{I}+\frac{p_{1n}^2\beta^2}{p_2}+p_{2n}\beta^2\right)\mu + \frac{C_n}{\kappa_1}\left(\frac{p_{1n}^2(2\mu_o+\lambda_o)}{p_2E}\frac{I^*}{I}+\frac{p_2(2\mu_o+\lambda_o)}{E}\frac{I^*}{I}+\frac{p_{1n}^2}{p_2}+p_{2n}\right)-\frac{p_{1n}}{p_{2n}}D_n \quad (13)$$

and substituting B_n in Eq. (12) into Eq. (11) gives the general solution expressed in terms of constants C_n and D_n alone. This result can be substituted into the moment boundary conditions Eq. (9a) at $x = L$ to obtain

$$C_n \cdot \Gamma_{1n} + D_n \cdot \Gamma_{2n} = 0 \quad (14)$$

were Γ_{1n} and Γ_{1n} are the constants extracted from applying the moment boundary condition, Eq. (9a) or (9b). After substituting the results of Eq. (4) and (13) into the shear boundary condition Eqs. (10a) or (10b) at $x = L$ can be expressed as

$$C_n \cdot \Gamma_{3n} + D_n \cdot \Gamma_{4n} = 0 \quad (15)$$

were Γ_{3n} and Γ_{4n} are the constants extracted from applying the shear boundary condition, Eq. (9a) or (9b) at the free end $x = L$. The results from the moment and shear boundary conditions given in Eqs. (14) and (15) can be expressed in matrix form as

$$\begin{bmatrix}\Gamma_{1n} & \Gamma_{2n}\\ \Gamma_{3n} & \Gamma_{4n}\end{bmatrix}\begin{bmatrix}C_n\\ D_n\end{bmatrix} = \begin{bmatrix}0\\ 0\end{bmatrix} \quad (16)$$

and the characteristic equation can be obtained from the determinant of Eq. (16) as:

$$\Gamma_{1n} \cdot \Gamma_{4n} - \Gamma_{2n} \cdot \Gamma_{3n} = 0 \quad (17)$$

The characteristic Eq. (17) can be solved numerically to compute the roots where κ_1, κ_2, η, a_n^4, β^2, μ and a_k^4 are the dimensionless constants for the beam and the spring-mass system.

4. Frequency equations for arbitrary boundary conditions.

The structure shown in Fig. (1), indicate a torsional spring with torsional spring constant κ_1 at $x = 0$. When the spring constant approaches zero ($\kappa_1 \to 0$), the restraint at $x = 0$ behaves as that of a pin support where there is zero resisting moment and the beam is allowed to spin freely. When the spring constant is not zero, there is a resisting moment at the boundary and therefore the torsional spring has an effect on the vibrations of the system. At the extreme end the spring constant approaches infinity ($\kappa_1 \to \infty$). In this case the support is completely rigid and the boundary condition is that of a cantilevered beam. In Eq. (12), when $\kappa_1 \to \infty$ the first two terms vanish in B_n above, and consequently in the characteristic equation too.

At $x = L$, a tip mass is attached to the beam by means of a transverse linear spring. When the linear spring constant is zero ($\kappa_2 \to 0$) the effect of the tip mass is not realized at the tip of the beam and therefore the tip-mass has no influence on the natural frequencies.

Table 1: Classical boundary condition derived from the system.

Boundary Conditions		κ_1	κ_2	η
Clamped-Free	CF	∞	0 or ∞	0
Simply supported-Free	SF	0	0 or ∞	0
Simply supported	SS	0	∞	∞
Clamped-Simply supported	CS	∞	∞	∞

However, as the linear spring constant increases ($\kappa_2 \to \infty$), the effect of the tip-mass become pronounced and when κ_2 is extremely large, the tip-mass is rigidly attached to the tip of the beam. By varying the torsional spring constant, linear spring constant and tip-mass ratio, we can derive the classic boundary conditions shown in Table 1. The frequency equation for the total system including torsional spring and spring-mass is given below in Eq. (21). The following frequency equations are derived from the boundary conditions in Table 1.

Clamped-Free (CF) with radial axial load:

$$\sinh(p_1L)\sin(p_2L)\left(\frac{2\beta^2}{p_1p_2}-\frac{p_2}{p_1}+\frac{p_1}{p_2}\right)+\cosh(p_1L)\cos(p_2L)\left(\beta^2\left(\frac{1}{p_2^2}-\frac{1}{p_1^2}\right)-2\right)-\beta^2\left(\frac{1}{p_2^2}+\frac{1}{p_1^2}\right)-\frac{p_2^2}{p_1^2}-\frac{p_1^2}{p_2^2} \tag{18}$$

Simply supported-Free (SF):

$$\frac{1}{\kappa_1}\left(\left(p_2+\frac{p_1^2}{p_2}\right)\cosh(p_1L)\sin(p_2L)+\left(-\frac{p_2^2}{p_1}-p_1\right)\sinh(p_1L)\cos(p_2L)\right)+\left(\frac{p_1}{p_2}-\frac{p_2}{p_1}\right)\sinh(p_1L)\sin(p_2L)-2\cosh(p_1L)\cos(p_2L)-\frac{p_2^2}{p_1^2}-\frac{p_1^2}{p_2^2} \tag{19}$$

Clamped-Simply supported (CS):

$$\frac{1}{\kappa_1\eta}\left(-\frac{p_1p_2^3\cosh(p_1L)\sin(p_2L)}{a_n^4}-\frac{p_1^3p_2\cosh(p_1L)\sin(p_2L)}{a_n^4}\right)+\frac{1}{\kappa_1\eta}\left(\frac{p_2^4\sinh(p_1L)\cos(p_2L)}{a_n^4}+\frac{p_1^2p_2^2\sinh(p_1L)\cos(p_2L)}{a_n^4}\right)+\frac{1}{\kappa_1\eta}\left(\frac{p_1^3p_2\cosh(p_1L)\sin(p_2L)}{a_k^4}-\frac{p_2^4\sinh(p_1L)\cos(p_2L)}{a_k^4}-\frac{p_1^2p_2^2\sinh(p_1L)\cos(p_2L)}{a_k^4}\right)+\frac{1}{\eta a_n^4}\left((p_2^3-p_1^2p_2)\sinh(p_1L)\sin(p_2L)+2p_1p_2^2\cosh(p_1L)\cos(p_2L)+\frac{p_2^4}{p_1}+p_1^3\right)+\frac{1}{\eta a_k^4}\left((p_1^2p_2-p_2^3)\sinh(p_1L)\sin(p_2L)-2p_1p_2^2\cosh(p_1L)\cos(p_2L)-\frac{p_2^4}{p_1}-p_1^3\right)+\frac{1}{\kappa_1}\left(\frac{p_2^3\sinh(p_1L)\sin(p_2L)}{p_1^2}+2p_2\sinh(p_1L)\sin(p_2L)+\frac{p_1^2\sinh(p_1L)\sin(p_2L)}{p_2}\right)+\left(\frac{p_2}{p_1}+\frac{p_1}{p_2}\right)\cosh(p_1L)\sin(p_2L)-\left(\frac{p_2^2}{p_1^2}+1\right)\sinh(p_1L)\cos(p_2L) \tag{20}$$

Torsional cantilever with spring mass system:

$$\frac{1}{\kappa_1}\left(\cosh(p_1L)\sin(p_2L)\left(\frac{p_2^3a_n^4\beta^2}{p_1^4a_k^4}-\frac{p_2^3\beta^2}{p_1^4}+\frac{p_2a_n^4\beta^2}{p_1^2a_k^4}-\frac{p_2\beta^2}{p_1^2}+\frac{p_2^3a_n^4}{p_1^2a_k^4}-\frac{p_2^3}{p_1^2}+\frac{p_2a_n^4}{a_k^4}-p_2\right)\right)+\frac{1}{\kappa_1}\left(\sinh(p_1L)\cos(p_2L)\left(\frac{p_2^2a_n^4\beta^2}{p_1^3a_k^4}-\frac{p_2^2\beta^2}{p_1^3}+\frac{a_n^4\beta^2}{p_1a_k^4}-\frac{\beta^2}{p_1}-\frac{p_2^4a_n^4}{p_1^3a_k^4}+\frac{p_2^4}{p_1^3}-\frac{p_2^2a_n^4}{p_1a_k^4}+\frac{p_2^2}{p_1}\right)\right)+\cosh(p_1L)\cos(p_2L)\left(-\frac{p_2^2a_n^4\beta^2}{p_1^4a_k^4}+\frac{p_2^2\beta^2}{p_1^4}+\frac{a_n^4\beta^2}{p_1^2a_k^4}-\frac{\beta^2}{p_1^2}-\frac{2p_2^2a_n^4}{p_1^2a_k^4}+\frac{2p_2^2}{p_1^2}\right)+\frac{1}{a_k^4}\left(\frac{p_2^2a_n^4\beta^2}{p_1^4}-\frac{a_n^4\beta^2}{p_1^2}-\frac{p_2^4a_n^4}{p_1^4}-a_n^4\right)+\frac{1}{a_k^4}\left(\sinh(p_1L)\sin(p_2L)\left(\frac{2p_2a_n^4\beta^2}{p_1^3}-\frac{p_2^3a_n^4}{p_1^3}+\frac{p_2a_n^4}{p_1}\right)\right)+\sinh(p_1L)\sin(p_2L)\left(-\frac{2p_2\beta^2}{p_1^3}+\frac{p_2^3}{p_1^3}-\right.$$

$$\frac{p_2}{p_1}\Big) - \frac{p_2^2\beta^2}{p_1^4} + \frac{\beta^2}{p_1^2} + \frac{1}{\kappa_1}\left(\sinh(p_1L)\sin(p_2L)\left(\frac{p_2^3\eta a_n^4}{p_1^5} + \frac{2p_2\eta a_n^4}{p_1^3} + \frac{\eta a_n^4}{p_1p_2}\right)\right) +$$
$$\sinh(p_1L)\cos(p_2L)\left(-\frac{p_2^2\eta a_n^4}{p_1^5} - \frac{\eta a_n^4}{p_1^3}\right) + \cosh(p_1L)\sin(p_2L)\left(\frac{p_2\eta a_n^4}{p_1^4} + \frac{\eta a_n^4}{p_1^2p_2}\right) + \frac{p_2^4}{p_1^4} + 1 \qquad (21)$$

The natural frequencies of the system R_n are obtained by making a substitution, $a_n = R_n/L$, into the into Eq. (17). The values of R_n are dimensionless natural frequencies used below to analyse the numerical results. When $\kappa_1 \to \infty$ the torsional spring becomes rigid and the boundary condition behaves like that of a cantilevered beam. The classic cantilever configure can be obtained by setting the mass to zero ($\eta = 0$) and the fundamental natural frequency of the system is $R_1 = 1.8750$ which corresponds to the results obtained by Magra [15] $R_1 = 0.5969\pi$. Furthermore, when $\kappa_1 \to \infty$ the linear spring is rigid and the system behaves like a cantilevered beam with concentrated tip mass because the centre of gravity of the attached mass coincides with the tip of the beam (see Fig. (1)).

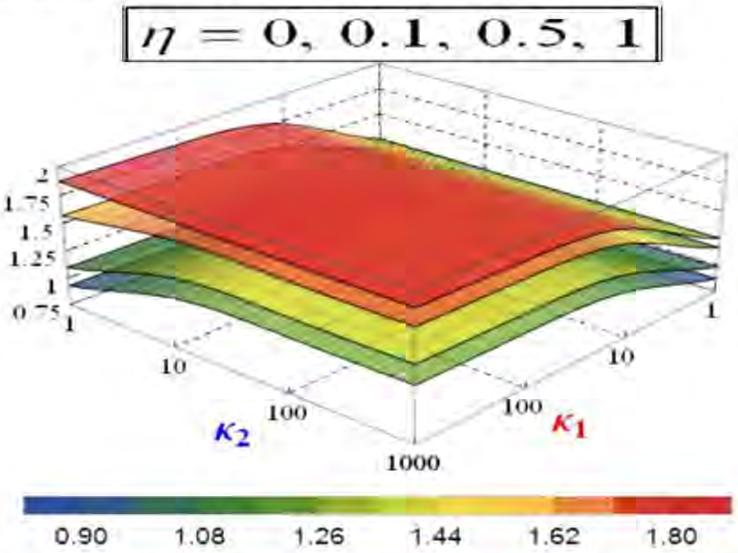

Fig. 3. Fundamental frequency plotted against spring constants κ_1 and κ_2 with tip mass ratio: a) $\eta = 0$, 0.1, 0.5 and 1.

For a tip mass ratio $\eta = 0.1$ and $\eta = 1$ the fundamental natural frequency is $R_1 = 1.7227$ and $R_1 = 1.2479$ which are the same result obtained by Magrab ($R_1 = 0.5484\pi$) and Gürgöze ($R_1 = 1.2479$), respectively [15,16]. In practical applications, the values for the parameters of interest will vary between zero and infinity ($0 < \kappa_1, \kappa_2, \eta < \infty$). The boundary conditions discussed above relate to extreme rigidity of the torsional and linear spring. It is also noted that the when the torsional spring is completely elastic $\kappa_1 \to 0$ the fundamental natural frequencies approach zero in the limit $R_1 \to 0$ and the other variables have minimal effect on the frequencies as seen in Fig. (1) above.

5. Conclusions.

In the present paper, small scale and surface effects on the fundamental frequency are investigated for a nanobeam with elastically restrained end conditions and carrying a tip mass attached via a linear spring to the end of the beam. The solution for the beam is obtained analytically by expanding the deflection in terms of its eigenfunctions and solving the resulting characteristic equation numerically. Furthermore, the characteristic equations are presented for parametric studies of the effect of support elasticity and tip mass on the fundamental frequencies of the nanobeam.

It is observed that the boundary conditions may lead to an increase or decrease of the fundamental frequency depending on the support flexibility. Boundary conditions can are expressed in terms of a torsional spring at $x = 0$, linear spring and tip mass at $x = L$. The classical boundary conditions correspond to setting the torsional and linear spring constants to zero $(\kappa_{1,2} \to 0)$ or infinity $(\kappa_{1,2} \to \infty)$.

It was observed that low torsional spring stiffness leads to a decrease in the fundamental frequency and high torsional spring stiffness to an increase in the fundamental frequency as the small scale parameter increases. The rates of decrease and increase depend on the relative values of the spring constants. The effect of the tip mass on the frequencies is to lower the natural frequencies as observed in [17] and [18].

6. Acknowledgment

The research of the author was supported by research grants from the Durban University of Technology (DUT). The author gratefully acknowledges the support provided by DUT.

7. REFERENCES

1. Eringen, A. C., and Edelen, D. (1972) On nonlocal elasticity. *Int. J. Eng. Sci.* 10 (3): 233–248.
2. Eringen, A. C., (2002) Nonlocal Continuum Field Theories, Springer-Verlag, New York.
3. Rahmanian, M., Torkaman-Asadi, M. A., Firouz-Abadi, R. D., and Kouchakzadeh, M. A. (2016) Free vibrations analysis of carbon nanotubes resting on Winkler foundations based on nonlocal models. *Physica B* 484: 83–94.
4. Moutlana, M.K. and Adali, S. (2019) Fundamental frequencies of a torsional cantilever nano beam for dynamic atomic force microscopy (dAFM) in tapping mode *Microsystem Technologies, 25(3), 1087-1098* , DOI 10.1007/s00542-018-4166-x
5. Eltaher, M.A., Khater, M.E. And Emam, S.A (2016) A review on nonlocal elastic models for bending, buckling, vibrations and wave propagation of nanoscale beams. *Applied Mathematical Modelling* **40** 4109-4128.
6. Eltaher, M. A., Alshorbagy, A. E., and Mahmoud, F. F. (2013) Vibration analysis of Euler–Bernoulli nanobeams by using finite element method. *Appl. Math. Modelling* 37: 4787–4797.
7. Kiani, K. (2015) Nanomechanical sensors based on elastically supported double-walled carbon nanotubes. *Appl. Math. Comput.* 270: 216–241.
8. Moutlana, M.K. and Adali, S. (2017) Fundamental frequencies of a nano beam used for atomic force microscopy (AFM) in tapping mode, The 9th International Conference of the African Materials Research Society (AMRS2017) GABORONE, BOTSWANA. (11 to 14 Dec 2017) MRS ADVANCES, Warrendale, PA. https://doi.org/10.1557/adv.2018.321.
9. Reddy, J. N., and Pang, S. N. (2008) Nonlocal continuum theories of beams for the analysis of carbon nanotubes. *J. App. Phys.* 103: 023511.
10. Ansari, R., Gholami, R. and Rouhi, H. (2012) Vibration analysis of single-walled carbon nanotubes using different gradient elasticity theories. *Composites*: *Part B*: 43: 2985-2989
11. Lu, L., Gou, X and Zhao, J. (2017) Size-dependent vibration analysis of nanobeams based on the nonlocal strain gradient. *International Journal of Engineering Science*. 116: 12-24.
12. Zhao, H.S., Zhang, Y. and Lie, S.T. (2018) Frequency equations of nonlocal elastic micro/nanobeams with the consideration of the surface effects. *Applied Mathematics and Mechanics* **39**(8), 1089-1102.
13. Eltaher, M. A., and Mahmoud, F. F., Assie, A.E. and Meltis, E.I. (2013) Coupling effects of nonlocal and surface energy on vibration analysis of nanobeams. *Applied Mathematics and Computation* 223: 760-774.
14. Gurtin, M.E. and Murdoch, A. (1975) A continuum theory of elastic material surfaces. *Archive for Rational Mechanics and Analysis* (57) 291-323.
15. Magrab, B. E. (2012) Magrab Vibrations of Elastic Systems: With Applications to MEMS and NEMS, New York, Springer.
16. Gürgöze M. (1996) On the eigenfrequencies of a cantilever beam with attached tip mass and spring-mass system. *J. Sound Vib.* 190(2): 149-162.
17. Moutlana, M. K., and Adali, S. (2015) Vibration of a cantilever beam with extended tip mass and axial load subject to piezoelectric control. *R & D J. South African Institution of Mech. Eng.* 31: 60-65.
18. Moutlana, M.K. and Adali, S. (2018) Effects of Elastic Restraints on the Fundamental Frequency of Nonlocal Nanobeams with Tip Mass. *International Journal of Acoustics and Vibration (IJAV)* (accepted for publication).

Chapter 8 – Paper 5: *Computation of the natural frequencies and dynamic behavior of the nanobeam subject to various boundary conditions*

8.1 Natural frequencies of a torsional cantilever nanobeam with spring-mass system and longitudinal linear spring, including buckling.

In this Section, Case 2 is studied in more detail with the inclusion of a directed axial load induced via a linear spring. (Sent for publication).

Frequencies of a torsional cantilever nanobeam with arbitrary boundary conditions under axial load including buckling.

MALESELA K. MOUTLANA
Department of Mechanical Engineering, Durban University of Technology, Durban, 4001, South Africa

Abstract.

Torsional cantilevers are gaining prominence in the field of nano-manufacturing at atomic scale, nano-biomedicine, hydrodynamics, etc. This class of cantilever (torsional) allows for greater control of the system and improved sensitivity of for scanning surfaces immersed in viscous environments. This report is concerned with the motion of a beam used in dynamic atomic force microscopy (dAFM). The AFM was discovered by Binnig and is used to scan the topographical features of samples at atomic level and this has led to the ability to manipulate and create structures with sub-nano building blocks. Manipulating of biological or pliable samples in general has led to great advances in the biomedicine and hydrodynamic nano sciences. These beams can be used to scan and modify samples by using high frequency oscillations to remove material or shape these structures at nanoscale. The scanning process is achieved by contact as a result of tapping the sample surface to determine the topographical profile of the sample. The tapping contact force can also be used to deform the sample surface and/or remove material using high frequency oscillations.

A nanobeam with arbitrary boundary conditions is studied to model different configurations and the effects on the parameters of interest for application in dAFM. Euler-Bernoulli theory is generally used to model beams and is exceedingly reliable at micro and micro level. At nano level, the theory is not reliable, and the modelling must be augmented with other modern theories to accurately describe the transverse motion in vibration. In this study Eringen's theory of nonlocal continuum or stress gradient theory is incorporated to consider the small-scale effects that are brought about due to size.

The classic cantilever has a clamped boundary condition called the fixed end with zero freedom to allow rotary and linear motion. In a torsional cantilever the boundary condition can be adjusted, by altering the torsional spring stiffness, to influence the natural frequencies. The boundary condition at the free end is a transverse spring with the other end attached to a mass i.e. a spring-mass system. A longitudinal linear spring is also attached to tip of the beam.

The motions of the tip of the beam and the tip-mass is investigated to determine the frequency response and force interaction at the contact point with the sample. The tip response frequency contains information about the maximum displacement amplitude and acceleration, and therefore the sample penetration depth and contact force.

Keywords: atomic force microscope, tip mass, elastic restraints, vibrations, nanobeam, small scale effects.

8.1.1 Introduction.

Carbon nano tubes/material have assumed a prominent role in engineering structures. Advanced research has resulted in the creation of nano electromechanical systems (NEMS) which have led to application that improve many aspects of life including research into sub-micron robotics, biomedicine, nano-resonator sensors, etc. Vibrations of nanobeam have found expression in atomic force microscopy for scanning and manufacturing.

The vibration characteristics of nano scale beams are examined within the Euler-Bernoulli framework underpinned by Eringen's nonlocal continuum theory due to the size of the beam [1-12]. At macro and micro level classic bending theories are used with a satisfactory result. When the beams reach nanoscale dimensions, modern advanced theories are employed i.e. nonlocal continuum (stress gradient) and strain gradient theories are incorporated in the modelling [3-8]. These stress gradient theories include Eringen's non-local theory (first order stress) and higher order theories like Reddy Beam Theory (RBT) and Levison Beam Theory (LBT). Eringen's theory postulates a unified groundwork for field equations of nonlocal continuum and provides a foundation for several stress-gradient theories [9]. Higher order stress/strain gradient theories are structured to allow the transverse stress at the surface approach zero as required. Lu *et. al.* [11-12] and Gholami *et. al.* [10] investigated strain gradient theories for beams at nanoscale by considering only the local higher order strains. All these theories above provide very accurate results compared to Molecular Dynamics (MD) simulations.

The nanobeam under investigation is restrained by a torsional spring to at $x = 0$ and is typically referred to as a torsional cantilever. This class of cantilevers have been shown to improve sensitivity in application for low aspect ratio beam according Sriramshankar and Jayanth [15], whereas comparable levels of sensitivity can be achieved by using long or high aspect ratio beams for conventional cantilevers. Furthermore, high aspect ratio beams are disadvantageous for applications in viscous medium because of the associated damping.

In the present investigation, the nanobeam carries a single degree lateral spring-mass system and a longitudinal constant force spring at $x = L$. This configuration is appropriate for manipulation of samples or structures at nanoscale i.e. removal of atoms or molecules to functionally grade nanomaterials for specific behaviour. The beam and spring-mass operate as a hammer and chisel, and the depth of penetration can be adjusted by tuning the elastic restraints to influence the vibration frequencies. The vibration frequencies contain information about the dynamic behaviour for the entire system i.e. displacements of beam tip and mass,

velocity and acceleration. The longitudinal spring provides a constant axial that is assumed to be directed in the horizontal direction for small deflection, in conformity with the theories mentioned above.

8.1.2 Nanobeam with spring–mass and axial load at $x = L$.

The nanobeam in this investigation is restrained by a torsional spring (k_1) at $x = 0$ and is modelled as a cantilever with a flexible restraint in Fig. (8.1a) and (8.1b). The stiffness of the spring can be adjusted to simulate an elastic beam support, with the spring providing a torsional force. At the other end of the beam $x = L$, a constant axial load $N(x,t)$ is applied in compression (+*ve*) and tension (-*ve*), and a single degree of freedom spring-mass system is attached. The lateral linear spring stiffness (k_2) can be adjusted to achieve the desired penetration depth by using the information contained in the frequencies of vibration.

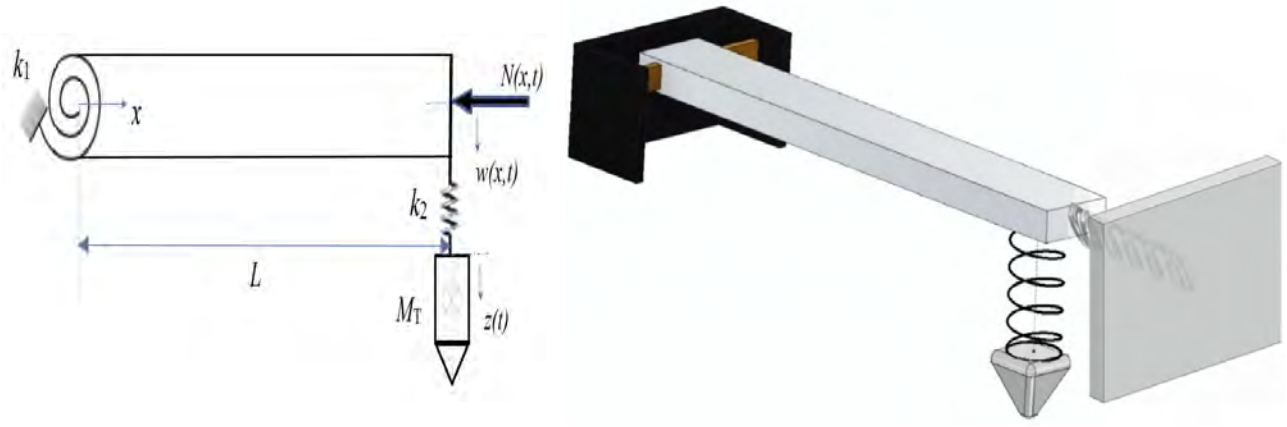

(a) (b)

Figure 8-1: Elastically restrained beam with concentrated axial load and spring-mass attached at free end.

The above diagrams are simplified in Fig. (8.2) to indicate the tip displacement of the nanobeam structure and the tip-mass. The displacement of the beam is indicated by $w(x,t)$, where $w(x,t)$ contains the temporal domain and the modal domain function, which includes the sum of the infinite numbers of modes in the modal domain.

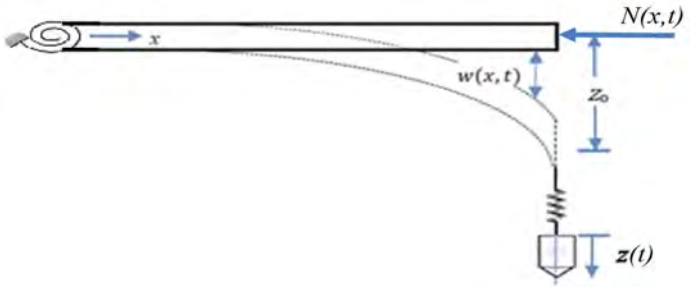

Figure 8-2: Deflection of the beam with constant axial load and spring-mass attached at free end.

The motion of the tip-mass is indicated by $z(t)$ and is dependent on time and the position of the spring-mass system along the beam is $0 < x < L$. The amplitude of vibration for the tip-mass is z_o and is coupled to the beam displacement. Attached to the free end of the beam at $x = L$ is a sculpting/scanning tool which can be modelled as a mass with a sharp tip, attached to the beam by means of a linear spring (k_2) and the centre of gravity of the tip mass coincides with the tip of the beam and this constitutes the spring-mass-system. Fig. (8.3a) shows the dAFM tip approaching the sample and Fig. (8.3b) shows the dAFM interacting with the sample in a viscous medium.

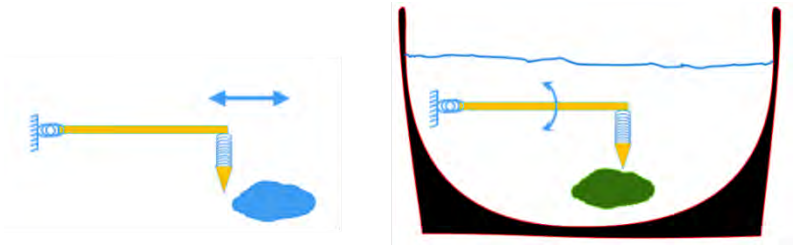

(a) (b)

Figure 8-3: Nanobeam probe with spring-mass approaching sample of interest (a) sample in open air (b) stubby probe in viscous fluid medium.

During the scanning process, a contact force is produced between the tip mass and the sample to be profiled. The spring-mass system is excited by the displacement of the tip of the nanobeam during motion, generating a multiplicative effect on the displacement of the mass. In order to proceed with the solution, the constitutive relation of stress-strain for the beam based on nonlocal theory of elasticity can be expressed as,

$$\sigma_{xx} - \bar{\mu}\frac{\partial^2 \sigma_{xx}}{\partial x^2} = E\mathcal{E}_{xx} \tag{1}$$

Where E is the effective Young's modulus, $\mathcal{E}_{xx}$ is the longitudinal strain, $\bar{\mu} = e_o l_i$ is the small-scale parameter with e_o denoting a material constant and l_i the characteristic length, which are determined using Molecular Dynamics(MD) simulations. The nonlocal expression for moment $M(x)$ is given by,

$$M(x) - \bar{\mu}\frac{\partial^2 M(x)}{\partial x^2} = EI\frac{\partial^2 w}{\partial x^2} \tag{2}$$

where I is the effective moment of inertia. The equation of motion for a nonlocal nano beam undergoing transverse motion with axial load is given by Reddy [9] and can be expressed as,

$$EI\frac{\partial^4 w(x,t)}{\partial x^4} + N(x,t)\frac{\partial^2 w(x,t)}{\partial x^2} - \bar{\mu}N(x,t)\frac{\partial^4 w(x,t)}{\partial x^4} + \rho A\frac{\partial^2 w(x,t)}{\partial t^2} + \bar{\mu}\rho A\frac{\partial^4 w(x,t)}{\partial x^2 \partial t^2} = F_o(x,t) \tag{3}$$

and the equation of motion for the spring mass system at $x = L$ is,

$$M_T \frac{\partial^2 z(t)}{\partial x^2} k_2 z(t) = k_2 w(L,t) \tag{4}$$

The density of the nanobeam is ρ and A is the cross-sectional area. $F_o(x,t)$ stands the external forcing function which is taken as $F_o(x,t) = 0$ for a nanobeam undergoing free vibration. The applied axial load, $N(x,t)$, is kept constant during vibration and simply referred to as N in the equations below. The dynamic motion of the tip mass is stated in Eq. (4) and the two discreet systems in Eqs. (3) and (4) are coupled through the motion of the tip $w(L,t)$.

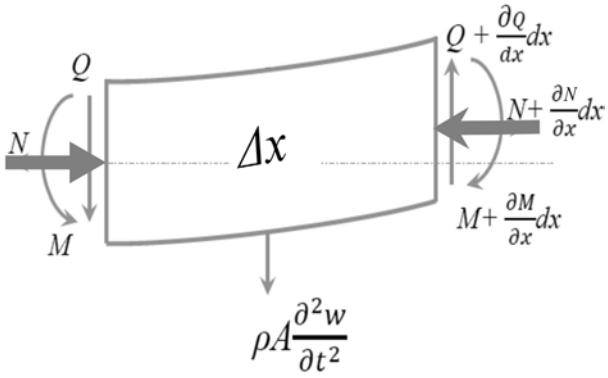

Figure 8-4: Infinitesimal section of beam showing forces and moments for beam displaced from equilibrium position.

An infinitesimal section (Δx) of the nanobeam is indicated in Fig. (8.4) and by taking the sum of the forces and moments we derive the governing equations of motion.

$$M = EI \frac{\partial^2 w(x,t)}{\partial x^2} + \bar{\mu}\left[N \frac{\partial^2 w(x,t)}{\partial x^2} - \rho A \frac{\partial^2 w(x,t)}{\partial t^2}\right] \tag{5}$$

$$Q = EI \frac{\partial^3 w(x,t)}{\partial x^3} + N \frac{\partial w(x,t)}{\partial x} - \bar{\mu}\left[N \frac{\partial^3 w(x,t)}{\partial x^3} - \rho A \frac{\partial^3 w(x,t)}{\partial x \partial t^2}\right] \tag{6}$$

Using Eqs. (5) and (6) incorporating the nonlocal effects, the equation of motion for a nonlocal nanobeam in transverse vibration is,

$$EI \frac{\partial^4 w(x,t)}{\partial x^4} + N \frac{\partial^2 w(x,t)}{\partial x^2} - \bar{\mu} N \frac{\partial^4 w(x,t)}{\partial x^4} - \rho A \frac{\partial^2 w(x,t)}{\partial t^2} + \bar{\mu} \rho A \frac{\partial^4 w(x,t)}{\partial x^2 \partial t^2} = 0 \tag{7}$$

8.1.3 Critical buckling due directed axial load at $x = L$.

The axial load is applied in both compression and tension and the magnitude of the force in compression should be limited in order prevent buckling failure. The choice of axial load is made by referencing the applied load (N) to the critical buckling load (N_{cr}) of the nanobeam.

$$N = k \cdot N_{cr} \tag{8}$$

where k is the axial load fraction and allows the for the axial load to be selected in an appropriate range, $k = +0.8, +0.4, 0, -0.4, -0.8$. To determine the critical buckling load of

the system, the equation of motion Eq. (7) is written below with the terms involving the time derivative equal to zero.

$$EI\frac{\partial^4 w(x)}{\partial x^4} + N\frac{\partial^2 w(x)}{\partial x^2} - \bar{\mu}N\frac{\partial^4 w(x)}{\partial x^4} = 0 \tag{9}$$

The above Eq. (9) is a 4th order differential equation of motion can be reduced to a 2nd order differential equation by integrating twice with respect to *x*. After integration twice we derive an equation with two integration constants, E and F.

$$(EI - \bar{\mu}N)\frac{\partial^2 w(x)}{\partial x^2} + Nw(x) = Ex + F \tag{10}$$

The LHS side of Eq. (6) has a homogeneous solution of the form

$$\frac{\partial^2 w(x)}{\partial x^2} + \lambda^2 w(x) = 0 \tag{11a}$$

$$\lambda^2 = \frac{N}{(EI - \bar{\mu}N)} \quad \text{or} \quad N = \frac{\lambda^2}{(1+\bar{\mu}\lambda^2)}EI \tag{11b}$$

The solution for this second order differential equation of motion has two solutions, a homogenous and a particular solution which is derived from the boundary conditions. The total solution is a sum of the homogenous and particular solution and can be expressed as,

$$w(x) = Asin(\lambda x) + Bcos(\lambda x) + \frac{1}{\lambda^2}(Ex + F) \tag{12}$$

The constants, A, B, E and F can be determined from the displacement and moment boundary conditions at $x = 0$:

$$w(0) = 0 \tag{13}$$

$$EI\frac{\partial^2 w(0)}{\partial x^2} - \bar{\mu}N\frac{\partial^2 w(0)}{\partial x^2} - k_1\frac{\partial w(0)}{\partial \mathrm{x}} = 0 \tag{14}$$

and, the moment and shear forces at $x = L$:

$$EI\frac{\partial^2 w(L)}{\partial x^2} - \bar{\mu}N\frac{\partial^2 w(L)}{\partial x^2} = 0 \tag{15}$$

$$EI\frac{\partial^3 w(L)}{\partial x^3} - \bar{\mu}N\frac{\partial^3 w(L)}{\partial x^3} - N\frac{\partial w(L)}{\partial \mathrm{x}} = 0 \tag{16}$$

After inserting the general solution into the boundary conditions, only three constants can be determined and the fourth constant is set to unity, and this results in a transcendental equation with roots corresponding to the various buckling modes. The lowest root of the transcendental equation corresponds to the critical buckling load and is written as follows for a torsional cantilever,

$$-\frac{\sin(\lambda L)}{k_1} + \gamma\cos(\lambda L) = 0 \tag{17}$$

for the lowest buckling load, $\lambda = 0$ is a trivial solution and therefore the transcendental equation is solved numerically for the non-trivial solutions. When $k_1 \to 0$ the transcendental

equation is that of a simply supported beam, $\sin(\lambda L) = 0$ and when $k_1 \to \infty$ the equation is that of a cantilever beam, $\cos(\lambda L) = 0$ in concurrence with Reddy [10]. The 1st root of the equation is substituted into Eq. (11b) to obtain the critical buckling load of the system (N_{cr}).

8.1.4 Method of solution for the governing equations.

Solution of the governing Eq. (3) is obtained by eigenfunction expansion of the displacement function as,

$$w(x,t) = \sum_{n=1}^{\infty} X_n(x)T_n(t) \tag{18a}$$

$$z(t) = \sum_{n=1}^{\infty} z_o T_n(t) \tag{18b}$$

$$\ddot{T}_n(t) + \omega_n^2 T_n(t) = 0 \tag{18c}$$

Inserting Eq. (18a) into Eq. (7) and using Eq. (18c), the differential equation of motion for the beam in the modal domain is obtained. For the spring-mass, after inserting Eq. (18b) into Eq. (4) and using Eq. (18c), the equation of motion of the tip mass is reduced to the modal domain. The natural frequency ω_n is the frequency of the n^{th} mode of vibration for the nanobeam which is directly related to the frequency parameter, a_n^4. The differential equation in the modal mode becomes,

$$P \cdot X'''' + \mathrm{Q} \cdot X'' - R \cdot X = 0 \tag{19a}$$

where,

$$P = 1 - \mu\beta^2 \tag{19b}$$

$$Q = \mu a_n^4 + \beta^2 \tag{19c}$$

$$R = a_n^4 \tag{19d}$$

and, $$\mu = \frac{\bar{\mu}}{EI}L \ , \ \beta^2 = \frac{N}{EI}L^2 \quad , \quad N = k \cdot N_{cr} \ , \ N_{cr} = \frac{EI}{L^2}\left(\frac{\pi^2}{4 + \bar{\mu}\pi^2}\right)$$

$$a_n^4 = \frac{\rho A \omega_n^2}{EI} \text{ and } a_n = \frac{R_n}{L}$$

The motion of the tip-mass can also be written in the modal domain and the modal displacement of the system is,

$$z(L,t) = a_n^4 \mathrm{X}(L) \Big/ \left(1 - \frac{a_n^4}{a_k^4}\right) \tag{20}$$

where $a_k^4 = \kappa_2/\eta$ is frequency parameter for the spring-mass system; κ_2 and η represent the linear spring constant ratio and the tip-mass ratio, respectively.

The frequency parameter a_n is associated with the circular frequency ω_n of vibration, μ and β^2 are the dimensionless constants corresponding to the small-scale parameter and axial load, respectively. The general solutions of Eq. (19a) is given by,

$$X_n(x) = A_n\cos(p_{2n}x) + B_n\sin(p_{2n}x) + C_n\cosh(p_{1n}x) + D_n\sinh(p_{1n}x) \tag{21}$$

where the wave numbers p_{1n} and p_{2n} are,

$$p_{1n} = \sqrt{\frac{Q+\sqrt{Q^2+4PR}}{2P}} \quad \text{and} \quad p_{2n} = \sqrt{\frac{Q-\sqrt{Q^2+4PR}}{2P}} \tag{22}$$

After substituting P, Q and R from Eqs. (19b), (19c) and (19d) into Eq. (22), the following two equations are obtained.

$$p_{1n} = \sqrt{\frac{\beta^2+\mu a_n^4}{2(1-\beta^2\mu)} + \frac{1}{2}\sqrt{\frac{(\beta^2)^2+4a_n^4-2\beta^2\mu a_n^4+\mu^2 a_n^8}{(1-\beta^2\mu)^2}}} \tag{23}$$

$$p_{2n} = \sqrt{\frac{\beta^2+\mu a_n^4}{2(1-\beta^2\mu)} - \frac{1}{2}\sqrt{\frac{(-\beta^2)^2+4a_n^4-2\beta^2\mu a_n^4+\mu^2 a_n^8}{(1-\beta^2\mu)^2}}} \tag{24}$$

The constants p_{1n} and p_{2n} are derived from the roots of the differential equation, Eq. (19a). The first and second term in Eq. (19a) contain the axial load ratio (β^2) which implicitly included in P and Q in Eq. (22) as indicated in Eqs. (23) and (24). For the roots of the differential equation to be real, the internal radical $\sqrt{Q^2+4PR}$ must necessarily be positive and the external radical must also be real. Since the axial load ratio (β^2) can be both positive (compressive) or negative (tensile), we must observe critical limits on the values of the axial load ratio (β^2) to ensure acceptable results. Moreover, $(1-\beta^2\mu) \neq 0$ because that would cause the terms under the radical to tend towards infinity. Furthermore, if the internal radical is positive, the first term under the radical must the greater than the second term and positive, to avoid imaginary roots.

The constants A_n, B_n, C_n and D_n are determined from the boundary conditions where, the boundary conditions at $x = 0$ are zero displacement and moment and can be expressed as,

$$w(0) = 0 \tag{25a}$$

$$EI\frac{\partial^2 w(0,t)}{\partial x^2} + \bar{\mu}\left[N\frac{\partial^2 w(0,t)}{\partial x^2} - (\rho A)\frac{\partial^2 w(0,t)}{\partial t^2}\right] - k_1\frac{\partial w(0,t)}{\partial \mathrm{x}} = 0 \tag{25b}$$

where k_1 is the torsional spring constant. Using Eqs. (18a) and (18b) the moment boundary condition can the transformed and written in the modal mode in Eqs. (26a) and (26b), where κ_1 the torsional is spring constant ratio.

$$X(0) = 0 \tag{26a}$$

$$(1-\mu\beta^2)X'' + \mu a_n^4 X - \kappa_1 X' = 0 \tag{26b}$$

At the free end, taking into consideration the small-scale effect, tip mass, the linear spring and axial load, the moment and shear boundary condition at $x = L$ can be expressed as,

$$EI\frac{\partial^2 w(L,t)}{\partial x^2} + \bar{\mu}\left[N\frac{\partial^2 w(L,t)}{\partial x^2} - (\rho A)\frac{\partial^2 w(L,t)}{\partial t^2}\right] = 0 \quad (27a)$$

$$EI\frac{\partial^3 w(L,t)}{\partial x^3} - N\frac{\partial w(L,t)}{\partial x} + \bar{\mu}\left[N\frac{\partial^3 w(L,t)}{\partial x^3} - (\rho A)\frac{\partial^3 w(L,t)}{\partial x \partial t^2}\right] = F_L(L,t) \quad (27b)$$

where $F_L(x,t) = k_2 \cdot z(t)$ is force due to the spring-mass system and k_2 is the linear spring constant ratio. Equation (20) is the solution to Eq. (4) is used to represent $z(t)$ in the shear boundary. Using Eqs. (18a) and (18b) in the moment and shear boundary conditions in Eq. (27a) and (27b), the transformed boundaries are written in the modal mode.

$$(1-\mu\beta^2)X'' + \mu a_n^4 X = 0 \quad (28a)$$

$$(1-\mu\beta^2)X''' + (\mu a_n^4 + \beta^2)X' - \frac{a_n^4\eta}{\left(1-\frac{a_n^4}{a_k^4}\right)}X = 0 \quad 28b)$$

where η is the dimensionless tip-mass ratio which can be expressed as, $\eta = M_T/\rho AL$, and M_T is the mass which is specified as $\eta = 0.1$ or 10% of the mass of the nanobeam. Substitution of Eq. (21) into the boundary condition Eq. (25a), we obtain,

$$A_n + C_n = 0 \quad (29)$$

The general solution Eq. (30) can now be expressed as,

$$X_n(x) = B_n\sin(p_{2n}x) + D_n\sinh(p_{1n}x) + (\cos(p_{2n}x) - \cosh(p_{1n}x))C_n \quad (30)$$

substituting Eq. (30) into Eq. (25b) gives,

$$B_n = \frac{C_n}{\kappa_1}\left(\frac{p_{1n}^2}{p_2} + p_{2n}\right)\mu\beta^2 + \frac{C_n}{\kappa_1}\left(\frac{p_{1n}^2}{p_2} + p_{2n}\right) - \frac{p_{1n}}{p_{2n}}D_n \quad (31)$$

and substituting B_n in Eq. (31) into Eq. (30) gives the general solution expressed in terms of constants C_n and D_n alone. This result can be substituted into the moment boundary conditions Eq. (28a) at $x = L$ to obtain,

$$C_n \cdot \Gamma_{1n} + D_n \cdot \Gamma_{2n} = 0 \quad (32)$$

where,

$$\begin{aligned}\Gamma_{1n} = {} & -\mu\sin(p_2L)a_n^4p_1^2 + \beta^2\mu^2\sin(p_2L)a_n^4p_1^2 - \mu\sin(p_2L)a_n^4p_2^2 + \\ & \beta^2\mu^2\sin(p_2L)a_n^4p_2^2 + \sin(p_2L)p_1^2p_2^2 - 2\beta^2\mu\sin(p_2L)p_1^2p_2^2 + \\ & \beta^4\mu^2\sin(p_2L)p_1^2p_2^2 + \sin(p_2L)p_2^4 - 2\beta^2\mu\sin(p_2L)p_2^4 + \\ & \beta^4\mu^2\sin(p_2L)p_2^4 + \mu\cos(p_2L)a_n^4p_2\kappa_1 - \mu\cosh(p_1L)a_n^4p_2\kappa_1 - \\ & \cosh(p_1L)p_1^2p_2\kappa_1 + \beta^2\mu\cosh(p_1L)p_1^2p_2\kappa_1 - \cos(p_2L)p_2^3\kappa_1 + \\ & \beta^2\mu\cos(p_2L)p_2^3\kappa_1\end{aligned}$$

$$\begin{aligned}\Gamma_{2n} = {} & (\mu\sin(p_2L)a_n^4p_1 - \mu\sinh(p_1L)a_n^4p_2 - \sinh(p_1L)p_1^2p_2 + \\ & \beta^2\mu\sinh(p_1L)p_1^2p_2 - \sin(p_2L)p_1p_2^2 + \\ & \beta^2\mu\sin(p_2L)p_1p_2^2)\kappa_1\end{aligned}$$

where Γ_{1n} and Γ_{1n} are the dummy constants introduced from applying the moment boundary condition, Eq. (27a). After substituting Eq. (31) into the shear boundary condition Eq. (28b) at $x = L$, the transformed equation can be expressed as,

$$C_n \cdot \Gamma_{3n} + D_n \cdot \Gamma_{4n} = 0 \tag{33}$$

where,

$$\begin{aligned}\Gamma_{3n} = {} & (a_k^4 - a_n^4)p_2 \left(\frac{\eta \cos(p_2 L) a_k^4 a_n^4}{(a_k^4 - a_n^4)} - \frac{\eta \cosh(p_1 L) a_k^4 a_n^4}{(a_k^4 - a_n^4)} - \beta^2 \sinh(p_1 L) - \right. \\ & \mu \sinh(p_1 L) a_n^4 p_1 - \sinh(p_1 L) p_1^3 + \beta^2 \mu \sinh(p_1 L) p_1^3 - \\ & \beta^2 \sin(p_2 L) p_2 - \mu \sin(p_2 L) a_n^4 p_2 + \sin(p_2 L) p_2^3 - \beta^2 \mu \sin(p_2 L) p_2^3 - \\ & \frac{\beta^2 \cos(p_2 L) p_1^2}{\kappa_1} + \frac{\beta^4 \mu \cos(p_2 L) p_1^2}{\kappa_1} - \frac{\mu \cos(p_2 L) a_n^4 p_1^2}{\kappa_1} + \frac{\beta^2 \mu^2 \cos(p_2 L) a_n^4 p_1^2}{\kappa_1} - \\ & \frac{\eta \sin(p_2 L) a_k^4 a_n^4 p_1^2}{(a_k^4 - a_n^4) p_2 \kappa_1} + \frac{\beta^2 \eta \mu \sin(p_2 L) a_k^4 a_n^4 p_1^2}{(a_k^4 - a_n^4) p_2 \kappa_1} - \frac{\eta \sin(p_2 L) a_k^4 a_n^4 p_2}{(a_k^4 - a_n^4) \kappa_1} + \\ & \frac{\beta^2 \eta \mu \sin(p_2 L) a_k^4 a_n^4 p_2}{(a_k^4 - a_n^4) \kappa_1} - \frac{\beta^2 \cos(p_2 L) p_2^2}{\kappa_1} + \frac{\beta^4 \mu \cos(p_2 L) p_2^2}{\kappa_1} - \frac{\mu \cos(p_2 L) a_n^4 p_2^2}{\kappa_1} + \\ & \frac{\beta^2 \mu^2 \cos(p_2 L) a_n^4 p_2^2}{\kappa_1} + \frac{\cos(p_2 L) p_1^2 p_2^2}{\kappa_1} - \frac{2\beta^2 \mu \cos(p_2 L) p_1^2 p_2^2}{\kappa_1} + \\ & \left. \frac{\beta^4 \mu^2 \cos(p_2 L) p_1^2 p_2^2}{\kappa_1} + \frac{\cos(p_2 L) p_2^4}{\kappa_1} - \frac{2\beta^2 \mu \cos(p_2 L) p_2^4}{\kappa_1} + \frac{\beta^4 \mu^2 \cos(p_2 L) p_2^4}{\kappa_1} \right)\end{aligned}$$

and,

$$\begin{aligned}\Gamma_{4n} = {} & -\eta \sin(p_2 L) a_k^4 a_n^4 p_1 + \eta \sinh(p_1 L) a_k^4 a_n^4 p_2 - \beta^2 \cos(p_2 L) a_k^4 p_1 p_2 + \\ & \beta^2 \cosh(p_1 L) a_k^4 p_1 p_2 + \beta^2 \cos(p_2 L) a_n^4 p_1 p_2 - \beta^2 \cosh(p_1 L) a_n^4 p_1 p_2 - \\ & \mu \cos(p_2 L) a_k^4 a_n^4 p_1 p_2 + \mu \cosh(p_1 L) a_k^4 a_n^4 p_1 p_2 + \mu \cos(p_2 L) a_n^8 p_1 p_2 - \\ & \mu \cosh(p_1 L) a_n^8 p_1 p_2 + \cosh(p_1 L) a_k^4 p_1^3 p_2 - \beta^2 \mu \cosh(p_1 L) a_k^4 p_1^3 p_2 - \\ & \cosh(p_1 L) a_n^4 p_1^3 p_2 + \beta^2 \mu \cosh(p_1 L) a_n^4 p_1^3 p_2 + \cos(p_2 L) a_k^4 p_1 p_2^3 - \\ & \beta^2 \mu \cos(p_2 L) a_k^4 p_1 p_2^3 - \cos(p_2 L) a_n^4 p_1 p_2^3 + \beta^2 \mu \cos(p_2 L) a_n^4 p_1 p_2^3\end{aligned}$$

where Γ_{3n} and Γ_{4n} are the dummy constants introduced from applying the shear boundary condition, Eq. (28b) at $x = L$. The results from the moment and shear boundary conditions given in Eqs. (32) and (33) can be expressed in matrix form as,

$$\begin{bmatrix} \Gamma_{1n} & \Gamma_{2n} \\ \Gamma_{3n} & \Gamma_{4n} \end{bmatrix} \begin{bmatrix} C_n \\ D_n \end{bmatrix} = \begin{bmatrix} 0 \\ 0 \end{bmatrix} \tag{34}$$

and the characteristic equation can be obtained from the determinant of Eq. (34) as,

$$\Gamma_{1n} \cdot \Gamma_{4n} - \Gamma_{2n} \cdot \Gamma_{3n} = 0 \tag{35}$$

The characteristic Eq. (35) can be solved numerically to compute the roots where κ_1, κ_2, η, a_n^4, β^2, μ and a_k^4 are the dimensionless constants for the nanobeam and the spring-mass system.

8.1.5. Frequency equations for arbitrary boundary conditions.

The structure shown in Fig. (8.1), indicate a torsional spring (κ_1) at $x = 0$. When the spring constant approaches zero ($\kappa_1 \to 0$), the restraint at $x = 0$ behaves as that of a pin support where there is zero resisting moment and the nanobeam spins freely. When the spring constant is not zero ($\kappa_1 \neq 0$), there is a resisting moment at the boundary and consequently the torsional spring influences the vibrations of the system. On the other hand, when the spring constant

approaches infinity ($\kappa_1 \to \infty$) the support is rigid, and the boundary condition is that of a cantilevered beam. In Eq. (31), when $\kappa_1 \to \infty$ the first two terms vanish in B_n above, and consequently in the characteristic equation too.

At $x = L$, a tip mass is attached to the beam by means of a transverse linear spring. When the linear spring constant is zero ($\kappa_2 \to 0$) the effect of the tip mass is not realized at the tip of the beam and therefore the tip-mass has no influence on the natural frequencies.

Table 8.1: Classical boundary condition derived from the system.

Boundary Conditions		κ_1	κ_2	η
Clamped-Free	CF	∞	0 or ∞	0
Simply supported-Free	SF	0	0 or ∞	0
Simply supported	SS	0	∞	∞
Clamped-Simply supported	CS	∞	∞	∞

However, as the linear spring constant increases ($\kappa_2 \to \infty$), the effect of the tip-mass become pronounced and when κ_2 is extremely large, the tip-mass is rigidly attached to the tip of the nanobeam. By varying the torsional spring constant, linear spring constant and tip-mass ratio, we derive the classic boundary conditions shown in Table 8.1. The frequency equation for the total system including torsional spring and spring-mass is given below in Eq. (39). By applying the limiting value in Table (8.1) the following characteristic equations are derived for the boundary conditions.

(i) Clamped-Free (CF) with constant axial load:

$$\sinh(p_1L)\sin(p_2L)\left(\frac{2\beta^2}{p_1p_2}-\frac{p_2}{p_1}+\frac{p_1}{p_2}\right)+\cosh(p_1L)\cos(p_2L)\left(\beta^2\left(\frac{1}{p_2^2}-\frac{1}{p_1^2}\right)-2\right)-\beta^2\left(\frac{1}{p_2^2}+\frac{1}{p_1^2}\right)-\frac{p_2^2}{p_1^2}-\frac{p_1^2}{p_2^2}=0 \quad (36)$$

(ii) Simply supported-Free (SF):

$$\frac{1}{\kappa_1}\left(\left(p_2+\frac{p_1^2}{p_2}\right)\cosh(p_1L)\sin(p_2L)+\left(-\frac{p_2^2}{p_1}-p_1\right)\sinh(p_1L)\cos(p_2L)\right)+\left(\frac{p_1}{p_2}-\frac{p_2}{p_1}\right)\sinh(p_1L)\sin(p_2L)-2\cosh(p_1L)\cos(p_2L)-\frac{p_2^2}{p_1^2}-\frac{p_1^2}{p_2^2}=0 \quad (37)$$

(iii) Clamped-Simply supported (CS):

$$\frac{1}{\kappa_1\eta}\left(-\frac{p_1p_2^3\cosh(p_1L)\sin(p_2L)}{a_n^4}-\frac{p_1^3p_2\cosh(p_1L)\sin(p_2L)}{a_n^4}\right)+\frac{1}{\kappa_1\eta}\left(\frac{p_2^4\sinh(p_1L)\cos(p_2L)}{a_n^4}+\frac{p_1^2p_2^2\sinh(p_1L)\cos(p_2L)}{a_n^4}\right)+\frac{1}{\kappa_1\eta}\left(\frac{p_1^3p_2\cosh(p_1L)\sin(p_2L)}{a_k^4}-\frac{p_2^4\sinh(p_1L)\cos(p_2L)}{a_k^4}-\frac{p_1^2p_2^2\sinh(p_1L)\cos(p_2L)}{a_k^4}\right)+\frac{1}{\eta a_n^4}\left((p_2^3-p_1^2p_2)\sinh(p_1L)\sin(p_2L)+\right.$$

$$2p_1p_2^2\cosh(p_1L)\cos(p_2L)+\frac{p_2^4}{p_1}+p_1^3\Big)+\frac{1}{\eta a_k^4}\Big((p_1^2p_2-p_2^3)\sinh(p_1L)\sin(p_2L)-$$
$$2p_1p_2^2\cosh(p_1L)\cos(p_2L)-\frac{p_2^4}{p_1}-p_1^3\Big)+\frac{1}{\kappa_1}\Big(\frac{p_2^3\sinh(p_1L)\sin(p_2L)}{p_1^2}+$$
$$2p_2\sinh(p_1L)\sin(p_2L)+\frac{p_1^2\sinh(p_1L)\sin(p_2L)}{p_2}\Big)+\Big(\frac{p_2}{p_1}+\frac{p_1}{p_2}\Big)\cosh(p_1L)\sin(p_2L)-$$
$$\Big(\frac{p_2^2}{p_1^2}+1\Big)\sinh(p_1L)\cos(p_2L)=0 \tag{38}$$

(iv) Torsional cantilever with spring mass system and axial load:

$$\frac{1}{\kappa_1}\Big(\cosh(p_1L)\sin(p_2L)\Big(\frac{p_2^3a_n^4\beta^2}{p_1^4a_k^4}-\frac{p_2^3\beta^2}{p_1^4}+\frac{p_2a_n^4\beta^2}{p_1^2a_k^4}-\frac{p_2\beta^2}{p_1^2}+\frac{p_2^3a_n^4}{p_1^2a_k^4}-\frac{p_2^3}{p_1^2}+\frac{p_2a_n^4}{a_k^4}-p_2\Big)\Big)+$$
$$\frac{1}{\kappa_1}\Big(\sinh(p_1L)\cos(p_2L)\Big(\frac{p_2^2a_n^4\beta^2}{p_1^3a_k^4}-\frac{p_2^2\beta^2}{p_1^3}+\frac{a_n^4\beta^2}{p_1a_k^4}-\frac{\beta^2}{p_1}-\frac{p_2^4a_n^4}{p_1^3a_k^4}+\frac{p_2^4}{p_1^3}-\frac{p_2^2a_n^4}{p_1a_k^4}+\frac{p_2^2}{p_1}\Big)\Big)+$$
$$\cosh(p_1L)\cos(p_2L)\Big(-\frac{p_2^2a_n^4\beta^2}{p_1^4a_k^4}+\frac{p_2^2\beta^2}{p_1^4}+\frac{a_n^4\beta^2}{p_1^2a_k^4}-\frac{\beta^2}{p_1^2}-\frac{2p_2^2a_n^4}{p_1^2a_k^4}+\frac{2p_2^2}{p_1^2}\Big)+\frac{1}{a_k^4}\Big(\frac{p_2^2a_n^4\beta^2}{p_1^4}-$$
$$\frac{a_n^4\beta^2}{p_1^2}-\frac{p_2^4a_n^4}{p_1^4}-a_n^4\Big)+\frac{1}{a_k^4}\Big(\sinh(p_1L)\sin(p_2L)\Big(\frac{2p_2a_n^4\beta^2}{p_1^3}-\frac{p_2^3a_n^4}{p_1^3}+\frac{p_2a_n^4}{p_1}\Big)\Big)+$$
$$\sinh(p_1L)\sin(p_2L)\Big(-\frac{2p_2\beta^2}{p_1^3}+\frac{p_2^3}{p_1^3}-\frac{p_2}{p_1}\Big)-\frac{p_2^2\beta^2}{p_1^4}+\frac{\beta^2}{p_1^2}+$$
$$\frac{1}{\kappa_1}\Big(\sinh(p_1L)\sin(p_2L)\Big(\frac{p_2^3\eta a_n^4}{p_1^5}+\frac{2p_2\eta a_n^4}{p_1^3}+\frac{\eta a_n^4}{p_1p_2}\Big)\Big)+\sinh(p_1L)\cos(p_2L)\Big(-\frac{p_2^2\eta a_n^4}{p_1^5}-$$
$$\frac{\eta a_n^4}{p_1^3}\Big)+\cosh(p_1L)\sin(p_2L)\Big(\frac{p_2\eta a_n^4}{p_1^4}+\frac{\eta a_n^4}{p_1^2p_2}\Big)+\frac{p_2^4}{p_1^4}+1=0 \tag{39}$$

The above characteristic equations (36 to 39) above are for classic local beam and do not take small-scale effects into account and can be used as a baseline. The small-scale effects are taken into consideration in the nonlocal characteristic equation, Eq. (35). The natural frequencies of the system R_n are obtained by making a substitution, $a_n = R_n/L$, into the into Eq. (35). The values of R_n are dimensionless natural frequencies used below to analyze the numerical results. When $\kappa_1 \to \infty$ the torsional spring becomes rigid, the boundary condition behaves like that of a cantilevered beam. The classic cantilever configure can be obtained by setting the mass to zero and the fundamental natural frequency of the system is $R_1 = 1.8750$ which corresponds to the results obtained by Magrab [17] $R_1 = 0.5969\pi$. Furthermore, when $\kappa_2 \to \infty$ the linear spring is rigid and the system behaves like a cantilevered beam with concentrated tip mass because the center of gravity of the attached mass coincides with the tip of the beam , see Fig. (8.5).

8.1.6. Numerical results: fundamental frequencies for arbitrary boundary conditions.

Elastic boundary conditions allow us to simulate different configuration by altering the stiffness of the supports. In Fig. (8.5), for each plot, the torsional spring stiffness ratio is varied

for a range $\kappa_1 = 10^1$, $10^{1.5}$, 10^2 and 10^3 and the linear spring stiffness is chosen for a range $\kappa_2 = 10^1$, $10^{1.5}$, 10^2 and 10^3 with the tip-mass kept constant at $\eta = 0.1$ or 10% of the beam mass. In the Fig. (8.5) the bottom most contour represents $\kappa_1 = 10^1$ which is the lowest stiffness ratio for the torsional spring and the upper most contour plot represents $\kappa_1 = 10^3$. It is noted here that the natural frequencies increase with increasing torsional spring ratio and the lowest $R_1 = 0.6873$, occurs at maximum compressive load $\beta^2 = +0.8$, minimal spring stiffness $\kappa_1 = 10$ and $\kappa_2 = 10$ exclusive of small-scale ($\mu = 0$). When the small-scale parameter increases steadily to $\mu = 0.6$, the frequency of the system increases. This change is not prominent when the axial load is compressive ($+0.4 \leq \beta^2 \leq +0.8$) but is clearly visible when the load is tensile $\beta^2 \leq 0$.

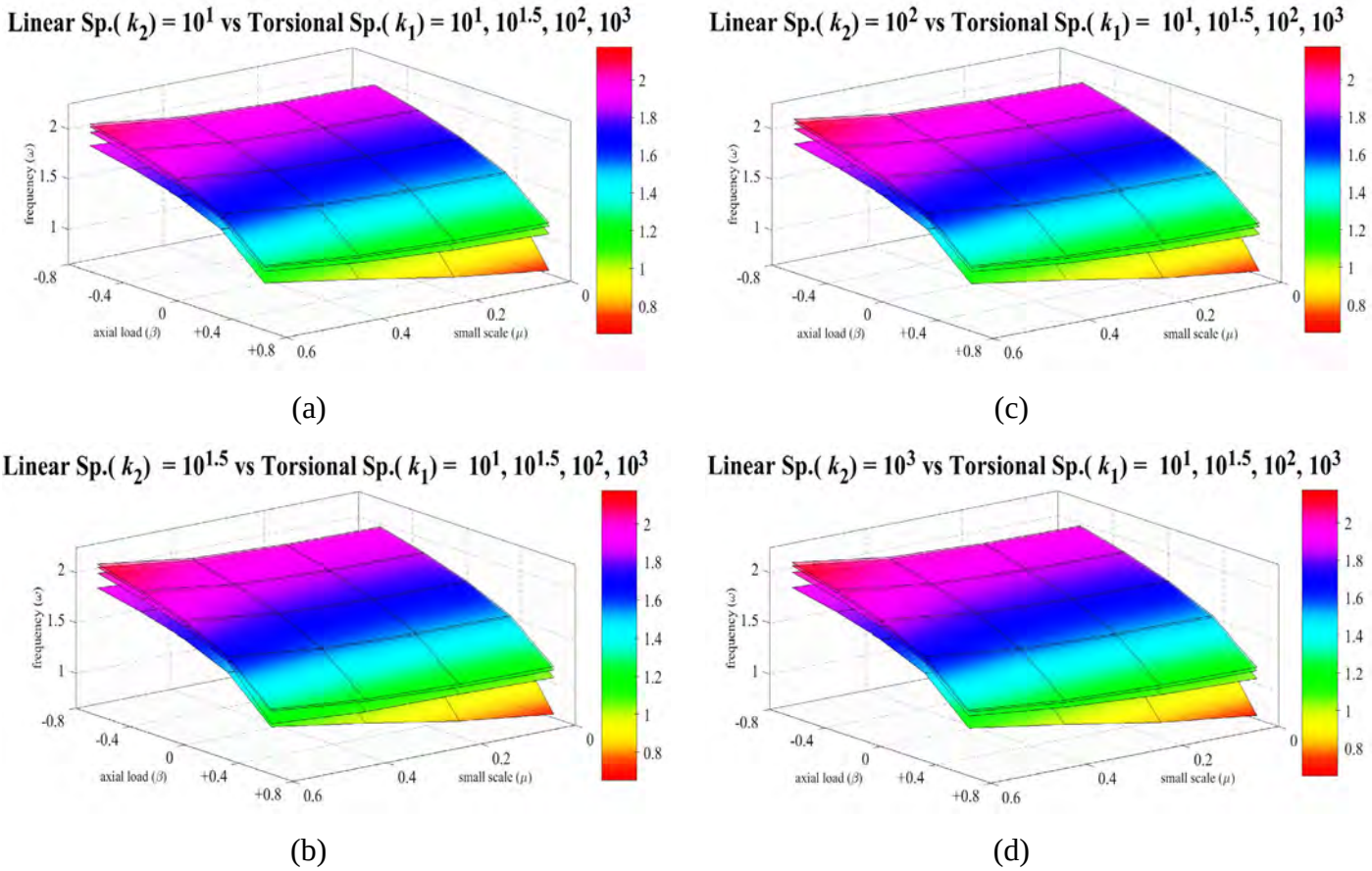

Figure 8-5: Fundamental frequency plotted for linear spring (κ_2 - constant) and torsional spring (κ_1 - varying) with tip mass ratio $\eta = 0.1$ and axial load (β^2) vs. small-scale parameter (μ).

In Fig(8.6), the 2D contour plots are presented for the parameters of interest i.e. $\beta^2 = -0.8$, 0, +0.8, tip-mass ratio $\eta = 0.1$ and the spring contact ratios are varied over a range, $10^1 \leq (\kappa_1$ and $\kappa_2) \leq 10^3$. In Fig. (8.5a) it is noted that that the contours are linear with respect to the linear spring ratio (κ_2) because once we set the linear spring ratio and vary the torsional spring

constant (κ_1), the changes in the natural frequency are minimal at best and close of null. This indicates that the axial load dominates the dynamics when it reaches a value close to the critical buckling load. Not only that, in Eqs. (23) and (24) we note that if frequency parameter of the nanobeam is zero ($a_n^4 = 0$ – null dynamic motion) and the small-scale parameter is zero ($\mu = 0$), the wave numbers, p_1 and p_2 are non-zero.

$$p_{1n} = \sqrt{\frac{\beta^2}{2(1)} + \frac{1}{2}\sqrt{\frac{(\beta^2)^2}{(1)^2}}} \quad \text{or} \quad p_{1n} = \sqrt{\frac{\beta^2}{2} + \frac{\beta^2}{2}} = \beta \tag{40}$$

$$p_{2n} = \sqrt{\frac{\beta^2}{2(1)} - \frac{1}{2}\sqrt{\frac{(-\beta^2)^2}{(1)^2}}} \quad \text{or} \quad p_{2n} = \sqrt{\frac{\beta^2}{2} - \frac{-\beta^2}{2}} = \beta \tag{41}$$

This shows that for a non-zero compressive axial load, the wave numbers are non-zero ($p_{1n} \neq 0$ and $p_{2n} \neq 0$) for zero frequency parameter. This implies that the low order vibrations below critical value of the wave numbers are suppressed, and unable to be exited for a nanobeam under axial compressive load [11]. If the above conditions, with respect to the frequency and small-scale parameter are met, and the axial load is zero ($\beta^2 = 0$), the characteristic equation for determining the natural frequencies (Eq. 35) vanishes. Earlier in the text we noted that $(1 - \beta^2\mu) \neq 0$ or $\beta^2 \neq 1/\mu$ and that the term under the radicals in Eqs. (23) and (24) need to be positive to avoid imaginary roots. Therefore, in the selection of the axial load, one needs to pay attention to the range of values of all relevant parameters selected in order to obtain meaningful results.

Fig. (8.6d) shows the frequencies of a nanobeam under compressive axial load and small-scale parameter $\mu = 0.6$ and we note that in the presence of nonlocal effects the frequencies tend to increase. At maximum torsional spring ratio ($\kappa_2 = 10^3$) the natural frequencies are maximum, and effect of the small-scale effects have a stiffening effect of the nanobeam as observed by Reddy and Wang [14]. For zero axial load ratio ($\beta^2 = 0$) in Figs. (8.6b) and maximum torsional and linear spring ratio (κ_1 and $\kappa_2 = 10^3$), the system behaves like a cantilever beam with concentrated tip-mass ($\eta = 0.1$) and the natural frequencies are widely published, $R_1 = 1.7227$ [4, 16, 17, 18] as indicated in the plot. As expected, when the torsional spring ratio increases ($\kappa_1 \to \infty$), the frequencies increase and in Fig. (8.6e) a further increase in the frequencies is attributed to the small-scale parameter. In Figs. (8.6c) and (8.6f) the nanobeam is under tensile load and the frequencies are higher than in the other two instances ($\beta^2 =$ +0.8 and 0).

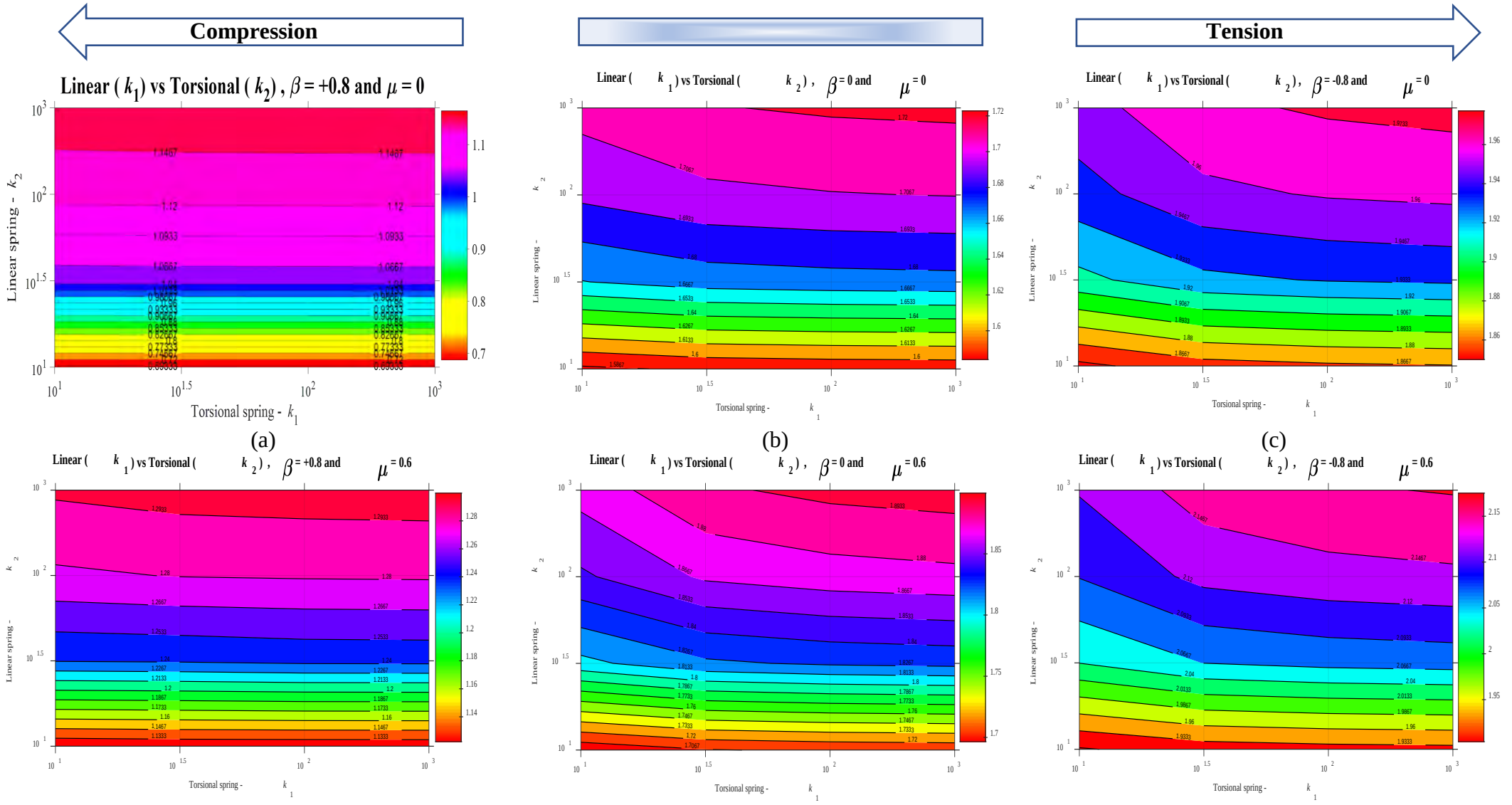

Figure 8-6: Contour plots for torsional (κ_1) vs. linear spring (κ_2) with axial load (β^2) and small scale-effects (μ).

Table 8.2: Frequency parameter (a_k) of spring-mass system.

	$a_k^4 = \kappa_2/\eta$			
κ_2 \ η	0	0.1	0.5	1
10^1	∞	3.1623	2.1147	1.7783
$10^{1.5}$	∞	4.2170	2.8201	2.3714
10^2	∞	5.6234	3.7606	3.1623
10^3	∞	10	6.6874	5.6234

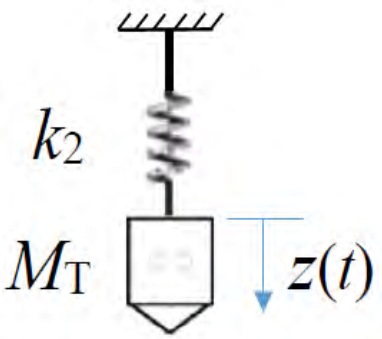

Figure 8-7: Spring-mass system at $x = L$

The spring-mass system can be isolated as shown in Fig. (8.7). This represents a single degree of freedom system and the frequency value for different combinations of linear spring constant and tip mass ratio is tabulated in Table (8.2). The frequencies of the beam are directly coupled to the frequencies of the spring-mass system and the data in Table (8.2) reveals pertinent details about the vibration characteristics of the entire system. Eq. (20) can be rearranged and written in the form below, where the left-hand side represents the ratio of the displacement of the mass from its equilibrium position to the displacement of the tip of the beam.

$$\frac{z(L,0)}{X_n(L)} = \left(\frac{a_n^4}{a_k^4 - a_n^4}\right) \tag{42}$$

It is clear from the relationship above that this ratio depends entirely on the frequency parameters of the beam (a_n) and the frequency parameters of the single degree of freedom system (a_k). Therefore, information about sample penetration depth can be obtain using the frequencies in Figs. (8.5) and (8.6) and Table (8.2). It is noted that when the rigidity of the linear spring increases ($\kappa_2 \to \infty$) the ratio is non-zero meaning that the tip-mass moves in synch with the nanobeam tip displacement.

$$\frac{z(L,0)}{X_n(L)} = \frac{1}{a_k^4}\left(\frac{a_n^4}{1 - a_n^4/a_k^4}\right)$$

after factoring out a_k^4, substitute $a_k^4 = \kappa_2/\eta$.

$$\frac{z(L,0)}{X_n(L)} = \frac{1}{\kappa_2/\eta}\left(\frac{a_n^4}{1 - a_n^4/(\kappa_2/\eta)}\right)$$

$$\frac{z(L,0)}{X_n(L)} = \frac{\eta}{\kappa_2}\left(\frac{a_n^4}{1 - \eta a_n^4/\kappa_2}\right)$$

therefore, $F_L(x,t) = k_2 \cdot z(L,t)$ in Eq. (27b) can be written as,

$$F_L(x,t) = \kappa_2 \cdot \frac{\eta}{\kappa_2}\left(\frac{a_n^4}{1 - \eta a_n^4/\kappa_2}\right) X_n(L)$$

$$\therefore \quad F_L(x,t) = \frac{\eta a_n^4 X_n(L)}{1-(\eta a_n^4)/\kappa_2} \tag{43}$$

When $(\kappa_2 \to \infty)$, the second term in the denominator vanishes and the shear boundary condition Eq. (27b) reduce to that of a beam with tip mass in concurrence with [16,18,19, 20]. To achieve maximum tip-mass deflection, the transverse spring constant ratio (κ_2) must be small. For example, we can achieve more than double additional tip-mass deflection by allowing $\kappa_2 \to 1$ and at maximum torsional spring ratio, and that is demonstrated by Moutlana and Adali [4], This means that the penetration depth in nanomanufacturing using dynamic atomic force microscopy (dAFM) can be controlled. Lastly, if $a_k^4 < a_n^4$ in Eq. (42) the denominator is negative, and consequently the displacement ratio is negative which indicated that the tip of the nanobeam motion is out of synch with the tip-mass displacement (they move in opposite directions).

Equation (42) articulates the relation between the frequency parameter (a_n) of the beam and the frequency parameter (a_k) of single degree of freedom system. The form of the equation shows that if the denominator on the right-hand side is equal to zero ($a_n = a_k$), this term tends to infinity, i.e. $a_n^4/(a_k^4 - a_n^4) \to \infty$. When this occurs, the term on the left-hand side must be infinite by necessity. Either the numerator tends to infinity, or the denominator tends to zero in the limit. When displacement of the mass from the equilibrium $z(L, 0)$ is infinite, the system undergoes the phenomenon of resonance which should be avoided in manufacturing tools. When plotting the characteristic equation, the resonance frequencies of the whole system can be identified, and the information is key to the design of mechanical systems.

8.1.7. Conclusions.

In the present paper, small scale and surface effects on the fundamental frequency are investigated for a nanobeam with elastically restrained end conditions and carrying a tip mass attached via a linear spring to the end of the beam. The solution for the beam is obtained analytically by expanding the deflection in terms of its eigenfunctions and solving the resulting characteristic equation numerically. Furthermore, the characteristic equations are presented for parametric studies of the effect of support elasticity and tip mass on the fundamental frequencies of the nanobeam.

It is observed that the boundary conditions may lead to an increase or decrease of the fundamental frequency depending on the support flexibility. Boundary conditions can be expressed in terms of a torsional spring at $x = 0$, linear spring and tip mass at $x = L$. The classical boundary conditions correspond to setting the torsional and linear spring constants to

zero $(\kappa_{1,2} \to 0)$ or infinity $(\kappa_{1,2} \to \infty)$. It was observed that low torsional spring stiffness leads to a decrease in the fundamental frequency and high torsional spring stiffness to an increase in the fundamental frequency as the small-scale parameter increases. The rates of decrease and increase depend on the relative values of the spring constants. The effect of the tip mass on the frequencies is to lower the natural frequencies as observed in [16, 18, 21].

8.1.8. Acknowledgment.

The research of the author was supported by research grants from the Durban University of Technology (DUT). The author gratefully acknowledges the support provided by DUT.

8.1.9. References.

1. Eringen, A. C., and Edelen, D. (1972) On nonlocal elasticity. *Int. J. Eng. Sci*. 10 (3): 233–248.
2. Eringen, A. C., (2002) Nonlocal Continuum Field Theories, Springer-Verlag, New York.
3. Rahmanian, M., Torkaman-Asadi, M. A., Firouz-Abadi, R. D., and Kouchakzadeh, M. A. (2016) Free vibrations analysis of carbon nanotubes resting on Winkler foundations based on nonlocal models. *Physica B* 484: 83–94.
4. Moutlana, M.K. and Adali, S. (2019) Fundamental frequencies of a torsional cantilever nano beam for dynamic atomic force microscopy (dAFM) in tapping mode *Microsystem Technologies*, 25(3), 1087-1098. DOI 10.1007/s00542-018-4166-x
5. Eltaher, M.A., Khater, M.E. And Emam, S.A (2016) A review on nonlocal elastic models for bending, buckling, vibrations and wave propagation of nanoscale beams. *Applied Mathematical Modelling* **40** 4109-4128.
6. Eltaher, M. A., Alshorbagy, A. E., and Mahmoud, F. F. (2013) Vibration analysis of Euler–Bernoulli nanobeams by using finite element method. *Appl. Math. Modelling* 37: 4787–4797.
7. Kiani, K. (2015) Nanomechanical sensors based on elastically supported double-walled carbon nanotubes. *Appl. Math. Comput*. 270: 216–241.
8. Moutlana, M.K. and Adali, S. (2017) Fundamental frequencies of a nano beam used for atomic force microscopy (AFM) in tapping mode. *MRS ADVANCES*, Warrendale, PA. https://doi.org/10.1557/adv.2018.321.
9. Reddy, J. N., and Pang, S. N. (2008) Nonlocal continuum theories of beams for the analysis of carbon nanotubes. *J. App. Phys.* 103: 023511.

10. Reddy, J. N. (2006) Nonlocal theories for bending, buckling and vibration of beams. *Int. J. Eng. Sci*. **45**: 288-307
11. Lu, Pin. (2007). Dynamic analysis of axially prestressed micro/nanobeam structures based on nonlocal beam theory. *Journal of Applied Physics*. 101. 073504 - 073504. 10.1063/1.2717140.
12. Gholami, R., Ansari, R. and Rouhi, H. (2012) Vibration analysis of single-walled carbon nanotubes using different gradient elasticity theories. *Composites*: *Part B*: **43**: 2985-2989
13. Lu, L., Gou, X and Zhao, J. (2017) Size-dependent vibration analysis of nanobeams based on the nonlocal strain gradient. *International Journal of Engineering Science*. **116**: 12-24.
14. Reddy, J. & Wang, C. (2016). Eringen's Stress Gradient Model for Bending of Nonlocal Beams. *Journal of Engineering Mechanics*. **142**. 04016095. 10.1061/(ASCE)EM.1943-7889.0001161.
15. Sriramshankar, R., and Jayanth, G. R. (2015) Design and Evaluation of Torsional Probes for Multifrequency Atomic Force Microscopy. *IEEE/ASME Transactions on Mechatronics*, vol. **20**, no. 4, pp. 1843-1853, Aug. 2015, doi: 10.1109/TMECH.2014.2356719.
16. Magrab, B. E. (2012) Magrab Vibrations of Elastic Systems: With Applications to MEMS and NEMS, New York, Springer.
17. Gürgöze M. (1996) On the eigenfrequencies of a cantilever beam with attached tip mass and spring-mass system. *J. Sound Vib*. **190**(2): 149-162.
18. Moutlana, M. K., and Adali, S. (2015) Vibration of a cantilever beam with extended tip mass and axial load subject to piezoelectric control. *R & D J. South African Institution of Mech. Eng.* **31**: 60-65.
19. Dowell, E. H. (1978) On some general properties of combined dynamical systems. *American Society of Mechanical Engineers*, Vol. **46**, Pages 206-209, Winter Annual Meeting, San Francisco, Calif., Dec. 10-15.
20. Gürgöze, M. (1996) On the eigenfrequencies of a cantilever beam with attached tip mass and spring-mass system. Journal of Sound and Vibration. **190**(2): 149-162.
21. Moutlana, M.K. and Adali, S. (2019) Effects of Elastic Restraints on the Fundamental Frequency of Nonlocal Nanobeams with Tip Mass. *International Journal of Acoustics and Vibration*. Vol. **24**, No. 3, pg. 520-530, https://doi.org/10.20855/ijav.2019.24.31368.
22. Zhao, H.S., Zhang, Y. and Lie, S.T. (2018) Frequency equations of nonlocal elastic micro/nanobeams with the consideration of the surface effects. *Applied Mathematics and Mechanics* **39**(8), 1089-1102.

Chapter 9 – Conclusion and future research.

9.1 Conclusion.

In this study, the effects of elastic and inertia elements on the boundary conditions of a nanobeam are investigated. These effects are very profound and are manifested in the natural frequencies of sub-systems and the entire combined system. Discreet systems, such as a nanobeam and a spring-mass system can be coupled to fabricate a tool that can be used in nano-manufacturing and hence, the natural frequencies are important for constructing robust devices. The system under investigation is a torsional cantilever with a spring-mass system at the other boundary. The stiffnesses of the springs can be varied to manipulate the natural frequencies of the system and this class of nanobeams demonstrates that there is room for improvement in applications such as AFM, nano-resonators and other novel NEMS devices.

Nano scale materials are known to have different properties as opposed to micro and macro scale materials due to size and this results in altered behaviour when modelled using classic tools like Euler-Bernoulli or Timoshenko beam theory. Modern theories integrating Eringen's nonlocal concepts i.e. stress gradient and strain gradient theories have been developed to model mechanical behaviour, and these have been shown to be consistent when compared to molecular dynamic simulations. The success of these theories relies on the fact that they take into consideration the small-scale effects. In this study small-scale effects are incorporated into the modelling to study a transversely vibrating nanobeam with torsional spring at $x = 0$ and a concentrated tip-mass that is laterally restrained at $x = L$. The 1st [Paper 1] model helps us to understand the dynamic forces that occur between the probe of an AFM and a sample of interest.

This model explores further understanding the bounds nonlocal stress gradient theories, where we note coalescence of successive mode eigenvalues when the small-scale parameter is beyond a specific value e.g. when $\mu = 0.565$, the natural frequency is $R_n = 2.5954$ and the when $\mu > 0.565$, there appears to be no real or non-trivial eigenvalues for cantilevered nanobeam with tip-mass and elastic restraint. This indicates that beyond certain bounds, nonlocal theories might not yield satisfactory results and scientist are further extending their scholarships into bulk to surface ratios of nano and sub-nano structures to gain a better appreciation of NEMS. It is also noted that when the stiffness ratio of the restraints increases, the natural frequencies increase. The mass has the opposite effects, the mass is inversely proportional to the increase in the natural frequency. Furthermore, it is noted that small-scale parameter has the effect of

stiffening or softening the nanobeam depending on the boundary conditions i.e. the natural frequencies of a simply supported beam and clamped-pinned support beam decrease as the small-scale parameter increases, exhibiting a softening effect. The opposite in seen for the cantilever because the natural frequencies increase as the small-scale parameter increases, exhibit a stiffening effect.

The 2nd model [Paper 2, 3, 4 and 5] is composed of a torsional spring at $x = 0$ and a spring-mass system at $x = L$. This model combines two systems with their own unique natural frequencies into a single system with universal natural frequencies. The universal frequencies can be altered by tuning the natural frequencies of the sub-systems. The frequency of the universal system tends to reside between the frequencies of the individual systems and this ability to tune each sub-system can be useful to prevent external force from inducing resonant behaviour. This model can be viewed as a hammer and chisel and is most suitable for removing or shaping nanomaterial. These types of nano tools are seen in applications for unfolding of DNA and RNA molecules or removing atoms to optimize material properties.

The torsional cantilever is critical development in that it allows more freedom in the design of probes for AFM. For example, when scanning in a viscous medium, thin lengthy probe are required to receive accurate reading but the force required can also be inadequate. The torsional cantilever allows us to use short stubby probes with adequate accuracy and the scanning AFM can be designed to be compact. Torsional cantilevers also have the capability of matching the compliance of the probe to the compliance of the sample of interest, thereby preventing damage to probe and sample during research. The additional advantage offered by the model with spring-mass system is the multiplicative effect it has on the displacement of the tip-mass i.e. the distance traveled by the mass for a standalone spring-mass can be increase by a factor of approximately 1.14 to 3.1 which means that the penetration depth of the tool can be manipulated, resulting in greater effectiveness for material optimization instruments. This can be achieved by setting the relevant parameters, including the elasticity of the springs, small-scale and tip-mass parameters.

Lastly, [Paper5], the 2nd model is further developed to include a longitudinal axial load. The axial load has real application in modern devices, and these is noted with emergence of piezo sandwiched nanobeam. In these applications, flexo-electricity is used to induce an axial load on the top and bottom of the beam surface resulting in moments at the boundaries. The moments are used to control the vibration frequencies, and this was studied extensively by Moutlana and Adali. The axial load exhibits complex behaviour for a beam under compression

and the buckling phenomenon must be carefully considered. The buckling phenomenon is explored as far as 1st mode is concerned. It is found that the compressive axial load decreases the natural frequencies, and a tensile load increases the frequencies of the system. This system offers even more control over the frequencies of vibration compared to the two systems mentioned above, where the axial load offers an additional degree of freedom.

The inclusion of the axial load provides us with information about the behaviour under longitudinal loading which could manifest as a result of flexo-electricity (in composite piezo nanobeams) or residual stress at the surface of the nanobeam. Scientist have recognized that at nano and sub-nano scale, the bulk to surface ratio could have a significant influence on the frequencies. The governing equation are therefore developed to include small-scale effects as well as surface effects. These effects involve the tractions normal to the surface and across the surface and the surface is assumed to experience a different environment compared to the bulk.

9.2 Future research.

Further studies will be undertaken to analyze a beam with elastic restraints, tip mass, axial load, flexo-electricity and surface effects. This will lead to exploring beams that are sub-nano scale to learn the behaviour and develop application to conduct further research. The governing equations developed in this research will be used to study the frequencies for nano/pico beams with surface effects.

Appendix

A. Natural frequencies for nanobeam with spring-mass system under axial load.

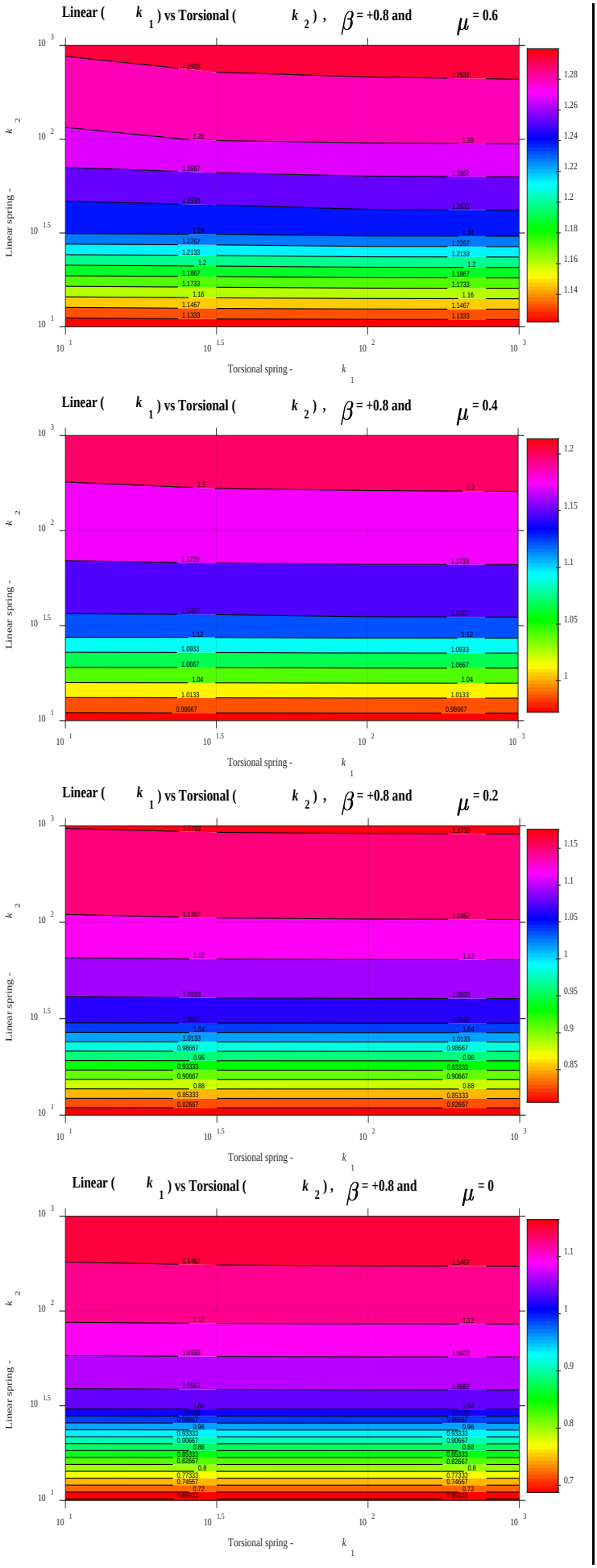

Figure A 8: Contour plot for compressive axial load $\beta = +0.8$ and $\beta = +0.4$.

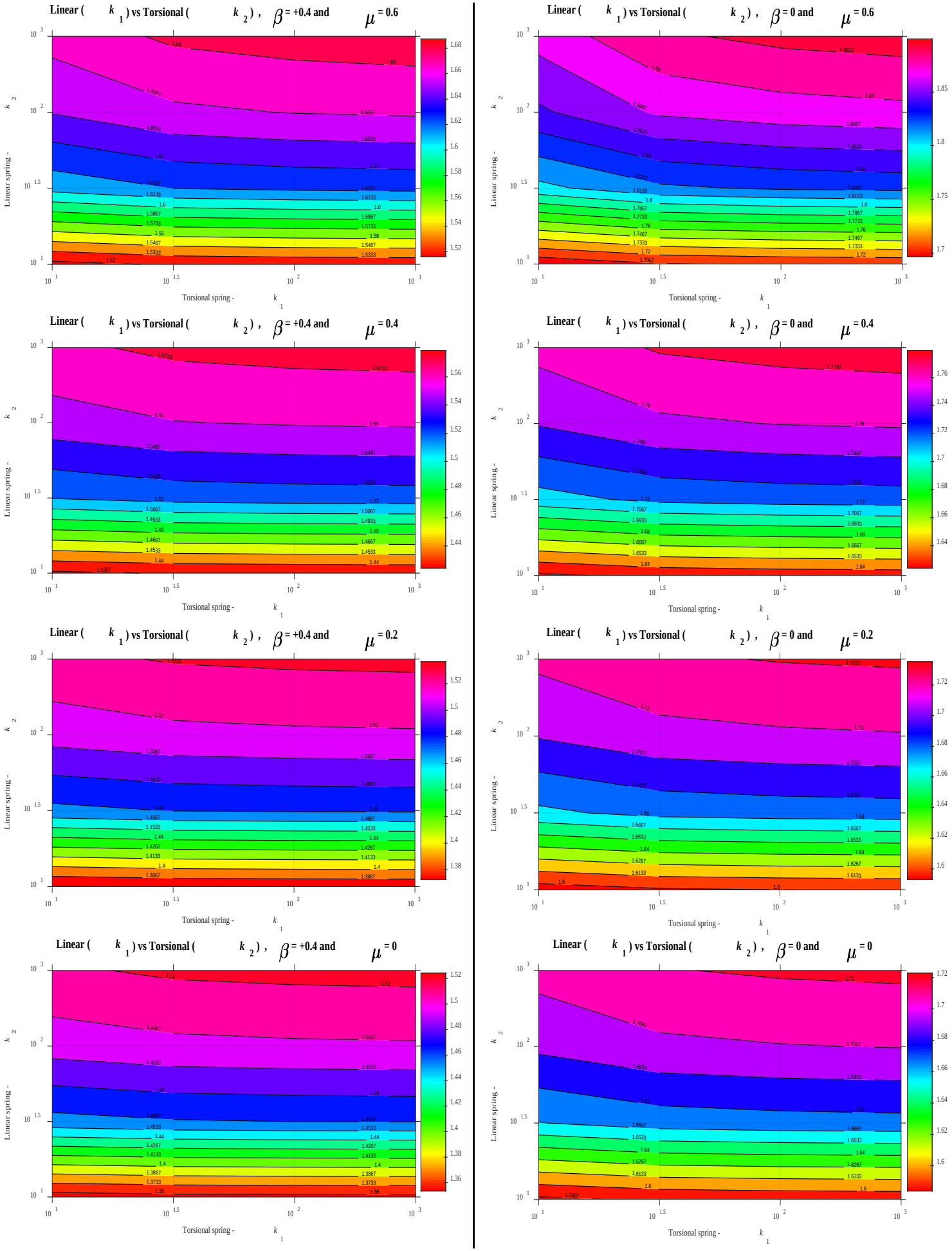

Figure A. 9: Contour plot for compressive axial load $\beta = +0.4$ and load $\beta = 0$ (zero axial load).

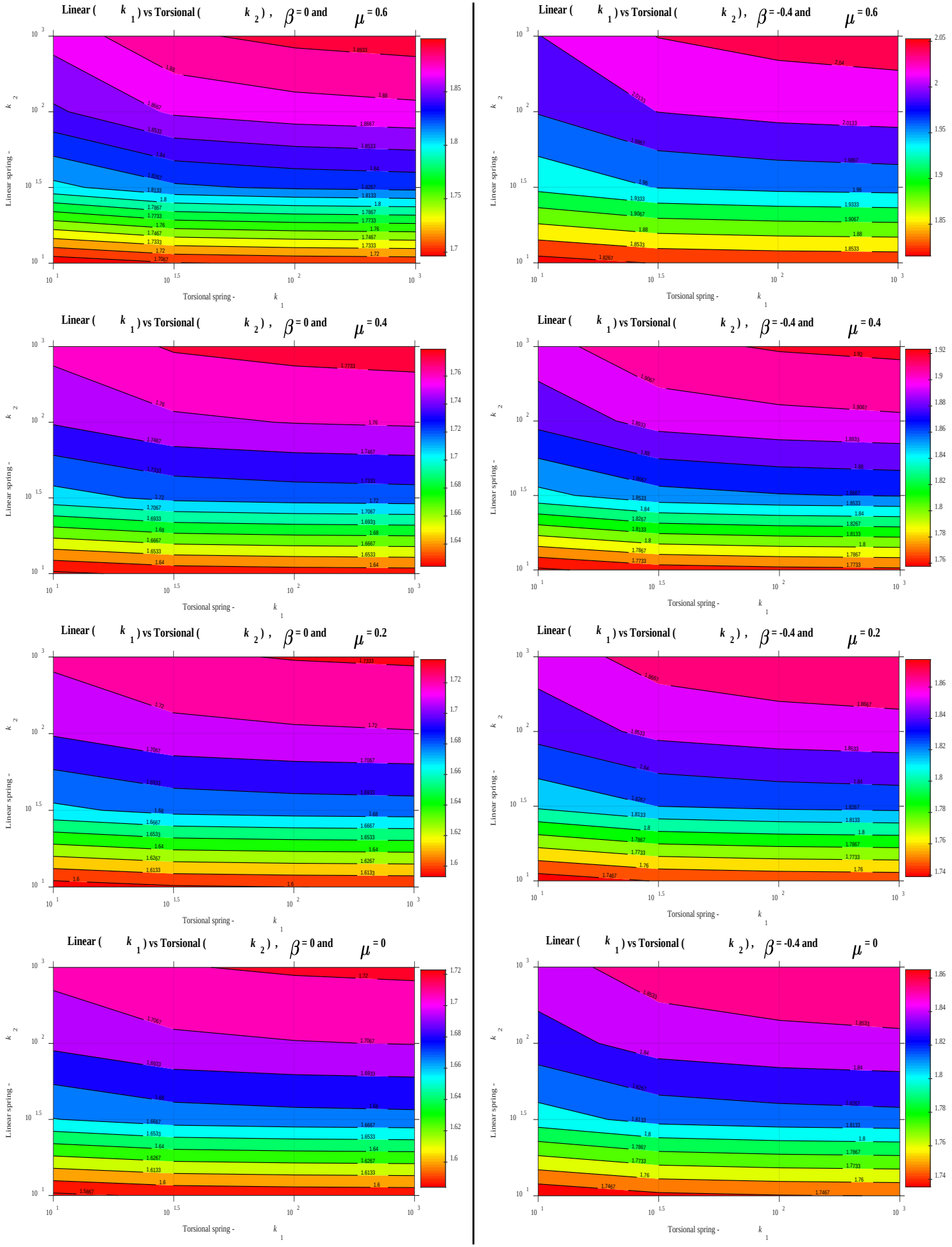

Figure A 10: Contour plot for zero axial load $\beta = 0$ and $\beta = -0.4$ (tensile axial load).

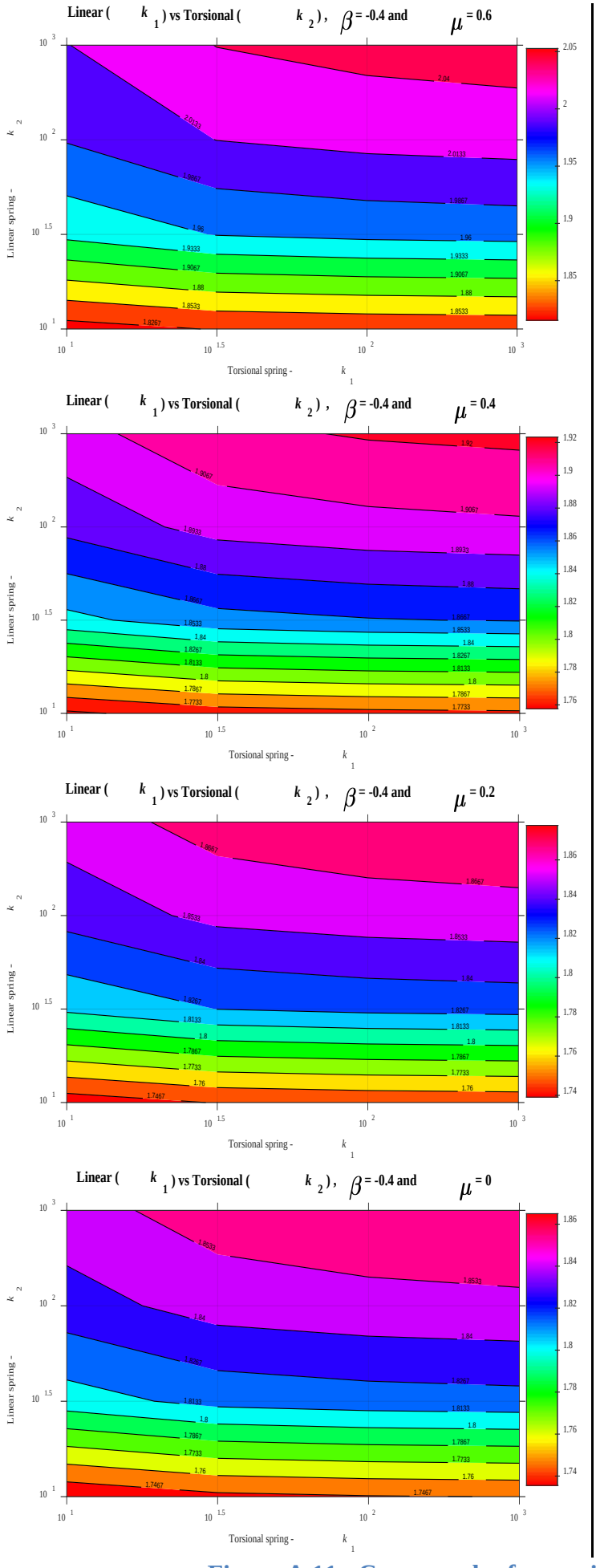

Figure A 11: Contour plot for tensile axial load β = -0.4 and β = -0.8.

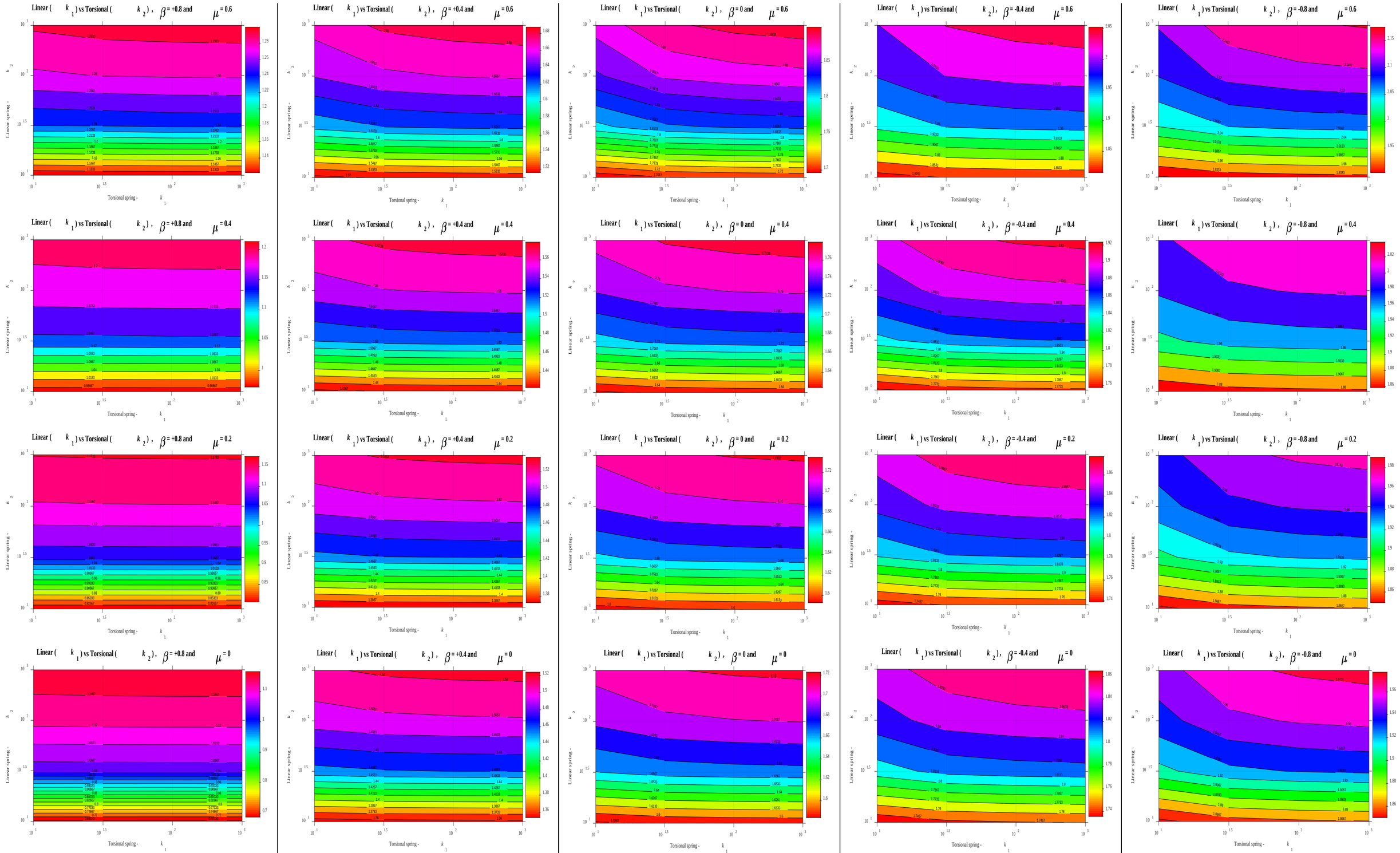

Figure A 12: Contour plots for nanobeam with axial load and spring-mass system.